Predictability Studies of Coastal Marine Ecosystem Behavior

Dem Fachbereich Biologie, Geo- und Umweltwissenschaften

der Carl von Ossietzky Universität Oldenburg

zur Erlangung des Grades eines

Doktors der Naturwissenschaften

vorgelegte Dissertation

von

Marcello Vichi

geboren am 06/04/1970 in Ravenna (Italien)

Oldenburg 2002

Erstreferent: ***Prof. Dr. W. E. Krumbein***
Korreferent: ***Prof. Dr. W. Ebenhöh***
Tag der Disputation: ***03.06.2002***

For unfortunately, Nature cannot be understood by pretending that it is simple.

C. Elton, *Animal Ecology* (preface to the 1965 edition)

quoted in Mann (1988)

Acknowledgments

First of all, I would like to thank the three people that addressed my wandering along this winding path. I am especially thankful to my external scientific supervisor Drs. Job Baretta, who began this all with the pioneering ERSEM project, and continuously helped me in the difficult meandering of this interdisciplinary work. I am very indebted to Drs. Piet Ruardij for the development of the OpenSESAME system, for his capability to solve any kind of problem with numerical coupled models and for providing me with the first implementation of the 3D model. I am particularly grateful to my co-advisor Professor Wolfgang Ebenhöh for giving me the possibility of benefiting from his knowledge of complex systems and for his supporting enthusiasm and trust in my capabilities.

I wish to thank my principal advisor Professor W.E. Krumbein for the great opportunity of presenting this thesis at Oldenburg University and all the staff of complex (and complicated!) modelling at ICBM, especially Cora Kohlmeyer and Kai Wirtz. Without the clever and accurate programming skills of Erwin Embsen, OpenSESAME would not exist. His ability in computer engineering was indeed an important aid during the whole model developing phase.

A special thank goes to Professor Nadia Pinardi, for having me introduced in this fascinating world of coupled physical/ecological models. I also wish to thank the Danish Hydraulic Institute staff and the Netherlands Institute for Sea Research staff for their interest and support in this research.

It has been a pleasure to work and discuss from time to time with exceptional modellers as Hanneke Baretta-Bekker, Marco Zavatarelli, Emanuele Dilorenzo (not only for his scientific help!), and all the past and present members of the SINCEM laboratory at the Marine Environmental Sciences Course, Ravenna.

And finally, last but not least at all, I will never forget the love and patience of my wife Patrizia Tonini, who literally followed me in this adventure, providing a continuous and substantial personal support.

The data support from the BASYS-EU Project, the Regional Meteorological Service (ARPA Emilia Romagna, Italy), the CNR Institute of Marine Biology (Venice), the Marine Biology Laboratory (Trieste) and the other PRISMA-I operational units (ICRAM and IGM) is greatly acknowledged.

This work was partially supported by the TMR Marie Curie Research Training Grant under contract MAS3-CT97-5050 and by the Italian Ministry for the Environment and Territory (Department for Global Environmental, International and Regional Conventions), co-ordinated by the National Institute of Geophysics and Volcanology.

Contents

List of Figures

List of Tables

1. Introduction

Starting from the consideration that marine ecosystem behavior appears unpredictable, our scientific interest is to understand what are the intrinsic reasons of this apparent unpredictability. Without involving into strictly philosophical grounds, the *unpredictability* of marine ecosystems is generally connected to the existence of emergent properties in natural systems, indicating with this term that systems behavior that cannot be obtained from the simple superposition of separate processes. These concepts entered marine ecology in the last 25 years, when "Systems Ecology" became an important branch of biological oceanography since the fundamental text of Odum (1983). Since then, the holistic view on the ecosystem behavior has evolved, considering community and population processes as a "continuum of functional responses to changing conditions" over a wide range of time scales (Pomeroy *et al.*, 1988). Moreover, it has become clearer that new sophisticated understanding of biological processes must be embedded in an appropriate physical setting in order to satisfy the requirements of each discipline (Robinson *et al.*, 1999), and that a substantial part of that wide range of time scales has to be taken into account to provide a proper description of ecological processes. This involves the inclusion of microbial food web processes, that have been found to play an important part in the oceanic carbon flux (Azam, 1998), but also of the physical disturbances that drive the dynamics at those smaller scales, not forgetting the buffering effect of the larger scale circulation processes and, especially in coastal basins, bentho-pelagic interactions. The integration of these diverse entities appears an overwhelming task, because it has to combine together several disciplines with different conceptions of how marine systems behave. As clearly stated by Robinson *et al*. (1999), solving these interdisciplinary problems requires a systems approach which includes a set of linked physical/biogeochemical models, as well as multisensor observational networks and general analysis schemes for the interpretation of ecosystem dynamical processes.

However, recent scientific efforts have shown that, although the predictability of the physical part of the system has improved in estimating the required dynamical fields, the predictability of the ecosystem behavior (as a whole) through the application of coupled models is still fairly uncertain. This occurs in spite of the consideration that when an ecosystem is measured synoptically at the system level (for instance, in small (en)closed natural systems or mesocosms), we find that processes such as photosynthesis, assimilation and respiration do go on at predictable and often remarkably stable rates (Pomeroy *et al.*, 1988). Therefore, a (still questionable) conclusion is that ecosystems do appear to exhibit properties that are self-generated within the system itself, and that are not always traceable to

external forcing functions with similar periodicity (Mann, 1988). There are several examples of cryptic interactions between physical and biological processes in the world ocean, and these occur from large scales events (as the El Niño-related changes in the fish stocks of the Pacific) to smaller scale coastal basins (salt marshes, coral reefs, see Mann (1988) for a more detailed review). An example of an emergent feature that is not clearly related to cause-effect dynamics can be also drawn from the Adriatic Sea, a basin that has been intensively studied during this thesis. The mucilage phenomenon in the Adriatic Sea (and also Tyrrhenian Sea) shows a puzzling unclear periodicity that does not appear to have any driving environmental forcing function. Although the effects and many of the involved variables are quite well understood, several hypotheses have been put forward to unravel the triggering mechanisms (Azam *et al*., 1999; Degobbis *et al*., 1995, 1999; Puddu *et al*., 2000, 2001), but, so far, what can be deduced from the observations is that mucilages seem to be an integrated response of a complex open system to various multiscale disturbances. Generally, the inherent complexity of ecosystems is considered to be a positive factor that fortifies the system itself by providing resistance and resilience to external perturbations (Odum, 1983; Choi *et al.*, 1999). However, as in the case of mucilages, the influence of external factors can be amplified within the ecosystem, exceeding the system's (re)cycling capacity and leading to dystrophic conditions. Other external physical factors, such as meteorological perturbations that modify the existing hydrodynamical conditions, then have to occur in order to reset the system functionalities to a more "climatological" behavior.

The representation of such a system behavior can only be achieved by applying multidisciplinary models as suggested by Robinson *et al*. (1999), but is important to remark that it is required that these models embody an appropriate degree of complexity. About 20 years ago, Platt *et al*. (1981) concluded that the construction of ecosystem simulation models by means of coupled differential equations had led to only very limited success in predicting the consequences of perturbing those systems. These statements lead to a reexamination of the premises of systems ecology, with the formulation of five distinct lines of inquiry that were thought to be promising directions for investigating marine ecosystem behavior (Ulanowicz and Platt, 1985). Those were: thermodynamics, statistical mechanics, input-output analysis, information theory and ataxonomic aggregation in coupled deterministic models. Especially this last line of research has been followed by many scientists, with a plethora of coupled models that have developed in last years. The advances in this field have greatly benefited from the progress in physical oceanography in defining and formulating the hydrodynamical environment with which marine biota have to cope, allowing the implementation of more refined coupled physical/biogeochemical models. This thesis belongs to this line of investigation and a more detailed treatment is presented in Chapter 2. Nevertheless, embarking into ecosystem analyzes through the application of mechanistic models cannot be kept separated from ecosystem perspective considerations. This point has recently been made by Jørgensen (1999):

> "Models will have to learn from systems ecology how ecosystems are working *as systems* and reflect this knowledge in the models, and models can be used to *observe new system properties* of ecosystems. Models have been used as tools in development of

ecosystem theory, and ecosystem theory has been applied to improve, verify and validate models." (my italics).

The possibility of building knowledge from model applications especially lies in the analysis of discrepancies, which means recognizing when a model is deviating from the observed behavior of a system. This is what we call "unpredictability" in a modelling sense, but it does not have to be considered with its negative acceptation only. In fact, it is important to understand whether such unpredictability stems from uncertainties in the initial conditions (as in the case of most physical systems) or from an insufficient description of the natural complex self-organization of biogeochemical processes in the implemented parameterizations of current mechanistic ecosystem models. If the predictability time scale is a function of the initial conditions, then the most appropriate strategy to employ is data assimilation, merging observational data with model dynamics in order to control the predictability error. If, instead, the predictability limit is caused by model deficiencies, then the process descriptions have to be improved by means of specific process studies. This does not necessarily indicate that the model is failing to reproduce the system, but, according to the citation above, it may imply that we are observing different system properties that need to be incorporated in the model formulation in order to accomplish realistic behavior. In this case data assimilation might work as well if dynamical model errors are treated adequately (Robinson *et al.*, 1998), although the absence of some of the basic dynamical principles in the deterministic models will limit the model applicability to the time periods or areas in which the implemented relationships are prevalent (stratified steady-state periods, single-nutrient growth limitations, etc.). There is also a third possible hypothesis, which is that the predictability limit is a combination of the previous causes originating from an inability of the mechanistic approach to elicit complex behavior. If this is true, the conclusions of Platt *et al.* (1981) would still be valid, and the (now refined) mechanistic models have to be abandoned as inappropriate tools for describing ecosystem behavior. Our efforts thus have to be redirected towards alternative methodologies to formulate complex system dynamics quantitatively..

1.1. Aims and methodologies of the thesis

Before testing this last hypothesis, we have to thoroughly assess the present formulations of deterministic coupled models. In fact, recent applications indicate that it is possible to introduce some degree of complexity in deterministic models, and that only such complex models or rather "complicated simple models" have a chance to reproduce the observed natural dynamical behavior (Ebenhöh, 1996).

A partial assessment of coupled model predictability skills has been done in this thesis. The chosen methodology was to apply the same "complex" conceptual principles of the functioning of the main biogeochemical processes to different marine systems, and represent the physical domain and the driving abiotic forcing functions with various stages of spatial and temporal resolution. The final aim is to investigate which observed properties of the ecosystem can be captured by the different rep-

resentations and, if a reasonable degree of agreement with the observed system behavior is achieved, examine the key factors in the model that determine such predictive capabilities. As explained above, a secondary (but important) aim is also to flag where and how the model "fails" in reproducing the system behavior, because this gives indications about the specific processes that need to be further investigated and eventually tested in improved forms within the modelling framework.

The model applications have focused on two very different semi-enclosed European marine ecosystems, the Baltic Sea and the Adriatic Sea. They are both highly-exploited basins with substantial land-derived inputs and distinct eutrophication events, but they differ fundamentally in their hydrodynamical features which makes the application of an ecosystem model with generic functional principles very interesting.

The work has been divided in two main parts. The definition and construction of the modelling tool is one, and the implementation at the various sites, with the performance of hindcasting and systems analysis experiments is the other. A large part of the thesis has been dedicated to the review and reanalysis of the biogeochemical flux model, and the theoretical equations both for the physical and biological parts have been collected in separate appendices because they are common to all the implementations.

Chapter 2 presents the numerical modelling tool, with the illustration of the basic principles of the model concept, the fundamentals of the ecological model (European Regional Seas Ecosystem Model, ERSEM, updated to version III) and the characteristics of the used general circulation model POM (Princeton Ocean Model). Some issues about the coupling of physical and ecological processes in high-resolution numerical models are discussed, and the solutions implemented in the modelling tool are presented.

The specific model applications begin at Chapter 3. Each chapter can be considered as a study in itself, with the modelling framework being the connecting feature. According to the motivations expressed above, I have decided to assess the model skills with different spatial and temporal domains, comparing model results with the known behavior of the analyzed systems.

In Chapter 3, emphasis is given to the analysis of seasonal behavior of the northern Adriatic Sea ecosystem as represented by a vertical high-resolution water column model located at three different, dynamically-relevant sites. The seasonally-averaged results have been compared with the climatological features of the ecosystem, and model-simulated primary and bacterial production rates have also been compared with corresponding *in situ* measured rates. The climatological nature of the implementation allowed to focus on limited aspects of systems study. The dynamics of the spring bloom have been analyzed at the different sites and the functional linkages with the hydrodynamics are presented. Particular attention has been paid to the cycle of dissolved organic matter and its interactions with the carbon transfers along the pelagic food web, especially because ERSEM III introduces improved parameterizations of this important component of the microbial dynamics. Indices of the dominant matter-transfer pathways derived from systems analysis considerations are applied, and the model behavior at the distinct sites is explained in the light of the specific hydrodynamical regimes.

A more detailed representation of the abiotic factors is illustrated in Chapter 4, with the use of a realistic high-frequency time series of meteorological and other external forcing functions at two implementation sites in the Baltic proper. Here, a model hindcasting of the decadal system behavior during the last long stagnation period (1979-1991) is shown, again by applying the one-dimensional version of the coupled model. Model skills in reproducing the dynamics of principal physical and hydrochemical components have been thoroughly compared against observations from the Baltic Environmental Dataset, and the overall system behavior has been analyzed by taking oxygen saturation dynamics as a proxy for system levels organic matter production processes. The importance of the physical water column conditions and the interaction with redox conditions, nutrient supplies and nitrogen (re)cycling have also been analyzed with the aim of increasing the predictability skill of the model on this sensitive component of the Baltic system. In particular, several predictability indices have been applied to evaluate the model-data (mis)fit and the biological significance of such objective measures is critically discussed. Finally, I investigated the role of the meteorological variability in determining the ecosystem model results, with interesting implications on the use of coupled ecosystem models with time-averaged forcing functions.

Chapter 5 presents a three-dimensional implementation of the modelling tool. The importance of mesoscale structures and variability in driving coastal ecosystem behavior has been analyzed with a fully 3D coupled model centered around the Po River delta area in the Northern Adriatic Sea. This exercise has focused on the uncertainties related to the partial initialization of comprehensive ecosystem models like ERSEM III and their interaction with the predictability of mesoscale spatial variability of biological components. The applied methodology is a novel technique in ecosystem modelling, called Observational System Simulation Experiments (OSSEs).

A concluding analysis is given in Chapter 6.

2. The modelling system

2.1. Physical/ecological coupled models

The word *coupling* has the generic meaning of bringing together two distinct entities, in some technical cases by making use of relationships or devices that connect adjacent parts. Concerning physical and biological properties of marine systems, the concept of "coupling" is almost indivisible from the scientific analysis of the system itself, because of the strong dynamical nature of the marine environment that makes impracticable a sharp separation of the two disciplines. Explicit dynamical modelling of marine ecosystems is a recent branch of science, born from the substantial improvements in the application of high-resolution circulation models and the availability of computational systems that are able to process the large amount of information needed for the description of the main physical/biogeochemical processes. Therefore the development of the fundamentals of this discipline are still a process *in itinere*, and most of the current approaches originate from equivalents in the separate disciplines, with just some adaptations in order to fit into this new world of applications. A real appropriate vision of the topic of physical/ecological coupled modelling is still missing and is likely to be a primary task for the coming years.

Essentially, physical/ecological coupled models divide in two main branches, Lagrangian and Eulerian models, which are the analytical ways of treating the transport of constituents in a moving environment. I will focus on Eulerian models, not only because the tools used in this work fall in this category, but also because the Eulerian approach is usually the preferred one since it allows a direct point-to-point comparison of model results with observations. The ecological limitations of the Eulerian approach (especially concerning the tractability of multicellular organisms) will be shortly reviewed in the section describing the ecological model (Section 2.2.3).

In its most generic form, the Eulerian equation for an ecosystem state variable C in the marine pelagic system such as phytoplankton biomass or detritus, is

$$\frac{\partial C}{\partial t} = \left.\frac{\partial C}{\partial t}\right|_{phys} + \left.\frac{\partial C}{\partial t}\right|_{bio} \tag{2.1}$$

where the first term on the right hand side denotes changes due to the transport processes and the second indicates source or sink terms solely induced by biogeochemical transformations. The transport

term is usually made explicit in the following vectorial form

$$\frac{\partial C}{\partial t} = -\nabla \cdot \left(\vec{U}C\right) + \nabla \cdot \left(\vec{K} \cdot \nabla C\right) + \left.\frac{\partial C}{\partial t}\right|_{bio} \tag{2.2}$$

where the advective velocities $\vec{U}$ and diffusion coefficients $\vec{K}$ are three dimensional vectors. The application of a three-dimensional model of marine ecosystems implies the simultaneous solution of several equations like (2.1), one for each component, at the points in space defined by a grid. Analytical solutions of (2.2) are not available and the application of the model is strongly dependent on the numerical implementation of the integration techniques.

A rigorous and unique solution for this set of differential equations is currently an unattainable ideal, both from a practical and a scientific point of view. Firstly, the knowledge of the source and sink terms is (still) incomplete, and covers only a part of the large time scale spectrum of ecological processes; there are no Navier-Stokes equations for ecological processes and most of the uncertainties lie in the choice of the key variables that control the main interactions. Unlike physical oceanography, in ecological modelling the degree of approximation is more on the number and type of the defined ecological state variables than in the processes themselves. Secondly, the interaction with the transport term is not always linear as it is described in (2.1), and occurs at all time scales. The approximation applied in the biological parameterizations usually leaves out lower order terms that nevertheless may be significant regulating factors at particular dynamical scales. Finally, and this is more a technical point, the computational tools needed to solve the set of equations in an efficient and yet accurate way are still developing, especially for coastal area applications, where the boundary conditions have a high variability and the dynamics are mainly determined by local processes (Prandle *et al.*, 1993). As consequence, the employment of deterministic coupled models in forecasting operations is in its infancy and a consistent validation of their hindcasting capabilities has not (yet) been performed. In a recent critical analysis of aquatic ecosystem models, Ebenhöh (2000) highlighted the fact that the modelling efforts in the last five years have moved from a systems-oriented approach to a more engineering, problem-oriented approach, aiming at an understanding of limited and local aspects of the ecosystem. A reason for this is that the interest in modelling is increasing because the need for prognostic tools capable of predicting the behavior of the ecosystem is becoming urgent due to the fast-varying and sometimes harmful changes in coastal areas and semi-enclosed basins. Some examples are eutrophication phenomena in the Gulf of Finland, more frequent toxic algal blooms and recent mucilage formation events in the Adriatic and Tyrrhenian Seas. Nevertheless, it is difficult to establish cause-effect relationships between observed apparently anomalous processes and system behavior.

2.1.1. Critical variables and dominant process scales

Hence, the identification of those system properties that need to be included in the description of marine ecosystem processes is the major task. The recommendations expressed in a recent workshop on

biological data assimilation in ecological models reads: “The most appropriate configuration should be chosen for the problem at hand. Model definition should be achieved by identifying critical variables and dominant space and time scales.” (Robinson and Lermusiaux, 2000). From this advice, it is even clearer that in recent years the focus has moved from a view of the ecosystem as “a system” - as requested by systems ecologists in the 80s (Chapter 1) - to the selection of the key variables that appear to give the highest degree of connectivity with the problem at hand. This partly explains the proliferation of models with such different structures and setups. An interesting example is given in Hofmann and Lascara (1998), where the authors made a review of existing three-dimensional coupled models. Table 2.1 presents the results from that work with some additional more recent publications. It is striking how the column listing the type of circulation model contains recurring keywords, which basically indicate the degree of approximation of the primitive hydrodynamic equations that is considered sufficient to produce an adequate representation of the physical features. Conversely, the column describing the ecological model has a much wider range of terms, mostly being a list of the variables interacting in the model, which are justified by the column stating the application’s objectives. Clearly, there appears to be a sort of general consensus on the appropriateness of physical representation, while there is a clear lack of consensus on what properly represents the biological/ecological response of marine ecosystems.

The choice of the critical variables is clearly complicated by the highly diverse species composition in natural communities. When different species belonging to a marine ecosystem are analyzed separately in laboratory or mesocosm conditions, we note a high range of variability in the species-specific functional response to environmental factors. However, as also pointed out in the Introduction, the corresponding ecosystem-level processes appears to be more stable and “immune” to the successional changes in the system. This has been attributed to the existence of guilds of species which perform a common function. Through time, the dominant species may change, but this has apparently lower influence upon the rate of the functional processes which are generally controlled by abiotic factors, indicating that ecosystems exhibit higher stability than do species populations (Pomeroy *et al.*,1988). Therefore, ataxonomic aggregation and size-dependent parameterizations embedding allometric principles (Platt, 1985) of biological functional processes appear to be a promising methodology to be used in coupled models.

Probably, the most highly abstracted form of ataxonomic aggregation is the one used in the so-called NPZ(D) models (Nutrients, Phytoplankton, Zooplankton and Detritus). Many of these models originates from the work of Fasham *et al.* (1990), and they are broad functional aggregations that do not make any distinction about intrinsic dimensionalities. The currency of the model is generally nitrogen, which may be converted to units of carbon or chlorophyll-*a* by means of constant conversion factors. An NPZD model is more or less equivalent to the concept of trophic levels (Lindeman, 1942) that has been demonstrated to be a much too coarse approximation of ecosystem complexity (Mann, 1988) and with a low inherent predictive capability (Cousins, 1985). Nevertheless, when used in conjuction with good representations of the abiotic factors, such models are able to explain a

Region	Circulation Model	Biological Model	Space/Time Scale	Objective	Reference
Gulf of Carpentaria	Barotropic, Ekman imposed	Lagrangian vertical behaviour	100s km, seasonal	Larval dispersal, penacid shrimps	Rothlisberg et al. (1983)
Mid-Atlantic Bight	Barotropic, Ekman imposed	NO_3, P	100s km, seasonal	Spring bloom	Walsh et al. (1988)
Gulf of Mexico	Two-layer baroclinic	NO_3, P	100s km, years	Primary production	Walsh et al. (1989)
California CTZ	Primitive equation	Lagrangian	100s km, weeks	Transport patterns	Hofmann et al. (1991)
Bransfield Strait	Primitive equation	Lagrangian bioenergetics	100s km, weeks	Larval growth and dispersal, Antarctic krill	Capella et al. (1992); Hofmann et al. (1992)
Georges Bank	Primitive equation	Lagrangian vertical behaviour	100s km, seasonal	Larval dispersal; cod, huddock, sea scallop	Werner et al. (1993); Tremblay et al. (1994)
North Sea	Baroclinic	Lagrangian vertical behaviour	100s km, months	Larval dispersal, herring	Bartsch (1993)
Bering Sea	$k-\varepsilon$	NO_3, NH_4, P, Z, D	100s km, seasonal	N and C flux	Nihoul et al. (1993)
North Atlantic	Quasi-geostrophic	NO_3, NH_4, DON, PON, P, Z, BAC	1000s km, years	Ecosystem dynamics	Sarmiento et al. (1993); Fasham et al. (1993)
South Atlantic	Primitive equation	NO_3, P	100s km, weeks	Primary production	Pribble (1994)
Conception Bay	Diagnostic	LF	10s km, weeks	Larval capelin dispersal	de Young et al. (1994)
Indian Ocean	Reduced gravity	SiO_4	100s km, years	Silicate distribution	Young and Kindle (1994)
North Sea	Baroclinic	NO_3, NH_4, PO_4, SiO_4, pelagic and benthic food webs (functional groups)	100s km, seasonal	Carbon and macronutrients cycling	Baretta-Bekker (1995); Baretta-Bekker and Baretta (1997)
North Atlantic	Quasi-geostrophic	NO_3, NH_4, P, HET, NEX	100s km, months	Spring bloom	McGuillicuddy et al. (1995a,b)
North Atlantic	Prescribed	N, P, Z	100s km, year	Primary production	Semovsky and Wozniak (1995)
California CTZ	Primitive equation	NO_3, NH_4, SiO_4, LP, SP, Z (3 sps.), D	100s km, weeks	N and C flux	Moisan et al. (1996)
California CTZ	Primitive equation	Lagrangian	100s km, weeks	C transport	Moisan and Hofmann (1996b)
Baltic Sea	Primitive equation	N, P, Z, D	mesoscale, days	Spring bloom	Fennel and Neumann (1996)
Adriatic Sea	Primitive equation	NO_3, NH_4, PO_4, SiO_4, pelagic food webs (functional groups)	100s km, seasonal	Primary production, Chl-a	Zavatarelli et al. (2000)

Table 2.1.: Characteristics of Three-Dimensional Models that have been developed for Marine Ecosystems. Adapted from Hofmann and Lascara, (1998, see paper bibliography for some of the references indicated in the table) and updated with more recent publications. Abbreviations: N, nutrient; NO_3, nitrate; NH_4, ammonium; PO_4, phosphate; SiO_4, silicate; P, phytoplankton (LP, >5μ; SP, <5μ); Z, zooplankton; D, detritus; DON, PON, dissolved and particulate organic nitrogen; NEX, exported nitrogen; BAC, bacteria; HET, heterotrophs; LF, larval fish.

reasonable portion of observed variance, especially when driven by high-resolution hydrodynamical processes (Hofmann and Lascara, 1998). From a biological point of view, NPZD models are basic approximations of ecosystem interactions, ignoring the role of the microbial loop in marine organic matter fluxes (Azam, 1998; Azam *et al*., 2000). But the idea of functional groups, particularly for the unicellular components, is enticing and can be extended to comprise more size-differential regulations, as is found to be the case in the planktonic world (Riegman *et al*., 1993). This tendency is also confirmed in the recent literature on coupled ecosystem models, where more components are added to the original NPZD structure in order to accommodate more aspects of ecosystem complexity.

To contribute to a coherent approach to ecosystem modelling, a revised modelling framework is proposed. This is based on generic functional, biological principles, grounded on strict adherence to mass conservation laws and realized by closing the different element cycles in the model domain, including (external) sources as well as (benthic) sinks. The modelling system described in details in the next section and in the Appendices attempts to capture those aspects of the system behavior which *grosso modo* are biogeochemical responses to the abiotic dynamics and the resultant (variable) temporal and spatial structure of the system. It therefore focuses on those variables that:

1. are passively transported;
2. can be expressed in terms of concentration;
3. complete their whole life-cycle *in* the model domain;
4. are responsible for the largest fraction of energy cycling through the system.

2.2. The HiROPE system

The coupled model described in this section and detailed in the Appendices, is the cumulation of a series of model development efforts spanning a series of EU-MAST funded projects (ERSEM I, ERSEM II, MATER, BASYS) with the aim of providing a comprehensive set of methodologies for building multi-purpose, high-resolution ecosystem models. For these reasons, the acronym is a concatenation of other acronyms that refer to the specific system that has been incorporated in the tool (**Hi**gh-**R**esolution **O**penSESAME **P**OM **E**RSEM). In other words, this is the most recent version of the European Regional Sea Ecosystem Model (ERSEM III; previous published versions were ERSEM I, Baretta-Bekker, 1995; ERSEM II, Baretta-Bekker and Baretta, 1997) coupled to the general primitive equations Princeton Ocean Model (POM, Blumberg and Mellor, 1987). The coupling has been done using the OpenSESAME simulation environment, which is illustrated in the next section. Other model applications have been performed by several authors using (slightly) different versions of the two models or with a different hydrodynamical model, and they have been applied to different basins as coastal seas, estuaries and open ocean areas (Allen *et al*., 1998, 1999; Obernosterer *et al*., 2001; Ruardij *et al.*, 1997; Vichi *et al*., 1998a,b; Zavatarelli *et al*., 2000).

Figure 2.1 shows the generic coupling between the different sub-models. The physical model transforms the information from the forcing functions (air-sea interactions and other boundary conditions) into dynamical fields, defining and driving the physical transport and the environmental information. The trophic interactions and the production/consumption of particulate and dissolved organic matter are calculated in the ERSEM pelagic and benthic models, together with the molecular diffusion of regenerated nutrients from the sediments. The input from external organic and inorganic sources, the sinking of particulate material and sedimentation, which is an input to the benthic system, are also included in the pelagic processes. The state of the system at a certain point in time and space is thus determined by the physical transport term and by the source/sink terms due to biogeochemical interactions. Actually there is still a one-way information flow from the physical model to the ecological model, because there are no feedback interactions (dashed lines in the scheme). The lack of information and process-studies on the impact of the biota on the physics of the water column make the opening of this door still a delicate task.

2.2.1. OpenSESAME

The core and basis of the implementation of the coupled models is the simulation environment OpenSESAME[1] (Open Software Environment for Simulation and Analysis of Marine Ecosystems, hereinafter OS) which has been developed at NIOZ by Piet Ruardij and Erwin Embsen. The package is a modification of the original SESAME (Ruardij *et al*., 1995) that was created to integrate the physical and biogeochemical sub-models in the ERSEM I and II projects for the modelling of the North Sea ecosystem dynamics (Baretta-Bekker, 1995; Baretta-Bekker and Baretta, 1997). OpenSESAME is essentially an equation solver that allows the user to construct ecological models by defining dynamical equations (fluxes) between the different biogeochemical components, specifying the elements which are exchanged (*i.e.* carbon, phosphorus, oxygen, etc.). The user-defined model structure and equations are written in a specialized meta-language that provides the statements needed for implementing the different types of ecological state variables and fluxes recognized in the ecosystem. The final output of the package is a plain C source code that is a rigorous translation of the user-defined model, which is also nested into a looping routine that takes care of the numerical time integration. One of the advantages of this translation maneuver is that many *a priori* controls can be imposed on the building of ecosystem models, directing the modeller towards the implementation of more coherent coding that is closer to the biological, theoretical form of the modelled process. Conservation of mass and unit equivalence are explicitly prescribed in the statements and the flow of mass across the boundaries of the model domain can be prescribed by using special source and sink variables. Moreover, the user is forced to implement a hierarchical structure of processes and functions that, on the one hand, make the model apparently more difficult to read in a traditional way, but on the other hand is suitable for building a graphical tree of the model, accessible through a Graphical User Interface (written in Tcl/Tk). Finally, specific arrangements of the computer representation of the set of state variables

[1] The OpenSESAME package is distributed freely and can be requested at sesame@nioz.nl

renders the ecosystem model open to the coupling with existing transport models, which provide the calculation of the transport term in (2.1). This last statement needs to be clarified, because a consistent and direct coupling between existing models is difficult to be done in practice. This is commonly known in ecosystem modelling, because all the existing setups of coupled models have introduced special features that modified the original code, at the price of losing the compatibility. In this respect, the model produced with OpenSESAME is an entity *per se*, and therefore hardly linkable with others. Furthermore, hydrodynamical transport models are usually written in FORTRAN, a language which is less than ideally suitable for the hierarchical and object-oriented programming that is needed when dealing with systems comprising of many variables and levels. Thus, the generated ecosystem model cannot be easily incorporated into transport models but the other way around can be done in a very efficient way, at the price of translating the physical model in the meta-language. This has been done in this specific case for the Princeton Ocean Model, and will be explained in more detail in the next section.

2.2.2. The Princeton Ocean Model

POM is widely used in physical oceanography as one of the reference primitive equation numerical models for the simulation of ocean and shallow water physical systems. The HiROPE simulation system comprises a complete recent version of the three-dimensional model (known as POM97) and also a one-dimensional version.

The one-dimensional version is essentially a vertically-resolved boundary layer model, which is based on the turbulence closure scheme proposed by Mellor and Yamada (1982, version 2.5, hereinafter referred to as M-Y). The model determines the dynamical vertical structure and the actual turbulent diffusive vertical transport in the water column, as driven by the boundary conditions at the air-sea interface and at the bottom.

The three-dimensional setup has some specific features that makes it particularly suitable for high-resolution applications in coastal areas, where the variability of the biological processes is a consequence of the variability of the hydrodynamical properties. In this respect, POM is characterized by the following attributes:

- open source and a large number of users around the world, with applications to all kinds of basins;
- sigma coordinate model, which allows the application to basins with highly-varying bottom topography;
- embedded turbulence closure to dynamically evaluate the turbulent diffusion coefficients. The numerical differentiation of the diffusion terms is also treated implicitly in order to allow the prescription of fine resolution boundary layers;

- free surface and mode splitting time stepping that efficiently provides the calculation of the vertically integrated equations (external mode) and the three-dimensional baroclinic equations (internal mode) with complete thermodynamics.

The analytical form of the main equations can be found in Blumberg and Mellor (1987) and Mellor (1998) and a brief description of the 3D and 1D implementations is presented in Appendix C. In this section I will focus on the specific implementation of POM into OpenSESAME (OS). The model has been first incorporated into OS by translating it to the meta-language (the acronym OSPOM97 will be used to indicate the stand-alone translation). Special care has been taken to maintain the original structure of the FORTRAN code and the flow chart of the resulting implementation is shown in Figure 2.2, where the link with the OS driver is also presented. POM users here can easily recognize the names of the main FORTRAN routines and the sequence of the calculations of the main variables both in the external and internal mode (for an explanation of the symbols see the POM User Guide, Mellor, 1998). In respect to OSPOM97, the OS driver is simply acting as a shell that increases the discrete time counter, prepares and reads the boundary forcing functions and stores the simulation results. The standard seamount test case has been used for comparison with the FORTRAN version, giving a complete matching of the simulation results. Therefore OSPOM97 is a "perfect" clone of POM, with the advantage of a more flexible structure that can be easily coupled to the ecological model.

2.2.3. ERSEM

The ERSEM model is a biomass-based ecosystem model which was originally constructed to simulate the dynamical cycling of carbon, oxygen and the macronutrients N, P and Si over the seasonal cycle in temperate marine systems. The model consists of an interlinked set of differential equations, describing the biological and chemical processes both in the water column and in the benthic system, as forced by light and the hydrodynamical environment. The detailed description of the reviewed equations of ERSEM III is given in Appendix A and B. Section A.1 gives an overview of the mathematical formulation and presents the different types of model state variables in Tables A.1 and B.1 for the pelagic and benthic system, respectively. All parts of the ERSEM I/II model system have been subjected to independent scientific scrutiny in that they have been published in peer-reviewed journals. I will refer to the papers listed in the cited tables for the biological reasons of the parameterizations chosen to represent the biogeochemical processes in the model.

The ERSEM model follows the functional group approach described in Section 2.1.1 (see also Baretta and Ruardij, 1988) and the defined functional groups are considered in terms of their carbon and macronutrient contents as detailed in Section A.1. Each sub-group constitutes an implicit size-class, that is, there is no internal size structure in the biological constituents. All the organisms considered to be in a particular group (e.g: diatoms or picophytoplankton) share the same functional properties in the ecosystem and have the same trophic interactions. The functional group approach has been shown to be a good choice for the description of unicellular organisms, but generally fails

when dealing with size-structured populations as mesozooplankton, where experimental data usually are derived from individuals (Baretta *et al*., 1995). The necessity to apply fixed physiological rate parameters to the bulk-biomass-population introduces serious errors, as physiological rates scale negatively with increasing size of individuals, not necessarily with a population of individuals. Hence, having to assume fixed specific rates is a coarse approximation, and the mesozooplankton description will remain pretty primitive as long as this group is modelled as bulk biomass. Individual-based models, using allometric relations defining the instantaneous physiological rates of differently-sized individual are needed in order to be coupled with the existing models for lower trophic levels. The present mesozooplankton models can be seen as an elaborate predation-closure term on the unicellular components of the system. As the mesozooplankton plays a relatively minor role in the cycling of carbon and nutrients (10-15%) we grudgingly accept the status-quo.

ERSEM was prepared as a compendium of the knowledge about marine ecosystems, joining together expertise from several disciplines, with everyone holding a specific point of view about how a model should be constructed. As hinted at in previous sections, the equations describing ecological processes will always tend to be dynamical entities, to be adapted as soon as new information upon process definition is obtained. Essentially, the ERSEM philosophy is to capture the (re)transformation of dissolved carbon and macronutrients N, P (and Si) into particulate forms. These elements are the basic building blocks of living organisms and their biogeochemical interactions in the model have been achieved by specifying the separate threads and the stoichiometry between the elements. Hence a source term in a specific fundamental equation corresponds to a sink term - corrected by the appropriate stoichiometric coefficients - in the fundamental equation of another state variable involved in the process. To ensure conservation of mass, it is thus necessary to close the organic matter cycles in the model domain, and this has been done by:

- explicit coupling between pelagic and benthic systems, and functional separation of the early-diagenetic processes;
- closing of the Oxygen cycle through surface re-aeration. The CO_2 pool is still considered to be an infinite source/sink and the dynamics are not explicitely followed, although a parameterization for the inorganic carbon species has been prepared for future applications on large scale Carbon cycling studies;
- explicit resolution of the microbial loop;
- food web structure with multiple food sources and multiple predators both in the pelagic and in the benthic system.

This last concept is better expressed by the following sentences in Baretta *et al.* (1995):

> The trophic interactions between the functional groups are defined using fixed parameters, with very uncertain values, depending strongly on the definition of the interacting

> functional groups. This approach precludes the adaptation and self-organization of the functional groups when the trophic interactions are organized in a food chain. However, (...) if functional groups have multiple food sources and multiple predators, the system can dynamically adapt to spatial or temporal variability in the environment by channelling mass fluxes through different components (...).

Therefore, self-regulating behavior is encouraged by introducing more "apparent degrees of freedom", although the feeding linkages between the biological state variables in the trophic web are fixed. The ERSEM choice is thus to apply and set-on-stage the major number of feedbacks in order to *suggest* relationships instead of imposing them; the idea is that the dominant features of the system should arise from the concurrent application of appropriate boundary conditions and the dynamical interactions between the state variables. In this respect ERSEM differs from the other ecological models, mainly based on the NPZD structure. As already introduced above, these models usually close the cycles by prescribing parameters that combine several processes and that have to be calibrated for each study case. Like other models that attempt to integrate detailed ecological and physiological knowledge, instead, ERSEM is so complex that a calibration procedure will not find a single optimal set of parameter values. This dilemma has been well posed by Beck (1987, quoted in Scholten and Smaal, 1999), when illustrating the pros and cons of simple *vs*. comprehensive physiological models. A simple model can have the advantage of being completely identified by the available observations, but in general predicts "wrong" although highly precise pictures of the system. On the contrary, a comprehensive model would intuitively be superior and produce "correct" results, but the large uncertainties in the unverifiable portions of the model decrease our confidence in it. The answer which one should be preferred for which application is still open.

Hence, I prefer to consider this work to be more a series of applications of a general ecosystem modelling approach to different systems than a calibration exercise. In the applications of HiROPE presented in the following chapters, the available data have not been used to calibrate the parameters of the model, but they have been considered just as the target to which the model should tend. Thus, if the model reproduces the observations it means that the modelled process has been provided with sufficient information to describe the observed system. Usually the term calibration indicates the process of fine-tuning model parameters in order to best fit the information coming from the observed system. However, the picture of the system that we obtain from the available data is rather sketchy and uncertain because of many reasons. First of all, the high degree of natural variability, which adds unexplained variance to the observations; secondly, the intrinsic complexity of measuring the dynamical marine system, which cannot be easily reduced to laboratory or mesocosm experiments, and which is too extensive to be completely captured even in the most elaborate field survey. Unfortunately the properties of the system that have to be known in order to describe its behavior correctly have to be inferred from this partial picture, and caution should be exercised not to introduce artificial relationships driven by the (compulsory) need to fit the observations. In the ERSEM approach, the system behavior should be the response of the first principles embedded in the model equations to the domi-

nant physical and biological scales, although this is still an idealized objective. Several parameters are still coarse shortcuts to processes, especially in the dynamics of the excretion and remineralization of micro/mesozooplankton components and also in the biologically-mediated chemical processes in the water column and at the sediment interface (e.g.: nitrification/denitrification, see Chapter 4). For all these parameters a preliminary sensitivity analysis is necessary, in order to test the most appropriate set of values for the problem at hand.

Indeed there are many sophisticated tools to calibrate numerical models especially involving data assimilation techniques (Matear, 1995; Hurtt and Harmstrong, 1996, 1998; Spitz *et al*., 1998, 2001; Robinson *et al*., 1998; Fennel *et al*., 2001), however, they are hardly suitable for complex ecosystem models like ERSEM (but see Vallino, 2000). This stems from the high number of variables and parameters involved in the processes and from the consequent high computational requirements. It is difficult to separate a portion of the model and to calibrate it using existing information, because the different equations of the model are coupled to each other, acting with several regulating mechanisms on the same process. Generally simultaneous changes of parameters belonging to different functional groups are necessary to tune the model in a desired direction. Paradoxically, this is also a simplification, because in a complex model where the redundancy of processes can compensate the incompleteness of some others, the model itself develops an internal coherence which reduces the sensitivity to many parameters and improves the reactivity to different scenarios (Ebenhöh *et al*., 1995).

2.3. The numerical coupling

Most of the literature about the modelling of the transport and fate of components in the marine environment concerns the dynamics of passive tracers, which are simply transported by currents as dissolved or suspended loads and/or sink in the water column settling on the sea floor. However, one of the key features of biogeochemical variables is that they are non-conservative tracers and their quantity changes through biochemical transformations while interacting with the hydrodynamical environment. As soon as source or sink terms are introduced in the transport equations, the modellers have to deal with the diversity of the temporal and spatial scales that are involved.

These kind of equations are commonly known as *stiff* equations, which are composed of terms that show different behavior and response according to the scale at which the system is analyzed. The range of time scales resolved in numerical models depends on the chosen parameterization of the dominant processes of interest and the interval used in the numerical integration (Hofmann and Lascara, 1998). The first is a combination of the knowledge of the process itself, the amount of empirical observations and the availability of experiments designed in order to identify some of the main cause-effect relationships. The latter is mainly the result of a compromise between the previous set of assumptions and the stability of the numerical scheme. This is the point where the science of ecological modelling leaves its “solid” scientific background and tentatively moves in the direction of

art. There are no hard rules for the combination of the main ingredients, and it is up to the modeller how to integrate the information with a reasonable accuracy while at the same time maintaining a fair degree of computational efficiency.

Generally speaking, equations defining biological source terms are parameterized and scaled in order to reproduce specific sets of observations gathered in specialized experiments. The extension of the application of these equations to a different range of time and space scales may lead to unpredictable results. This needs to be carefully considered in the assessment of model performance, especially due to the practical difficulty of parameterizing the numerous regulating factors existing in living cells, which are able to adapt the functional response in a relatively short time. Following this line of thought, it appears important to use numerical schemes that are able to track any "alarming" response given by the chosen representative (but not self-adapting) equation terms, applying a kind of feedback control similar to the ones found in the biological processes of organisms. Moreover, another relevant attribute is the necessity of having a modular and computationally inexpensive integration scheme, because ecosystem models need to be expanded and enlarged in the number of variables and source terms, to incorporate advancements in the relevant research fields. A cumbersome, although more precise, integration scheme is less flexible and would lead to a continuous re-discussion about the suitability of the integration method itself.

These considerations make it attractive to use simple integration schemes such as the first order Euler forward scheme in deterministic models. The main argument against this simple approach is the low accuracy and stability in the calculation of the forward-in-time value of the variables. It is true that a comparison of the numerical solution of a limited set of differential equations using an Eulerian integration method and a high-order Runge-Kutta method may show considerable discrepancies of up to 40%. Nevertheless, the degree of discrepancy decreases with the shortening of the time step, and comparative application of both methods to complex ecosystem models like ERSEM has shown only limited differences, which are negligible when compared to the computational savings offered by the Eulerian methods (Baretta *et al*., 1995). Accuracy, with respect to complex ecosystem models, appears to be more a matter of using the proper equations for the proper time-scales, and as long as an appropriate time step is used for describing the dynamical processes the use of first-order integration schemes appears justified.

Another key point in the numerical coupling is the well-known undershooting/overshooting problem that arises from the interaction between numerical noise caused by numerical dispersion or discontinuities in the physical fields, and the advection schemes of three-dimensional coupled models, which are not always positive-definite. The natural smoother of these effects should be turbulent diffusion, but the sub-grid-scale parameterizations used in models are not always able to handle these problems when using realistic forcing functions. Therefore, in the case of fast-varying components, this numerical instability may generate negative values in some transported variables. In the OpenSESAME integration driver we have chosen to stop a model run as soon as a negative value of a biological state variable is encountered. This is a fundamental requirement because of the unrealistic meaning

of negative (mass) concentrations, even if this problem occurs quite frequently in numerical models of the coastal ocean (Haidvogel and Beckmann, 1998). The topic of overshooting/undershooting has been studied extensively, especially in atmospheric modelling, and several solutions have been proposed. The common methods are the inclusion of numerical diffusion terms of various orders in the prognostic equations, or to periodically apply a filter after the calculation of the forward-in-time value; for reviews of the suggested methods see Shapiro (1970, 1971), Raymond (1988) and Xue (1999). The two methods lead to equivalent results and involve a set of further calculations that in the case of large ecosystem models slow down the computation considerably. Zavatarelli *et al.* (2000), in the idealized Adriatic implementation of the POM/ERSEM model, have side-stepped this problem by correcting negative concentrations to small positive values. This leads to an addition of mass in the model domain that the authors have tracked as being less than 1% of the total mass content. However, this is not desirable, although apparently unavoidable in order to carry on the simulations (different model implementations could require more substantial mass additions that would conflict with the system mass conservation). Following this approach, we have applied and tested a simplified local filter that acts only where negative values are found. The algorithm preserves mass conservation, has a higher computational efficiency but is less theoretically grounded than the previous ones. It is based upon a redistribution of mass from the surrounding grid-points by means of control volumes, and the rate of redistribution is a function of the relative gradient. It is clear that as soon as robust advection schemes are suitable for high-resolution coupled models of marine ecosystems, this problem will disappear. MPDATA (Multidimensional Positive Definite Advection Transport Algorithms) such as the ones from Smolarkiewicz (1983, 1984; see also Pietrzak, 1995, for a comparison) are generally implemented in recent hydrodynamical models, although the high computational overhead still makes these algorithms too cumbersome for large coupled ecosystem models. Thus, in the current state of the applications, the inclusion of filtering schemes is necessary in order to control the simulation results and allow sufficiently long model runs.

The prototype of the three-dimensional on-line coupling between a complex ecosystem model like ERSEM and POM has been initiated in Zavatarelli *et al.* (2000) together with other one-dimensional applications by Allen *et al.* (1998, 1999) and Vichi *et al.* (1998a,b). The basic idea of the scheme is to run the physical model at the required constant time step and pass the abiotic dynamic conditions to the ecological model. A time step cutting procedure originally proposed (and still being developed) by Ruardij *et al*. (1995) is used for the integration of the biogeochemical source terms with the transport terms by means of the Euler forward scheme, which prescribes that during the execution of smaller time steps (with respect to the fixed physical time step, and caused by ecology), physics is not calculated and the transport terms are held constant. Starting from these concepts, the HiROPE system implements a time step control procedure that combines in an efficient way the requirements of a robust integration scheme and the adaptability of the biological parameterization. The core of the coupling is a decisional procedure called *TakeStep* that controls the length of the integration time of the ecological terms according to the magnitude of the local time scales of the processes themselves.

The major underlying inference is that biological processes may be faster than transport rates, and that the modifications in the concentration of a state variable caused by biogeochemical source/sink terms are essentially local events. An indication of this is that ecological constituents can present marked vertical gradients also in the absence of a gradient in the vertical structure of the water column (Townsend *et al*., 1992). The numerical details of the scheme go beyond the scope of this dissertation and will be published separately. For completeness, it is important to remember that the main aim of this procedure is to flag the presence of ecological rates of change that are faster than a prescribed "physiological" limit, and to accordingly adapt the length of the integration time step, in order to follow the evolution of the process without the risk of unrealistic numerical overestimations that may lead to negative values.

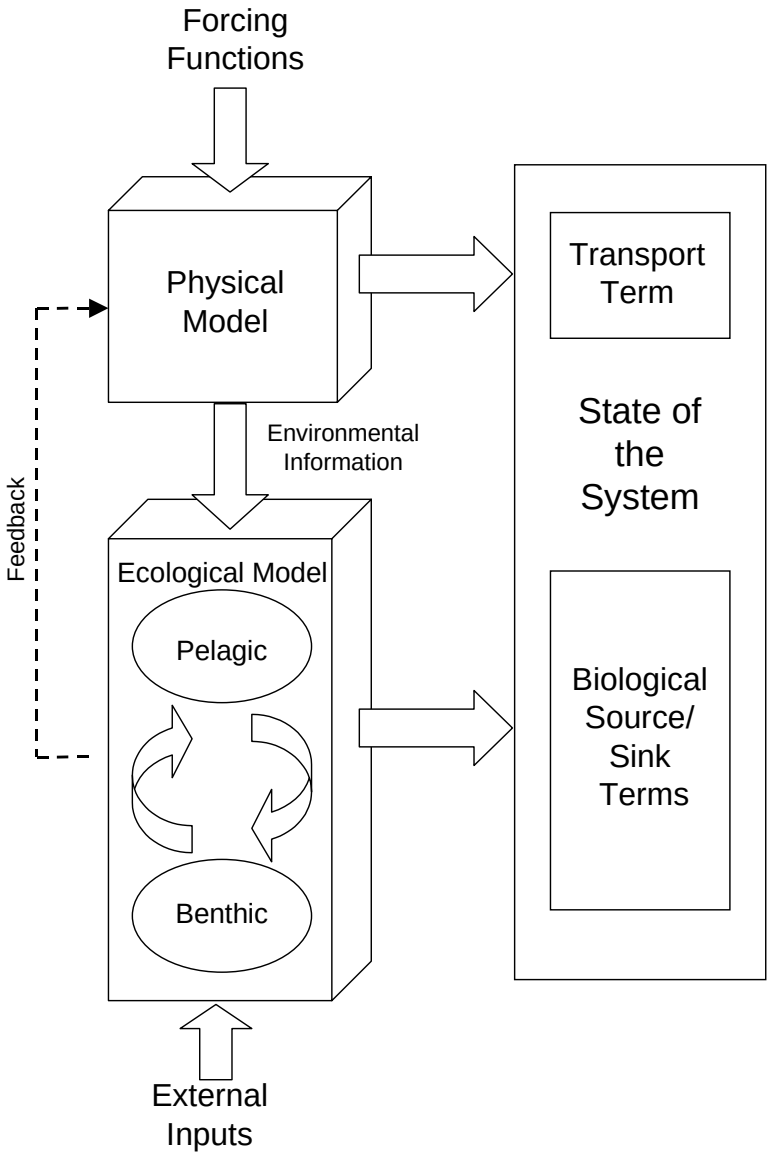

Figure 2.1.: Generic scheme of the coupling between the physical and the ecological models. See text for a detailed explanation.

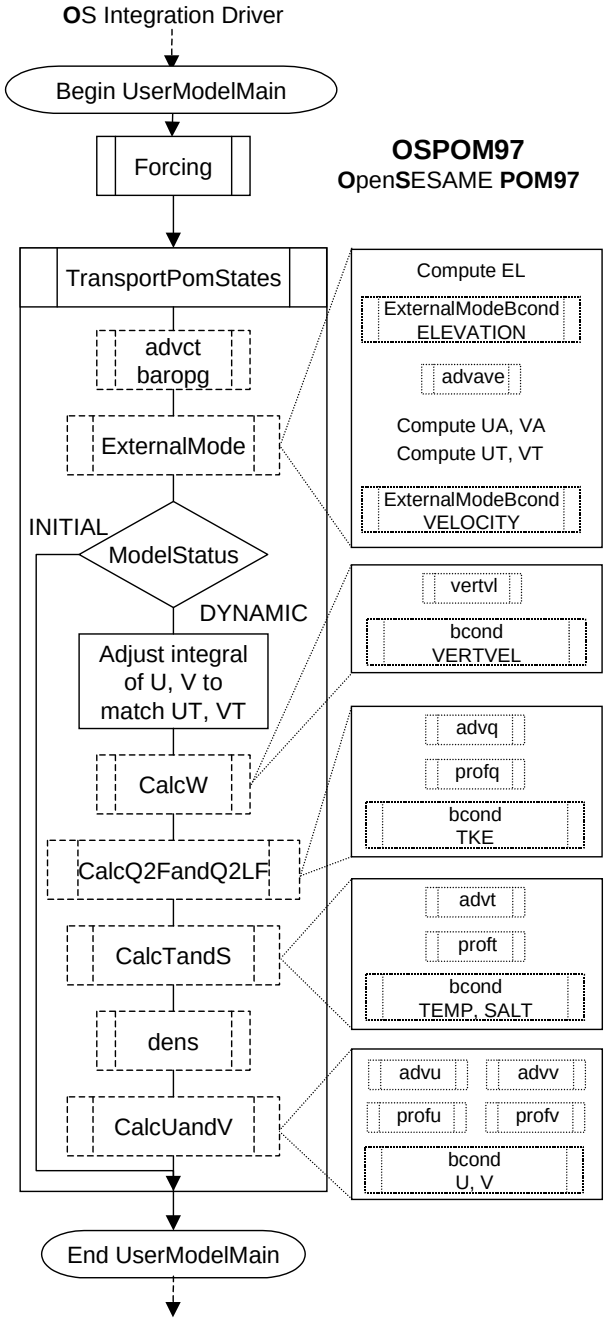

Figure 2.2.: Flow chart of the OS implementation of POM97, OSPOM97. UserModelMain is the routine that is linked with the OS library driver, which takes care of the integration loop following the integration limits and POM internal time step.

3. Climatological applications of HiROPE in the northern Adriatic Sea. Simulation of ecosystem seasonal cycles and carbon transfer pathways

3.1. Introduction

Among the coastal regions of the Mediterranean Sea, the northern Adriatic basin (Figure 3.1) emerges as a very interesting area where to carry out physical/biological model exercises. The coastal ecosystem is characterized by a wide spatial and temporal variability determined by the atmospheric forcing functions, the general circulation, the continental (riverborne) inputs of nutrients and organic matter and the water column-sediments interactions. Trophic conditions varies from mesotrophic (with occasional dystrophic crisis) in areas directly affected by external inputs, to oligotrophic in the central part of the basin (Zavatarelli *et al.* 1998; Stachowisch, 1984; Giordani *et al.* 1992; Fonda Umani, 1996). This variability imposes a strong constraint on the ecological model to be used in this area, as the model has to be generic enough to reproduce this wide trophic range, and the associated biogeochemical interactions, in dependence only of the physical and biogeochemical boundary conditions used. Therefore, this area is a suitable test site for the HiROPE model, and specifically, this Chapter deals with one-dimensional (vertical, 1D-V) climatological applications.

The HiROPE 1D-V model has been implemented at three different locations of the northern Adriatic Sea that are representative of the spatial environmental variability of the basin and that have been interested by monitoring programs, so that their distinctive features can be defined and compared with the model results. These implementations are considered to be preliminary for the setting-up of three-dimensional models of the basin, because the 1D-V approach can be used as a testing platform to provide parameter estimation, sensitivity assessments and also initial and/or boundary conditions for the 3D model.

Two of the investigated locations were already the subject of a modeling exercise in the past (Vichi *et al.*, 1998a, b). I present here new simulations for this two locations, because the original FORTRAN model implementation has been substituted with HiROPE and the biogeochemical model updated with the new formulation of ERSEM III discussed in the Appendices. Therefore, the choice was made to perform a re-assessment of the simulations previously carried out. Moreover, here we

go further in the comparison between model results and observations, since I extended it to the model predicted biogeochemical rates (primary and bacterial production), in an effort to provide insights on the model behavior in reproducing correctly the fluxes of matter within the planktonic food web.

The analysis of the ecosystem functioning at the three implementation sites and the role of the different food chains in transferring matter from lower to higher compartments have also been subject of investigation. Extending the work done in Vichi *et al.* (1998b) I have analyzed model results from the point of view of the conceptual marine ecosystem functioning scheme proposed by Legendre and Rassoulzadegan (1995), with particular emphasis on the role of DOM and microbial community processes in the dynamics of the northern Adriatic Sea.

Section 3.2 presents a general characterization of the implementation sites, while Section 3.3 illustrates the model set-up highlighting the specific changes in the set of physical and biogeochemical parameterizations of HiROPE. Results are described, discussed and validated with observations in 3.4. In Section 3.5 some biological questions on the features of the Adriatic food web functioning and carbon cycling are addressed with emphasis on the cycling of dissolved organic matter, and Section 3.6 illustrates the major conclusions from these numerical experiments.

3.2. Sites of implementation

Three different areas have been chosen (Figure 3.1), each one representing some characteristics of the northern Adriatic shelf and having different interactions with the hydrodynamic features of the basin. Sites S1 and S3 are placed in the north western part of the Adriatic Sea, site AA1 is located in the Gulf of Trieste in the north-eastern part of the Adriatic Sea. Each of these locations have been interested by multidisciplinary monitoring programs aimed to define the seasonal characteristics of the marine ecosystem.

The hydrodynamical behavior of S1 is directly influenced by the Po river runoff (1500 $m^3\ s^{-1}$ on annual average). S1 is located at about 5 km offshore the Po delta. The bottom depth is 20 m. S3 reflects conditions more typical of an open sea area, less influenced by riverine discharge. It is located at about 37 km offshore of the western Adriatic coast, the bottom depth is 30 m and is located in the middle of the northern Adriatic cyclonic gyre (Artegiani *et al.* 1997). They show a similar seasonal variability in the physical parameters, but the water column in S1 is stratified for most of the year due to the freshwater input, while the S3 site is well mixed during the winter and autumn seasons.

S1 site is characterized by the Po river input of large amounts of inorganic nutrients, organic and inorganic suspended matter (Cozzi *et al.* 1999; Pettine *et al.* 1998, 1999; Giani *et al.* 2000, 2001), the latter mainly constituted of clay and finer silt. The hydrodynamics of site S3, instead, is mainly influenced by the cyclonic general circulation system of the northern Adriatic basin, even if intermittent phytoplankton blooms can be associated to the offshore spreading of the Po river plume.

The Gulf of Trieste, where the AA1 station is located (Figure 3.1), is a semi-enclosed basin with a surface area of about 600 km^2 and a maximum depth of 26 m. The whole area is strongly affected

by rivers runoff, expecially along the shallow north-western coast (Isonzo river), with an average freshwater input ten times lower than the Po river (150 $m^3 s^{-1}$) (Stravisi, 1983a,b; Naudin *et al.* 1996). However, due to the small volume of the basin (9.5 km^3) the average volume-specific discharge is nearly three times higher than in the northern Adriatic as a whole (Malej *et al.* 1995). The hydrological features of the basin show a very large interannual and seasonal variability due to the strong easterly winds characteristic of the northern area (Bora) and particularly intense in the Gulf of Trieste. The structure of the plankton community reflects the variability of the abiotic factors: species composition and relative abundances, in fact, show dramatic changes from year to year (Fonda Umani *et al.* 1995; Malej and Fonda Umani, 1995; Cataletto *et al.* 1995; Mozetič *et al.* 1998). The AA1 site is located in the very central part of the basin where the bottom depth is about 20 m, and it is an operational site of the monitoring programme of the Marine Biology Laboratory (LBM, Trieste).

3.3. Model set-up

The equations for the biogeochemical and hydrodynamical model are presented in detail in the Appendices. In particular, the 1D-V version of HiROPE has been implemented, and the proper set of dynamical equations for the physical transport part can be found in Section C.3. In this section, the forcing functions used to derive the boundary conditions and the main changes/assumptions in the parameter space are illustrated. I will make reference to the equations in the Appendices when specifically needed for the comprehension of the model implementation.

3.3.1. Vertical discretization

The water column at the modelling sites have been discretized in the vertical applying a logarithmic distribution of layer depths at surface and at the bottom, and a uniform depth distribution in the interior. The vertical grid at S1 and AA1 is composed of 30 levels with 6 logarithmic levels both at surface and at the bottom (the depth of the first layer is 0.1 m, the central layers are 1 m deep). site S3, which is deeper, has been divided in 40 vertical levels, in order to have the same resolution of 1 m in the central layers (surface layer is 0.05 m deep).

3.3.2. Forcing functions

The 1D-V model is mainly controlled by surface exchange fluxes imposed as boundary conditions to the model equations as described in Section C.4. The wind stress forcing function in (C.36a) and the heat flux loss terms for the temperature boundary conditions also reported below in (3.1), plus the short-wave incoming radiation flux Q_s in (C.41), were all calculated from the 6-hours surface reanalyses of meteorological parameters from the European Center for Medium-range Weather Forecast (ECMWF) for the period 1982-93 (Gibson, 1997). The surface fluxes are computed following the procedures described in Maggiore *et al.* (1998) and Zavatarelli *et al.* (2002). Surface salinity data have been used to evaluate the surface boundary condition in (C.42). For S1 and S3, data are taken from the

Adriatic BiogeoChemical Dataset (ABCD, Zavatarelli *et al.*, 1998) as monthly mean climatological time series considering an appropriate area centered around the implementation sites. Climatological values of salinity at AA1 site were calculated from timeseries collected between years 1993-2000.

Another important external forcing function that has been shown to largely affect the simulated biological properties is the Inorganic Suspended Matter (ISM) in the water column (Vichi *et al.*, 1998a). The concentration of suspended sediments modifies the ambient light through extinction processes and consequently decreases the productivity of phytoplankton. The ISM profiles are applied in the model as external factors affecting the light extinction coefficient for biology as in (A.9). Unfortunately, there are scarce climatological information concerning the seasonal mean concentrations of ISM in the northern Adriatic. In the AA1 site we used observations collected monthly over the period 1997-2000 from which we have calculated the seasonal mean concentration profiles. For S1 and S3, we used the PRISMA-I data collected during only four seasonal surveys. Therefore, those data are not climatologically representative. This additional degree of uncertainty has been taken into account especially for the S1 site in the Po prodelta area; in the validation phase (Section 3.4.2) additional sensitivity experiments have been done to assess the importance of a good representation of light processes in coastal biogeochemical deterministic models. The applied ISM concentrations at the three sites are shown in Figure 3.2.

Perpetual time series of nutrients used in the surface boundary conditions (N^* in (C.46)) are climatological mean seasonal values extracted from the ABCD dataset in the case of S1 and S3, and seasonal mean values from the LBM dataset at the AA1 site. The seasonal frequency was the only possible because of the systematic lack of observations in some months. The main differences in the three time series (not shown) are that both S1 and AA1 show high nitrate and phosphate surface concentrations typical of river-affected coastal stations while S3 presents lower surface values indicating oligotrophic characteristics proper of open-sea areas. Besides, in S1 all nutrients show a distinct and strong peak in autumn (concentrations are about 10 times more than in other sites), while S3 and AA1 do not show such a significant autumn increase.

3.3.3. Physical parameterizations

The application of 1D-V models for the representation of hydrodynamical processes usually requires the use of additional parameterizations to account for the absence of horizontal dynamics. In the specific case of the northern Adriatic Sea, vertical processes alone, which are determined by the specification of surface heat, momentum and water fluxes, are not completely sufficient for an appropriate description of the seasonal evolution of the water column structure. Therefore, it is necessary to include a closure of the annual heat and water budgets in order to let the model reproduce a perpetual climatological year for the physical variables.

The annual heat flux budget is negative in the northern basin (Supić and Orlić, 1999) and is likely to be compensated (on a climatological time scale) by the advection of warm waters from South (Artegiani et al. 1997). This has been specified in the model as proposed in Vichi et al. (1998), by

calculating the annual surface heat loss in the forcing functions and distributing this bulk value along the year in the form of an empirical heat correction function added to the surface boundary condition (C.39a) as follows:

$$(K_H + \chi_1)\left(\frac{\partial T}{\partial z}\right)_{z=0} = \frac{-Q_b - Q_h - Q_e + Q_{corr}}{\rho_w c_p}. \tag{3.1}$$

The most suitable shape of this empirical function at the three sites was established by means of trial and error methods analyzing the simulated seasonal profiles of T with respect to the observed means and their range of variability.

Concerning the closure of the water fluxes, a crucial problem when dealing with 1D models is that the local buoyancy losses are not compensated by long-term basin-wide lateral advection of buoyancy in order to maintain a perpetual dynamical equilibrium in the water column. The imposition of local net positive or negative heat and water fluxes at surface produces a model drift; in reality, the water column heat and salt budgets are closed by the horizontal advection processes. In a purely one-dimensional model the horizontal advection terms are neglected and so it is necessary to parameterize the lateral advective adjustment process. In early works (Vichi *et al.*, 1998a) we have applied a closure of the water cycle based on the imposition of a surface salt flux correction as done for the heat flux in (3.1). In this work I use the same parameterization of local lateral advection that will be applied also in Chapter 4, Section 4.3.3, which mimics the basin-scale contribution to the vertical water column stability. The method consists in the introduction of a climatological time-varying vertical profile of salinity, to which the dynamics of the water column has to adjust within a given time scale. An additional source term is added in the model equation for salinity (C.32), which is parameterized as

$$\omega_S = \alpha_{adv}(z)\,(S - S_{clim}), \tag{3.2}$$

where $\alpha_{adv}(z)$ is the depth-varying relaxation frequency (in d^{-1}), defined to be 0 up to a given depth δ_{adv}. Values of α_{adv} and δ_{adv} used at the different implementation sites are given in Table 3.1. The time series of climatological profiles S_{clim} has a monthly frequency consistent with the surface salinity forcing data S^* used in (C.42).

During the calibration phase, the seasonal vertical thermal structure of these shallow sites has been found to be highly sensitive to the parameterization of the radiative heat penetration, the last term in the general equation (C.31). Downward irradiance is usually parameterized with a depth-dependent exponential attenuation, considering that the infrared portion of the light energy spectrum is completely absorbed at surface. In shallow coastal areas it is necessary to have a finer resolution of the heating of upper layers and thus the approximation of imposing the whole infrared radiation at surface is insufficient. Following Paulson and Simpson (1977), HiROPE utilizes a partitioning of the incoming short-wave irradiance in a portion extinguished in the first upper layers (simulating the infrared components of the spectrum) and a portion that can penetrate the water column (visible light) as parameterized in (C.41). Therefore, there are two different extinction coefficients, one for

the “infrared” part (λ_i) and one for the visible (λ_v) plus an apportioning non-dimensional coefficient ε_i, whose values used in the climatological experiments are given in Table 3.1. The different values of ε_i at the three implementation sites (Table 3.1) have been calibrated through trial and error sensitivity experiments comparing with the observed seasonal vertical profiles of temperature at the three sites. The adopted values account for the specific local optical properties in the three areas that are not considered in the physical parameterizations. In fact, the value of ε_i increases from pelagic (S3) to coastal sites (AA1, S1) and the need for a higher value at S1 is justified by the larger presence of attenuating suspended matter originating from the Po river.

3.3.4. Biogeochemical parameters and assumptions

The main parameterization improvement with respect to the previous modeling works (Vichi et al. 1998a,b) in which the standard ERSEM II implementation was used (Baretta-Bekker *et al.* 1995, 1997), is the inclusion of dissolved detritus as a dynamical model state variable (Section A.6). In early implementations it was assumed that the Dissolved Organic Matter (DOM) produced at each numerical time step was directly uptaken by bacteria, independently from the nutrient-content of the substrate. The implications of such a parameterization were that it was not possible to simulate any accumulation of DOC as observed by Pettine *et al.* (1999) and pointed out in Vichi *et al.* (1998b). Since the modeled dynamics of carbon in phytoplankton is decoupled from the nutrient uptake processes (Baretta-Bekker *et al.* 1997), the DOM excreted by primary producers can present different degrees of nutrient content in the model.

Generally, the utilization of DOM by marine bacterioplankton is mainly dependent on the nutrient availability in the substrate itself (Puddu e*t al.* 2000). In this work, the ERSEM III detailed representation of bacterioplankton dynamics related to DOM utilization has been used. Bacterioplankton functional processes now include the concept of refractory organic matter, and the degree of refractoriness is determined by the carbon:nutrient ratios of DOM that regulates the uptake of the organic matter itself. Optimal uptake is achieved when the C:N:P ratios in DOM and in bacterioplankton correspond to the optimal intracellular bacterial ratio of 45:9:1 (Goldman *et al.* 1987). Therefore, bacteria require more phosphorus for a proper assimilation into cells with respect to phytoplankton, where the optimal observed ratio is 106:16:1 (Redfield *et al.* 1963). The formulation of carbon uptake (BCD, bacterial carbon demand) in the bacteria functional group and the details of the functional parameterization are extensively given in Appendix A, Section A.3.

Since our aim is mainly on the analysis of the climatological behavior of the system, the food web structure of ERSEM III has been slightly simplified. The state variable $P_i^{(4)}$ representing large phytoplankton with low growth and predation rates (usually identified as dinoflagellates) has not been applied in this experiment. The choice was made to incorporate dinoflagellate into the generic autotrophic flagellate functional group $P_i^{(2)}$, and thus the standard values of both the predation and growth rates have been decreased to the values shown in Table 3.1. Also the potential growth rates for the other phytoplankton groups have been modified , applying the same values used in the previous

Parameter description	S1	S3	AA1
Background turbulent diffusivity for T and tracers (χ_1, m^2s)	$2.5\,10^{-5}$	$1.3\,10^{-5}$	$1.0\,10^{-5}$
Background turbulent diffusivity for S (χ_2, m^2s)	$1.3\,10^{-6}$	$9.0\,10^{-6}$	$1.3\,10^{-6}$
Apportioning coefficient for infrared/visible light (ε_i, %)	90	50	80
Attenuation coefficient for visible light (λ_v, m^{-1})	0.17	0.17	0.17
Attenuation coefficient for infrared light (λ_i, m^{-1})	5.0	5.0	5.0
Relaxation constant for S at surface(α_S, md^{-1})	0.5	0.5	5
Relaxation constant for nutrients at surface (α_{nut}, md^{-1})	0.22	0.6	0.6
Relaxation constant for local advection term (α_{adv}, d^{-1})	1/60	1/60	1/5
Depth-scale for local advection term (δ_{adv}, m)	5	5	5
Percentage of PAR (ε_{PAR}, %)	50	50	50
Sediment porosity (ϕ, $-$)	0.7	0.4	0.75
Adsorption coefficient for phosphate in sediments ($-$)	400	100	400

Table 3.1.: Values of selected physical and biogeochemical parameters used in the HiROPE climatological simulations.

works in order to compare with the past results (Table 3.1).

The potential reactivity of sediments is a function of biological activity (bioturbation, bioirrigation) and also of morphological properties such as the grain size. In early works (Vichi et al. 1998a,b), we have calibrated some of the sediment parameters at the S1 and S3 sites, focusing on the porosity ϕ and the non-dimensional adsorption coefficient for orthophosphate (Ruardij and van Raaphorst, 1995, both described in Section B.7) by means of measurements extracted from the PRISMA-I dataset (F. Frascari, personal communication). The same approach has been used for the AA1 site, where the sediments are composed primarily of clay and silt, and the mean porosity value has been taken from Cermelj et al. (1997). All the mentioned parameters are given in Table 3.1.

3.4. Model results

3.4.1. Initial conditions for climatological runs and model spin-up

The models at the three implementation sites have been initialized with climatological winter profiles of temperature and salinity extracted from the data sets described in Section 3.3.2. Climatological initial condition definitions for biogeochemical pelagic components are more difficult to obtain for all the model state variables and it becomes almost impracticable in the case of benthic variables. The latter are generally considered to be the buffer of the system, especially concerning nutrient recycling and availability, and thus their appropriate initialization could be crucial for long-term climatological simulations. The usual methodology applied for the initialization of the benthic system is to start from guesstimate and perform long-term simulation until an equilibrium with the pelagic dynamics is reached. Winter profiles of pelagic biogeochemical constituents in the northern Adriatic basin are usually homogenous due to the mixed conditions of the waters (Zavatarelli *et al.*, 1998). I have

performed some sensitivity tests to the initial conditions, initializing the models with different homogenous profiles for the major pelagic state variables, and I have found that the pelagic and benthic systems converge to almost the same dynamical perpetual year cycle in 4-5 years of simulation in presence of the external nutrient inputs described in Section 3.3.2. This result may not be *a priori* generalized to all marine ecosystem models in all areas, but is valid in the case of the ERSEM model in these particular implementations. Therefore, the 1D-V models have been initialized with the same vertically-homogeneous values of biogeochemical variables and results of the 6^{th} year of simulation have been taken as reference, considering the first 5 years as the specific spin-up time of the benthic system for reaching the equilibrium with the forcing functions.

3.4.2. Validation of seasonal model results

The choice was made to validate model results by computing the seasonal mean vertical profiles of selected variables and comparing them with the corresponding climatological data as already proposed in Vichi et al. (1998a,b). The seasonal means (calendar seasons) of model state variables have been plotted against the means and ranges of variability of the available observations in the data sets for the three sites, and the results for temperature (T), salinity (S), phosphate $(N^{(1)})$ and chlorophyll-*a* $(Chla)$ are shown in Figure 3.3, 3.4, 3.5 and 3.6 respectively. Each figure is divided in rows corresponding to the different sites (S1, S3 and AA1, respectively) and columns that represent the seasons (winter, spring, summer and autumn).

Temperature and salinity

Figure 3.3 shows the seasonal profiles of temperature at the three implementation sites. The seasonal cycle is similar at all sites, with well mixed conditions in winter, a thermal stratification starting in spring, and autumn conditions with the characteristic heat storage in the bottom layers. The seasonal observed variability is satisfactorily captured by the simulated profiles. The deeper S3 site shows the best agreement with the climatological data with the exception of 1-2 degrees discrepancies in winter at the bottom and in autumn at surface. At S1, the model underestimates the temperature in winter and especially in spring, where the simulated profile is off the range of variability. AA1 has an intermediate behavior that is always within the range of variability, although the modelled profiles are slightly misplaced with respect to the seasonal observed means.

The seasonal profiles of salinity (Figure 3.4) show the main differences that characterize each site. S1 has the largest variability in the surface salinity due to the influence of the Po river runoff. This signal, in spite of surface boundary conditions imposed with a fast relaxation constant (see (C.42) and Table 3.1), is only partially captured by the model; this is particularly evident in autumn, where the surface value is not matched, and the surface freshwater signal is mixed down to a greater depth (with respect to observations) by momentum fluxes. It is important to note that the discrepancies mentioned above in the description of temperature profiles (Figure 3.3) occur in the seasons when the salinity mean profiles are in worse agreement with the observations, indicating that the introduced

parameterizations of local advection of salt (Section 3.3.3) are not completely sufficient to describe the seasonal system dynamics. This is especially true in winter and autumn at S1 and AA1. In the Gulf of Trieste station, in fact, the model is not completely capable to capture the vertical location of the halocline and the upper layers salinity structure in general. In winter, the halocline is placed at depth of 15 m, while the data show its location at about 5 m and a similar misfit is visible in autumn. The 1D-V approach and the imposition of surface salinity data appear not to be sufficient to completely contrast the wind mixing and to maintain the strong stratification observed at the AA1 site, although they do provide a reasonable representation of the seasonal variability and the coastal features of the area. Besides, the model-data discrepancies at S1 and AA1 can also be attributed to the fact that observations at these sites are less representative of a climatological situation, due to the high dynamical variability of such coastal areas.

Biogeochemical pelagic variables

Since it is widely accepted in oceanography that much of the variance of the marine biogeochemical component behavior is directly determined by the abiotic dynamics, we can expect to have a more satisfactory simulation of climatological means of biogeochemical state variables at the S3 site, where the simulated physical variables have shown the best agreement with observations. This is actually true both in case of phosphate and Chlorophyll-*a* shown in Figure 3.5 and 3.6 respectively. The simulated seasonal profiles of phosphate at S3 are within the range of variability in all seasons except at the bottom in winter and spring. This discrepancy with the observed concentrations could be due to the inclusion of observations taken at sites with depth greater than S3, where the concentration increase at the bottom is located deeper in the water column. The winter phosphate concentration predicted by the model at S1 shows a clear increase with depth (as found in the observations) but the concentration of orthophosphate is overestimated. The excessive bottom nutrient concentrations during winter in the model results are also observed in the other nutrient profiles (not shown). This is not likely to be caused by an overestimation of autumn remineralization processes, because at that time the overall concentrations at the bottom are comparable with observations, but rather by the lack of nutrient removal due to advective processes that are particularly intense in the Po prodelta area. Another cause can be the underestimation of biological uptake because of improper inorganic suspended matter boundary conditions determining an unfavorable light environment. Since the contribution of advective processes cannot be taken into account in a purely 1D model, we have tested the second hypothesis by performing a sensitivity analysis to the ISM forcing function. The ISM winter concentration at S1 (Figure 3.2) is the highest with respect to all the other seasons and sites. As noted above in Section 3.3.2, this profile is not derived from climatological observations, but has been collected during a single winter campaign. Therefore, I have applied the ISM seasonal profiles used as forcing functions at AA1 (Figure 3.2), which are still proper of a coastal area, but are derived from a three year monthly time series. The results of the seasonal phosphate profiles obtained with the sensitivity run at S1 have been superimposed to the standard run in Figure 3.5 using a dashed line. It is clear

that changing the ISM concentration affects the phosphate vertical distribution, and this is mainly due to an increase of the winter phytoplankton standing stock that uptakes more nutrients (see Figure 3.6 and paragraph below). The phosphate profile falls within the observed winter range of variability at surface and get much closer to the observed mean profile than in the standard run. The same behavior is observed in spring, while summer and autumn do not show any significant change. The sensitivity of the model to an appropriate representation of the vertical light distribution shows, on the one hand, the importance of having data concerning the ISM distribution and, on the other hand, the necessity to include more sophisticated parameterization of light processes in deterministic models.

Spring and summer profiles are in satisfactory agreement at surface at all sites except AA1 where the surface value is underestimated, due to the strong uptake by phytoplankton during wintertime. The winter AA1 phytoplankton biomass (Figure 3.6) is in fact the largest one with respect to the other site, and this can be explained by the favorable earlier onset of the stratification occurring at AA1, as discussed in the next section.

The comparison of simulated phytoplankton biomass is shown in Figure 3.6 as seasonal profiles of chlorophyll concentrations. Model state variable representing Chlorophyll-*a* (*Chla*) is a diagnostic variable in the model, which is derived from phytoplankton carbon content using the formulation shown in Section A.2.5. The simulated profiles fall within the observed ranges in almost all seasons especially in AA1, although there is a systematic underestimation in S3 particularly during spring. Winter profiles can be conveniently compared with sufficient climatological data only at AA1, where the climatological model predicts an overestimation with respect to the observed mean profile; concentrations, however, still lie within the observed ranges.

On the contrary, in S1, the low number of observations indicate a possible underestimation of the biomass stock during winter, which can partially justify the high nutrient concentrations given by the model. Given the model equations for phytoplankton (Section A.2.3), two reasons can explain the limited primary production in the model at S1 in spite of the high nutrient availability: a) light limitation due to high ISM concentration; b) unfavorable mixing conditions which move the phytoplankton in and out from the euphotic zone limiting the adaptation to light. Actually, these two factors are tightly coupled each other, and the occurrence of the spring bloom is strictly determined by the interaction of the vertical light distribution and the hydrodynamics of the water column, as it will be discussed in detail in the next section. The sensitivity experiment on the ISM forcing function described above has confirmed that the winter phytoplankton mean concentration is strongly affected by light limitation. The chlorophyll-*a* profile computed from the sensitivity run forced with the ISM climatological profiles used at AA1 (dashed line in Figure 3.6) is more in agreement with the observations than in the standard run (continuous line). Moreover, we note that the subsurface maximum developed by the model during spring is completely dependent on the light conditions; this feature is slightly visible in S3 as well and absent in AA1, while none of the observed mean spring profiles show any clear subsurface maximum. In spring, the S1 site is already stratified (see Section 3.4.3 and Figure 3.7a) and the occurrence of subsurface maxima is directly correlated to low concentrations of ISM (Figure 3.2). As

soon as surface ISM values are increased (sensitivity test not shown), we observe the shallowing of the maximum and the outcropping to the surface, while, with a decrease in the ISM concentration as obtained by applying the AA1 ISM spring profiles (Figure 3.2, corresponding to the dashed line profile in Figure 3.6), the maximum is moved deeper in the water column. Therefore, these experiments with an improved biogeochemical model confirm the importance of the knowledge of proper ISM profiles for a good representation of primary production processes as already concluded in previous works (Vichi et al. 1998b).

3.4.3. Physical-biological interactions

In this section model results are comparatively analyzed in order to explain some of the different features observed at the three sites and described in previous section. Particularly, I focus on the seasonal cycle of primary producers as affected by the seasonal vertical dynamics of the water column. Figure 3.7 shows the depth-averaged seasonal cycle of state variable *Chla* at S1, S3 and AA1 sites plotted against the corresponding cycles of the mixed layer depth and of the critical compensation depth (D_{cr}). The *Chla* means are computed over the depth-range comprised between surface and D_{cr}, which is defined (following Sverdrup, 1953) as the level where the vertically-integrated primary production rates equal the integrated autotrophic respiration rates. The dynamical time evolution of D_{cr} at the 3 sites shows the largest variability at S1 (Figure 3.7a) progressing from near-surface (winter) to the bottom (summer), while has a more gentle deepening at S3 (Figure 3.7b) but with a sharp shallowing in October. Site AA1 (Figure 3.7c) has an intermediate behavior, with a longer winter shallow value, a steep deepening in March/April and a recovery similar to S1 in late summer/autumn. One of the main factors driving the vertical location of the D_{cr} is the underwater light climate, which, as shown in the previous section, is strongly affected by the presence of light-attenuating suspended particles. The shallower location of the D_{cr} in winter at S1 can thus be explained by the high concentration of ISM with respect to the other sites, which limits the penetration of light in the deeper layers.

The seasonal cycle of *Chla* follows the typical behavior of mid-latitude temperate coastal areas, with a distinct spring bloom, a summer decay and an autumn bloom, particularly intense at S1 (Figure 3.7a). The onset of the “spring” bloom is slightly shifted at the three locations: it occurs in late winter at S3 and AA1, while we find it in early spring at S1. These results are in partial agreement with the 30 years long-term analysis by Degobbis et al. (2000) of surface Chl-*a* data collected in a transect from the Po Delta to the Croatian coast. However, their open-sea site does not show any clear evidence of an earlier spring bloom with respect to coastal sites as seen in S3 (Figure 3.7b). This early winter bloom is, as mentioned above, more pronounced in AA1 (Figure 3.7c), which is partially in contrast with climatological observations, although, due to the high interannual variability observed in the Gulf of Trieste, there have been observations of phytoplankton spring development from late February to June.

The seasonal primary producer cycle simulated by the model shows distinct differences in the 3 study cases, and they can be interpreted as consequences of the coupling between the environmental

factors - mainly represented by the light availability - and the hydrodynamical conditions that develop at S1, S3 and AA1. If it can be demonstrated that the timing of the bloom in the basin is mainly dependent on the shallowing of the mixed layer and the deepening of the euphotic zone according to a Sverdrup (1953) mechanism, then it is important for a good predictability skill to have appropriate predictions of the surface mixing processes driven by momentum and heat exchanges. At the same time, due to the intrinsic coupled nature of this process, it is also required to provide a good estimate of the underwater light climate as determined by the amount of suspended matter in the water.

To verify if the bloom timing is strictly coupled with the hydrodynamical conditions, I have computed the square of the Brunt-Väisälä frequency (N^2) from model results and outlined in Figure 3.7 the time series of the depths where N^2 is maximum and also greater than 0.5 10^{-4} $rad^2 s^{-2}$ (below which these shallow water columns can be considered neutral). The obtained depth is assumed to be indicative of the extension of the mixed layer (the bottom of the mixed layer should always be shallower of this depth), and has been superimposed to the D_{cr} time evolution in Figure 3.7.

At all the three model implementation sites it can be noted that the chlorophyll increase in winter/spring is matched by the reduction of the mixed layer thickness and the deepening of D_{cr}. The biomass peaks are achieved when the lower limit of the mixed layer is either shallower than D_{cr} (S1 and S3) or has a comparable depth (AA1). This leads to the conclusion that at the three sites the winter/spring bloom onset is indeed controlled by the relative location of D_{cr} (driven by light penetration processes) with respect to the lower limit of the mixed layer (driven by turbulent dynamics), as originally observed by Gran (1931) and quantitatively described by Sverdrup (1953). Given the model results at the three locations shown in Figure 3.7, we can speculate that in shallow areas, it is apparently not necessary that the depth of the mixed layer is much less than the critical depth to stimulate the major growth in phytoplankton biomass as suggested by Sverdrup (1953). It appears sufficient to have a small increase in the stability of the water column to enhance the phytoplankton production as shown by the time-matching of the gradient change both in the biomass curve and in the mixed layer depth of Figure 3.7.

During summer, D_{cr} is always deeper than the lower limit of the mixed layer, but the water column is nutrient depleted (see also Section 3.5 and Figure 3.10b) and phytoplankton biomass is at minimum. In autumn, a recovery of the phytoplankton biomass occurs. The biomass increase is particularly evident at S1 where the autumn bloom has a magnitude comparable with the winter/spring one. The autumn breaking of the stratification, marked by the deepening of the mixed layer, brings bottom benthic remineralized nutrients back in the euphotic layers of the water column enhancing the primary production. This increase of nutrient availability is amplified at S1 by the input of nutrients at surface prescribed in the boundary conditions, giving rise to the high biomass peak.

In order to further confirm the strict dependence of the spring bloom mostly on just the mechanical mixing, I have applied the nutrient surface boundary conditions used at AA1 as forcing functions of the model at S1. The two sites have the same depth and equivalent distance from coast, but nutrient concentrations observed at AA1 are generally much lower than S1, except during the spring period.

Period	**site**	**PP** (mg C m^{-2} d^{-1}) mean (cv%)		**BCP** (mg C m^{-2} d^{-1}) mean (cv%)		**BA** (10^9 cell l^{-1}) mean (cv%)	
		Model	*Obs.*	*Model*	*Obs.*	*Model*	*Obs.*
January	S1	12 (30)	121 (30)	23 (80)	80 (18)	0.43	0.44
	S3	141 (14)	311 (-)	85 (47)	39 (-)	0.62	0.32
April	S1	1448 (9)	895 (4)	280 (15)	173 (62)	0.99	0.60
	S3	1014 (4)	500 (9)	180 (8)	31 (41)	0.76	0.85
July	S1	1898 (20)	2237 (60)	362 (3)	344 (16)	0.81	0.78
	S3	887 (2)	629 (11)	279 (2)	160 (1)	0.68	-
October	S1	1568 (3)	3181 (47)	531 (6)	553 (15)	1.02	0.78
	S3	567 (15)	853 (21)	314 (0.5)	169 (8)	0.73	-

Table 3.2.: Comparison of model simulated rates of primary production (PP), bacterial carbon production (BCP) and bacterial abundances (BA) with observations. Field observations are three-days mean values integrated along the water column from Table 4 in Puddu *et al.* (1998). Model data are monthly averages integrated on the water column at each model implementation site (S1 and S3). Averages are given with the coefficient of variation (cv%).

Therefore, by changing the surface boundary conditions in this way, we prescribe a higher nutrient availability during the bloom period that should lead to more favorable growth conditions. However, the timing of the winter/spring bloom (not shown) is completely unaffected by the changes of the nutrient import in the system. In contrast, the bloom duration and the summer/early autumn further developments show a different behavior with respect to the standard run. This indicates that the system has a delayed response to these conditions which shows up during the more stratified period, when the related benthic remineralization and biological interactions act as positive feedbacks that enhance the primary production.

Obviously, the results described above have general validity only in a climatological context and in the absence of biological control on the physical dynamics, as in our case where the radiative heat penetration is not affected by suspended particles. The feedback that can occur between the biological events and the physics of the water column have recently re-opened the discussion on the Sverdrup mechanism (Townsend, 1992; Stramska and Dickey, 1993) and it is important in the future to explore the effects of this coupling and the response of phytoplankton productivity to high-frequency changes in the mixed layer dynamics (Vichi, 2000 and Chaper 4).

3.4.4. Comparison with available *in situ* rates

In recent years, the availability of *in situ* measured biological rates has increased, and it is essential that a biogeochemical flux model is validated not only with observed concentrations, but also in terms of fluxes of matter along the trophic web. At S1 and S3, I have used the primary production, bacterial production and bacterial abundance data collected during the PRISMA-I cruises (Puddu *et al.*, 1998) for a comparison/validation with corresponding modelled rates and concentrations. It is important to state that the comparison can only be done as order of magnitude, because observed rates where estimated as two-days means measured four times in a specific year, while model rates

are given as monthly climatological averages of the corresponding month of sampling. Table 3.2, modified from Puddu *et al.* (1998), shows the vertically integrated daily rates with the associated coefficients of variation of primary production (PP), bacterial carbon production (BCP) , and mean water column bacteria abundances (BA) at S1 and S3 sites during the PRISMA-I campaign of April, July, October 1995 and January 1996. The observed PP has been compared with the mean monthly gross PP calculated by the model and integrated along the water column. BCP in the model has been computed as net production by subtracting the respiration term from the bacterial carbon demand described in Section A.3. This is assumed to be consistent with the rates computed by Puddu *et al.* (1998) in the experimental observations. Bacterial abundances have been derived by vertically-averaging the bacterial carbon concentration and applying a conversion factor of 20 fg C $cell^{-1}$ (Lee and Fuhrman, 1987).

Considering the coefficients of variation given in Table 3.2, the simulated PP is generally in the order of magnitude of the observations except in January at S1 where the value is underestimated by one order of magnitude. At S1, besides, the maximum production is found in July with a diminution in October, while the observations report an increase from July to October. There is, however, a good accord with data in the relative behavior at the two sites: S1 has rates 2-3 times higher than S3 as found in the observations (except in winter).

BCP rates at S1 match the observations in April, July and October, partially indicating the validity of the new bacteria uptake dynamics in ERSEM III. The January mean in the model is 4 times lower, and the low winter bacterial activity in the model is clearly related to the low PP rates discussed above. In fact, the winter BCP/PP rate simulated by the model (~50%) is lower than the observed value of 70% (Puddu *et al.* 1998). This discrepancy might be explained with the absence of direct riverborne DOM input in the model, which should enhance the bacterial carbon demand as it is thought to happen under the influence of the Po river (Puddu *et al.* 1998, Pettine *et al.* 1999).

Concerning the bacterial production at S3, we observe an overestimation with respect to the measured values, although the order of magnitude is still comparable. The higher bacteria activity in S3 is also reflected in the values of bacterial abundances, which are about twice the observed values in winter. The vertical distributions of bacteria (not shown) are in good agreement with the observations of Puddu *et al.* (1998) and, as a general consideration, the model seems to partially confirm the hypothesis that the variability of bacteria is more pronounced in their activity rates than in their biomass (La Ferla *et al.* 1998; Puddu *et al.* 1998; Zaccone *et al.* 1999). In fact, for about a doubling in the model BCP from April to October in S1 (Table 3.2), the simulated abundances increase only of a small percentage (from 0.99 to 1.02 10^{-9}cell l^{-1}).

Biological rates at AA1 have been compared with surface PP data and vertically-integrated BCP data for the period 1998-2000. Figure 3.8 outlines the measured monthly rates for three distinct years plotted against the monthly averaged surface gross PP computed by the climatological model. Since the model PP is given as daily mean using the parameterization described in Section A.2, it has been converted in the units of observations taking into account the day-length derived from the Dobson

and Smith (1988) astronomical light formulation. The overall time evolution of the simulated PP is comparable with observations, although it is evident the high interannual variability of plankton activity in the data of the Gulf of Trieste (Fonda Umani *et al.* 1995; Mozetič *et al.* 1998) that cannot be reproduced with a climatological simulation. Longer time series (at least 5 years) of observations are needed for a better estimation of the climatological variability of primary production rates and for a better comparison/validation against climatological model results. However, the model is already capable to capture the average magnitude of the spring bloom production peak and also the lower amplitude of the autumn recovery of phytoplankton production, indicating a satisfactory functional behavior of the model at AA1 as well.

The seasonally averaged BCP (over the period 1998-2000) measured at AA1 is compared with the model simulation in Table 3.3. Here, the simulated daily BCP has been converted to the units of observations dividing by the number of hours per day (bacteria activity is assumed to be independent from the light cycle). The annual evolution of BCP is correctly reproduced by the model with a progressive increase along the year and a stabilization in summer and autumn. However, the predicted values are twice the observations (although the coefficient of variation in the measurements is rather high), and the spring decrease observed in the data is not matched by the model. I have performed some additional sensitivity experiments in order to explain model discrepancies with respect to observations. The dynamical value of BCP in the model is dependent on both the bacterial carbon demand and the bacterial growth efficiency (BGE, η_B in the model equations) parameter that control the amount of carbon burned in the respiration process as shown in Section A.3.1. The value of bacterial efficiency considered appropriate for the Gulf of Trieste is 0.3 (S. Fonda Umani and F. Azam, personal communication) while in the model we use 0.4 that is the average of the values used by Baretta-Bekker *et al.* (1995, 1998). A sensitivity experiment on this parameter has shown that simulated BCP can be reduced of about 17% in winter and 23% in the other seasons with a reduction of the efficiency of 25% as shown in the last column of Table 3.3. However, the general behavior of BCP is not modified and the model is still not able to explain the decrease of BCP observed in the spring average value. I have thus performed an additional sensitivity experiment by applying a recently proposed empirical parameterization of the BGE dependency on the environmental temperature by Rivkin and Legendre (2001). By analyzing several observations in the world ocean they have found a significant inverse linear relationship between BGE and temperature and the corresponding parameter η_B in the standard model parameterization (A.36d) has been modified as:

$$\eta_B = 0.374 - 0.0104T \tag{3.3}$$

I make reference to Appendix A and Section A.3 for a detailed explanation of the model equations.

The simulated BCP time evolution obtained with the improved parameterization is much more satisfactory and the new curve is shown in Figure 3.9 compared with the model result obtained with the constant BGE of 0.3 and the observations from Table 3.3. There is a slight decrease in the winter bacterial activity and the spring average value is still not within the observed range of variability, but

Season	**Observed BCP** (mg C m^{-2} h^{-1})	**Modeled BCP** eff. = 0.4 (mg C m^{-2} h^{-1})	**Modeled BCP** eff. = 0.3 (mg C m^{-2} h^{-1})
Winter (DJF)	5.56 (56)	7.77 (63)	6.27 (57)
Spring (MAM)	2.96 (39)	8.82 (31)	6.75 (30)
Summer (JJA)	6.49 (117)	14.20 (4)	10.75 (5)
Autumn (SON)	7.76 (60)	15.52 (2)	12.01 (3)

Table 3.3.: Comparison of model simulated rates of bacterial carbon production (BCP) with observations at AA1 site (Gulf of Trieste). Model results and data are computed as seasonal averages integrated along the water column. and given as mean with the coefficient of variation (cv%). Results from simulations with a bacterial efficiency of 0.4 (standard value in the experiments) and 0.3 are shown.

the overall behavior of the modeled BCP is more in accord with observations compared to the model results with a constant BGE. Thus, temperature appears to be a determining factor in the formulation of bacteria efficiency, and it is necessary to perform further experiments in order to assess the consequences of such effect on the other system components. Supplemental investigations and longer time series of BCP measurements are needed to refine the knowledge of long-term variability of bacterial activity and the related parameterization issues. Indeed, there is a clear sensitivity of the model to the microbial dynamics, and these processes are key factors that control the evolution of DOM in the northern Adriatic, as will be further discussed in the next section.

3.5. Trophic interactions and DOM dynamics

In an early work (Vichi et al. 1998b) we analyzed the carbon pathways in an aggregated structure of the pelagic food web of ERSEM II with climatological simulations at the same S1 and S3 sites described in this research. In that analysis we found that the role of bacteria in channelling the organic carbon was comparable to the "classical" herbivorous flux from phytoplankton to zooplankton. This was found to be valid not only at S3, which, having more open-sea features, is likely to be driven by internal remineralization processes, but also at the S1 site that, on the contrary, should be dominated by new production and particulate matter formation. Therefore, we concluded that the multivorous food web concept proposed by Legendre and Rassoulzadegan (1995) is also a possible food web pattern in the coastal areas of the northern Adriatic affected by substantial allochtonous input of inorganic nutrients.

In this Section, that work has been extended in order to get further insights on the ecosystem functioning, focusing on the central role of DOM and the bacteria-phytoplankton coupling that has been improved in ERSEM III. The assessment of the model capabilities in the description of microbial processes is an important step towards the development of predictive ecosystem models, especially in the light of recent findings in the microbial ecology of the Mediterranean Sea (Azam *et al.* 2000). The DOM dynamics in the northern Adriatic is of great concern because of the mucilage formation

events occurred in recent years (Azam *et al.* 1999; Degobbis *et al.* 1995, 1999; Puddu *et al.* 2000 and references therein). Recent data on DOC distribution in the northern Adriatic Sea (Pettine *et al.* 1999; 2001) show a tendency to accumulate during the summer period, and high concentration of DOC are expected to be pre-conditioning of the mucilage formation.

Figure 3.10a illustrates the climatological time evolution of the modeled DOC concentration averaged within the critical compensation depth D_{cr} (see Section 3.4.3) at the investigated sites. The model predicts substantial DOC accumulation during the spring/summer periods at all locations. Accumulation starts as soon as the stratification is established (see Section 3.4.3) and has a clear different behavior at the three sites. The accumulation mechanism developed by the model is a consequence of the coupling between parameterized biological functional processes and hydrodynamics: the onset of the stratification enhances phytoplankton production and depletion of dissolved inorganic phosphorous (DIP, Figure 3.10b). As a consequence of the decoupling between phosphorus and carbon dynamics in phytoplankton (Section A.2.3), the unbalanced nutrient conditions inhibit the carbon assimilation into biomass, and the photosynthesized carbon is exudated by autotrophs in the form of nutrient-impoverished organic matter. This flux leads to dissimilar DOC accumulation rates at the three sites (Figure 3.10a): AA1 and S3 show an early buildup because of the earlier shallowing of the mixed layer discussed in previous section, but AA1 reaches higher values ought to the greater production rates typical of coastal zones. The maximum value at the other coastal site (S1) is comparable to AA1 but shows a more dynamical evolution towards the late summer maximum, indicating the formation of more complex biogeochemical pathways of the organic matter flow in the trophic web.

In order to thoroughly understand the biogeochemical dynamics developed by the model and their interactions with the hydrodynamical regimes, I have analyzed the model results in term of fluxes among system components by computing a set of ratios reflecting the status of the planktonic food web as proposed by Legendre and Rassoulzadegan (1995). The original scheme has been slightly modified to adjust to a phosphorus-limited system instead of a nitrogen-limited one. The principal aim here is to investigate the model behavior to see if the deterministic non-linear coupling of simple empirical biogeochemical relationships with the hydrodynamical transport let emerge features that are indeed observed in marine ecosystem. The first measure (Figure 3.11a) allows us to distinguish among the diverse trophic web patterns developed by the model. It is computed as the ratio between the transfer flow of carbon from autotrophs to zooplankters (sum of carbon grazing rates of all the micro/mesozooplankton groups upon phytoplankton state variables) and the equivalent from bacteria to zooplankters (both computed as average within the D_{cr}). The value of this ratio indicates if carbon is transferred to higher trophic levels through the classical herbivorous chain (greater than 1), the microbial loop (lower than 1), or, in the case of values close to 1, through a multivorous food web (Legendre and Rassoulzadegan, 1995). An additional measure is the "quality" of dissolved organic matter as a proper substrate for bacterial growth, which we define as the DOC:DOP ratio ($R_c^{(1)}/R_p^{(1)}$ as described in Section A.3.1). The time series of this ratio, averaged within the D_{cr} is shown in Figure 3.11b. The third index illustrates the role of bacteria with respect to the uptake/release of phosphorus.

This is computed as phosphate flux between bacteria and the DIP pool, defined positive when bacteria release DIP and negative when bacteria compete with phytoplankton for the inorganic resource. The integrated value of this flux within the D_{cr} is shown in Figure 3.11c.

The type of grazing (Figure 3.11a) is a function of the available resources for zooplankton. In winter/spring, when the phytoplankton spring bloom develops at all sites, the transfer of carbon is mainly through the herbivorous food chain as indicated by ratios higher than unity. In the decaying portion of the bloom, which is sharper at S1 and with a more gentle slope at S3 and AA1, the autotrophic phase is followed by the development of a microbial web as also observed in many realistic meso- and eu-trophic ecosystems (Legendre and Rassoulzadegan, 1995). The quality of the substrate (Figure 3.11b) deteriorates after the bloom, and this determines the shifting of the microbial community from nutrient remineralizers to competitors for inorganic resources as depicted in Figure 3.11c. The microbial food web pattern (indicated by values lower than 1 in Figure 3.11a) lasts for the whole summer period, with a more steady behavior at S3 and AA1 than at S1. In particular, S1 shows a series of oscillating phases which are also reflected in the behavior of the DOM quality (Figure 3.11b), indicating that either the input of nutrients from the Po River and/or more active remineralization processes give rise to small recoveries of the multivorous transfer pathways.

In autumn, at the breaking of the stratification, the three sites show again a different behavior. S1 develops a clear multivorous food web with the microbial "grazing" comparable to the herbivorous grazing, whilst S3 and AA1 remain in the status of a microbial throughflow of carbon. Thus, the quality of DOM released in the environment improves more rapidly at S1 than at S3 and AA1 (Figure 3.11b), changing the activity of bacteria to phosphorus remineralizers (Figure 3.11c). Examples of marine systems with these alternating trophic pathways can be found in Legendre and Rassoulzadegan (1995) for coastal and open-sea areas. Model results suggest that the concurrent existence of different mass-transfer patterns takes place in the shallow northern Adriatic Sea as well, and the shifting from one to the other is essentially modulated by the physical conditions of the water column, the underwater light climate and by the external nutrient inputs.

3.6. Summary and conclusions

This Chapter has presented a climatological application of HiROPE with emphasis on the comparison with observations and on the analysis of the ecosystem functioning of the northern Adriatic Sea. This exercise was considered preliminary and necessary to the development of the three dimensional simulations of the ecosystem behavior presented in Chapter 5.

The comparison with the seasonal observed means described in Section 3.4.2 confirms the model capability to capture the major seasonal local biogeochemical and physical dynamics at the three implementation sites. The climatological model behaves better at those locations, such as S3, where the variability induced by coastal processes and riverine input is reduced. Discrepancies at the more coastal sites (S1 and AA3) can be attributed to the lack of this variability in the climatological bound-

ary conditions and to the absence of horizontal advective processes that cannot be taken into account with a 1D model. Sensitivity analyses performed on the inorganic suspended matter forcing functions have shown how model results are substantially affected by such external boundary conditions, strengthening the need of coherent data sets for the improvement of predictability skill of deterministic biogeochemical flux models.

Comparisons with observed biogeochemical rates such as primary and bacterial production, are also (within the limit of the climatological implementation) indicating the general qualitative agreement of the model results with observations. Simulations also confirm the model skill to adjust to different trophic conditions, being able to accommodate high productivity rates typical of areas under direct influence of river input (S1 and AA1) and oligotrophic offshore regions (represented here by the S3 site). The partial accordance of the simulated bacterial carbon production with observations encourages the inclusion of more sophisticated deterministic parameterizations of microbial web processes (such as the differential DOM utilization included in ERSEM III), which are expected to have a large impact on the simulation of organic matter transfers in the ecosystem. Especially the temperature dependence on the bacterial growth efficiency (Section 3.4.4) has been found to be an important factor for improving model skills in reproducing the observed microbial rates.

The onset of the winter spring bloom at the three implementation sites appears driven by the local evolution of the water column stratification conditions in relation with the underwater light climate (according to a Sverdrup-like mechanism); the different timing of the bloom development seems to condition also the subsequent evolution of the microbial web dynamics.

Analyses of model results carried out in the framework of the conceptual scheme of ecosystem functioning proposed by Legendre and Rassoulzadegan (1995) seem to confirm that also for a coastal basin such as the northern Adriatic Sea, the major carbon transfer pathway can shift from the classical herbivorous food web to the microbial one, and the development of multivorous food web is likely, in particular at locations such as S1, characterized by strong nutrient external inputs. However, our simulations indicate that after the winter spring bloom, during the summer season, the main carbon pathway is the microbial one. The important role of the microbial community revealed by the model is consistent with the conclusions of Puddu *et al.* (1998) based on direct observations, which suggested that a large fraction of primary production is processed by bacteria during summer. Therefore the dynamics of DOM should be regarded as a central issues for a complete comprehension of the northern Adriatic ecosystem functioning.

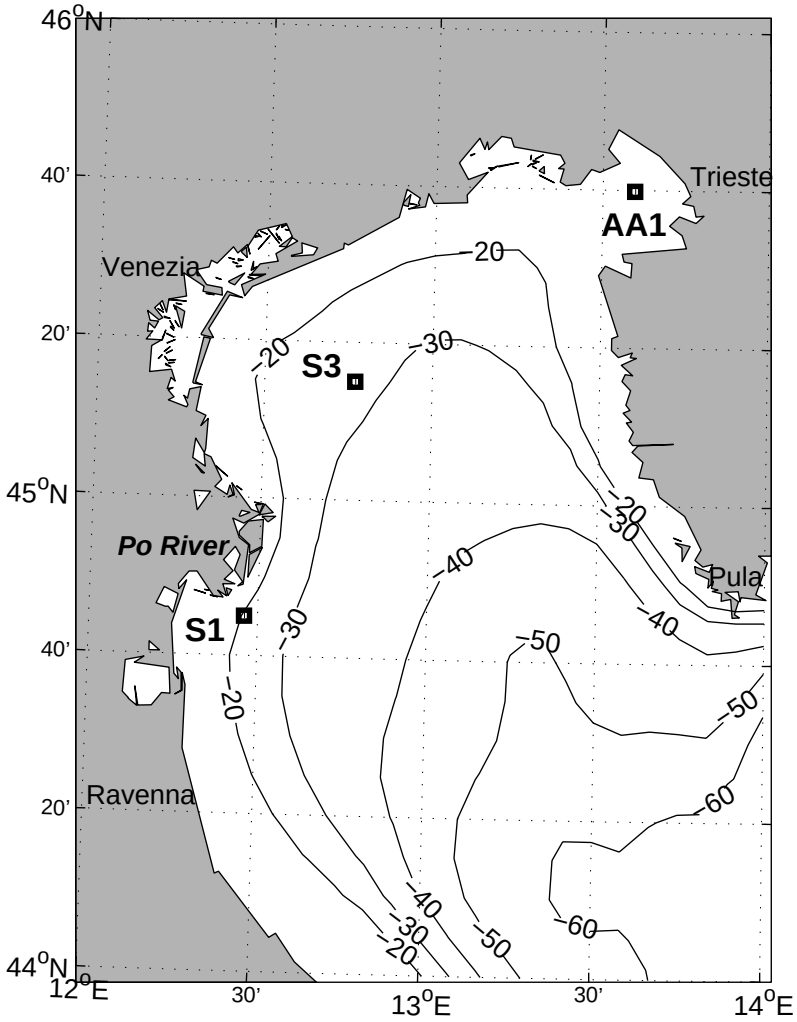

Figure 3.1.: Map of the northern Adriatic shelf with location of the model implementation sites (S1, S3 and AA1).

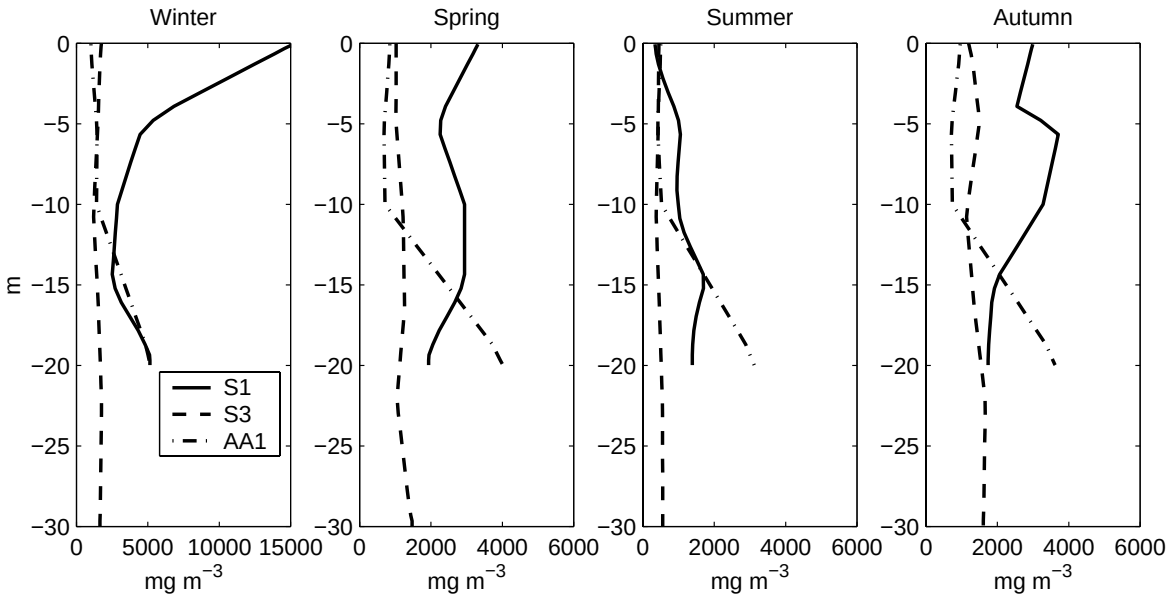

Figure 3.2.: Seasonal vertical profiles of Inorganic Suspended Matter (ISM) concentration used as external forcing functions at the three implementation sites.

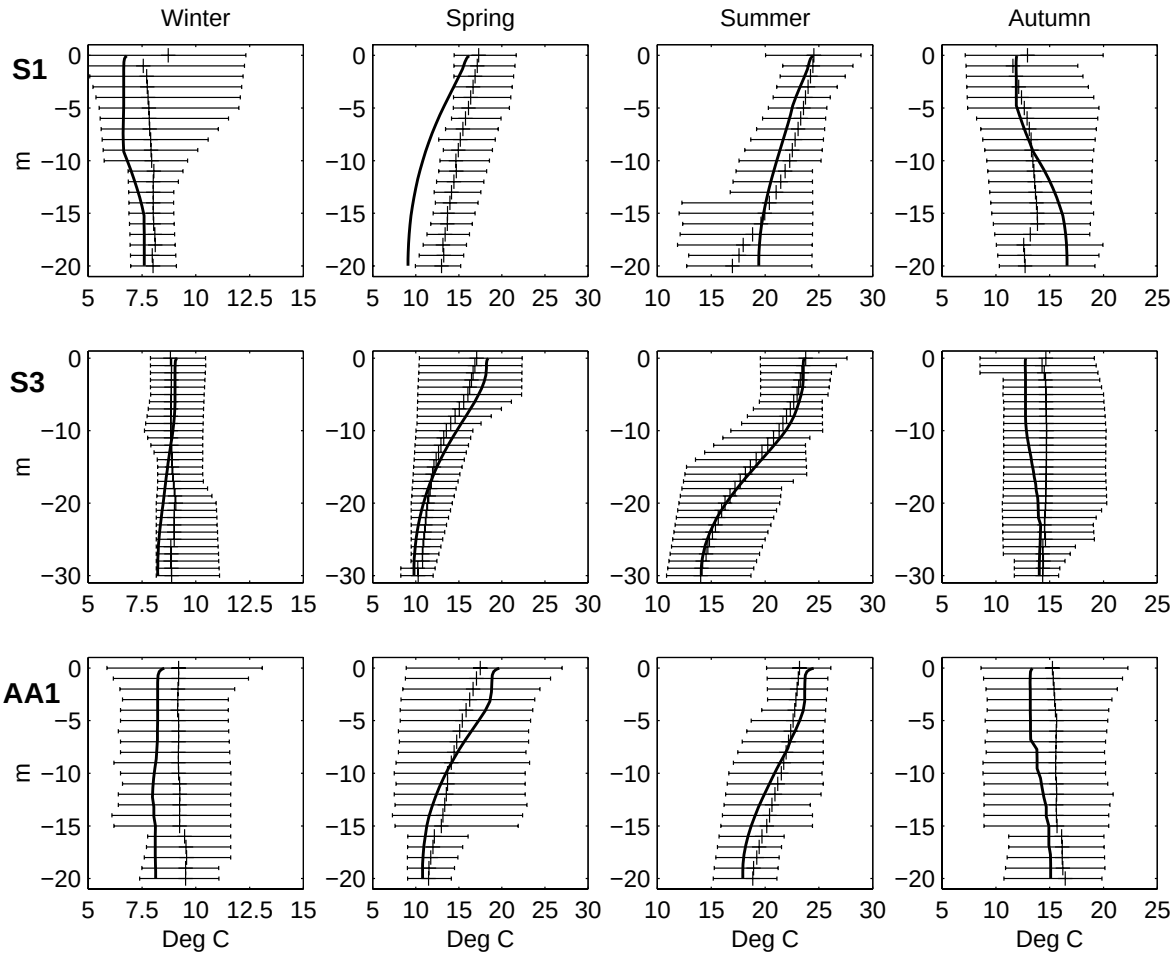

Figure 3.3.: Model and data comparison for temperature as climatological seasonal profiles at S1, S3 and AA1. The continuous line is the simulated mean seasonal profile for each site and season and climatological observations are plotted as seasonal means within the range of variability.

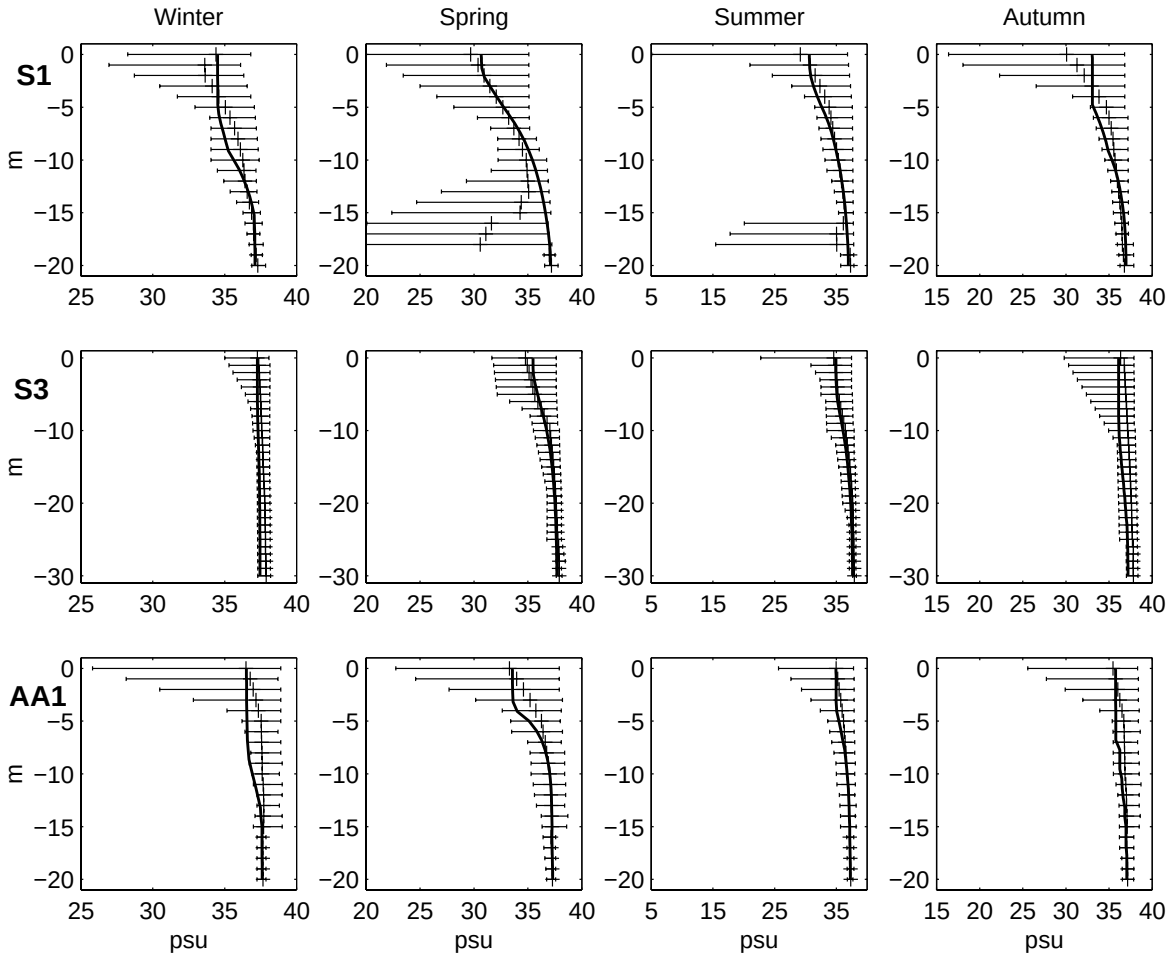

Figure 3.4.: Model and data comparison for salinity as climatological seasonal profiles at S1, S3 and AA1. The continuous line is the simulated mean seasonal profile for each site and season and climatological observations are plotted as seasonal means within the range of variability.

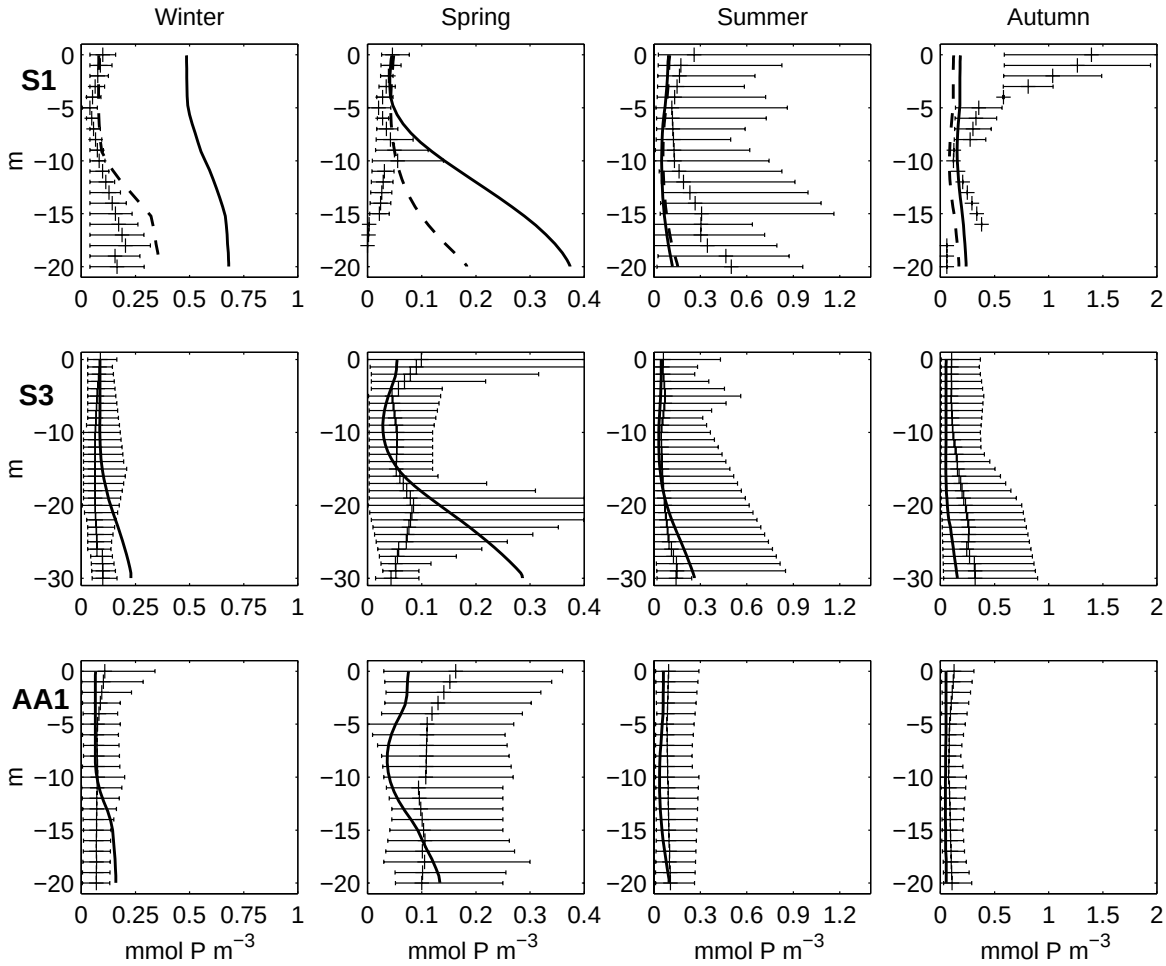

Figure 3.5.: Model and data comparison for biogeochemical model state variable phosphate ($N^{(1)}$) as climatological seasonal profiles at S1, S3 and AA1. The continuous line is the simulated mean seasonal profile for each site and season and climatological observations are plotted as seasonal means within the range of variability.

The dashed line profiles at S1 (first row) derive from a sensitivity experiment on the concentration of Inorganic Suspended Matter applied in the model as external forcing functions. The continuous lines are the model results with the standard ISM profiles for the S1 site described in Section 3.3.2, while the dashed lines are the seasonal means computed from a run in which the AA1 ISM climatological profiles (Figure 3.2) have been imposed.

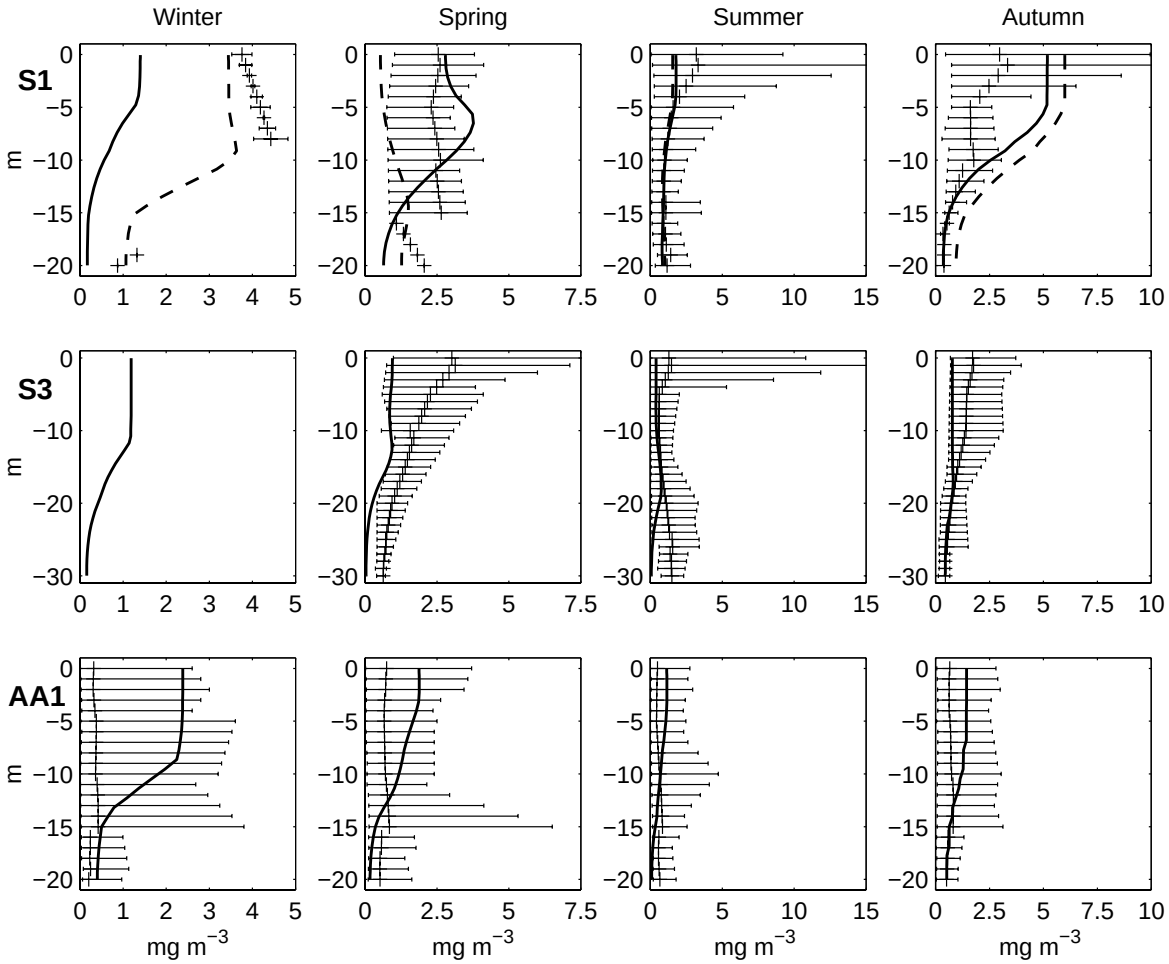

Figure 3.6.: Model and data comparison for biogeochemical model state variable chlorophyll-*a* (*Chla*) as climatological seasonal profiles at S1, S3 and AA1. The continuous line is the simulated mean seasonal profile for each site and season and climatological observations are plotted as seasonal means within the range of variability.
The dashed line profiles at S1 (first row) derive from a sensitivity experiment on the concentration of Inorganic Suspended Matter applied in the model as external forcing functions. The continuous lines are the model results with the standard ISM profiles for the S1 site described in Section 3.3.2, while the dashed lines are the seasonal means computed from a run in which the AA1 ISM climatological profiles (Figure 3.2) have been imposed.

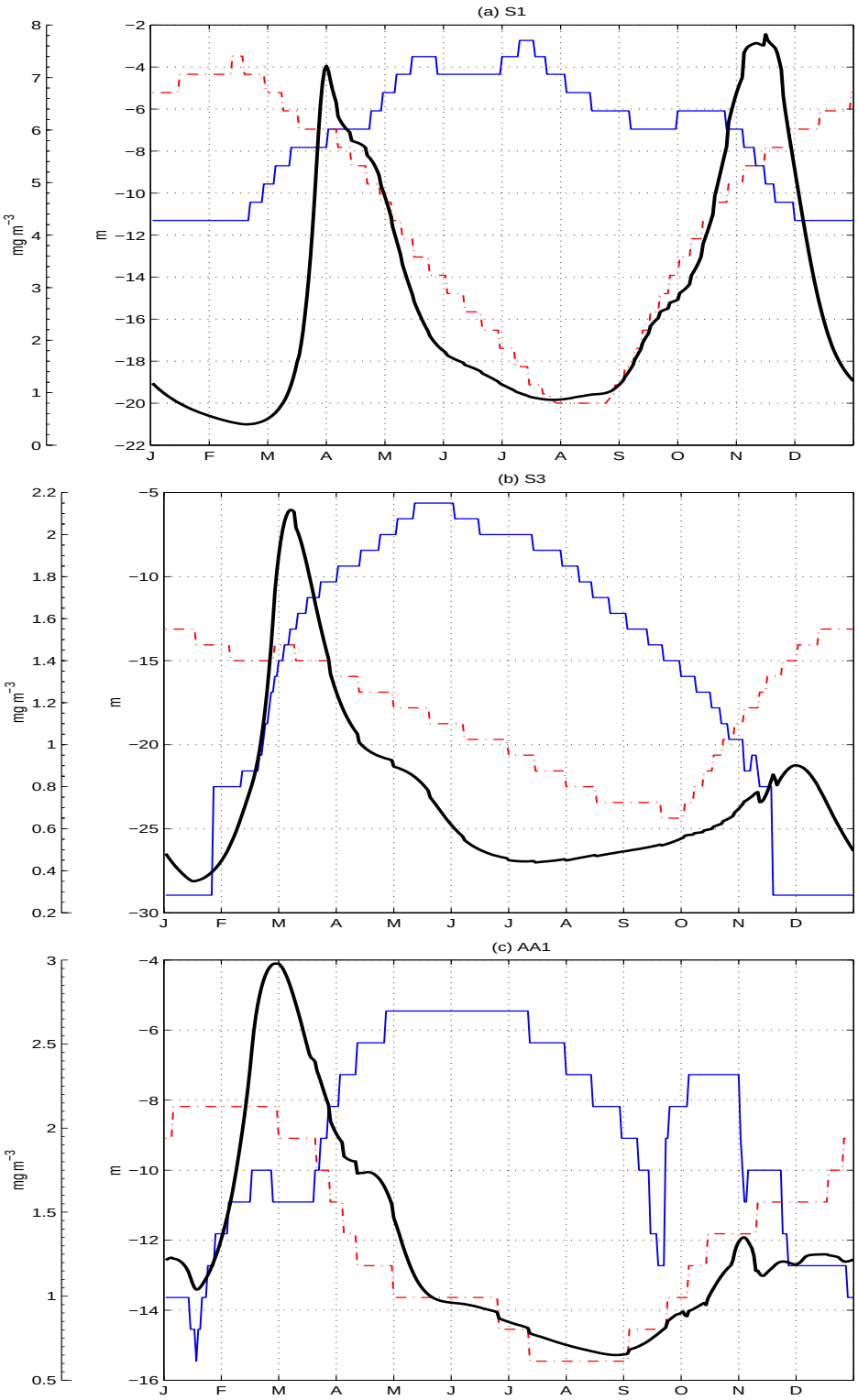

Figure 3.7.: Biological-physical interactions at the three implementation sites: (a) S1, (b) S3 and (c) AA1. Thick continuous line is the model simulated chlorophyll concentration (in mg m^{-3}) averaged within the critical compensation depth D_{cr} (defined as the depth where vertically-integrated primary production rates equal autotrophic respiration rates). The dynamical evolution of D_{cr} (dashed thin red line) and of the mixed layer depth (in m, continuous thin blue line) simulated by the model are superimposed to the chlorophyll curve.

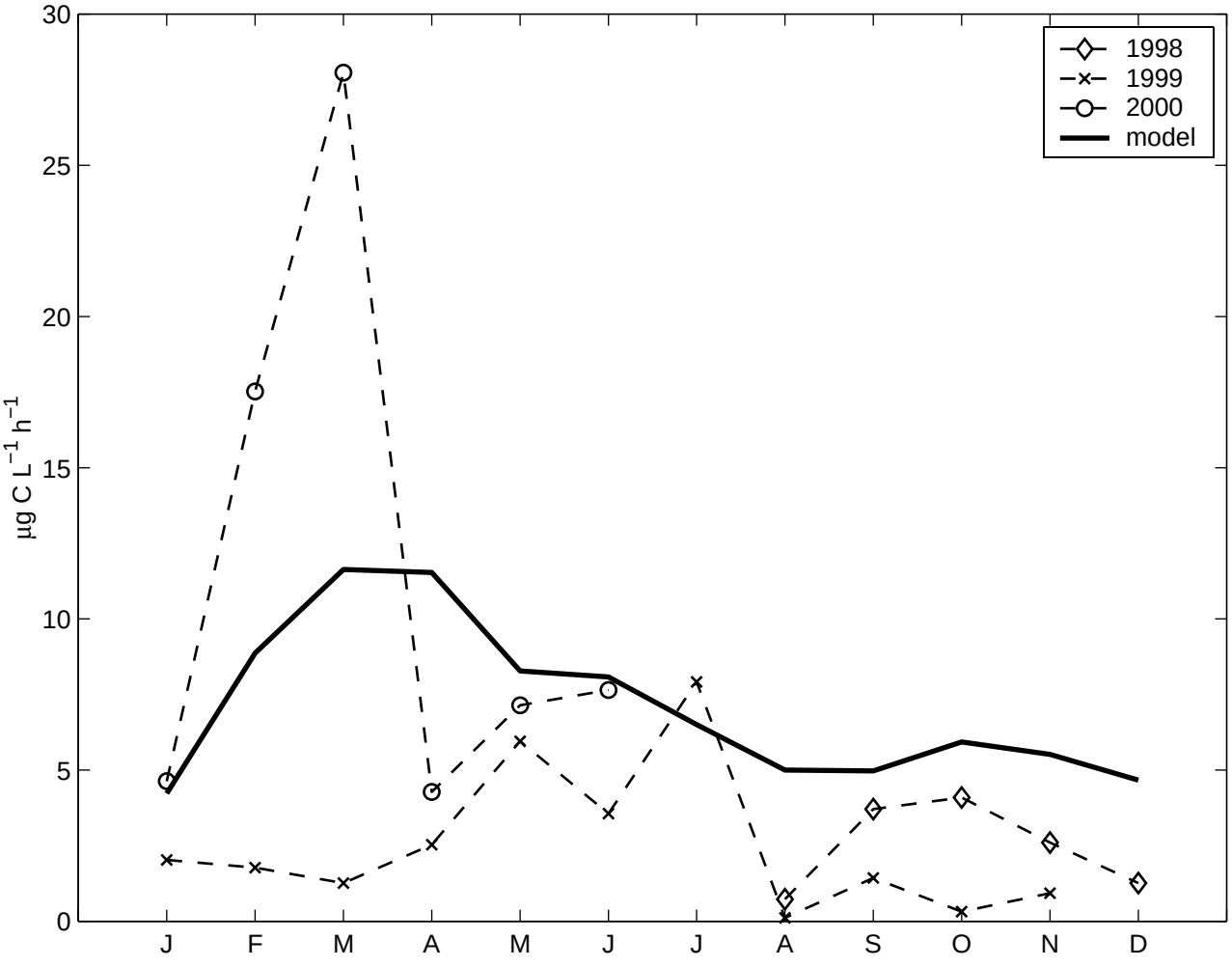

Figure 3.8.: Comparison between time series of model simulated primary production rates and observations at AA1 site in the Gulf of Trieste. Model data (continuous thick line) are computed as monthly climatological average of surface primary production rates. Observations are single field measurements collected once per month in the period 1998-2000.

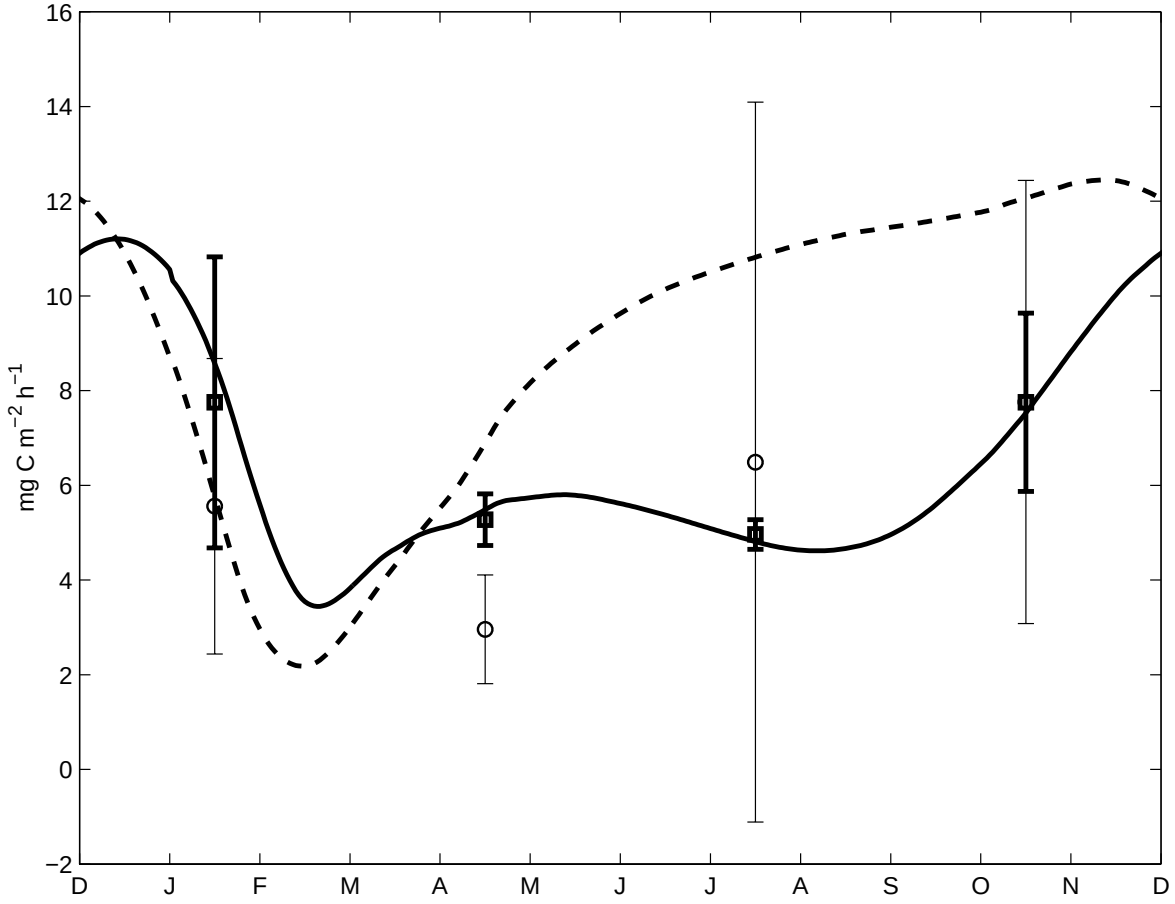

Figure 3.9.: Results of the sensitivity experiment on the formulation of bacterial growth efficiency (BGE). Comparison between time series of model simulated bacterial carbon production (BCP) rates obtained with the BGE parameterization proposed by Rivkin and Legendre (2001) and observations at AA1 site in the Gulf of Trieste. The circles (○) are the seasonally averaged observations in the period 1998-2000 plotted with the standard deviations. The dashed thick line (- -) is the modeled depth-integrated BCP with constant BGE of 0.3, the continuous line (-) is the BCP with the temperature-dependent BGE (the relative seasonal means and standard deviation bars are also given with the symbol □).

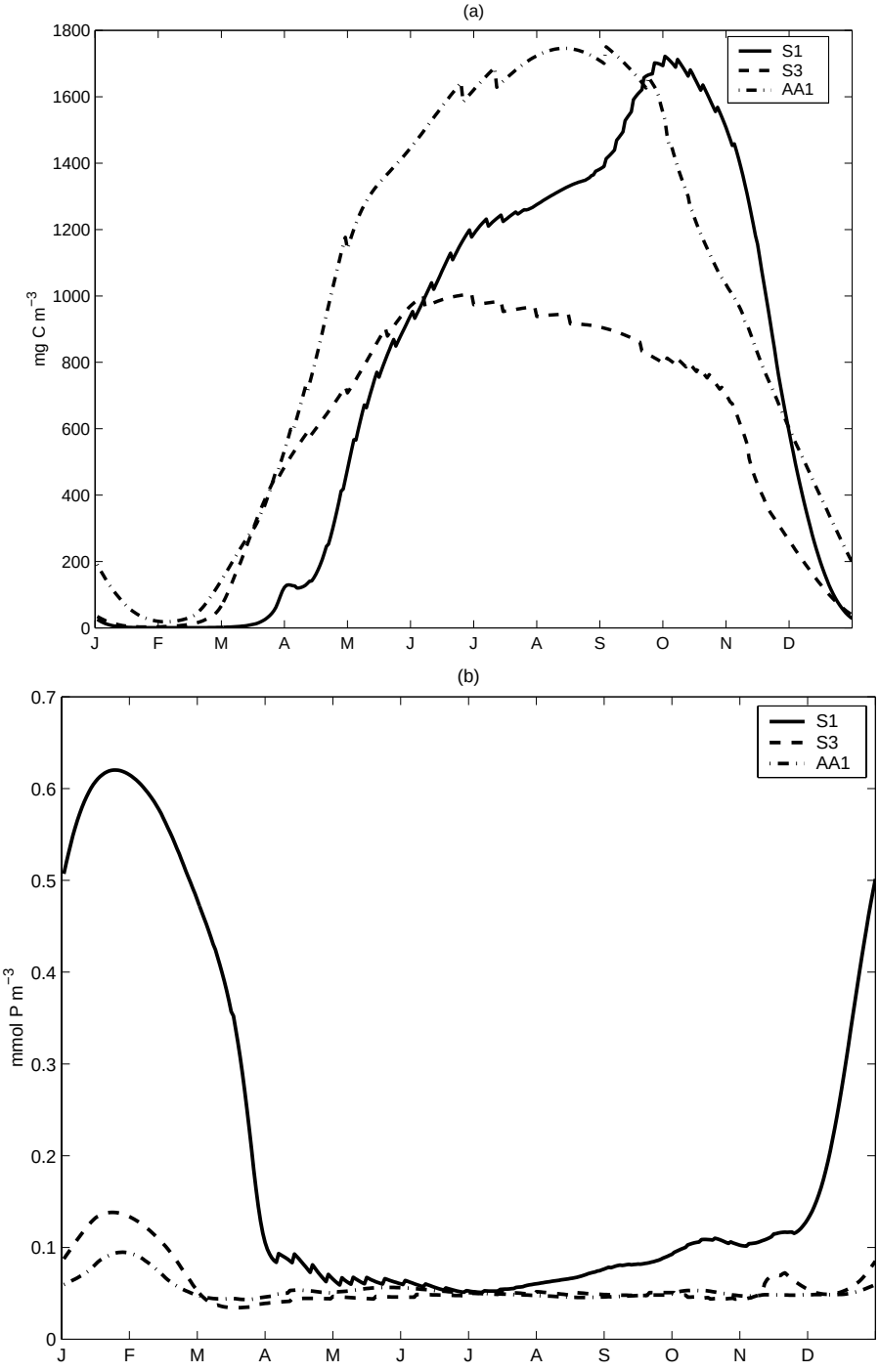

Figure 3.10.: Model simulated concentration of (a) dissolved organic carbon (DOC) and (b) dissolved inorganic phosphorus (DIP) as average within the critical compensation depth at the three implementation sites.

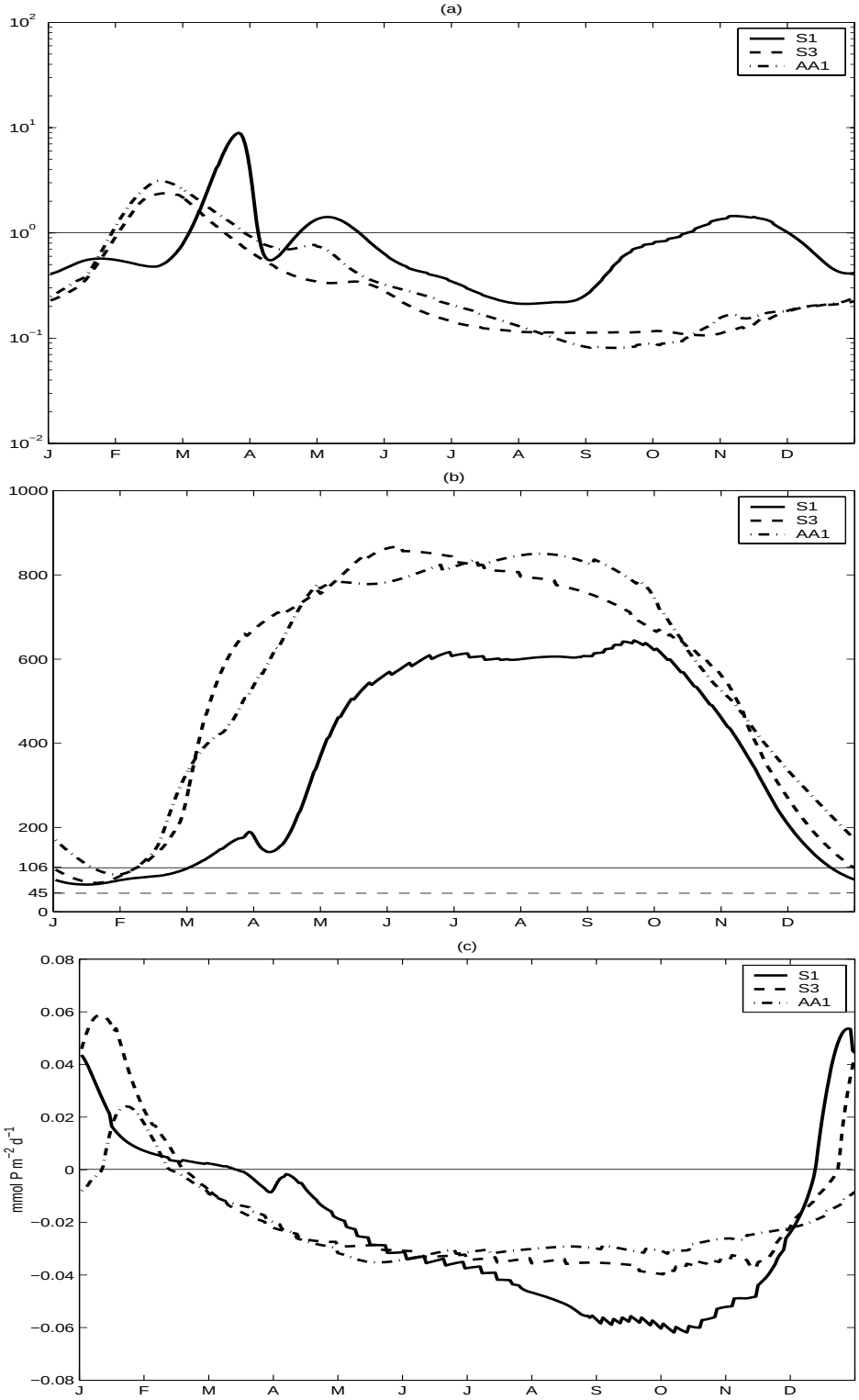

Figure 3.11.: Indices of ecosystem functioning and matter-transfer pathways. (a) ratio between the carbon flows of herbivorous grazing (from autotrophs to zooplankters) and microbial grazing (from bacterioplankton to zooplankters; in semi-logarithmic scale). (b) ratio between the C-component and P-component in dissolved organic matter (DOC:DOP). The optimal ratios for phytoplankton (106:1; Redfield *et al.* 1963) and bacteria (45:1; Goldman *et al.* 1987) are indicated. (c) phosphorus flux between bacteria and dissolved inorganic phosphorus (DIP).

4. Long-term dynamics of the Baltic Proper ecosystem behavior. One-dimensional hindcasting simulations with high-frequency realistic forcing functions

4.1. Introduction

This Chapter presents a Baltic Sea application of the one-dimensional vertical (1D-V) version of the HiROPE modelling tool. Specifically, this implementation focuses on the simulation of the shorter time scales of the hydrodynamical fields by applying realistic high-frequency forcing functions, and analyzing how the different time scales of the physical and biogeochemical processes interact in the long-term decadal behavior of the Baltic ecosystem.

Such a study gives an opportunity to increase our understanding of system level properties, because, as explained in Chapter 2 and in the Appendices, the HiROPE model aims to simulate the coupling between several fundamental biogeochemical processes and the transport dynamics (vertical, in this case). These dynamical interactions are hardly measurable directly at sea, and they can only be investigated with the support of a numerical model. In addition, such a study can also be used to assess the performance and the genericity of the biogeochemical parameterizations in ERSEM III against the observed system behavior of this complex semi-enclosed sea, in order to identify specific model deficiencies or key processes that needs to be further investigated. Therefore, the results of this work are manifold, and I have focused on the following objectives:

- analyze the long-term hindcasting skill of the model and the suitability of the one-dimensional implementation in the description of decadal Baltic system processes;
- study the dynamics of the nutrient cycles in combination with the hydrodynamical characteristics of the system;
- understand the impact of external nutrient loads on the ecosystem dynamics;
- study the impact and functional importance of high-frequency forcing functions;

- assess - with objective measures for the (mis)fit between model results and observations - the potential predictability skill of the model for future forecasts of the system behavior.

Clearly, giving an exhaustive answer to these points is an overwhelming task, but the overall approach has given promising results that deserve a future continuation. The philosophy behind this Chapter is that a good description of physical processes is of paramount importance when trying to predict system-level properties (also when dealing with the longer time scales), and the use of one-dimensional realistic simulations can help in determining some of the main interactions, but also the major limits of the implementation itself. The model has thus been applied at two different locations, one in the Bornholm Basin, and one in the deeper Gotland Basin (Figure 4.1), in order to analyze possible localized processes and test the model capabilities under different conditions. Some specific model adaptations have been necessary to capture the Baltic dynamics reinforcing the conclusion that the hindcasting skill (and to some extent the predictability) cannot be separated from the proper inclusion of a minimum required amount of biotic interactions.

This Chapter is divided in two main parts. On the one hand, the description of the Baltic system and the analysis of the simulation results, with the identification of the sensitive processes that seem to affect the response of the model. On the other hand, the quantitative assessment of the goodness of fit with respect to the observations, and a critical analysis of the application of these objective measures. Finally, in the last section, it has been analyzed how the representation of the smaller scale variability induced by the abiotic environment affects the system properties as described in the model. Such experiments can help in partially understanding what are the essential abiotic features that have to be included in mechanistic models for their future utilization as predictive tools.

4.2. The Baltic proper system: overall description

The Baltic Sea in general has been extensively studied in past years and in particular has been the site of periodic assessment reports that partially allow to track the long term changes in the hydrodynamics and biogeochemistry of the system (HELCOM, 1987; HELCOM, 1990; HELCOM, 1996). These publications have been used as reference in order to draw out the general description of the basin, and critically interpret the modelling results where more specific information is lacking.

The Baltic proper (Figure 4.1) is the largest basin in the physiography of the Baltic Sea, and its maximum depth of 240 m is found in the Gotland Deep. The main hydrographic feature is the permanent salinity stratification, which is maintained by intermittent inflows of salt water through the Belt Sea and the Sound into the Bornholm basin, and by runoff of the major drainage rivers (Odra, Vistula, Nemunas). The inflows are usually divided in major and minor events, depending on the salinity of the incoming water (greater or lower than 17 psu). The two major effective inflows in last 25 years occurred in 1975/76 and in 1993, delimiting a long stagnation period without a renewal of the waters in the deeper part of the basin. This period, in concurrence with the eutrophication conditions observed in most of the basins, had remarkable consequences on the oxygen depletion and formation of hydrogen

sulphide, because the oxic state of the deeper waters is strongly dependent to the advective exchange of more oxygenated salt waters (ventilation) from the seaward boundary. The local advective transport due to the general circulation dynamics is probably a second-order effect in the long-term behavior, although it participates in the short-term variability of the water column, changing the stability features and carrying oxygen re-supply. In spite of the numerous studies on the hydrodynamics of the basin, the three-dimensional structure of the general circulation is not well known, especially due to the high variability in the meteorological fields over the region. However, some persistent circulation patterns can be identified with the aid of numerical models, and results show circulation cells mostly confined to the sub-basin level, with small horizontal exchanges between the basins (Lehmann and Hinrichsen, 2000). Hence, the presence of a weak horizontal circulation enhances the relevance of the mesoscale patterns (Fennel and Neumann, 1996) and the vertical turbulent transport processes driven by the exchange of momentum and heat at the air-sea interface.

The vertical structure of the water column is of clear importance in the overall behavior of the vertical distribution of nutrients, because the halocline is also a "nutricline" separating the bottom reservoirs from the surface layers. The major seasonal resupply of nutrients occurs during the winter period, with the deepening of the pycnocline following the vertical thermohaline convection. Winter maxima of nitrates and phosphates are clearly identified throughout the entire Baltic proper, and a rapid decrease to lower levels is observed during the spring period, in concomitance with the development of phytoplankton blooms (HELCOM, 1996). The nutrient considered to be the key factor in the Baltic proper is nitrogen and it is generally accepted that phytoplankton activity is nitrogen-limited (Graneli *et al*., 1997). A surplus of P with respect to N is usually observed in the various sub-basins, although it is important to remark that considering only the nutrient concentration levels is not sufficient to determine the trophic state of the system. From budget considerations (Stigebrandt and Wulff, 1987; Wulff and Stigebrandt, 1989), the residence time of nitrogen in the basin is about 1 year, while phosphorus has a residence time of about 10 years. However, nutrient budgets are primarily based on computations of inflows/outflows, the external loads plus other point sources and the atmospheric inputs, not considering the possible internal sources (Wulff *et al*., 1998, Rahm *et al*., 2000). The potential internal recycling capacity of the system is still a substantial ignorance factor, which severely reduces the predictability of the ecosystem behavior and the assessment of possible remediation measures. The (re)cycling of the organic matter through the Baltic food web is affected by the input of nutrients from land and from the bottom reservoirs, and it involves not only the classical grazing chain (large phytoplankton towards zooplankton), but also the microbial loop, because bacteria actually participate in the control of the inorganic nutrient pools (Kuparinen and Heinänen, 1993; Zweifel, 1993). The mediating ecological role of bacteria in the marine environment has been strongly pointed out in recent years since Azam's first introduction (Azam *et al.*, 1983), stressing the necessity of a complete integration of microbial dynamics within the description of the continuum of trophic interactions in the marine ecosystem (Legendre and Rassoulzadegan, 1995). In fact, the different regimes of the hydrodynamic vertical features could lead to different distributions of the organic matter fluxes in the

trophic web, resulting in a short-scale variability of these smaller components that could also affect the long term dynamics of the system.

With regard to the pelagic biology, the climatology over the period 1979-1993 for the Bornholm and Eastern Gotland basins, presents a large interannual variability, complicated by the risk of inadequate sampling that could miss the shorter term developments (HELCOM, 1996). Available observations from the whole Bornholm basin show three apparent phytoplankton biomass peaks. In April-May the main species are diatoms (*Chaetoceros* spp., *Skeletonema Costatum*, *Thalassiosira* spp.) followed by dinoflagellates (*Peridiniella catenata*, *Dinophysis* spp. and *Gymnodinium* spp.), with a shift, in later years, towards flagellate dominance. During summer, blooms of cyanobacteria are observed, although a diminishment has been reported after 1984. In this period, a rather diverse community develops, which is probably connected to the different meteorological and hydrographic conditions. The start of the spring bloom seems to shift from May towards April (might be due to mild winters as suggested in Schulz *et al.*, 1992, although hard to determine owing to the scattered data). In autumn, diatoms are the dominating group. In the Eastern Gotland Basin, the bloom is found later in the year (up to May in the Gotland Deep), and, as in Bornholm, diatoms and dinoflagellates are the more abundant groups. A distinct summer peak of cyanobacteria is less reflected in the data from this basin, while the autumn peak mainly consists of diatoms.

4.3. Model setup

The numerical hindcasting experiments at the two selected locations (Fig. 4.1) have been carried out using the same procedures and both start on January 1st 1979. The HiROPE implementation in the Bornholm basin will be indicated as BORNHOLM, while the model in the Eastern Gotland Basin is called GOTLAND. BORNHOLM is centered at 55.5N 15.5E and the depth of the water column is 80 m. The model has 20 levels with a logarithmic depth distribution both at the surface and at the bottom (the depth of the first layer is 0.3 m, the depth of the bottom layer is 1 m). In the remainder of the water column the levels are uniformly spaced every 5 m. GOTLAND is located on the slope of the Gotland Deep at 57.5N 19.5E with a depth of 150 m. The number of levels is 20 as well, and the depths of the first and bottom layers are 1.2 m and 1.5 m, respectively. In the middle of the water column, the layers are uniformly distributed with a depth of 10 m.

In order to set up both models, it is necessary to evaluate the initial conditions for all the model state variables. The reference dataset that has been used for this task and throughout the entire assessment phase is the Baltic Environmental Database (BED, Wulff and Rahm, 1990) accessed via the SwingStations web-interface (Sokolov and Wulff, 1999). The data extraction regions roughly covers an area of 1×1 degrees around the model locations.

There are no direct biological data available in the BED database, and the information that can be derived from the literature are sparse and mostly coming from different areas of the Baltic. Some initialization experiments have demonstrated that both models show some sensitivity to the initial

pelagic conditions only for the first 1-2 years of the time integration. By that period, the trajectories of the pelagic variables in the phase space converge to almost the same state, indicating the strong dominance of the external forcing functions with respect to the internal pelagic dynamics. For most of the benthic variables, however, this is not true. The carbon and nutrient pools in the sediments are important properties of the system, which partly determine the time scales of nutrient cycling in the marine environment. The forcing functions that determine the seasonal cycles do not have the same synchronizing impact on the benthic components as for the pelagic state variables.

The approach used to initialize the models takes into account the previous issues. Firstly, a set of guesstimate of the carbon and nutrient content of the pelagic variables is made. Small winter carbon concentrations have been given to the functional groups and the internal nutrient amount was obtained by means of the optimal internal ratio defined in the model. The values of the winter initial main physical and hydrochemical variables were directly derived from the BED database, linearly interpolating the vertical profiles of temperature, salinity and the dissolved nutrient concentrations to the model levels at both the locations. Bulk values of the organic carbon content in the sediment were evaluated from literature (Picker *et al*., 1998) and an initial guesstimate of the nutrient richness was given. After some tests, the choice was made to initialize with rather high nutrient contents, in order to spin up the oxidation of the organic matter in deeper layers. The models are then run for 3 years, starting from the previously described initial conditions and vertically homogeneous dissolved O_2 values. Oxygen in the bottom layer is fast depleted, organic matter is consumed and rearranged with respect to the nutrient content and the thickness of the oxic layer in the sediment is reduced to some millimeters. End values of the simulations were used as initial conditions for the standard runs at both sites, but dissolved nutrients and physical parameters were re-initialized to the profiles extracted from the BED database.

Another problem is connected to the setting-up of proper initial conditions for the benthic fauna. In BORNHOLM, where only data concerning macrofauna are available (HELCOM, 1996 and references therein), the same procedure described above has been applied. In the Eastern Gotland Basin (GOTLAND) the model depth is 150 m, hence it is within the range of the so-called “benthic desert zone” with no macrofauna (depth > 120 m; Olenin, 1994). There is no specific information regarding meiofauna, but these functional groups in the model decreased to very low levels in the 3 years of the spin-up period because of the oxygen depletion. Therefore in GOTLAND the model was initialized without benthic fauna except for microbial aerobic and anaerobic decomposers.

4.3.1. Meteorological forcing functions for the physical model

The atmospheric forcing functions have been extracted from the BASYS meteorological database (BASYS-MET, L. Müller, SMHI, personal communication), which contains gridded meteorological data with 1 by 1 degree resolution. The parameters in the database are: air pressure, zonal and meridional geostrophic wind, air humidity, cloud cover, precipitation and solar radiation. The frequency of the meteorological data is three hours except for precipitation (half-daily) and solar radiation (daily).

The data have been checked for missing values and missing days have been substituted with the corresponding information from the day before. The model interpolates between two three-hourly values to the actual numerical time step via a linear interpolation. From these parameters, the surface exchange fluxes of momentum and heat have been computed by means of the bulk formulae collected by Castellari *et al.* (1998) (see also Appendix C, Section C.4. Since we are dealing with high frequency observations, the astronomically-derived solar radiation (according to Dobson and Smith, 1988) corrected by three-hourly cloud cover data has been preferred to the daily averaged value given in the database.

The Bornholm sub-basin

The meteorological data from grid-point 55.5N, 15.5E have been chosen to be representative for the Bornholm basin. The available time series over the period 1979-1994 have first been analysed in order to find special features that could be connected to the behavior of the ecosystem when analyzing the model results. Figure 4.2 shows the running averages at different intervals of the air temperature extracted from the BASYS-MET database. The long term mean is 7.8 Celsius degree, with a standard deviation of 6.5 degrees. The 30-days running average shows a clear seasonal cycle and a large interannual variability, while there is no recognizable trend in the one and five years averages. The running averages of three-hourly wind data are shown in Figure 4.3. The geostrophic wind has first been converted to 10 m wind using a scaling factor of 0.7 and then the running averages have been computed. The 1979-94 long-term mean gives a value of 7.4 m/s, and from the 1-year average we can see that the mean value is exceeded intermittently before 1991, and constantly after that year (with the maximum in 1993). The years with highest wind velocity appear to be 1989-90, with other high energetic periods in 1983-84. It is difficult to see a clear seasonal cycle, although the analysis of the 30-days average always shows an overall decrease in the wind speed during the summer periods.

The Eastern Gotland sub-basin

Figure 4.4 shows the air temperature running averages calculated at the grid-point 57.5N, 19.5E, and representative of the Eastern Gotland sub-basin. The comparison with the Bornholm data shows a lower mean value of 7.2 degrees over the period 1979-94, but no relevant differences in the behavior of the running averages with wider intervals (1-year, 5-years), remarking the absence of trends. It is interesting to note that the Gotland 30-days mean during summer periods is lower than Bornholm only in the last two years of the time series, while the winter monthly minima are always lower. The main feature in the 10 m wind distribution (Figure 4.5) is a general lower speed compared to the Bornholm sub-basin. The mean over the period is 6.4 m/s with a standard deviation of 3.7 m/s, which is comparable with the 5-years running averages line. Also in this basin the more energetic periods in 1983-84 and 1989-90 are visible as well as the maximum in 1993, but the 1-year running average shows a different distribution pattern with respect to Bornholm, highlighting the presence of local meteorological events at the sub-basin scale.

4.3.2. Forcing functions for the ecological model

This term collects all the physical boundary processes which affect the distribution (in the 1D-V case, the surface time distribution) of biogeochemical state variables in the system. This list includes the input of nutrients and suspended matter from rivers, the atmospheric deposition of chemical compounds and other anthropogenic point sources.

It is difficult to assess the real weight of external forcing functions when dealing with ecological components. One of the main reasons is that, some times, uncertainties concerning the quality of the observations are of the same order as the changes in the dynamical environment. Moreover, the low sampling frequency can mask the real time distribution of events, missing some special features that take part in the determination of the system state. Hence, the risk is to constrain the model to include signals that probably have different interactions with the scales of the internal processes, leading to the development of artificial or incorrect dynamics in the model. However, the need for external forcing functions in ecological modelling is unquestionable in order to approximate a description of the real ecosystem. A very simple example is the river load of inorganic suspended matter. The inclusion of different parameterizations of this forcing leads to dramatic changes in the behavior of primary producers' bloom in very shallow waters, stressing the importance of the correct timing in the boundary conditions' imposition (Vichi *et al*, 1998a).

Nevertheless, the Baltic is a strongly eutrophicated system, mainly due to the input of terrigenous nutrients (Melvasalo, 2000). Therefore, external nutrient loads to the Baltic proper have been included in the simulations, although care must be taken in the interpretation of results because of the difficulty in considering river inputs in a 1D-V model. The distance from the sources and the transformations of dissolved nutrients into particulate organic matter have to be taken into account, notwithstanding the uncertainties in the quantity and quality of the horizontal export fluxes out from the model domain that are not considered in the 1D approximation.

The chemical compounds considered important for the marine environment that can be deposited via atmospheric processes are mostly nitrogen and phosphorus. The information concerning these inputs in the Baltic sea are mainly annual budgets at basin-level for phosphorus (6000-7000 tons; Davidavichiene and Sopauckiene, 1989; HELCOM, 1989) and monthly wet atmospheric nitrogen deposition with a 1 by 1 degree spatial resolution (L. Grannat, Department of Meteorology, Stockholm University, collected in the framework of the BASYS project). Since the known amount of phosphorus deposition does not have any temporal or spatial distribution, it has been decided to neglect this term and only include the nitrogen deposition as external forcing function. These data have spatial variability, and higher frequency deposition information can be derived using the consistent precipitation data from the BASYS-MET database. In order to obtain a half-day deposition, which is the frequency of the precipitation data, I computed the monthly total precipitation in both the Bornholm and Eastern Gotland sub-basins at the chosen locations. Afterwards, the monthly wet deposition was divided by the obtained total precipitation, and the resulting deposition per unit of precipitation was multiplied by the amount of precipitation every 12 hours. Scaling this value to the day, gives an esti-

mation of the deposition flux of nitrate and ammonium (both in mmol N m^{-2} d^{-1}) with a half-daily frequency for the Bornholm and Gotland areas, and this value is held constant for all the integration time steps within that period. A background deposition has also been considered , accounting for the dry deposition flux. This is a constant fraction, which may range from 5 to 20% of the wet deposition, and has been set to 20%. Such time series of fluxes are used as vertical boundary conditions for the dynamical equations of nitrate and ammonium in the ecosystem model (Appendix C, Section C.4.4).

The inclusion of river loads to the Baltic proper has been done taking a very simplistic approach. The total nutrient loads to the Baltic proper have been estimated from monthly time resolution data over the period 1979-90 (Stålnacke, 1996; Stålnacke *et al.*, 1998). The available information concerns the input of inorganic P as phosphate, inorganic N as nitrate plus nitrite, inorganic Si as silicate and the total P and N loads. The organic P and N inputs have also been estimated as difference between the total load and the inorganic part. The flux per meter squared per day for each component was finally obtained dividing by the total surface of the Baltic proper (211,069 Km^2, HELCOM, 1996) and by the number of days in each month. Such fluxes (Figure 4.6) have been imposed as boundary conditions in the corresponding dynamical equation of the model state variable, as done for the atmospheric deposition above. An estimation of the input of organic carbon related to the load of organic N and P is necessary to balance the organic matter input in the ERSEM III biogeochemical cycles. A Redfield ratio with the N-component was assumed, as this gives the higher absolute amount of POC due to the N-enriched characteristic of the organic inflows (actually this is an ignorance factor, but it seems not to show any particular sensitivity of the model results).

4.3.3. Physical parameterizations

The absence of any representation of horizontal transport processes, both advective and dispersive, in one-dimensional water column models implies that such models only may be expected to reproduce *in situ* observations if and when vertical transport processes dominate over the horizontal ones. When horizontal terms are neglected, it is assumed that the horizontal gradients are less important, although this is generally a matter of time-scales. Many features in the Baltic are helpful in applying these assumptions. First of all, the absence of a well-defined general circulation (Section 4.2), which allows the assumption of horizontal homogeneity at least at the sub-basin scale. Second, the weakness of the tidal forcing, which eliminates the superimposition of the high-frequency tidal transports to the local concentration values. Therefore, the reasons to use 1D models in the Baltic are multiple.

However, the interaction with the slower horizontal transport especially in the bottom layers is essential in the determination of the long-term behavior of the vertical water-column structure. Omstedt and Axell (1998) have demonstrated that the long-term behavior of the Baltic Sea can be simulated with 13 sub-basins treated as horizontally-uniform, vertically-resolved systems, which exchange waters with the adjacent basins. In this is way it is possible to simulate the persistence of the permanent stratification plus the intermittent entrainment of saltier waters from the Danish straits that also determines the formation of the bottom dense currents. This implies that, if we are interested in a long-term

analysis of the system by using a one-dimensional model, we have to be able to give to the biology enough physical variability at the small scales through the imposition of surface exchange fluxes, but also provide for a sort of partial closure of the annual cycle in the water column. The interaction between these different time-scales is of paramount importance for the description of the observed system behavior, especially where it concerns the timing of the phytoplankton spring blooms and the maintenance of the summer plankton stocks, as will be shown in Section 4.4.3.

In a 1D-V model, the vertical turbulent mixing induced by wind energy cannot be counteracted by long-term horizontal adjustment of the buoyancy of the water column. The imposition of realistic forcing functions at the surface tends to increase the instability and destroy the permanent vertical density gradient (assumed here to be mostly a function of the salinity), which should be restored by the horizontal general circulation structure. Since the horizontal terms are neglected, it is necessary to find a parameterization which could help in maintaining the stratification, mimicking the local advective adjustment and closing the local salt budgets. A similar approach was first done by Lascaratos *et al.* (1993) and Vichi *et al.* (1998a) in a climatological context, and here a slightly different formulation is presented.

Referring to Appendix C, the salt transport equation for the three-dimensional turbulent flow can be written - neglecting the horizontal diffusion terms - as:

$$\frac{\partial S}{\partial t} = -\mathbf{U}_H \cdot \nabla_H S + \frac{\partial}{\partial z}\left(K_H \frac{\partial S}{\partial z}\right), \tag{4.1}$$

where K_H is the turbulent diffusion coefficient according to the Reynolds decomposition . In place of the horizontal term, one introduces a parameterized equivalent source term like the following:

$$\frac{\partial S}{\partial t} = F(S) + \frac{\partial}{\partial z}\left(K_H \frac{\partial S}{\partial z}\right), \tag{4.2}$$

where F can be dependent both on time and space. It is proposed to parameterize this source term as a relaxation to long-term climatological profiles of the observed salinity distribution. The necessary assumption here is that the horizontal distribution of salinity is quite uniform at the sub-basin scale, and the main local dynamical processes are the consequence of momentum and heat fluxes at surface. This hypothesis can be considered valid for the Baltic proper because of the rather constant influence of freshwater sources. The main problem arises when considering the inflow of deep waters across the seaward boundary; this process has indeed an important interannual signal that cannot be accommodated using this method and other modelling techniques have to be used (Omstedt and Axell, 1998). The method uses a climatological vertical profile of salinity derived from the available observations, to which the dynamics of the water column have to adjust within a given time scale. This profile can be an annual mean or have a seasonal variability, in order to track the seasonally-varying freshwater

influence. The form of (4.2) becomes:

$$F(S) = -\frac{\Delta(z)}{\tau}(S - S_{clim}) \tag{4.3}$$

with $S_{clim} = S_{clim}(z,\tilde{t})$ and $\tilde{t}$ is discrete. The parameter τ represents the adjustment time scale of the relaxation process, and $\Delta(z)$ is a non-dimensional function that is zero down to a given depth δ and 1 below. Hence, the parameterization of local advection represents here the basin contribution to the stability process. The climatological salinity profiles S_{clim} have been computed from the BED database. The salinity profiles used in BORNHOLM and GOTLAND are the long term averages over the investigated period 1979-90. It was also considered to use a seasonally varying climatological profile, but the seasonal profiles derived from the data are only marginally different from the long-term annual mean and do not affect the behavior of the models. Several tests and comparisons with the available data have been done in order to determine the more appropriate values for the parameters in the current implementations. The standard simulations have been performed with $\tau = 60$ days for BORNHOLM and $\tau = 360$ days for GOTLAND. The different values are due to the different depths of the water columns, and thus, to the different interactions with vertical processes. The restoration in BORNHOLM is much faster because it is shallower, and the influence of surface exchange processes penetrates more at depth in the water column with respect to GOTLAND. Here, the buoyancy flux is stronger and thus, the erosion of the dense water layers takes longer periods. The function $\Delta(z)$ is the same for both models, being equal to 0 in all the layers down to 5 m below the surface, and 1 in the reminders.

It will be shown (Section 4.4) that this parameterization enters directly in the determination of the long-term nutrient dynamics of the basin. The diapycnal transport of nutrients, and thus the net phytoplankton production in the euphotic layers, is controlled by the turbulent diffusion process in the deep waters which is, in turn, a function of the vertical stability. Recently, it has been proposed that the observed deep-water mixing has a seasonal variability (with higher rates in fall and winter, Stigebrandt, 1985; 1987) and is dominated by the energy input from the wind via inertial currents and internal waves (Axell, 1998). This is confirmed by observations in the deepest part of the eastern Gotland basin, while below 150 m as in the presented cases, also the active coastal boundary layer can play an important role (Axell, 1998). Turbulence-closure models like the M-Y cannot appropriately represent the vertical shear of the horizontal velocities in deeper waters, and therefore, in this case, the turbulent mixing is parameterized as a sub-grid scale process with a constant background diffusivity (see Section C.3). This parameterization was the one used in the first preliminary results given in Vichi *et al*. (1999). However, this makes the model results much too sensitive to the value of this constant, because the dynamical values of K_H given by the M-Y are unrealistically low. This lack of representation of the energy flux density in the layers below and in the surroundings of the halocline has been parameterized as done by Stigebrandt (1987) and Omstedt and Axell (1998) (see also Axell, 1998, for more background information). When internal waves are responsible for the transport of energy at smaller scales, the turbulent vertical diffusivity is an inverse function of the buoyancy

frequency N, defined as

$$N^2 \equiv -\frac{g}{\overline{\rho}}\frac{\partial \overline{\rho}}{\partial z} \tag{4.4}$$

where g is the acceleration of gravity and $\overline{\rho}$ is the mean density field. The parameterized form of K_H is used in the model only when the computed value is smaller than the typical value found in the Baltic (1.0×10^{-5} m^{2}s^{-1}; Axell, 1998), and is written as:

$$K_H = \alpha N^{-1}. \tag{4.5}$$

The parameter α has been found to be in the order of 2.0×10^{-7} m^{2}s^{-2} in a vertically-resolved model of the whole Baltic basin (Stigebrandt, 1987). However, as pointed out by Axell (1998), this value underestimates the energy flux derived from observations in shallower waters, and in order to have a diffusivity comparable with 1.0×10^{-5} m^{2}s^{-1}, α has been increased to 1.5×10^{-6} m^{2}s^{-2}. This value gives the best fit with long-term observations of the available physical and hydrochemical variables, as will be shown further on in the model result presentation, although the model sensitivity to this parameter is quite marked. Figure 4.7 shows the time evolution of K_H computed by the M-Y and with the parameterization (4.5) in the surface layers of GOTLAND and just below the permanent pycnocline for the period spring-autumn in 1983. During the summer more stratified period, the total energy flux computed by the turbulence closure scheme (Figure 4.7a) is limited to the first 20 meters, because the buoyancy flux is stronger. Owing also to the presence of the relaxation flux (4.3), which continuously restores the buoyancy flux independently from the season, the values of K_H below the seasonal thermocline are very small and unrealistic. With the implementation of (4.5), it is possible to dynamically increase the energy in the interior of the water column, as shown in Figure 4.7b. This has several implications for the vertical nutrient dynamics, and helps to improve the model skill in the simulation of the spring bloom onset and the maintenance of the summer phytoplankton stocks (Section 4.4.3). It is also important to mention that, with the 1D implementation, the vertical advection and the effects of the density currents are completely neglected. This is an additional process that transports nutrients and oxygen along the water column, because the denser waters operate a ventilation of the bottom layers and lift up the nutrient-rich bottom or intermediate waters. Some of the discrepancies between model results and observations can be explained by the absence of such a process, and the 1D model appears to be particularly useful in pinpointing the time periods when such processes are more effective.

4.3.4. Biogeochemical parameterizations

Some specific model refinements with respect to the original ERSEM II implementation were necessary to capture the main "Baltic" processes, especially related to the occurrence of persistent anoxic conditions in the Eastern Gotland basin. The description of these features has been achieved thanks

to the modularity of the model structure described in the Appendices and the explicit formulation of the coupling between benthic and pelagic processes.

The main concern in the Baltic proper system analysis is connected to the description of the nitrogen dynamics, because this element is considered to limit the primary production in the basin (Section 4.2). In general, the biogeochemical cycle of N in coastal or semi-enclosed marine systems is subject to a complex array of regulatory mechanisms involving the two main species NO_3^- and NH_4^+ and the microbially mediated processes of ammonification (remineralization), nitrification, denitrification and nitrogen fixation (Herbert, 1999). Such processes (excluding fixation) mainly take place in the sediments, therefore the simulation of early diagenetic dynamics are of great importance. The dominance of one process over another is largely determined by the redox conditions in the water column, which are, in turn, connected to the hydrodynamics and to the rate of detritus sedimentation and decomposition. The standard ERSEM II formulation already comprised the parameterization of these processes in the sediment model (Ruardij and van Raaphorst, 1995), mainly described as first order reactions. In this study, the parameterization of the denitrification has been modified (see Sections A.5.1 and B.7.3 for further details), because this mechanism is considered to be the major sink for nitrogen in the Baltic (Wulff and Stigebrandt, 1989; Eilola and Stigebrandt, 1999), and has been demonstrated to occur also in the water column (Rönner and Sörensson, 1985). Nevertheless, the denitrification sites are first and foremost the sediments (Tuominen *et al*., 1998; Herbert, 1999), and this process is dynamically linked to the supply of organic matter and the bottom redox conditions.

In order to incorporate the dependence on the organic matter availability, denitrification has been coupled to the biological oxygen demand under hypoxic/anoxic conditions (anoxic mineralization), both in the water and in the sediments. Since the Baltic proper has shown an alternation of positive and negative redox conditions during the investigated stagnation period, it is important that the model is able to deal with both situations, in order to shift from nitrification to denitrification. In the denitrification reaction, nitrate is used as an electron acceptor for metabolic activity at low oxygen concentrations and the model formulation has been set up in order that pelagic bacteria switch to nitrate consumption modifying the redox conditions as shown in Sections A.3 and A.5.1). When oxygen is completely depleted, hydrogen sulphide is formed at the water-sediment interface, as a result of the bacterial reduction of sulphate ions. The bacterial oxygen demand is thus redirected to the sulphate ions, and the formation of one sulphide ion corresponds to the consumption of two oxygen molecules. The concept of "negative oxygen" (Fonselius, 1969; 1981) is based on this reaction, and multiplication with 2 of the H_2S value gives the "negative" O_2. This process was parameterized by allowing the dynamical coexistence of oxygen and HS^- in the sediments and in the water column (in the model "reduction equivalents" $K^{(6)}$ and $N^{(6)}$, respectively), and the molecular diffusion of reduction equivalents at the water-sediment interface. Therefore, the absolute oxygen amount (and hence the redox conditions of the system) is given by the actual oxygen concentration minus the concentration of reduction equivalents multiplied by the stoichiometric factor 2. In presence of oxygen, reduction equivalents are again reoxidized to sulphate with a fast first-order reaction (see Appendix A.5.2 and

B.7.6).

The other important process concerning the nitrogen cycle in the Baltic Sea is nitrogen fixation by cyanobacteria. The attention toward this group has been raised especially because the nitrogen budgets for the basin could not be closed without the introduction of this additional source of nitrate (Wulff *et al.*, 1998). Nitrogen fixation has not been introduced in the present implementation of the model, because a major concern was to analyze the model behavior with the generic implementation that was already applied to other areas. Nevertheless, results will show that during summertime there is an underestimation of the primary producer activity, as it is derived from the indirect signals of the oxygen oversaturation and the nutrient depletion. This discrepancy might be due to the absence of this important biological group, and the possible implications are further discussed in Sections 4.4.3 and 4.7.

4.4. Discussion of model results and comparison with observations

BORNHOLM and GOTLAND have been integrated from the 1st January 1979 to the 1st January 1991, and the results have been stored as daily averages. In the following sections model results will be compared with the corresponding independent data extracted from BED. The compared variables are: temperature (degrees Celsius), salinity (psu), phosphate (mmol P m^{-3}), nitrate (sum of nitrite and nitrate, mmol N m^{-3}), ammonium (mmol N m^{-3}), silicate (mmol Si m^{-3}) and oxygen. Percentage of oxygen saturation is used in the interior of the water column instead of dissolved oxygen. It is computed from the observed oxygen, temperature and salinity profiles using the same formulation applied in the model (Weiss, 1970). At the bottom of the water column data and models are compared making use of the “negative oxygen” concept (Fonselius, 1969 and Section 4.3.4) in order to point out any occurrence of anoxic conditions. Thus, the bottom oxygen concentration is given in ml l^{-1}.

The chosen comparison depths are: top (-1.25 m, first level in the BED database), middle and bottom of the water column. The latter are site-dependent, and the mid-column layer has been chosen as the depth where the permanent halocline can be usually found, resulting in -40 m for BORNHOLM and -60 m for GOTLAND. As detailed in Section 4.3.2, the external nutrient loads from rivers and atmosphere have been included as surface boundary conditions. The results from such standard simulations are plotted together with the run without the loads (called BORNHOLM-NoLoads and GOTLAND-NoLoads) in order to analyze the behavior of the Baltic proper in a scenario without any land-derived input. The only external source of nutrients in the latter is the atmospheric deposition, which only affects the N-compounds and has a smaller order of magnitude with respect to the surface pools. Therefore, in this case, the simulations only reflect the internal capabilities of the system to regenerate the initial stocks of nutrients and distribute them throughout the different compartments.

4.4.1. Physical structure of the water column

The long-term behavior of the water column structure is well-described by the one-dimensional approximations, particularly concerning the surface layers. With the aid of the local advection parameterization explained in Section 4.3.3, the model is able to hindcast the development of the observed temperatures at both sites in the layers down to the pycnocline. This happens both at the seasonal time scale as well as for the long term (decadal) time scale, also matching the site-specific variability. The model "hindcastability" generally deteriorates with depth, indicating the decreasing dominance of the surface forcing in determining the water column structure. In such cases, the use of the 1D-V model is still of help in identifying the possible occurrence of horizontal processes at time scales that are comparable with the vertical ones.

BORNHOLM

Figures 4.8 and 4.9 show the results of the BORNHOLM temperature at the three selected levels. At surface, the modelled temperature is in near-perfect agreement with the observations. Also the warming trend in the winter minima from the beginning of 1988 is perfectly matched by the model. Such good results indicate that the empirical formulations used to compute the surface fluxes from the meteorological data are appropriate for this basin, and that the time evolution of the sea surface temperature (SST) is fully determined by surface exchange processes. Deeper in the water column (40 m depth, Figure 4.9a), the heating of the intermediate layers shows a strong interannual variability, which is, to a large extent, well matched by the model. The increase of temperature due to the heat transfer from the surface layers is, in some years, a slow process on the order of months, and the intermediate layers heat up only in middle summer. In other years (1984 and 1987, for instance), there is an abrupt warming in spring with the formation of a plateau and then the occurrence of another peak. Particularly in 1987, the model predicts temperatures higher than the observed ones. This discrepancy can be explained from the simulated time evolution of the bottom temperature depicted in Figure 4.9b, where it is clear that the bottom temperature signal is not driven by the seasonal variability in the surface forcing but rather by the entrainment of saltier waters from the Sound. There are periods in which the bottom waters remain warmer because of the buoyancy flux connected to the presence of denser waters, and this feature lasts throughout more energetic mixing periods as in winter 1986-87. The model completely fails in reproducing the variability of the bottom temperature evolution because it does not consider the horizontal entrainments of saltier waters, highlighting the basin-scale nature of this phenomenon. In the 1D case, the salinity distribution below the pycnocline in BORNHOLM (Figure 4.12a) is completely determined by the relaxation to the climatological long-term profile, except in 1882-83 and 1990 where some strong mixing events penetrate down to the bottom. The use of the parameterization of horizontal advection given in Section 4.3.3 is necessary for maintaining the proper long term dynamical behavior of the water column, but, unfortunately, it is not sufficient to provide the time evolution of the deeper layers observed at this site (HELCOM, 1996).

GOTLAND

As in BORNHOLM, the SST development (Figure 4.10) is well matched by the model, especially in the warming periods, further stressing the importance of the surface exchange fluxes. However, the winter minima predicted by the model are lower than observed. Possibly, the meteorological forcing functions at this site are affected by the low temperature in the northern region because of the coarse data resolution. Indeed, the observed winter SST are comparable with the one at the Bornholm site (Figure 4.8), while the winter air temperature averages are lower (Figures 4.2 and 4.4). The seasonal variability is still visible at the depth of -60 m (Figure 4.11a), and the model is able to pick up most of the signal found in the observations. During some periods, especially in the summers 1983/84, the heat reaching the intermediate layers is not sufficient to increase the temperature to the observed values. Nevertheless, the bottom temperature (Fig. 4.11b) is generally well matched by the model and the slope of the decreasing trend is correctly reproduced. The variability in the bottom water temperature is much less than in BORNHOLM, because the larger distance from the open boundary to the North Sea reduces the influence of the dense water entrainments.

The salinity signal at surface at both locations (Figure 4.12) is prescribed by the boundary conditions and the short time scale of the applied relaxation condition gives a strong constraint to the surface salinity. In the middle levels the action of the restoration process is more evident in GOTLAND, manifesting itself more during the summer stratified periods . Here the effects of the parameterization of the eddy diffusivity discussed in Section 4.3.3 must also be considered. The salinity increase during late summer/autumn is a feature that can be distinguished also in the observations (not shown), but the real dynamics is more intermittent and unsteady. Notwithstanding the absence of sufficient variability, the adopted parameterization is able to maintain a qualitatively correct salinity evolution over the long term, contributing to the stability of the water column. However, the absence of a correct simulation of the inflow events can be a severe limitation to the proper reproduction of the energy fields with which the biology has to cope.

4.4.2. Model hindcasting of the Baltic Proper hydrochemistry

Due to the lack of time-series of direct observations on the relevant biological components in BED, it is required to draw out some information on ecosystem behavior from the available hydrochemical measurements. Nevertheless, the comparison with the experiment without the river nutrient loads allows to discriminate and (within the limit of the model parameterizations) to evaluate the remineralization capacity of the system as a function of the stratification conditions of the water column.

BORNHOLM

Oxygen saturation. The only (indirect) information we have to compare the model behavior with system-level biological activity is oxygen saturation. In Figure 4.13 the modelled oxygen saturation at Bornholm site in the surface layer from the standard run and from the run without the nutrient

river loads are compared with the observations. The model is in good accordance with the data over the full 12 years' period, especially in describing the timing of the oversaturated conditions. This is indirectly a confirmation of the model capabilities to match the seasonality of the production periods and the biological interannual variability in the long term. It also suggests that most of the variability in the data can be explained by the interaction between the seasonal light availability and the other physical forcing functions at surface. An important remark is that there are no clear evidences of autumn oversaturation peaks either in the data (except for 1982-83, 1985 and 1988) and, especially, in the model. However, the frequency of the sampling is too low to extrapolate information regarding the system behavior at these short time scales. The absence of a marked autumn oversaturation in the Arkona and Bornholm basin is also visible in literature data as, for instance, the estimation of the climatological net carbon production derived from oxygen saturation values done by Stigebrandt (1991).

It is difficult to note differences between the two model runs (BORNHOLM and BORNHOLM-NoLoads), although the increased nutrient availability clearly enhances the primary production in BORNHOLM (not shown). This has no consequences for the surface oxygen, because an increased production results in an increase in the consumption as well and in an increased diffusion to the atmosphere, leading to zero net gain in the percentage of the oxygen saturation. The differences between the standard run and the scenario without nutrient loads begin to show deeper in the water column. The comparison with the observations is less satisfactory in the lower layers. Close to the pycnocline (Figure 4.13b), the observed oxygen conditions are characterized by a clear seasonal signal with undersaturation troughs reaching values of 70% or lower, and episodes of oversaturation (especially in 1981 and 1985-88). This interannual variability is not matched by the model, which is indeed capable to capture the presence of a seasonal signal, but the simulated time distribution is always within the range 90%-100%.

The bottom layer (Figure 4.13c) is where BORNHOLM and BORNHOLM-NoLoads simulation results depart the most. The observations are better described by the standard run, although the model cannot simulate the entrainments of more oxygenated waters from the Sound that have a characteristic interannual variability. As explained above, the inclusion of such features is, of course, beyond the limits of this 1D-V implementation. However, the model can identify that portion of the variance that is driven by vertical processes, as for example in 1982-83 and in 1990 (years with the highest mean wind speed looking at the running averages in Figure 4.3). The long-term decrease in the bottom oxygen concentration appears to be explained by the interaction between the hydrodynamics, the local organic matter production/consumption and the nutrient availability. In fact, in the scenario without the river load inclusion, the bottom oxygen reaches a sort of oxic steady state that is just modified by the mixing event of 1990. This indicates that indeed the long-term oxygen conditions of the bottom waters at this site are directly linked to the input of nutrients from the land.

Nitrogen species. One of the aims of this study is also to focus on the biogeochemical cycle of nitrogen but considered in conjunction with all the other cycles of the elements. As detailed in Sec-

tion 4.3.4, oxygen dynamics determine the pathways of nitrogen transformations in marine systems. Figures 4.14 and 4.15 show the comparison between observations and model results for nitrate and ammonium, respectively. The hindcasting of nitrate time distribution is satisfactory at the surface and at the bottom layers, while the model is less capable to simulate the time evolution at the intermediate layer (Figure 4.14b).

The importance of the nutrient loads in establishing the winter concentration maxima is clear when looking at the surface time evolution of nitrate (Figure 4.14a). The experiment BORNHOLM-NoLoads considers only the internal recycling sources of nitrogen, resulting in about half of the observed values, whereas the inclusion of loads in BORNHOLM leads to a more satisfactory agreement between the surface observations and the model results. The spring decay signal due to the phytoplankton bloom appears to be reasonably reproduced at surface, although it is difficult to assess the exact timing of the bloom from just the hydrochemical observations. The observations suggest that nitrate consumption extends to the intermediate layers above the pycnocline, where the seasonal summer depletion is still visible (Figure 4.14b). At this level, the model gives a correct winter replenishment but partially fails in reproducing the summer decay, indicating the absence of some processes in the model formulation. The summer increase simulated by the model is due to the diapycnal diffusive transport of nitrate, which just accumulates there and is not utilized in the model as it appears to be in the observations. A likely explanation for this discrepancy is that phytoplankton growth in the model is not limited by nutrients but by the light availability at this level, and this seems not to be the case in the real system, at least looking at the indirect information extrapolated from the nutrient concentrations. Comparison with observed photosynthetic rates at this depth are therefore necessary for getting a correct estimation of the production processes in order to improve the model hindcasting capability.

Despite the large observed variability, the simulated bottom nitrate is within the range of the observations. This is mainly due to the improvements in the formulation of the nitrogen cycle in the model (Section 4.3.4), as will be shown in Section 4.5 where a comparison with the older ERSEM II parameterization has been done. The observed low nitrate concentrations are clearly due to the increase of organic matter production processes after the input of land-derived nutrients and the subsequent export to the bottom layers. In fact, the scenario without river loads gives a steady increase in the nitrate bottom concentration, which is in contrast with the observations.

The observed ammonium dynamics are poorly described by the model at all the levels (Figure 4.15), although NH_4^+ is difficult to be determined with sufficient accuracy. Therefore, a large part of the discrepancy with observations could be due to the data themselves, although usually measurements tend to overestimate the real concentrations. Ammonium accumulates especially in the intermediate and deeper layers. Analysis of the modeled fluxes shows that the high concentration above the pycnocline is not locally produced but rather is a consequence of the sediment release and the subsequent diffusion to the upper layers. The cause of this discrepancy has apparently to be searched for in the processes occurring at the sediment-water interface. There are two possible

explanations for the accumulation: an excess of production (remineralization) or a lack of consumption/transformation processes. Because the hypoxic conditions prevent ammonium losses via oxidation to nitrate (nitrification), it is hypothesized that the regeneration processes are too effective. Since the run BORNHOLM-NoLoads has a much lower concentration, it can also be argued that most of the ammonium comes from ammonification processes during organic matter decomposition. The high ammonification rate is indeed confirmed by the benthic ammonium flux which is about 5 times larger in the standard run (not shown). A comparison with benthic chamber fluxes might help in determining whether such discrepancy is due to too high N-content in the organic matter reaching the sediments (and thus low utilization/regeneration rates in the surface layers) or rather to an improper simulation of the microbial remineralization activity in the sediments.

Dissolved phosphate. The hindcasting of the observed phosphate time evolution is correctly matched by the model at the Bornholm site (Figure 4.16). The long term variability of the surface concentration is well reproduced by the standard run BORNHOLM (Figure 4.16a), especially in the period 1983-86 where the model is capable to partially capture the observed increase in the winter concentrations. It is interesting to note that this feature is not caused by the external nutrient availability (the run BORNHOLM-NoLoads shows the same behavior) but rather by the internal nutrient regeneration dynamics in combination with the interannual dynamics in the physical conditions. The model hindcasting underestimates the observations in that specific period, although this does not seem to be the case in the other years. During the summer periods the N-limitation controls the uptake of phosphate at surface, and the input of external N is clearly necessary in order to simulate the observed low concentrations. Such a behavior could also be intensified by the nitrification operated by cyanobacteria (process not considered in the model), although it is difficult to clearly separate the contribute of each specific process that determines the evolution of the observed summer nutrient concentrations. The sparse summer observations concerning oxygen oversaturation give some hints of a larger biological activity that would involve an increased uptake of nutrients. However, the origin of such nutrients cannot be clearly identified, especially whether it is from diapycnal diffusion, local regeneration in the euphotic zone or bacterial-mediated nitrification. As reported in the introduction, distinct biomass peaks of cyanobacteria are observed in the Bornholm basin (HELCOM, 1996), although the model seems already capable without any additional nitrification inflow to simulate some of the observed summer variability. The availability of measured nitrification rates (such as in Rahm *et al.*, 2000) in combination with observed primary production rates and the current modelling tool could be of help in understanding the origin and the fate of the inorganic nutrients within the Baltic biogeochemical cycles. With the current information it is only possible to see that the nitrification process is probably not the only closure of the nitrogen cycle in this marine system, but rather one of the components, and only with the comparative analysis of all the nutritional elements as done in this work it is possible to come closer to a comprehensive scientific explanation of the system behavior.

Indeed, the comparative analysis of other components is helpful in understanding some mechanisms of the nutrient cycling. For instance, the above-pycnocline concentration of PO_4 (Figure 4.16b)

has a time evolution that is similar to the nitrate curve (Figure 4.14b). In both the components there is a summer depletion at this level, while the model simulates an overall replenishment of the concentrations due to the diffusive transport from the bottom layers. In the PO_4 curve, such feature is slightly reproduced by the model, indicating that the model is actually capable to give a qualitatively correct estimation of both the remineralization and diffusion fluxes. The fact that both nitrate and ammonium behave differently indicates that there are different mechanisms regulating the cycling of these components around the pycnocline. As already pointed out in the nitrate description, phytoplankton is limited by the light availability during this period, and the euphotic zone does not extend to the intermediate layers, which instead appears to be still active from the point of view of the primary production processes (see also Section 4.4.3). If the background extinction coefficient of the underwater light is decreased (from the standard value of 0.1 to 0.08 m^{-1}, experiment not shown) the curves of the N species concentrations in these layers move towards the observations. Ammonium and nitrogen are consumed by the phytoplankton standing stock that extends more at depth, enlarging the shape of the subsurface maximum. However, the behavior of the phosphate concentration does not change much, because the increased production also increases the inorganic P remineralization, enhanced by the hypoxic summer conditions. Thus the model is able to adjust to the new conditions leading to a better matching with the nutrient observations at this depth, but also shows that this is not the proper mechanism, because the surface summer/autumn production is strongly decreased as a consequence of the shifting of the phytoplankton activity closer to the nutricline location. Therefore, it seems that it is not just a matter of the water optical properties and a larger penetration depth of the light, but rather it is the phytoplankton composition that is probably more adapted to the low light conditions at such depths. Future improvements in the simulation of the underwater light climate and phytoplankton adaptation, also taking into account the dynamical presence of inorganic suspended matter, should be done in order to achieve a better description of such processes.

Dissolved silicate. The dynamics of silicates are shown in Figure 4.17. This nutrient is considered to be non-limiting for diatoms in the Baltic proper, because distinct concentrations remain in the surface layer also during the spring/summer period (HELCOM, 1996). The model accordingly gives no silicate limitation for diatoms, although the diatoms behavior can be strongly controlled by modifying the value of the Michaelis-Menten constant in the regulating factor for silicate (A.14). The value of 3.0 mmol Si m^{-3} is a reasonable estimate in order to get a clear seasonality at surface as shown in Figure 4.17a, and a good agreement with the observations. In addition, these results have been obtained after the introduction of a first-order silicate remineralization term in the water column, as shown in (A.62). This terms needs to be further investigated and supported by measurements of the realistic dissolution rates, but, nevertheless, judging from the model, it seems to be a necessary process for a proper simulation of the near-surface silicate dynamics. In the observation time series, the same increase in the winter observations is visible during the period 1983-86 as in phosphate (Figure 4.16a). In contrast to phosphate, the model is not able to capture this feature for silicate, although a small increase of the winter concentrations is visible in the first years of the integration. The compar-

ison with BORNHOLM-NoLoads again highlights the tight coupling between all the nutrient cycles in the system. In fact, without the inclusion of the river nutrient loads, the surface silicate concentration shows a quite reduced seasonal variability with higher spring/summer values with respect to the standard BORNHOLM simulation, which is clearly more in accordance with the observations.

GOTLAND

The model hindcasting of the surface variables at GOTLAND is quite similar to the one for BORNHOLM. Indeed, apart from the values of the maxima that are lower in the Eastern Gotland Basin, the behavior of the surface hydrochemical components shows the same dynamical features. I have therefore concentrated on those aspects that are peculiar to this area, mostly linked to the more stratified water column conditions (Figure 4.12).

Oxygen saturation. Figure 4.18 shows the oxygen saturation at GOTLAND in the surface, middle and bottom layers (the bottom layer is in units of dissolved oxygen concentration as in BORNHOLM). The same considerations on the lack of a clear autumn oversaturation period valid for BORNHOLM apply also here. In particular, the absence of the small summer peaks is more evident, indicating that the model develops a lower phytoplankton activity. Like in BORNHOLM in the middle layer, the summer low oxygen concentration is underestimated by the model. The combined analysis of such discrepancies would hint at the existence of more complex carbon and nutrient (re)cycling dynamics in the surface and intermediate layers at this site. Probably these processes are regulated by a more efficient microbial web (*sensu* Legendre and Rassoulzadegan, 1995), in which the production of organic matter in the upper layers is counteracted by the microbial decomposition in the lower layers, which in turn sustains the production itself by providing recycled nutrients. The model is partially able to simulate such interactions, but it seems to miss some biological features as for instance, the phytoplankton species adaptation to low light and low nutrients regimes or a more sophisticated preferential recycling. This hypothesis is partially confirmed by looking at the run GOTLAND-NoLoads, where the absence of the summer external inputs of nutrients (although quite small) results in lower oxygen consumption fluxes during this period. The role of nitrifying bacteria might also be important under such stratified conditions and needs to be assessed in future experiments.

An indication of the role of the external inputs in the oxygen dynamics of this site is given by the behavior of the bottom oxygen concentration in the standard experiment GOTLAND and in GOTLAND-NoLoads (Figure 4.18c). Without the inclusion of external nutrient loads, the bottom concentration rapidly increases to oxic conditions. This is in contrast with previous experiments (Vichi *et al.*, 1999) in which the parameterization of the sub-grid turbulent (physical) mixing was done with a simpler method than the one used here (Section 4.3.3). It also indicates that the diapycnal diffusion is a key flux in the determination of the oxic state of the water column, and a good description of this process is essential for a future use of this coupled model for forecasting of the system properties. The inclusion of loads leads to the development of a clear trend, with oxygen being consumed to a

major extent and anoxia propagating in the upper layers. The trend is in good accordance with the observations, although there is a quite relevant interannual variability determined by the horizontal advection of more oxygenated waters that cannot be reproduced with the 1D-V approximation.

Nitrate and other dissolved nutrients. As discussed above, the nitrate dynamics are strongly linked to the redox conditions, therefore it can be expected that the differences between the runs with/without loads are also visible in this component (Figure 4.19). Apart from the surface concentration, where the observations are clearly matched only in the standard run case, and in the middle layer where the scarce amount of observations make the interpretation difficult, it is in the bottom layer where the two runs diverge the most. The characteristic low bottom nitrate concentration found in the area can only be reproduced when sufficient organic carbon is transferred from the productive layers to the bottom ones. If this export flux is reduced as in the case of BORNHOLM-NoLoads, the nitrate concentrations increase due to nitrification in the presence of oxygen of the ammonium regeneration fluxes.

Unfortunately, as in BORNHOLM, the model is not able to obtain the same good results of nitrate in the case of ammonium (not shown). However, the bottom concentration is better reproduced in GOTLAND, with an increase of the NH_4^+ concentrations during the period, as also reported in HELCOM (1996) for the Gotland Deep area. In general, also all the other dissolved nutrients follow the considerations already discussed in the previous section and the results are not given graphically. A special remark should be made for phosphate, because GOTLAND shows an increase in the surface concentration at the end of the simulation while BORNHOLM shows a reduction of the winter maxima. This is probably related to the fact that BORNHOLM has a larger flow of nutrients from the bottom remineralization layers, while in GOTLAND the strong stratification acts as a barrier for the resupply of nitrogen, thus leading to the accumulation of phosphate in the surface layers.

4.4.3. Long-term dynamics of the biological components

There are some interesting differences in the development of the trophic web structures at both the locations, but without specific relevant data, a description of these features would reduce to just a speculative exercise. Nevertheless, a qualitative comparison between selected biological state variables and rates can be useful to investigate how the generic ecological model captures the different characteristics of the two sub-basins. There is indeed a site-dependent behavior of the biology at the two locations, and this is mainly determined by the differences in the meteorological forcing functions (irradiance and wind energy), their interaction with the water column depth and the consequent spatial separation between biological production and consumption processes. The analysis of the differences between BORNHOLM and GOTLAND in the timing of the bloom is an interesting example of this coupled behavior. According to the observations (HELCOM, 1996), the bloom progresses from west to east and from south to north, following the increase in the surface heat fluxes and the establishment of a shallower mixed layer according to the Sverdrup (1953) mechanism, as also suggested by Stigebrandt and Djurfeldt (1996). The model was initially not able to develop this important feature (Vichi

et al., 1999), but the improvement of the physical parameterizations as described in Section 4.3.3 corrected the model behavior, giving the time evolution of the biomasses shown in Figure 4.20 as Chl-*a* surface monthly means. The thermal stratification starts earlier in BORNHOLM and the surface phytoplankton stock begins to increase in late winter, while it is still in a decaying phase at GOTLAND. Chl-*a* at BORNHOLM is generally higher than GOTLAND, both in the spring peaks and over the nitrogen-depleted summer period. Since the input fluxes of the external nutrients are the same at both sites, we can state that the different hydrodynamical features are dominant in the determination of the biogeochemical dynamics. However, there is a substantial interannual variability, and in the last years the GOTLAND spring bloom is first comparable with and then larger than in BORNHOLM. This happens after 1987, a peculiar year in which both models shows a single phytoplankton biomass peak from spring to autumn. A possible explanation of this behavior is connected to a reduction of the vertical thermal stratification which enhances the nutrient diffusion through the seasonal thermocline, sustaining the summer primary production (in fact, the annual GPP is larger in this year, as shown below in Figure 4.25a). Data are not sufficient for supporting and analyzing the model predicted rates. The available amount of observations collected in HELCOM (1996) indicate that prior to 1985-86 the phytoplankton biomass in the Bornholm Basin was usually more abundant than in the Eastern Gotland Basin. The decreasing trend is evident particularly in the summer concentrations (HELCOM, 1996). Indeed, after 1985, BORNHOLM develops lower spring peaks, and a small summer decrease is present but not properly significant.

Oxygen fluxes and biological production rates

The only possible comparison can be done with climatological means and comparing with the seasonally average behavior of the model over the simulated period. I have focused especially on the oxygen fluxes and the resulting oxygen saturation, because the latter can be used as a proxy for the biological activity as also done in Stigebrandt (1991). It is, as a first instance, possible to relate the oversaturated conditions to the presence of net biological production processes, and similarly, the undersaturation to the predominance of the oxygen consumption fluxes. Since the model is able to differentiate the production, the consumption and the exchange rates with the atmosphere, it is possible to draw some inferences on how the observed value of the oxygen saturation reflects the biological processes, assuming that we consider reasonable the model estimation estimation of the rates. Figure 4.21 shows the long-term monthly mean values, averaged over the first 20 m, of oxygen saturation, gross (GPP) and net (NPP) primary production (for the latter, the integrated values are computed instead of the means). The top panel also shows the climatological oxygen saturation values over the period 1957-1982 in the Arkona Basin (station BY1) and in the Eastern Gotland (station BY15, both data from Stigebrandt, 1991). The BY1 is located western of the Bornholm Island, and closer to the Belt Sea, therefore the features of this station are more affected by the inflows from the Skagerrak and the Kattegat. The simulated Bornholm site could thus be considered as intermediate between BY1 and BY15. The model shows a mean seasonal cycle that is in good agreement with the climatological observa-

tions, especially if we take into account the limits of station BY1 as an indicator of the Bornholm Basin. The relationship between the two stations is well represented, with BORNHOLM showing an earlier oversaturation, a higher value in GOTLAND in the first summer months and similar decaying curves for the two areas in autumn. Stigebrandt (1991), has derived an estimation of the NPP using the climatological data by means of considerations on the net oxygen production flux and the exchange through the air-sea interface parameterized as also done here in the HiROPE model (C.4.4). With such method, the estimated NPP is higher in BY15 than in BY1, according to the evolution of the oversaturation, although in contrast with the knowledge on the system behavior (HELCOM, 1996). This discrepancy was explained by the author with the upwelling of undersaturated waters at BY1. However, with the aid of the model, it is possible to show that the higher oversaturation in the Eastern Gotland Basin is consistent with an inverse relationship in the gross production rates (Figure 4.21b). Actually, this surplus of oxygen at GOTLAND is determined by the difference in the diffusive flux across the pycnocline. This flux is stronger in BORNHOLM for two reasons: (1) its weaker stratification and (2) the larger oxygen consumption rates below the euphotic zone due to the larger amount of the sinking organic matter. Nevertheless, even if the model-computed values of GPP in the first 20 m are consistent with the current findings (Stigebrandt, 1991; Stigebrandt and Wulff, 1987; HELCOM, 1996), the resulting NPP computed subtracting the ecosystem respiration is much lower than expected and with comparable values at both sites (Figure 4.21c). The integrated value of NPP is an estimation of the export of carbon out of the photic layer (Platt *et al*., 1989), therefore the model is probably underestimating this flux, which could result in an exacerbation of the currently hindcasted hypoxic/anoxic conditions in the bottom layers of BORNHOLM and GOTLAND shown in the previous sections.

Phytoplankton group distribution

The indications of a lower production activity in the model are more evident during summertime. Both the oxygen oversaturation values and the low nutrient concentrations from the BED data in the surface layers, together with some observations of the presence of a summer GPP peak (HELCOM, 1996), suggest that the phytoplankton standing stocks are more abundant than the values simulated by the model. Part of this discrepancy can be explained by an improper parameterization of the light availability (or phytoplankton adaptation to low light) in the sub-surface layers, as discussed in Section 4.4.2. The monthly surface mean values of the phytoplankton species distribution over the investigated period are shown in Figure 4.22. The time evolution and overall distribution is similar at both sites, with a spring bloom mainly composed of diatoms and flagellates. In BORNHOLM, the model also shows a small presence of dinoflagellates. It is important to remember that, due to the absence of carbonate dynamics in the model, the functional separation between generic autotrophic flagellates and dinoflagellates is not that sharp, because the main differences just lie in the potential growth rates (which are higher for the smaller flagellates), and the predation rates (which are lower for dinoflagellates, again owing to their larger size). Therefore, flagellates can be considered as smaller

dinoflagellates, and dinoflagellates could also describe the functional dynamics of larger flagellates or even toxic/inedible species that develop such mechanisms as strategical chemical-defense. An interesting finding is that the summertime biomass can be maintained only by including such a functional group (state variable $P_i^{(4)}$ in the model). This could also be an indication of the need of including cyanobacteria, that are actually the most abundant summer group in the Bornholm Basin, although the rather diverse phytoplankton community found in this period in Gotland complicates the choice of the generic functional grouping. So far, model results suggest that a sufficient condition for the summer dominance of a specific phytoplankton group is a combination of slow growth rates and low predation rates, which is the parameterized functional strategy of group $P_i^{(4)}$ in the model. Further investigation are needed in order to analyze the possible behavior of cyanobacteria functionalities, although in that case it is expected that the predation rates by heterotrophic flagellates would play a major role in controlling the abundance dynamics of this group.

As discussed in Section 4.2, the observed climatological autumn peaks in both the basins are mainly composed of diatoms, with a small presence of flagellates. The model (Figure 4.22) instead shows a dominance of dinoflagellates at the surface (consequence of the summer growth and of the low predation rates) and a small recovery of diatoms (especially in the sub-surface layers, not shown). This discrepancy could be explained again by the broad ecological significance implemented in the parameterization of dinoflagellates. When nutrients become available in the beginning of autumn, this group has attained a large standing stock, which partially outcompetes the diatom development. Further sensitivity simulations are needed for clarifying the role of the summer species in combination with the hydrodynamical regime shift in autumn.

In addition, the role of picophytoplankton should also be investigated with major details and with the aid of some specific observations. Model results (Figure 4.22) show a strong persistency of this group under almost all seasonal conditions because of the competitive ecological functionalities parameterized in the model (fast growth rates and only one predator, the heterotrophic flagellates). This behavior needs to be supported by more accurate information.

4.5. Assessment of the hindcasting skill

The previous sections have shown that the present implementation of the HiROPE model in the Baltic proper is able to capture a reasonable portion of the variability observed in the system. Clearly, model results are dependent on the imposed boundary conditions (nutrient loads, meteorological forcing functions, etc.), and it is rather important to know how strong this dependency is, and what kind of predictability error we can expect if such information has further errors that add to the existing model error. First of all, it is important to assess, as objectively as possible, the hindcasting skill of the model with respect to the available observations, and to evaluate the model performance on the various aspects of the ecosystem that the model tries to reproduce. Afterwards, in the next section, the effect of the imposition of different meteorological boundary conditions has been assessed by means

of twin experiments, with the aim of studying the associated sensitivity of the model components.

A visual comparison of model results has already been done in Section 4.4. Though it is helpful to do a direct model-to-data graphical analysis of the possible misfits in order to understand the overall behavior of the model over the simulation period, it is difficult to asses whether the model has a significant predictability ("hindcastability" would be more appropriate). The misfit measure has been estimated by means of the root-mean-square (RMS) difference or error between the model results and the observations ("the model error"). This measure is generally applied in geophysical sciences, and here two variants have been used:

$$RMSE_n = \left[\frac{1}{n} \sum_{i=1}^{n} (\phi_i - \phi_i^o)^2 \right]^{\frac{1}{2}} \tag{4.6}$$

$$nRMSE_n = \left[\frac{1}{n} \sum_{i=1}^{n} \left(\frac{\phi_i - \phi_i^o}{\phi_i^o} \right)^2 \right]^{\frac{1}{2}} \tag{4.7}$$

where $n = 1, \cdots, N$ is the index counting the number of observations, ϕ_i^o represents the observed value, and ϕ_i indicates the value of the corresponding model state variable taken at the the same time and (vertical) location of the observation. Equation (4.7) is a normalized version of (4.6). The analyzed pairs of model variable results (daily means) and observations concern the timeseries of temperature, oxygen and nitrate at the surface.

Nitrate has also been specifically analyzed at the bottom in order to show how important is the correct parameterization of the denitrification processes (explained in detail in Section 4.3.4) for a correct simulation of the observed bottom values, and more in general, of the overall cycle of nitrogen in the system. The fundamentals of the parameterization used in this work are the introduction of improved denitrification processes (both in the water column and in the sediments) that are coupled with the bacterial metabolism at low oxygen concentrations. Figure 4.23 shows the predictability RMS errors for nitrate at the surface and at the bottom for the standard simulation run compared with a simulation that uses the uncoupled parameterization (the standard ERSEM II formulation). In the latter, the consumption of nitrate through denitrification is parameterized as a first-order term only dependent on the nitrate concentration through a (best-fitted) constant specific consumption rate. With the improved parameterization, the model is able to control the increase of the predictability error after the first 6 years of the integration, whereas the uncoupled parameterization gives a clear divergence from the observations after that period. It is not possible to control the error by tweaking the constant specific denitrification rate or introducing an oxygen-dependent regulating factor, because denitrification is actually non-linearly related both to the substrate availability and to the redox potential. Therefore, only the introduction of the coupling with the bacterial activity appears to give the proper estimation of the consumption rates, at least according to the time evolution of the observed concentrations, although it is further necessary to verify the rates computed by the model with direct measurements.

Concerning the behavior of the other model variables with respect to the observations, it can be shown that the model is generally able to keep the hindcasting error within reasonable values. Nevertheless, I think it is necessary to point out that the methods used to "objectively" analyze the model performances against the observations are, in the case of biogeochemical components, not as objective as for the hydrodynamical variables in general. To give an example, the comparison with the observed concentrations of nutrients can be very bad in terms of RMSE, but the model behavior as a system can still be appropriate. This particularly happens in the case of the hindcasting of non-limiting nutrients. If the model gives a large RMSE for silicate (considered to be non-limiting in the Baltic), this discrepancy could be of less relevance than a small absolute RMSE during the late spring period in the case of nitrate (Evans, 1995). This is the main reason why both the absolute and normalized RMS in (4.6) and (4.7) have been introduced. Only by looking at both the measures, and knowing some general aspects of the biological system behavior, it is possible to extract sensible information on the model representation of the biological processes.

Figure 4.24, shows the RMSE for the SST, oxygen saturation and nitrate, respectively, in the near-surface layer both for GOTLAND and BORNHOLM. The fourth panel presents the normalized RMS errors for the same variables, but focusing on the BORNHOLM model for which more observations are available. As already presented in Figures 4.8 and 4.10, the hindcasting of the SST is very good at both the sites, and the RMSE is constrained around 1ºC after the initial divergence period. The initial physical state of the water column is not much important in the evolution of the RMSE. The shape of the RMSE curves in the first 2 years of the integration is dependent on the initial values, but in the longer term, the convergence value is the same for different initial conditions. As expected, this is not valid in the bottom layers below the pycnocline, especially in the deeper Gotland basin (not shown), where the lower exchanges with the surface layers and the dynamical limitations of the 1D-V implementation give more importance to the initial state of the water column. A similar behavior in the RMSE evolution is observed in the case of oxygen saturation (Figure 4.24b), for which the model shows a significant predictability. The average model error is kept below 10% of saturation, and the initial divergence in GOTLAND is fast recovered by the internal dynamics and the adjustment with the external forcing functions. The surface dynamics of oxygen are thus well captured by the model, also hinting to a reasonable representation of the carbon transformation fluxes to which oxygen dynamics are linked at the system level.

The RMSE for nitrate at surface (Figure 4.24c) has been already partially discussed for BORNHOLM in Figure 4.23. Here the comparison with GOTLAND is shown, where it is visible how the model is able to recover an inappropriate initialization of the water column nitrate content. In contrast with BORNHOLM, the initial values for GOTLAND have been obtained from a 12 year average of the January observations, because no measurements were available for January 1979. Within the first year, the internal nitrate dynamics are able to effect a redistribution of the unbalanced quantities, reducing the discrepancy with observations. However, the predictability error at both sites still increases with time, even if it appears to reach an asymptotic value of 1 mmol m^{-3} in the last 4 years. Now,

this makes it necessary to consider the biological significance of a RMS predictability error of such an entity. If the discrepancy occurs during the winter period, when high concentrations are found in the system, then the direct consequences to the model behavior would be of less relevance. Thus, it is also convenient to study the normalized RMSE, in order to extend the spectrum of information. In Figure 4.24d, we see that the nRMSE for nitrate is above 1 already from the third year of integration and with a constant increase. This indicates that, although the mean RMS difference is apparently low, when scaled with the observed value, the obtained normalized value indicates a worse model performance in the case of nitrate. The largest increases in the RMSE occur every year mainly during the spring production phase, when nitrate is consumed at a fast rate. This is an indication that the model is not exactly matching the timing of the bloom, as can also be argued from Figure 4.14. However, this relative error is apparently compensated during other periods, leading to the relatively small absolute long-term RMSE.

The same is not completely valid for the other considered variables such as SST and oxygen saturation. In the case of oxygen, the nRMSE is very small, around 0.1, and this value is maintained throughout the entire simulation. The nRMSE for SST shows an initial increase, and afterwards the index steadily decreases to 0.5. There are two more sudden divergences in winter 1982 and 1985. Such high values are usually linked to the model misfit of the observed SST during cold conditions. This is dynamically less important than in the previously discussed nitrate case, because the surface layers are completely mixed and the contribution to the density difference caused by this misfit is not much effective.

Thus, the use of both RMS estimators has proven to give more insights into the model behavior against the observations. Unfortunately, the lack of more biologically significant measurements (biomasses, Chl-*a*, etc.) hampers a thorough assessment of the model capability. Nevertheless, the good representation of the surface oxygen dynamics, indicate that the interaction between the exchange of oxygen with the atmosphere and the biological production/consumption processes could be properly represented by the model, even if it is necessary in the future to validate the model rates with measured ecosystem respiration and primary production rates when they will be made available at the proper time frequencies.

4.6. Influence of the meteorological forcing functions on the predictability of the ecosystem behavior

The aim of this section is to understand to which extent the time scales of the imposed external forcing functions affect the behavior of the modeled ecosystem components. Specifically, the surface meteorological data have been applied with different frequencies to a series of twin experiments, and the response of the biotic components has been analyzed with respect to the standard simulations described in the previous sections.

The underlying hypothesis is that the model parameterization of the turbulent energy in the wa-

ter column is, on the one hand, sufficient to provide an acceptable description of the sub-grid scale hydrodynamics, but, on the other hand, it could be insufficient at the scales of the biological functional processes, for instance because the time-averaging of the short mixing events could decrease the nutrient resupply during stratified periods. This could lead to a generally reduced activity of the biological components, mainly in the primary producers' functional groups, and have consequences in the longer scale dynamics of the whole ecosystem.

Previous modelling experiments have performed in order to study such hypotheses on an annual basis with one-dimensional (only) physical and coupled physical/biogeochemical models (Ridderinkhof, 1992; Ruardij *et al*., 1997; Lacroix and Nival, 1998). These simulations have two opposite approaches: a) a less detailed but still realistic representation of the physics (mixed layer model) and a comprehensive description of the biogeochemical processes, as in Ruardij *et al*. (1997); or b) a simple biological model (of the type NPZD) coupled with a realistic high-resolution simulation of the hydrodynamics as in Lacroix and Nival (1998). Lacroix and Nival concluded that the use of monthly and daily means of wind intensity (intended as wind energy) results in reduced phytoplanktonic biomass and delayed blooms at an oligotrophic modelling site in the Ligurian Sea (western Mediterranean) in comparison to a standard simulation with 3-hourly values. If the solar radiation is averaged, both biomass and gross production are higher than in the standard simulation. In contrast, Ruardij *et al*., by applying a mixed-layer model coupled with ERSEM II at a North Sea site, found that the forcing with weekly averaged wind energy has no significant effect on the modeled total primary production in the water column, although the depth of the surface mixed layer is indeed reduced. However, they also showed that the sequence and presence of incidental small-scale events, which determines the interannual signal of the wind climate, have an impact on the timing of the onset and maximal concentration of the spring bloom in the North Sea.

Therefore, there are some model indications that the small-scale meteorological and (thus) hydrodynamical variability induces an enhanced response of the biological processes, and also that this response can differ depending on the specific model implementations and assumptions. In this study, I have applied a similar experimental setup, but extend the analysis to the influence of the small-scale perturbations on ecosystem behavior at the longer time scales (decadal). Moreover, the HiROPE coupled model has comparable levels of detail both in the hydrodynamics and in the implementation of the biogeochemical processes, completing the spectrum of cases explored by the other authors. The analysis presented here is for the BORNHOLM model, but similar conclusions are valid for the GOTLAND model as well.

Since phytoplankton reacted differently to changes in wind and irradiance timeseries (Lacroix and Nival, 1998), here I have taken the complete approach, decreasing the frequency of all the meteorological data, but making sure that the physical representation of the water column was still in accordance with the observations when applying the low-frequency meteorological timeseries. The experiment with the 3-hourly frequency is considered to be the standard run. For the low-frequency experiments, the wind energy and the other meteorological parameters have been averaged to 6-hourly, daily and

weekly values (simulations RUN6H, RUN1D and RUN1W, respectively). A monthly frequency was not used, because with the derived surface boundary fluxes the model is not able to reasonably reproduce the observed long-term physical dynamics of the water column.

4.6.1. Results and discussion

The response of the biota to the different forcing scenarios has been analyzed using the vertically integrated annual net and gross carbon primary production rates (NPP and GPP, respectively). The NPP is defined as in the previous sections, by computing the difference between GPP and the vertically integrated ecosystem respiration rate. Figure 4.25a shows the magnitude of both terms as annual integrals for the standard BORNHOLM simulation with 3-hourly meteorological forcing functions. The carbon respiration fluxes are generally parameterized to be proportional to the production rates, although some other terms, as for instance the intracellular nutrient-contents, contribute to the activity respiration terms (cfr. Section A.2.3). The net annual carbon production thus has some small interannual variability which is different from GPP (Figure 4.25a).

The assessment of the variation between the low-frequency runs and the standard one has been done by computing the following percentage difference:

$$\eta = \frac{\psi_{3h} - \psi}{\psi_{3h}} \times 100 \tag{4.8}$$

where ψ_{3h} is the timeseries of the integrated annual values (NPP or GPP) from the standard 3-hourly run and ψ is the corresponding value from RUN6H, RUN1D and RUN1W simulations, respectively (Figure 4.25b). The percentage η is always positive except for 1990 in RUN6H and RUN1D, and increases as the frequency of the meteorological forcing decreases. This indicates an overall reduction of the biological activity, whose dynamics is thus linked to the small-scale variability induced by the meteorological boundary conditions.

Moreover, the difference with the standard run is larger in the NPP signal than in the GPP, as shown in Figure 4.25b only for the weekly run (the other runs have analogous behavior). The fact that NPP is reduced more than GPP implies that a “calmer” abiotic environment results in a higher degree of coupling of carbon and nutrient (re)cycling in the euphotic zone, a reduction in export production (NPP is a measure of export; Platt *et al.*, 1988) and reduced benthic-pelagic coupling both in the form of lower sedimentation fluxes and in the diminishment of nutrient fluxes from the benthic system back to the water column. The response of the system to such low-energy conditions is thus a higher retention of its primary production above the pycnocline, while at the same time receiving less nutrients from below to stimulate the production in the euphotic zone. On the contrary, the variability in the physical environment at the shorter time scales enhances the biological activity in the model with a marked non-linear behavior, resulting in the generation of positive feedbacks to the system maintenance itself.

We can also calculate the total long-term production over the period 1979-90 from the annual

values, resulting in relative differences of -6% when decreasing the frequency from 3-hourly to 6-hourly, -14% from 3-hourly to daily and -27% in the case of weekly frequency. These are significant, but acceptable differences in the estimation of the total local primary production over such a long integration period, especially when considering the practical errors in the realistic measurements of this rate. However, this discrepancy could be larger for longer integration periods as in the case of climate change studies, and this underestimation could become important in the overall calculation of the carbon and nutrient budgets.

It is also interesting to analyze the discrepancy between the different forcing scenarios at the seasonal scale by means of objective measures as the ones defined in Section 4.5. Another additional form of the root-mean-square (RMS) differences defined in (4.6) and (4.7) has been used as a measure of the model trajectories deviation. Since the result matrices have the same dimensions for each run, I have applied the following vectorial formula:

$$nRMS_i = \frac{1}{\bar{\phi}_i^{3h}} \left[\frac{1}{k} \left(\vec{\phi}_i^{3h} - \vec{\phi}_i \right)^T \left(\vec{\phi}_i^{3h} - \vec{\phi}_i \right) \right]^{\frac{1}{2}} \tag{4.9}$$

where k is the number of elements in the ordered data vector (number of vertical levels), i the discrete time index, $\vec{\phi}_i^{3h}$ indicates the state variable vector from the standard model with the 3-hourly frequency, $\bar{\phi}_i^{3h}$ is the standard run long-term mean, and $\vec{\phi}_i$ represents the corresponding variable from the forcing function scenarios. This measure has been applied to the result matrices of temperature, nitrate, Chl-*a* and GPP (Figures 4.26 and 4.27). The temperature simulation (Figure 4.26a) shows differences below 0.3 for most of the integration period, indicating that the averaging of the meteorological variability up to the daily scale is still sufficient to provide a large portion of the signals found in the standard run. There is a seasonal variability with higher winter values in all the experiments. This seasonality is a steady signal in RUN6H and RUN1D, but it shows additional frequencies in RUN1W. Moreover, there are some years in which the RMS shows a substantial increase (1982 and 1985-87), and this is particularly evident in RUN1W, where the high discrepancy in winter 1987 lasts throughout the whole year. Such years are characterized by a reduced wind velocity (Figure 4.3), when the importance of smaller scale events in forcing the dynamics of the water column is particularly enhanced.

The threshold value of 0.3 mentioned above is an arbitrary choice, but appears reasonable when compared to the results of the biogeochemical variables. In the case of nitrate (Figure 4.26b), the shape of the RMS curves shows a larger non-linear variability between the different simulations. Apart from the peak in 1990, RUN6H has a small RMS for the whole simulation period, while both RUN1D and RUN1W show a strong interannual signal with marked seasonal oscillations and peaks above 0.5. The seasonal RMS highs are centered in the summer period, indicating that the reduced meteorological variability maintains a more steadily-stratified water column, generally damping the diapycnal transport of nutrients induced by the smaller scale wind events. The consequences of such a lower nutrient availability are reflected in the more biologically relevant variables such as Chl-a and GPP (Figure 4.27). In RUN6H this effect generates small acceptable RMS values in both components,

while, especially in RUN1W, the RMS during summer is always larger than 0.5 reaching values close to 1 in the case of the GPP (Figure 4.27b) over the years with low wind intensity mentioned above. It is also interesting to note that although the RUN1W GPP rates show a larger discrepancy with respect to the standard run, the phytoplankton biomass expressed as Chl-*a* shows a lower misfit, although the two components are not always linearly related, as indicated for instance by the inverse correlation in 1984 and 1988.

The combined effect of low-frequency wind variability and irradiance leads to a clear overall reduction of the biological activity. Of course, with only the partial assessment of the model performances done in the previous sections, it is not possible to state that the standard run is closer to the realistic behavior than the simulations with the averaged forcing functions. Nevertheless, the sensitivity of the biological components to these boundary conditions is high, and the current results suggest that coupled physical/biogeochemical models underestimate the biological rates when using an averaged description (in time, and probably in space as well) of the hydrodynamical features. Model estimation of primary production should therefore be performed by applying the highest available time resolution in the surface forcing functions, in order to take into account the smallest achievable time-scale variability in the hydrodynamics.

4.7. Conclusions

The first overall conclusion is that the one-dimensional coupled approach of HiROPE is able to explain a large portion of the variance observed in the investigated areas of the Baltic, particularly in the surface layers where the bulk of the organic matter production processes occur. The good agreement with the observed surface temperature indicates that the calculated heat and momentum fluxes are correct, and that the vertical mixing processes above the pycnocline are to some extent properly represented. The high vertical resolution in the upper model layers and the high frequency of the surface forcing functions are considered to be necessary requisites to have a description of the hydrodynamical processes that is suitable for modelling biological dynamics in the Baltic. Comparative analyses of modelled hydrochemical components with respect to observations have shown that the long-term system behavior of the model remains internally consistent and within “likely” boundaries. In particular, the model hindcasting capability has been assessed in Section 4.5 by means of objective measures of model-data (mis)fits. On a decadal time scale, the model error generally presents an initial increase which tends to remain constant after the first three years of the simulation period. The model has skills in reproducing the surface oxygen concentration, which is an indirect measure of the carbon-conversion processes. In fact, the long-term average of the systematic error in the predicted value of oxygen saturation is just a few percentage, and unbalanced initial conditions are fast recovered by the internal model dynamics and the synchronizing effect of the surface forcing functions. On the other hand, the model error for nutrient concentrations shows an overall increase that appears to reach an asymptotic value at the end of the simulated period. In the case of nitrate, which

is considered to be the component limiting the phytoplankton growth in the Baltic, the discrepancy with the observations is particularly enhanced during spring periods, when this nutrient is fast depleted. The biological significance of this error appears to be restricted to the next summer, because the model shows a partial recovery of the misfit during autumn and winter, when nutrient stocks are replenished through vertical convection and external inputs. An appropriate use of data assimilation procedures might help in controlling the model error during such periods, but the experience with complex ecosystem models suggests that data assimilation should be applied and tested in conjunction with multivariate observations of the ecosystem state. In fact, the lack of comparison with more biologically relevant measurements makes a careful interpretation of this analysis necessary, although the used methodology does appear to be a valid tool for testing model skills.

Nevertheless, the improvements in the nitrogen dynamics of ERSEM III with respect to previous model formulations are a partial confirmation that the strategy of including more (although uncertain) interactions among the system components can increase the model skill in reproducing observations. Results have demonstrated that the predictability error is much larger and steady if the denitrification process - one of the major nitrogen sinks in the system - is not connected to the biological oxygen demand that determines the redox conditions in the water column. This is especially true in the sediments, indicating the large impact on the entire system behavior of the benthic-pelagic coupling.

However, the nitrogen cycle needs to be carefully checked against more relevant biological indicators (rates), also to clarify the possible role of nitrifying bacteria. Another aspect that needs to be further investigated is ammonium dynamics and its significance in the model. As shown in Section 4.4.2, ammonium is generally overestimated by the model. This model component is considered to be a proxy for all reduced N-compounds, and urea (up to 50% of excreted N) is not explicitly represented. If 50% of the model state variable $N^{(4)}$ is supposed to be composed of urea, the matching with NH_4^+ observations improves. Indeed, the best comparison with measurements occur in the deeper layers, where most of the reduced nitrogen is only in the form of ammonium. A possible suggested improvement would be to test the introduction of urea as a model state variable and analyze the impact of this supplemental component of the nitrogen cycle.

If we consider the overall behavior at the two implementation sites, we can state that the HiROPE system has shown a remarkable robustness in accommodating the main Baltic ecosystem dynamics. Thus, it is proposed as an auxiliary tool for systems ecologists and biological oceanographers to test and verify biological hypotheses on the system functioning within a dynamical framework capable to reproduce the main coupled physical/biological features of the Baltic.

Concerning the several biological questions posed in the Introduction on the Baltic ecosystem functioning, the model allowed to identify a series of interconnected processes that affect the long-term evolution of the system state. The key processes are organic particle production in surface layers, sedimentation through and regeneration in the water column interior, organic matter decomposition in the bottom layers and, finally, the diapycnal diffusion of remineralized inorganic components. All these elements are tightly coupled to the hydrodynamics, and their interaction is reflected in the oxic

state of the water column. Therefore, it is confirmed that oxygen is an optimal candidate for the indication of system level properties. In fact, the peculiar oxygen conditions during the investigated stagnation period appear to be driven by two main factors: 1) the external nutrient inputs from river discharge, 2) the turbulent transport in the intermediate layers of the water column. Indeed, the timing of the phytoplankton spring blooms and the description of the summer plankton stocks have been improved with respect to observations thanks to the partial amelioration of the turbulent energy fluxes in the water column interior (Section 4.3.3).

Especially the hindcasting of summer dynamics is largely connected to the parameterization of diffusion in a stratified system, but the model suggests that it is not just this physical process that controls the system state. Summer is in fact characterized by two opposite gradients in nutrients and oxygen (except for nitrate in the very deep layers that is consumed via denitrification). The lower layers generally have high nutrient and low oxygen concentrations, and it is the opposite in the surface layers. The diffusive transport through the permanent pycnocline determines the shape of both curves and an increase of these terms results in a double diffusion of both components. Evidences of the presence of a substantial vertical nutrient transport come from the high oxygen saturation observed in the system, which indicates an active phytoplankton standing stock in the surface layers. Moreover, since lower layers are always oxygen-depleted, we can argue that the export of organic matter from surface layers and the oxygen consumption associated to degradation is always sufficient to counteract the downward oxygen diffusive flux. Nevertheless, an increase of diffusive transport in the model result in a substantial oxygenation of bottom waters and only in a slight increase of surface organic production rates. The low production might also be due to light limitation, as discussed in Section 4.4.2, or better to a more efficient light utilization by phytoplankton that is not sufficiently well parameterized in the model. Indeed, nutrient levels in the intermediate layers are higher than observed indicating low utilization rates, but the artificial increase of light penetration depth is still not enough to provide a satisfactory description of the primary producer behavior. Light availability and/or light adaptation seem to be key issues for the phytoplankton dynamics in the area during summertime.

All these results suggest that the Baltic proper, for its permanent stratified conditions, is a site where nutrient and carbon cycling are strongly uncoupled (Thomas *et al.*, 1999; Osterroht and Thomas, 2000), and that there is an efficient preferential recycling of nutrients that maintain large organic matter fluxes towards the bottom layers impoverishing the oxygen conditions. In addition this appears only to happen if an external source of nutrients is provided in the system, as demonstrated by the scenario experiments without the inclusion of river nutrient loads. Therefore, the model gives indications that, even during the investigated stagnation period, the vertical oxygen replenishment would be sufficient to prevent the formation of anoxic conditions. The presence of supplemental nutrient sources stimulates the ecosystem production leading to the enhancement of organic matter fluxes and the oxygen consumption processes.

Model results also hint at a strong dependence of these positive feedbacks of the ecosystem carbon production on the short-term variability induced by surface meteorological forcing functions. Experi-

ments shown in Section 4.6 have given indications that local high-frequency variability in the physical forcing is the driver for much of the observed seasonal and interannual variability. The time-averaging of the meteorological forcing leads to damping of the vertical exchange fluxes with an overall reduction of the biological activity especially of primary producers. The model responds to the short-scale events in the hydrodynamics with a marked non-linear behavior that acts in the direction of generating positive feedbacks. Since observed biogeochemical rates derived from oxygen dynamics considerations appear to be more active than the model predicts, it implies that coupled physical/biogeochemical models underestimate the biological rates when using an averaged description of the hydrodynamical features. The changes in the interannual variability observed in such scenario simulations also indicate that long-term (and perhaps large-scale) variability is the integral of a cascade of variability at the smaller scales. This long-term discrepancy could be larger for integration periods longer than a decade - for instance, in the case of climate change studies - and this underestimation could become important in the predictability of system behavior in terms of carbon and nutrient budgets.

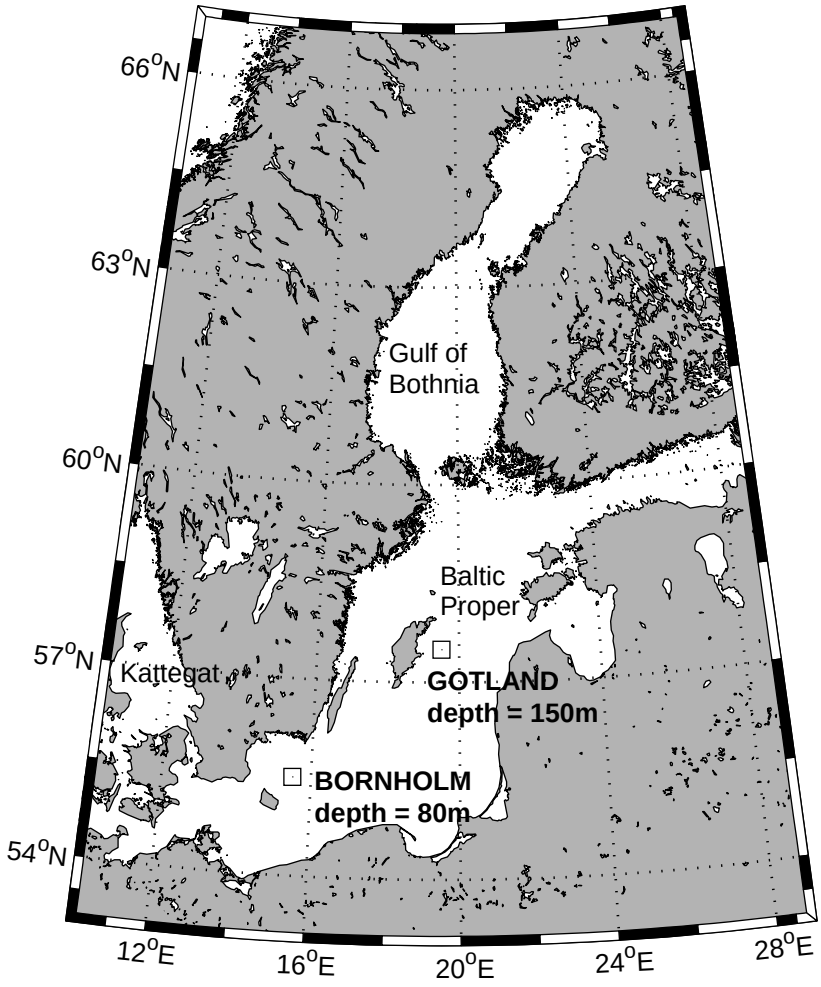

Figure 4.1.: Locations of the 1D-V HiROPE models in the Baltic Proper (map made with the m_map mapping toolbox by R. Paulowicz, http://www2.ocgy.ubc.ca/~rich/map.html).

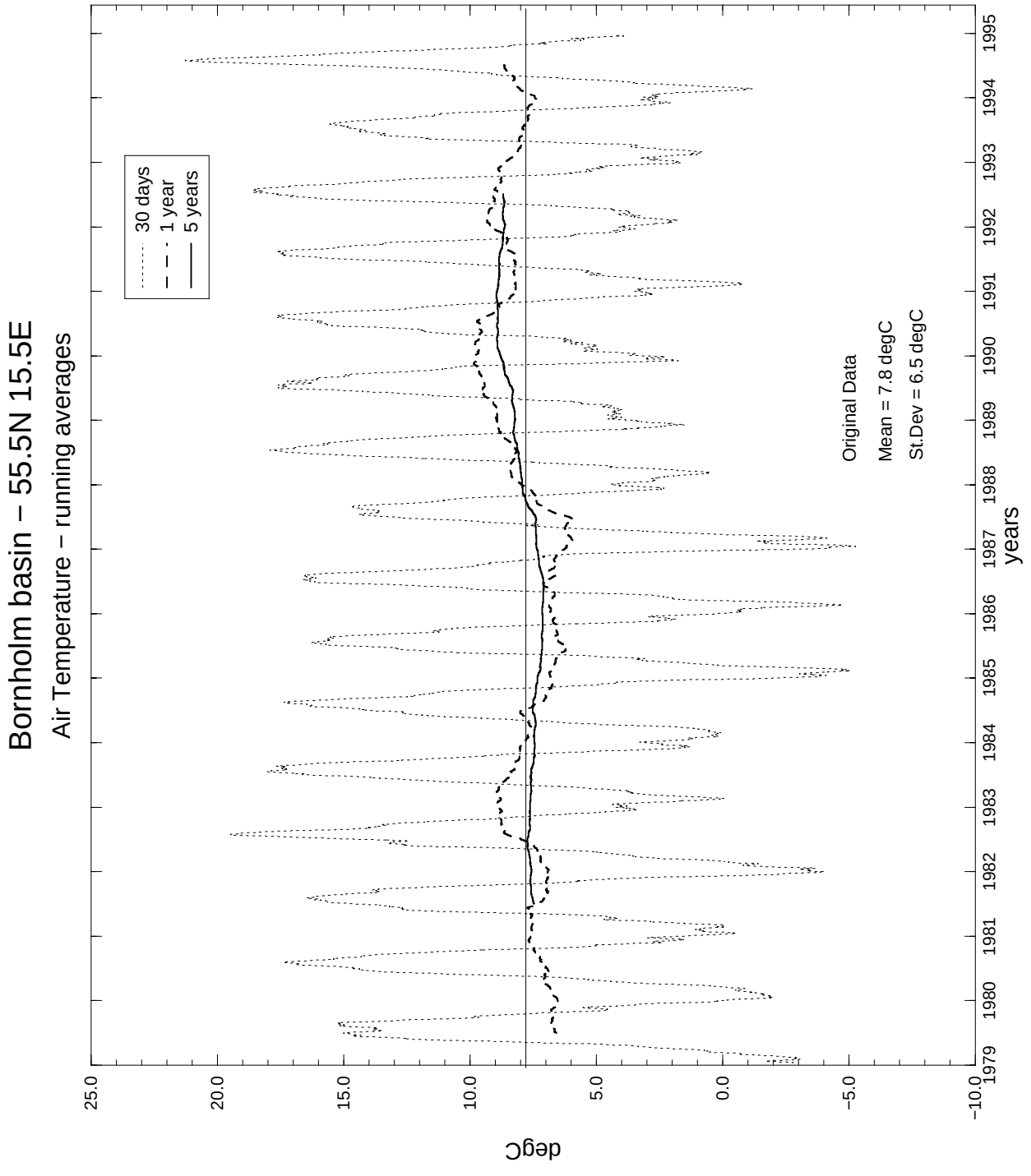

Figure 4.2.: Air temperature in the Bornholm area from SMHI data. Mean and running averages.

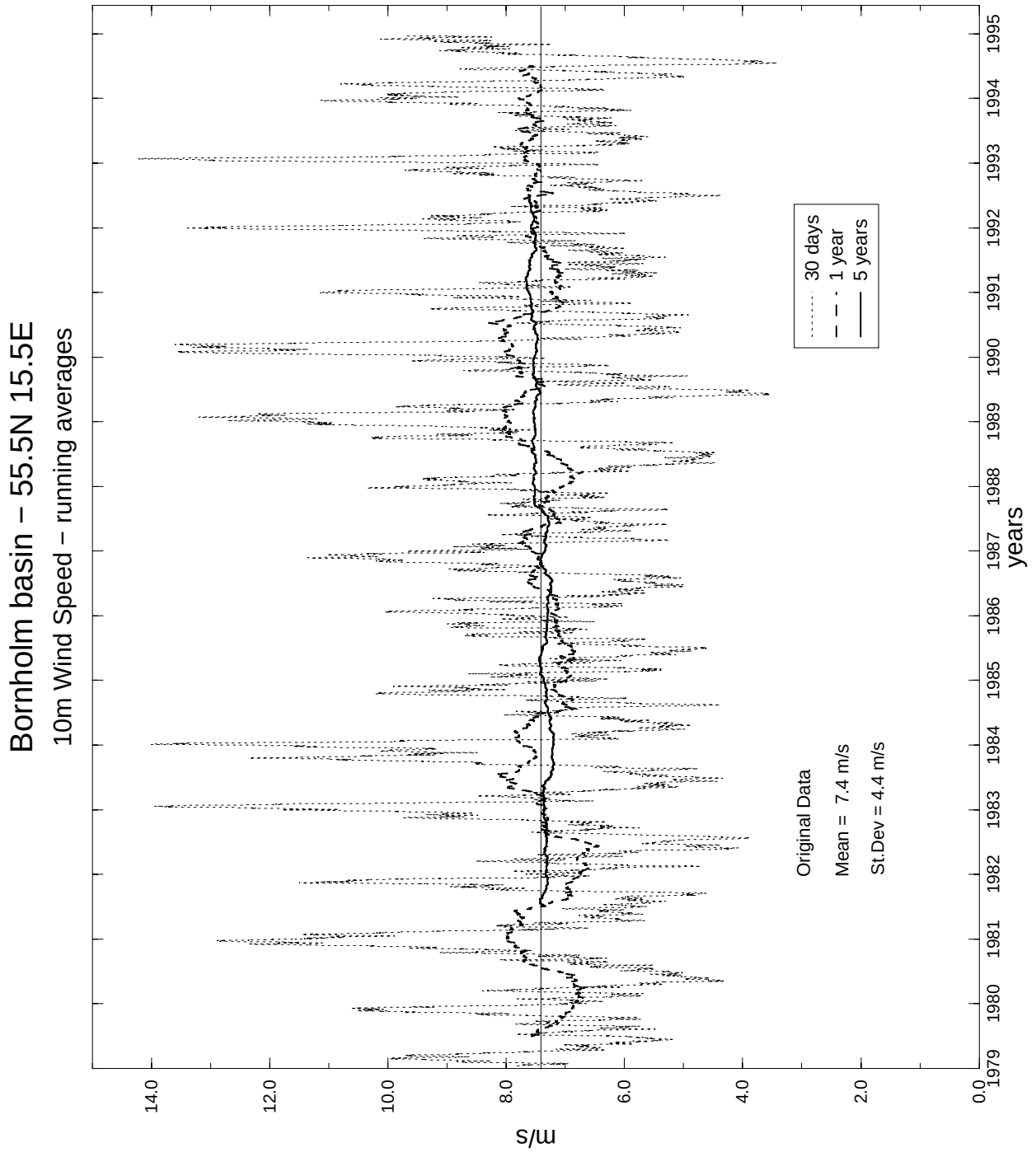

Figure 4.3.: Wind velocity in the Bornholm area from SMHI data. Mean and running averages.

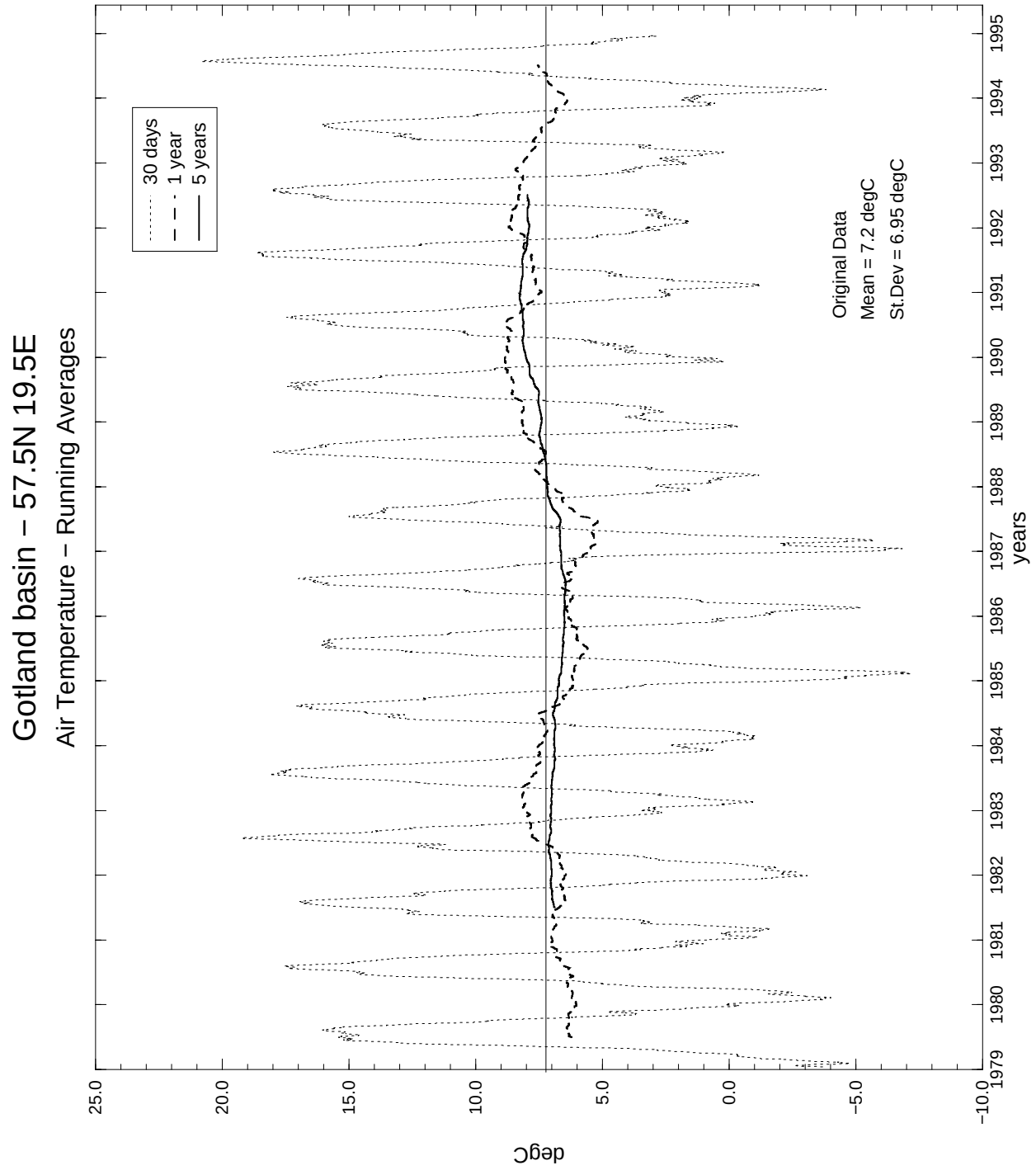

Figure 4.4.: Air temperature in the Eastern Gotland area from SMHI data. Mean and running averages.

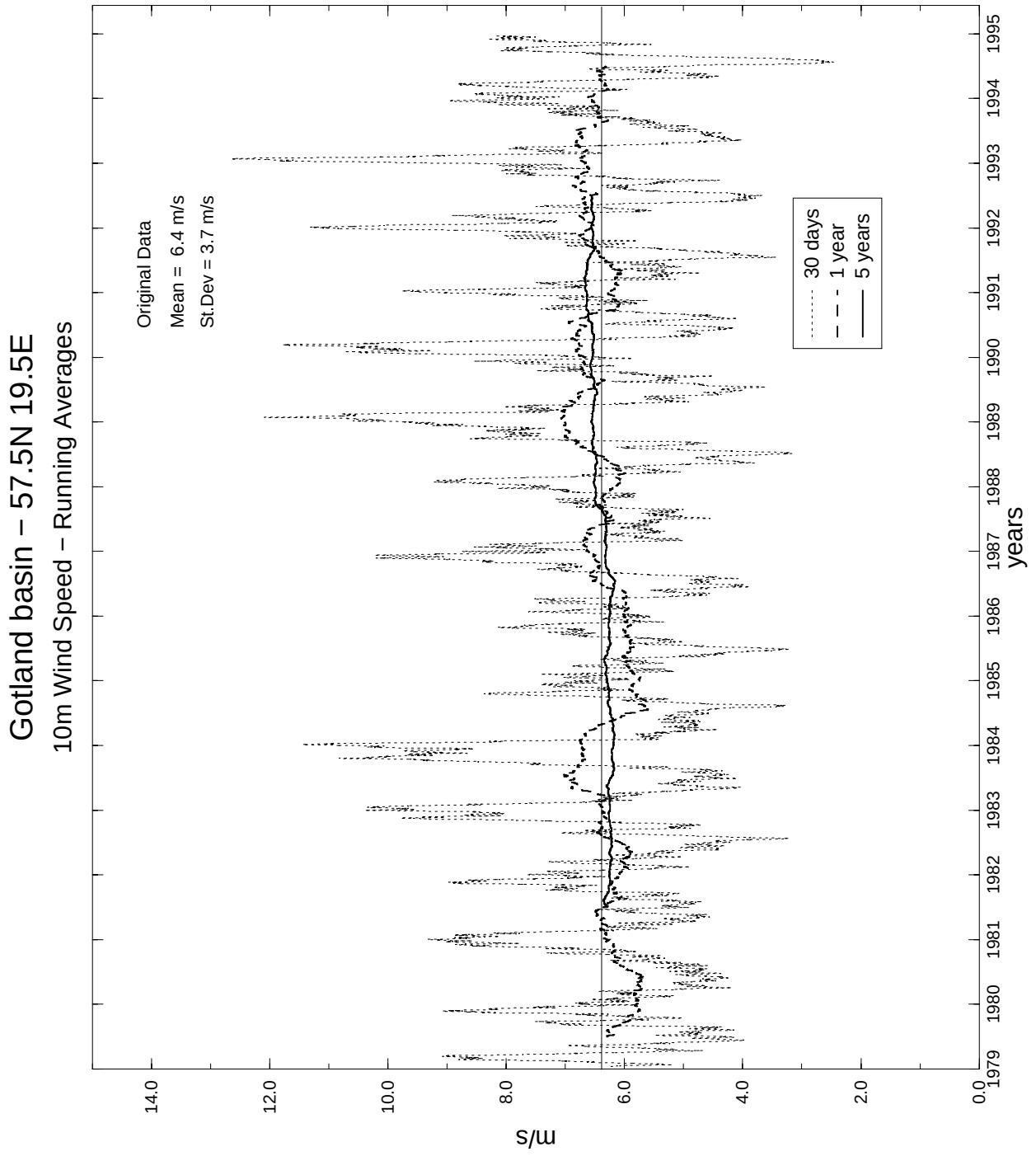

Figure 4.5.: Wind velocity in the Eastern Gotland area from SMHI data. Mean and running averages.

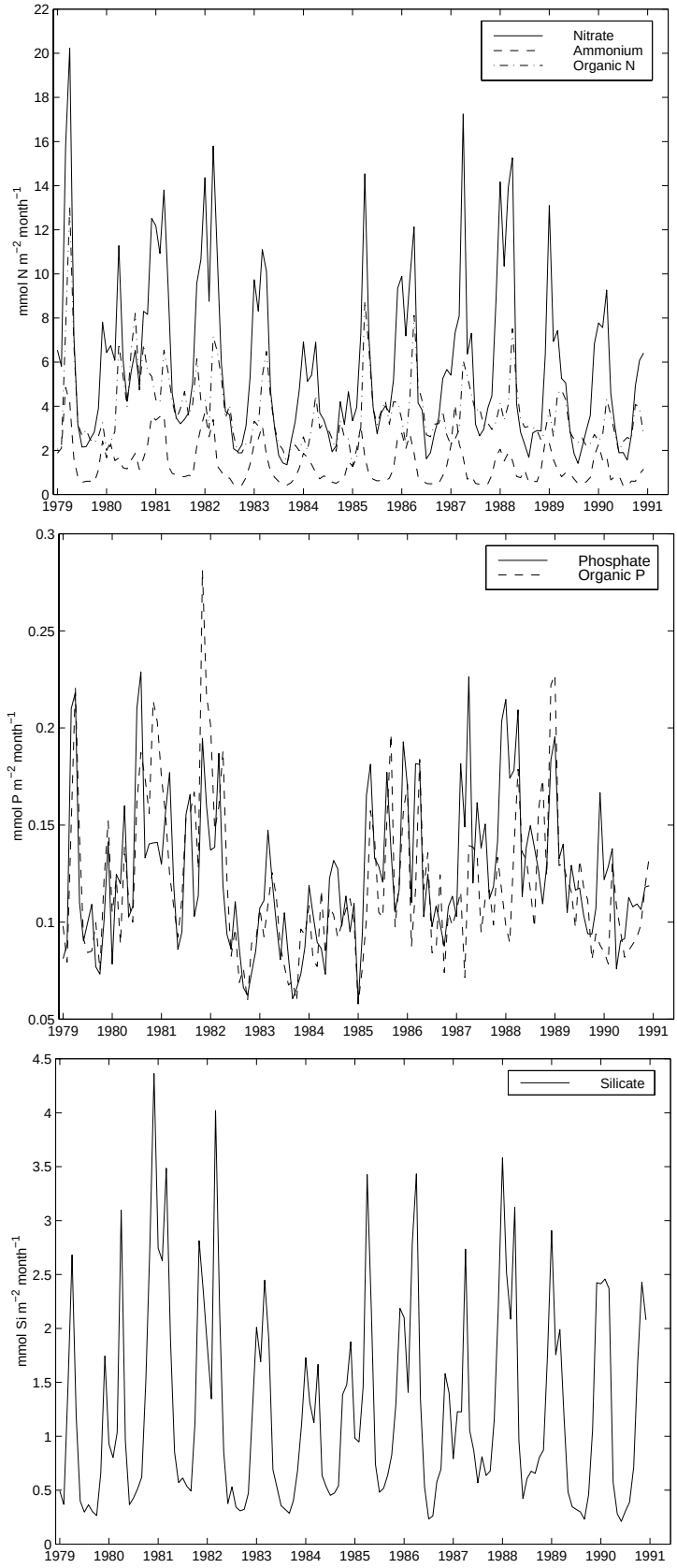

Figure 4.6.: Nitrogen, phosphorus (both organic and inorganic) and silica loads to the Baltic proper.

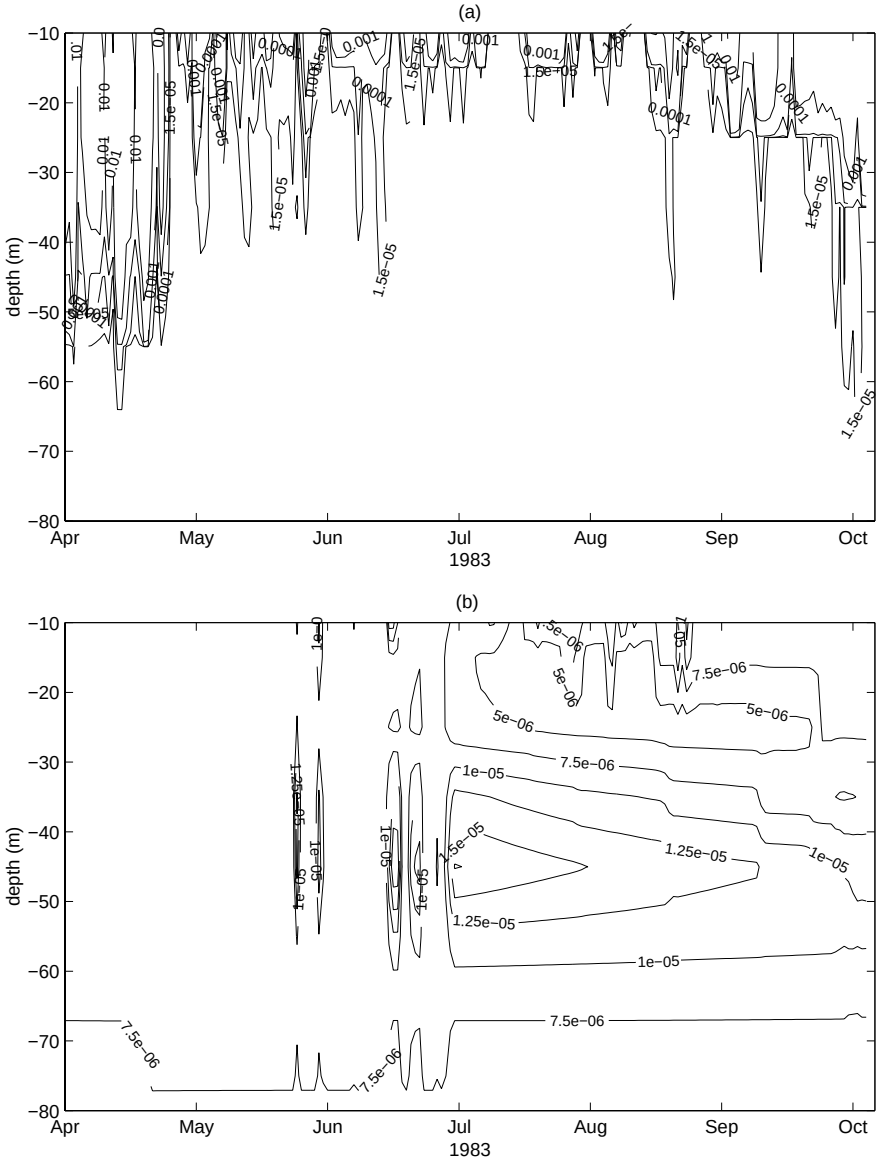

Figure 4.7.: (a) Vertical turbulent diffusivity K_H computed with the M-Y turbulence-closure scheme in GOTLAND (spring-autumn 1983, C.I. = 1.5×10^{-5}, 1.0×10^{-4}, 1.0×10^{-3}, 1.0×10^{-2}). (b) Parameterized diffusivity as the inverse function of N^2 for the same model site and period.

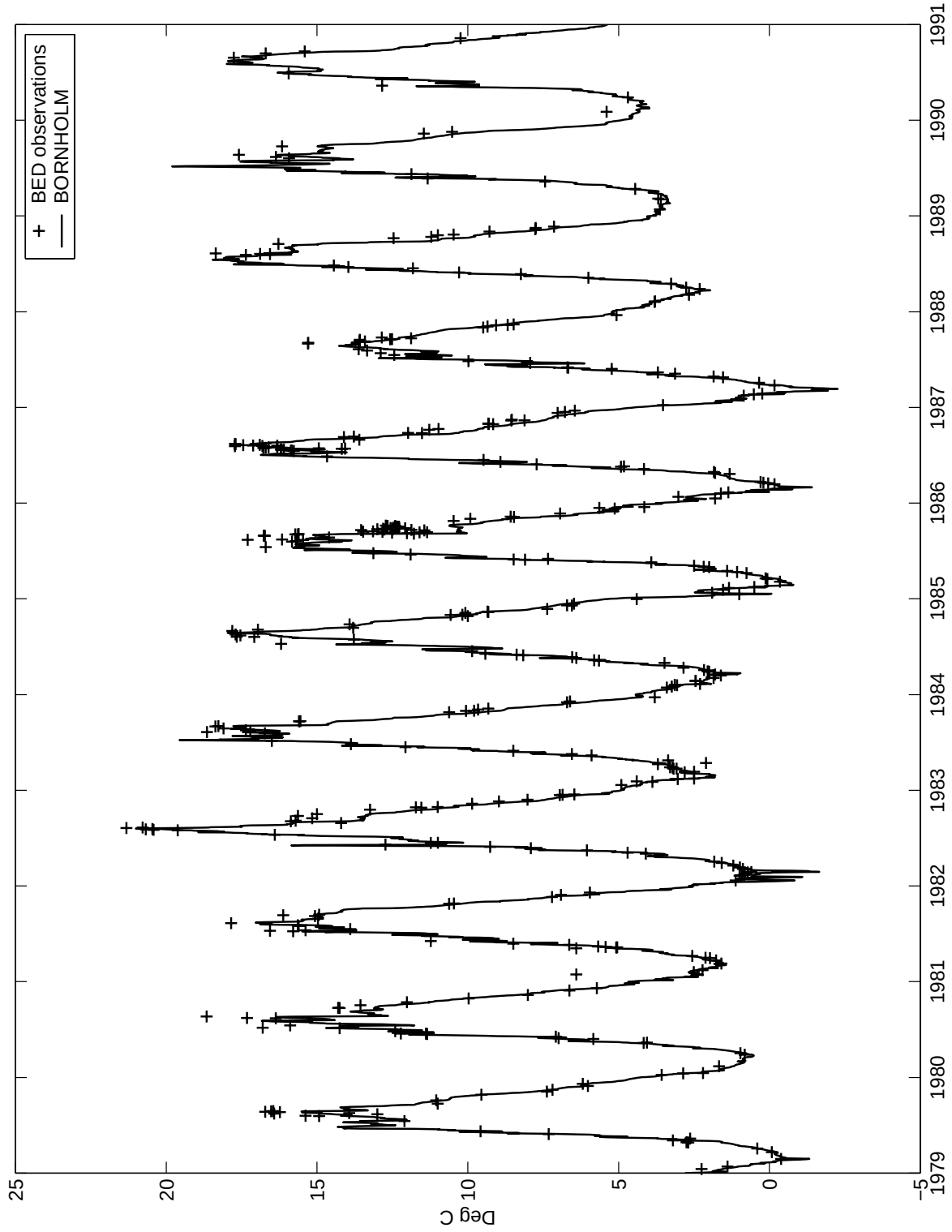

Figure 4.8.: BORNHOLM: near surface temperature. Comparison between BED data and model results.

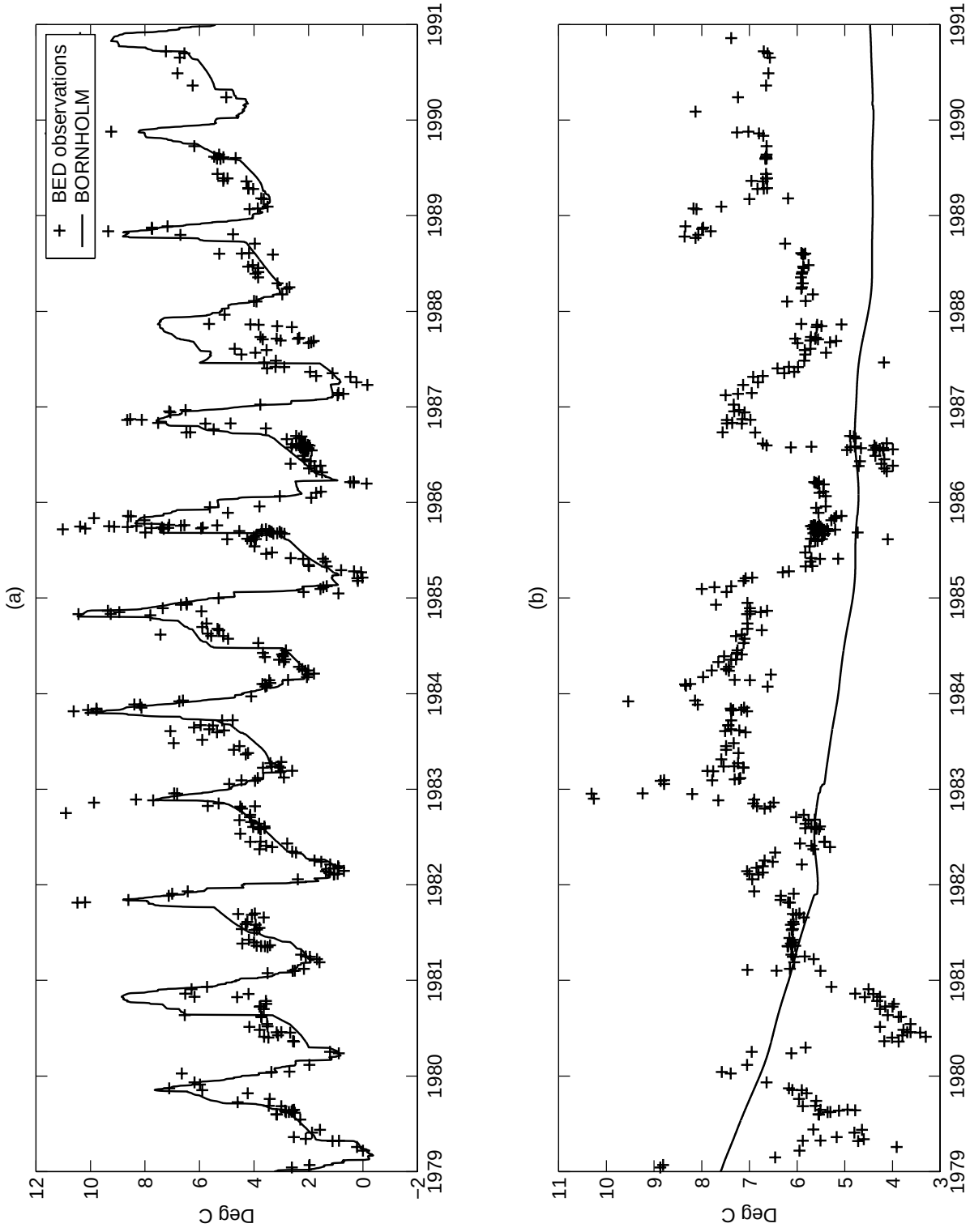

Figure 4.9.: BORNHOLM: temperature at (a) -40 m and (b) at the bottom. Comparison between data and model results.

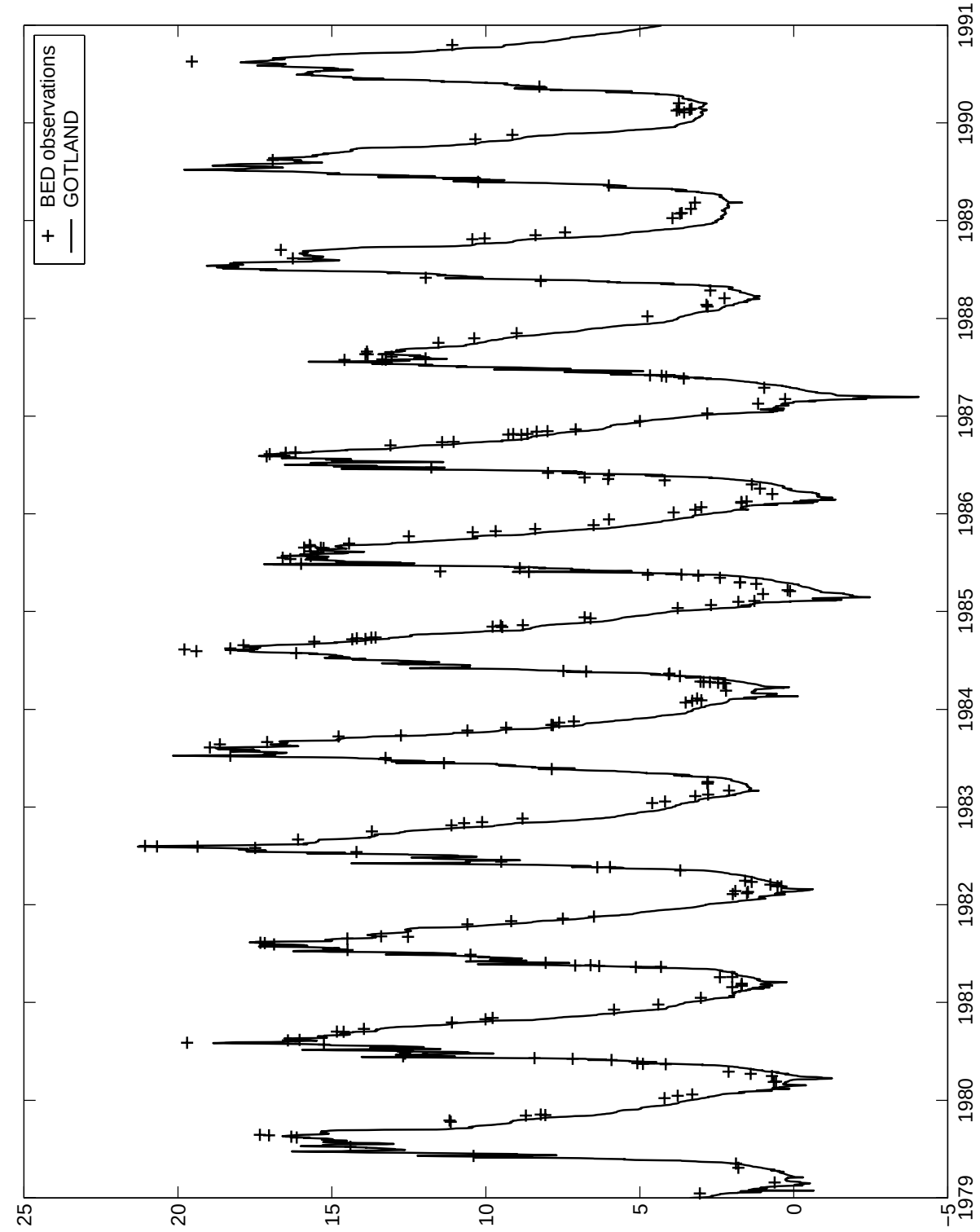

Figure 4.10.: GOTLAND: near surface temperature. Comparison between BED data and model results.

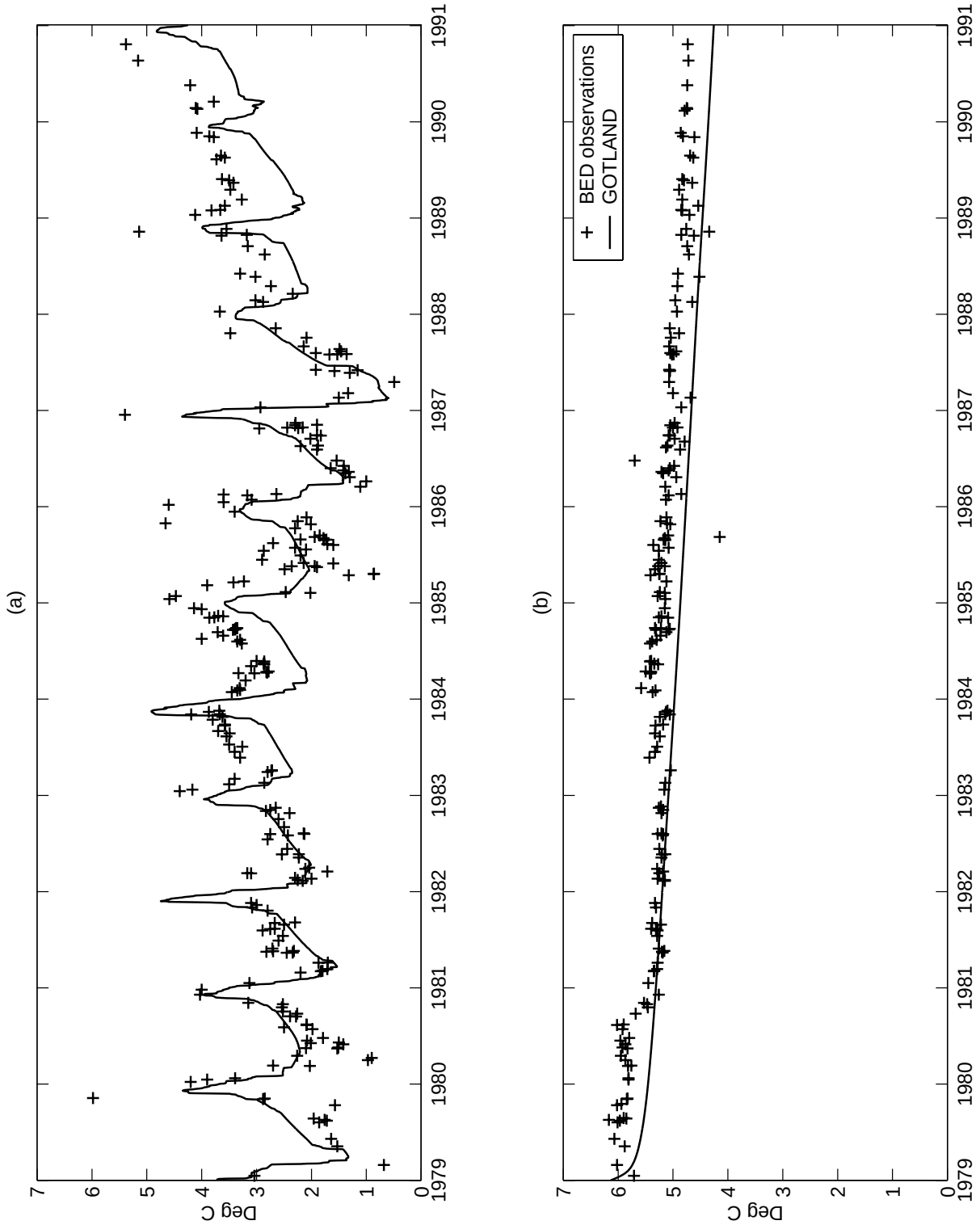

Figure 4.11.: GOTLAND: temperature at (a) -60 m and (b) at the bottom. Comparison between data and model results.

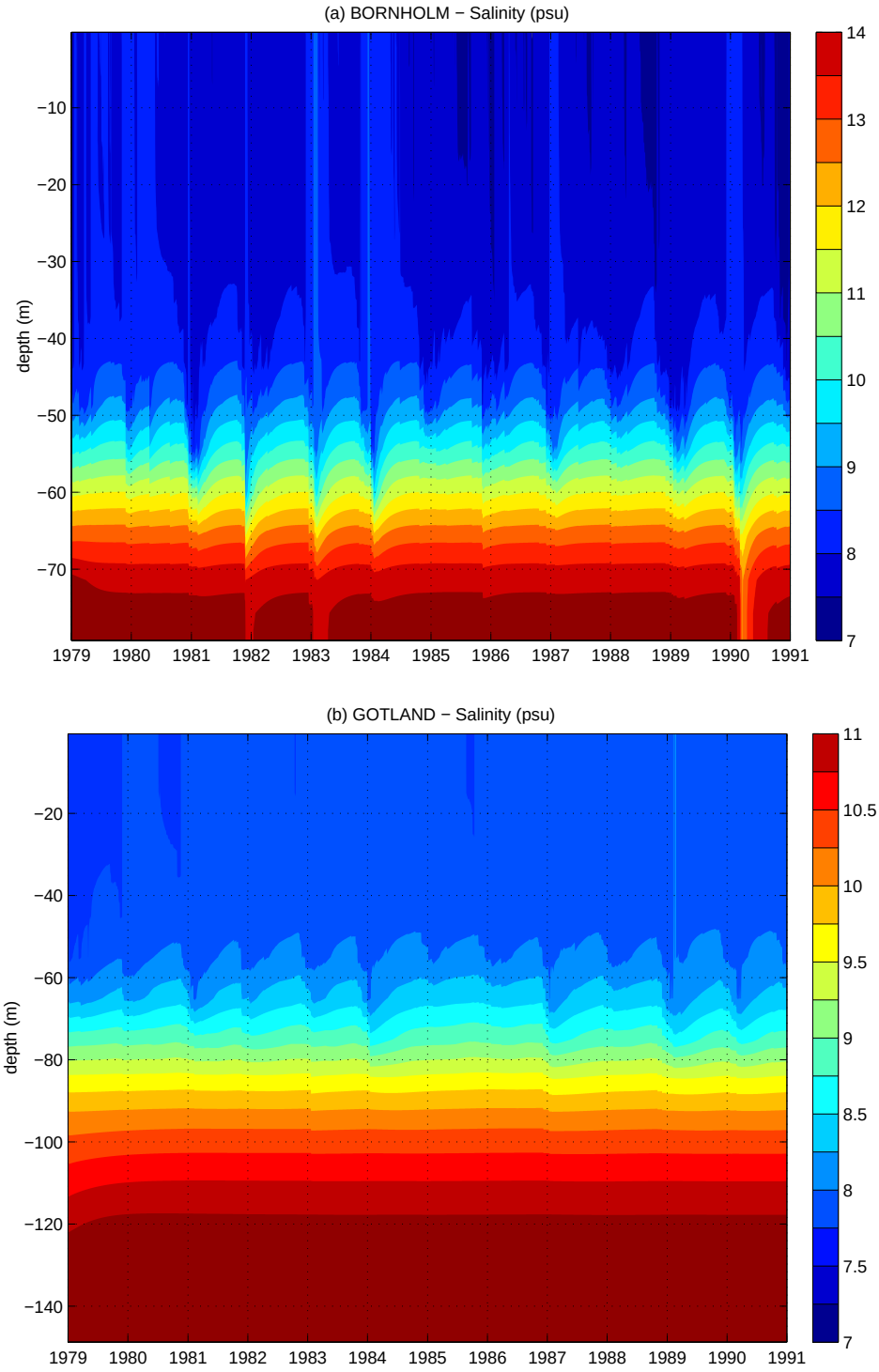

Figure 4.12.: (a) Salinity distribution in BORNHOLM (1979-1991). (b) Salinity distribution in GOTLAND (1979-1991).

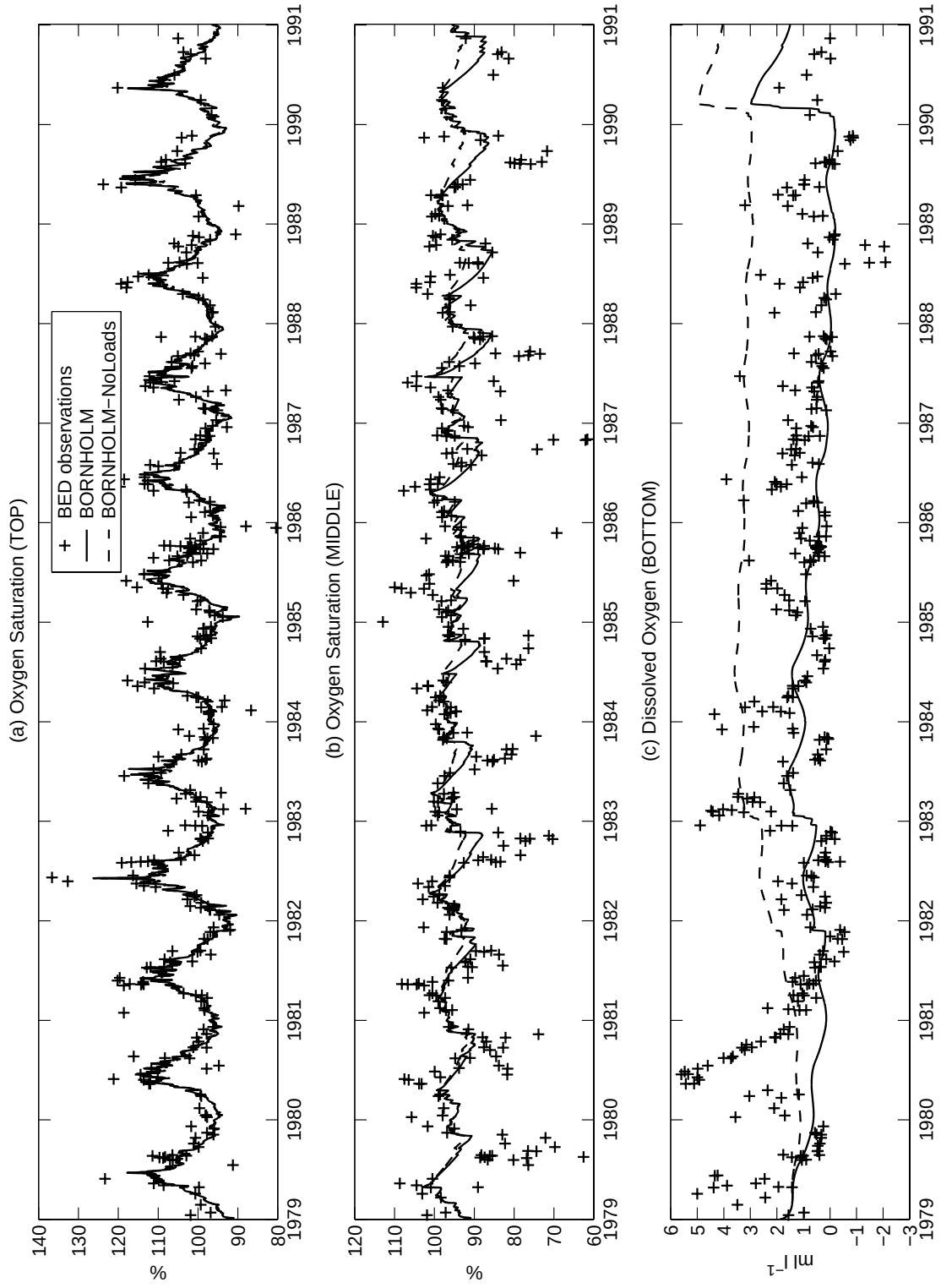

Figure 4.13.: BORNHOLM: percentage of oxygen saturation at (a) near surface, (b) -40 m and (c) bottom (-80m). Comparison between model results and BED data.

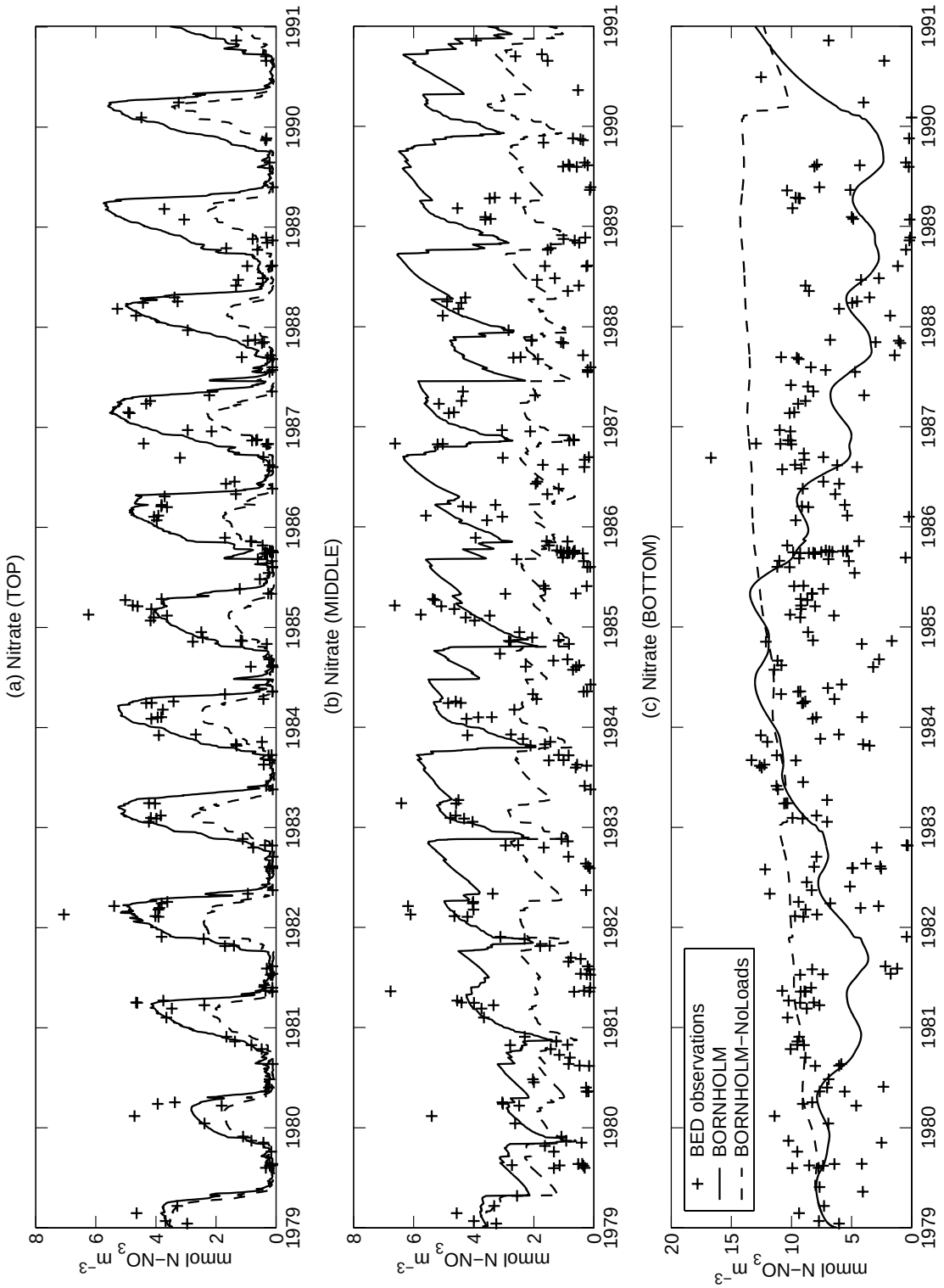

Figure 4.14.: As in Figure 4.13 but for nitrate.

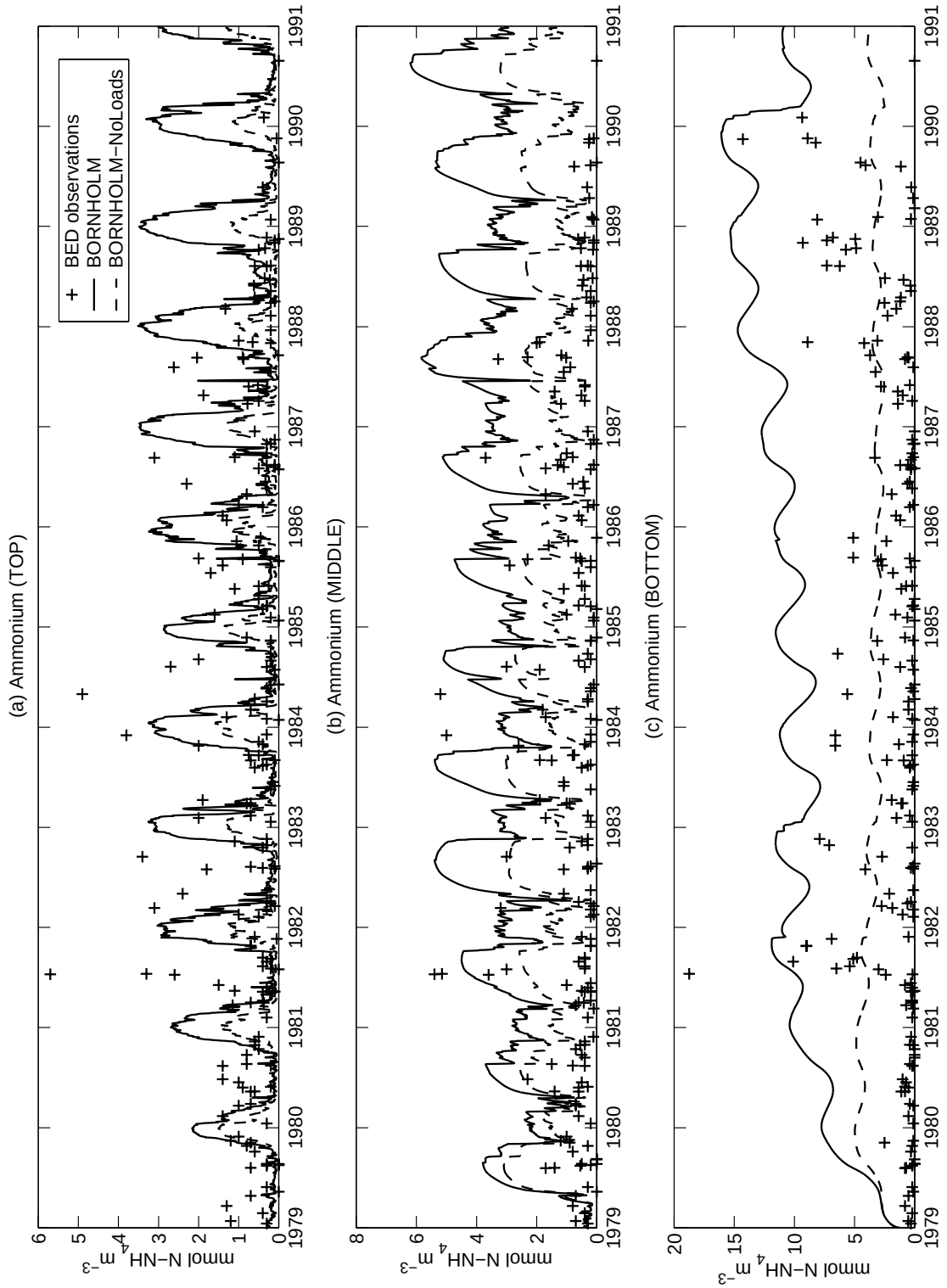

Figure 4.15.: As in Figure 4.13 but for ammonium.

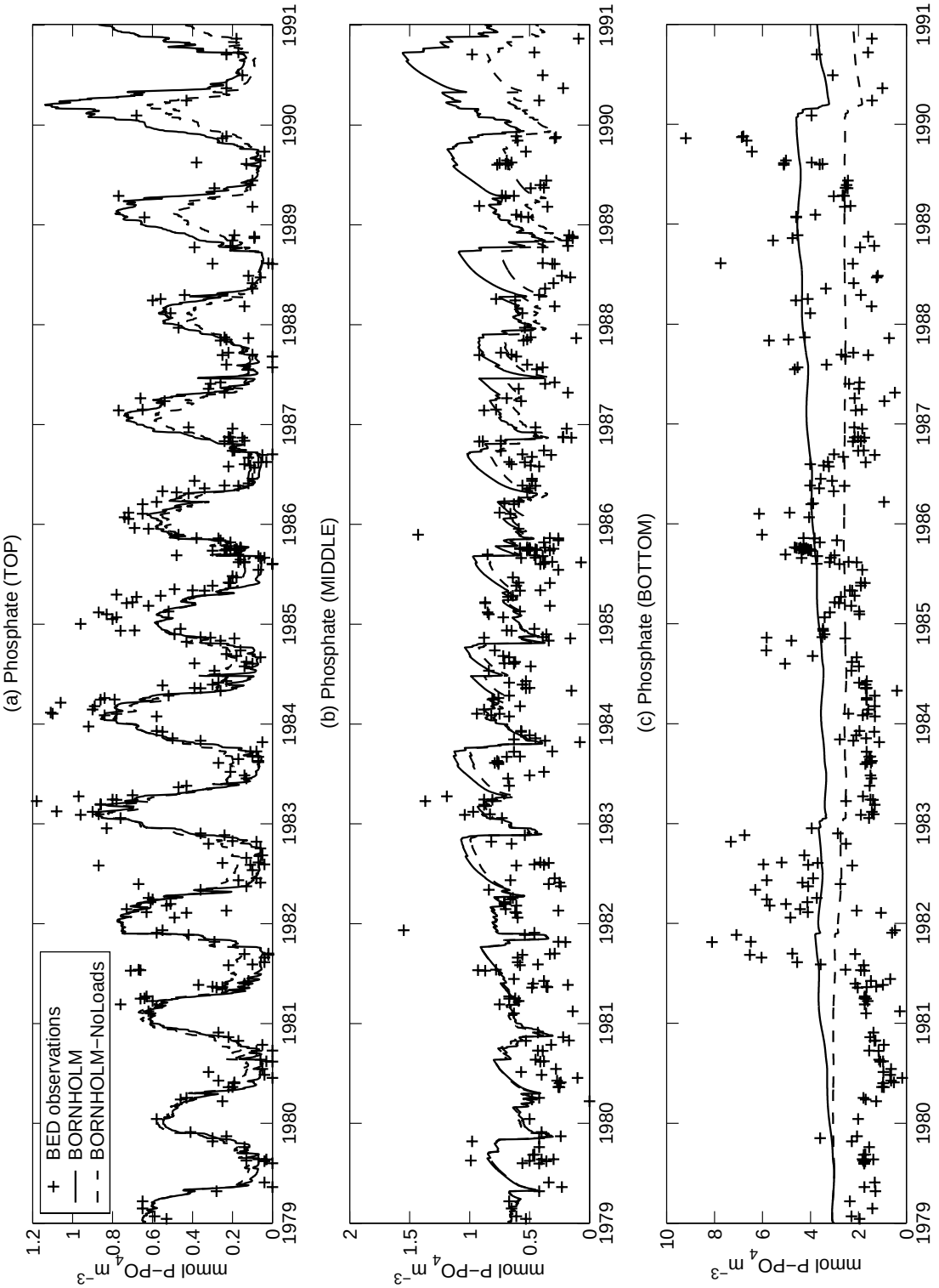

Figure 4.16.: As in Figure 4.13 but for phosphate.

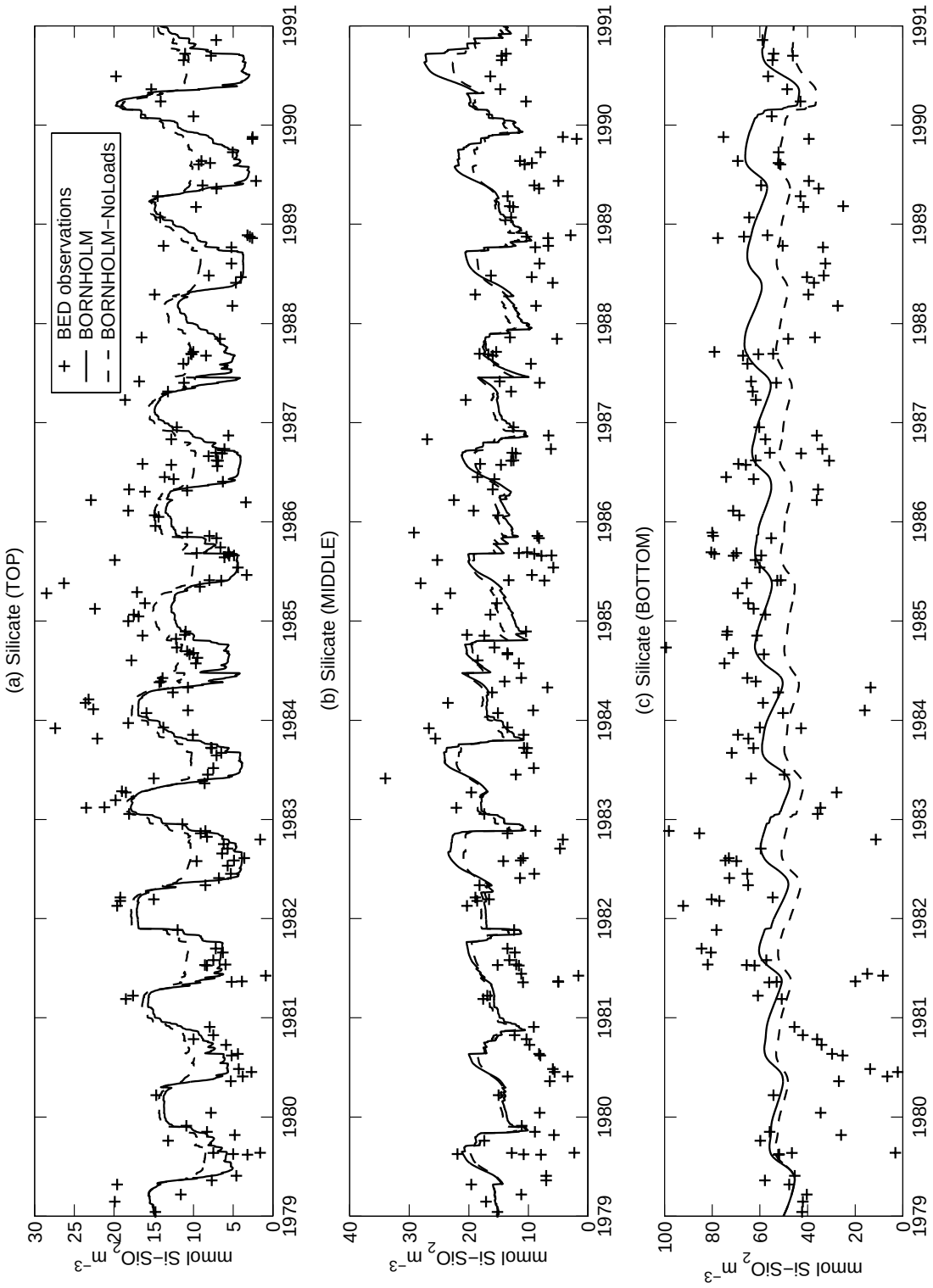

Figure 4.17.: As in 4.13 but for silicate.

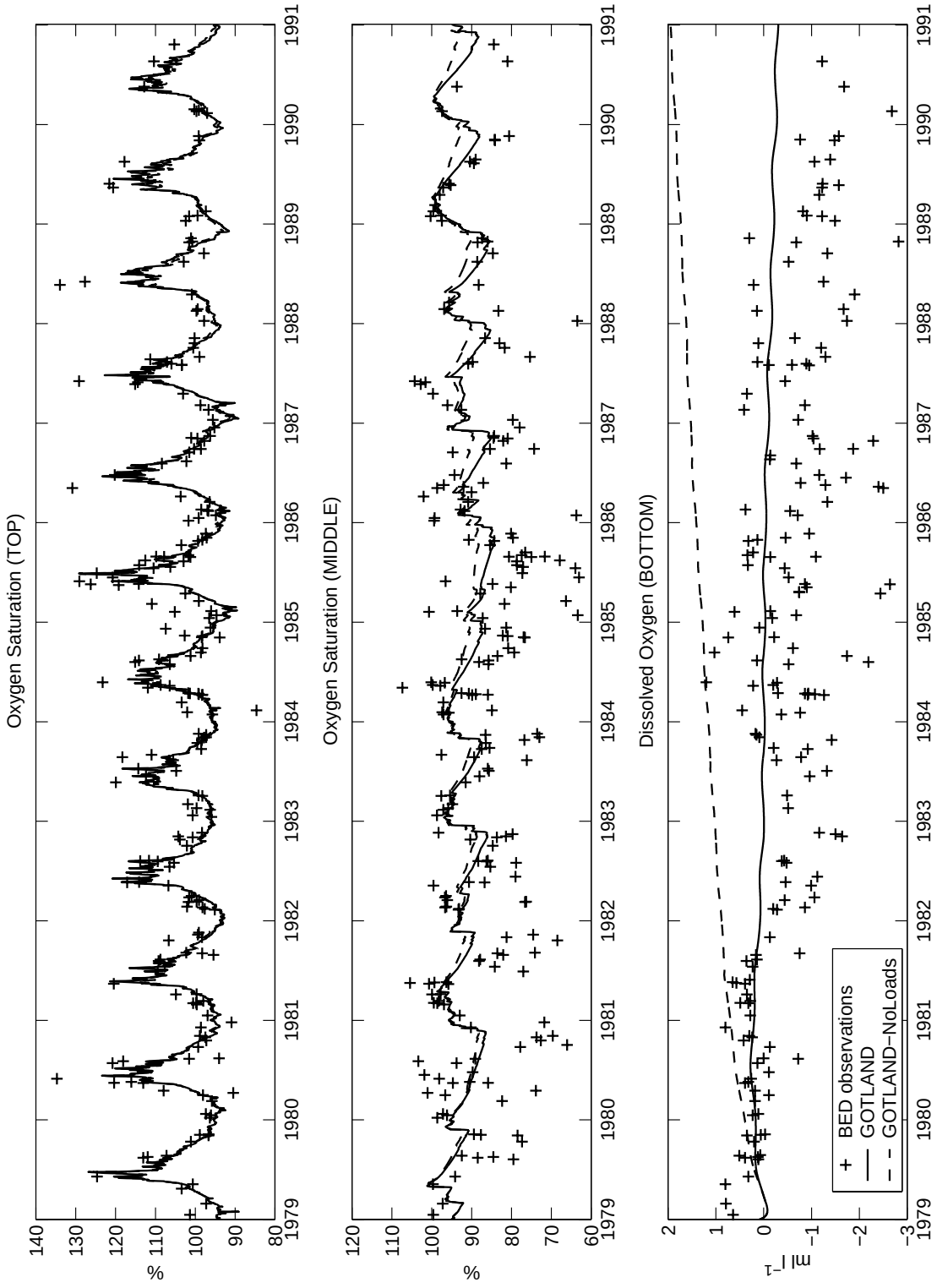

Figure 4.18.: GOTLAND: percentage of oxygen saturation at (a) near surface, (b) -60 m and (c) bottom (-150m). Comparison between model results and BED data.

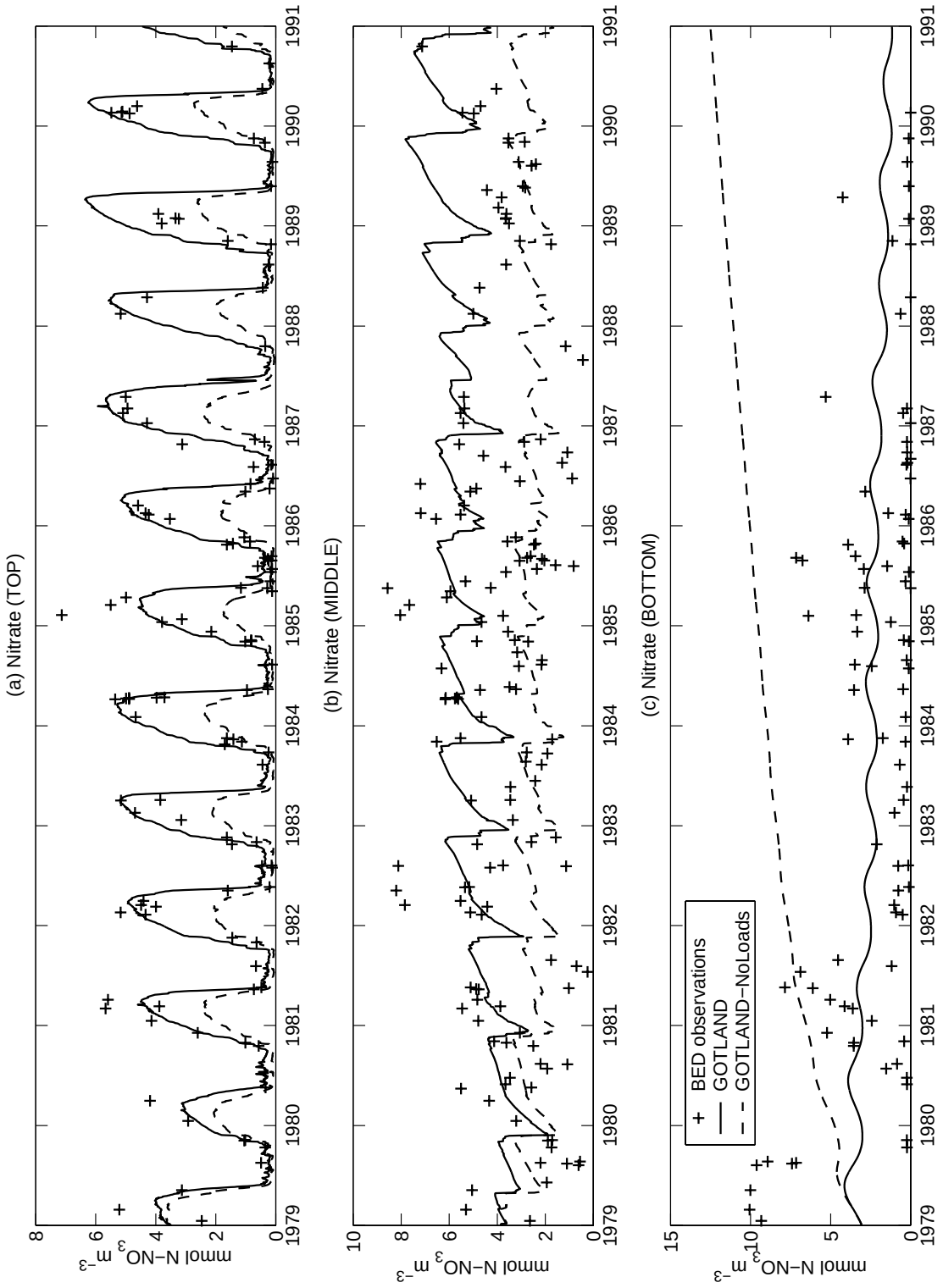

Figure 4.19.: As in Figure 4.18 but for nitrate.

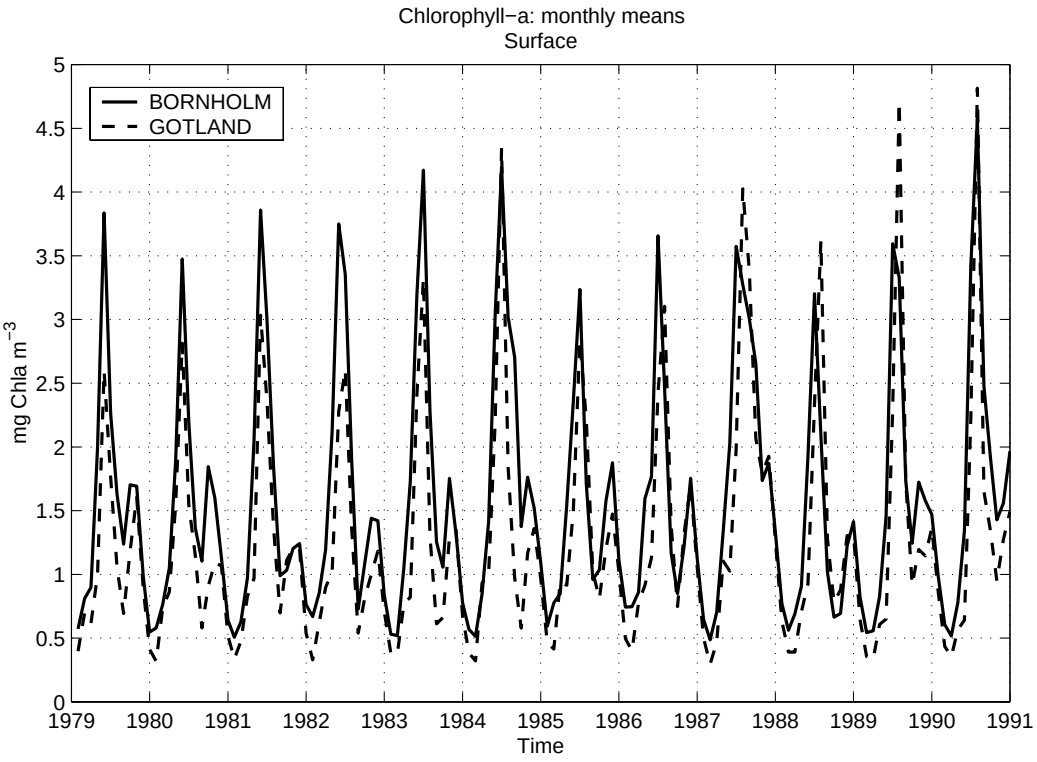

Figure 4.20.: Comparison between BORNHOLM and GOTLAND model results. Time distribution of monthly means of chlorophyll-*a* concentrations at surface.

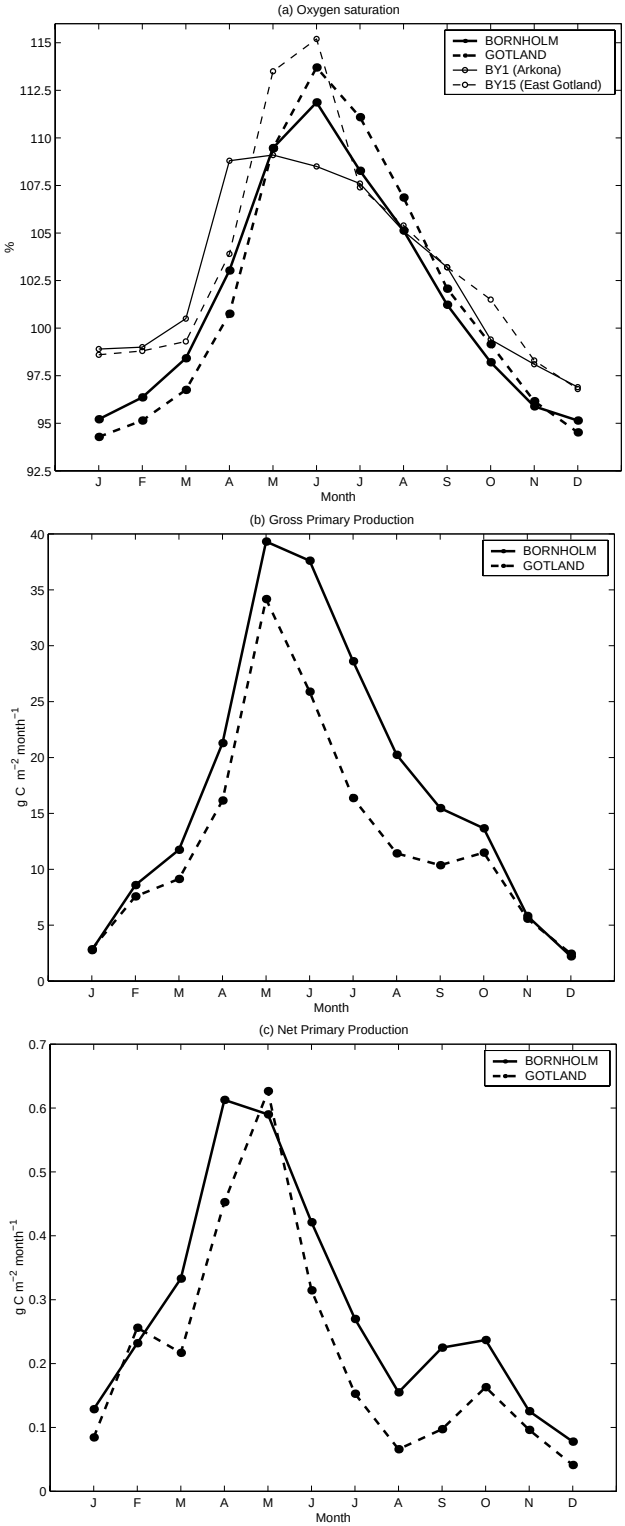

Figure 4.21.: Comparison between BORNHOLM and GOTLAND simulated monthly values over the investigated period. (a) Time distribution of monthly means of oxygen saturation in the first 20 m. The thin lines are the climatological monthly means over the period 1957-1982 at stations BY1 and BY15 from Stigebrandt (1991). (b) Time evolution of the monthly gross primary production (GPP) integrated in the first 20 m. (c) as in (b) but for the net primary production (NPP), computed as difference between GPP and the ecosystem respiration.

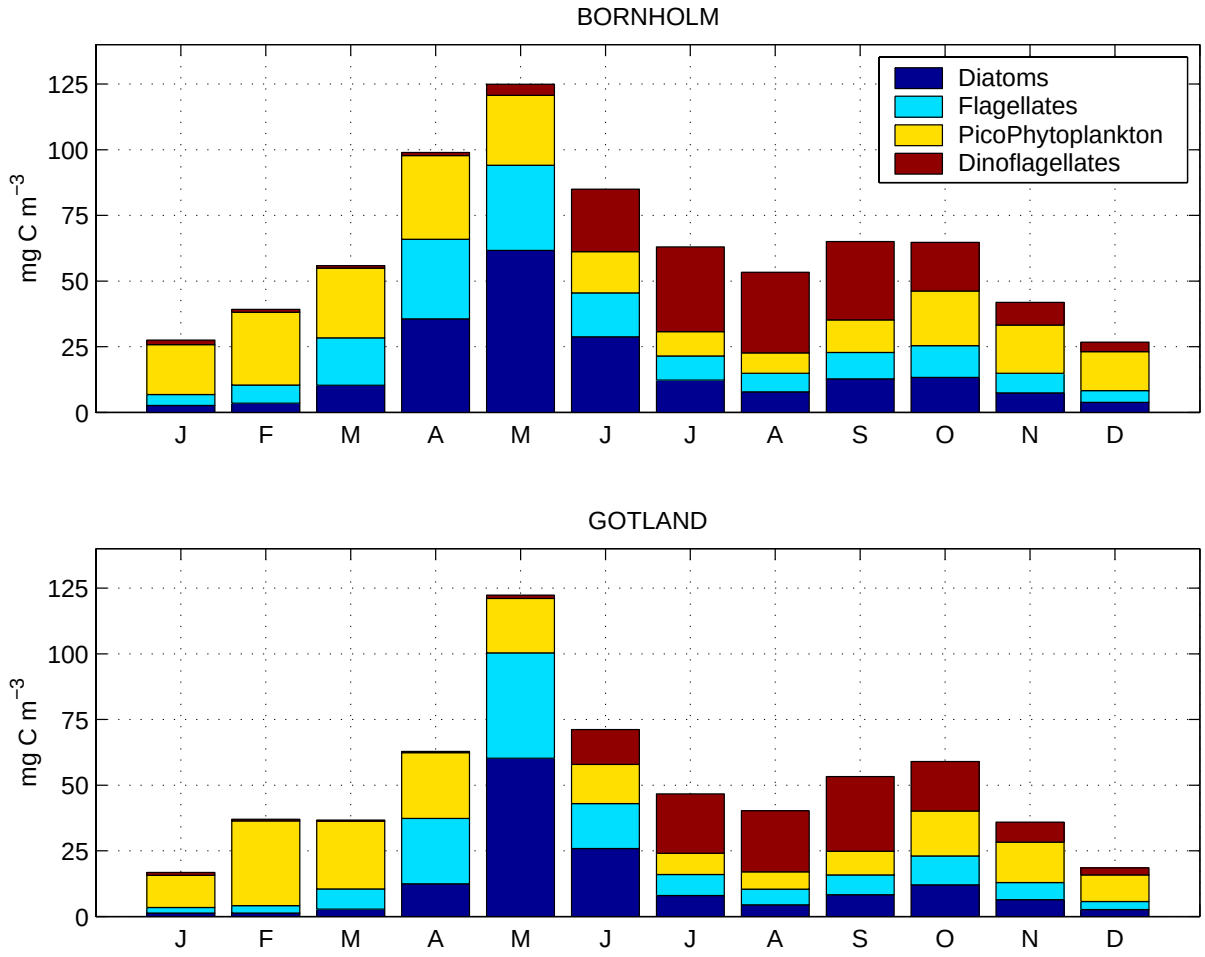

Figure 4.22.: Monthly means over the simulation period of the surface phytoplankton biomasses at BORNHOLM and GOTLAND.

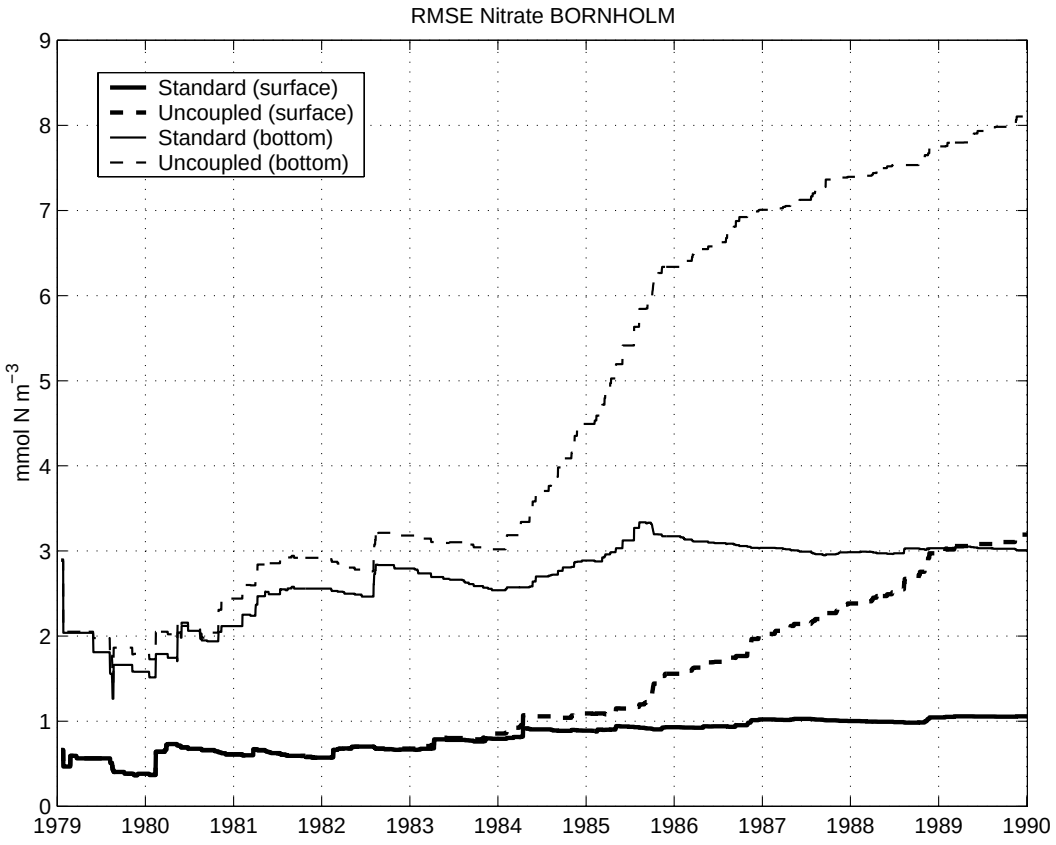

Figure 4.23.: RMSE between model and observations in BORNHOLM with uncoupled and coupled (standard) parameterization of the denitrification process.

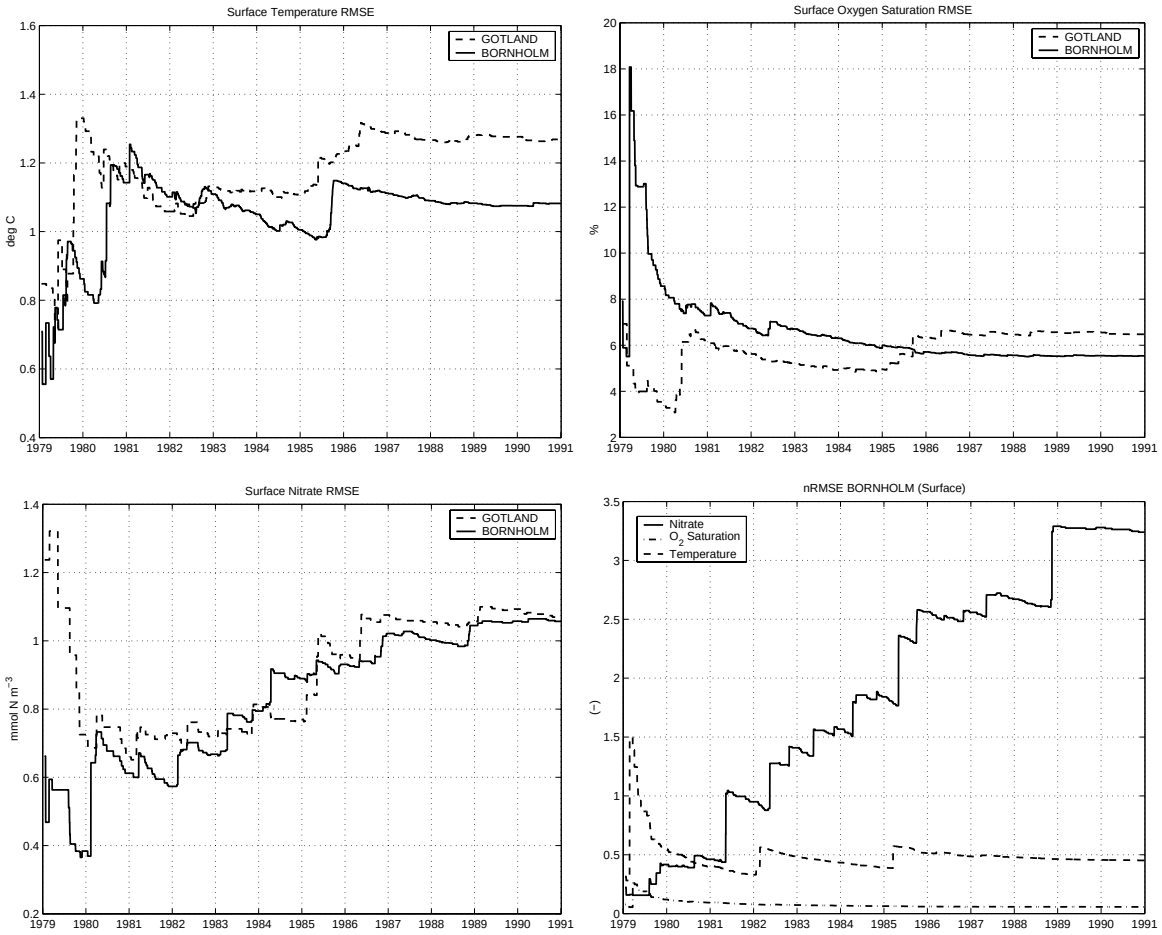

Figure 4.24.: RMSE between BORNHOLM and GOTLAND models and observations for: (a) SST; (b) surface oxygen saturation; (c) surface nitrate concentration. (d) normalized RMSE of the previous variables but only for the BORNHOLM model.

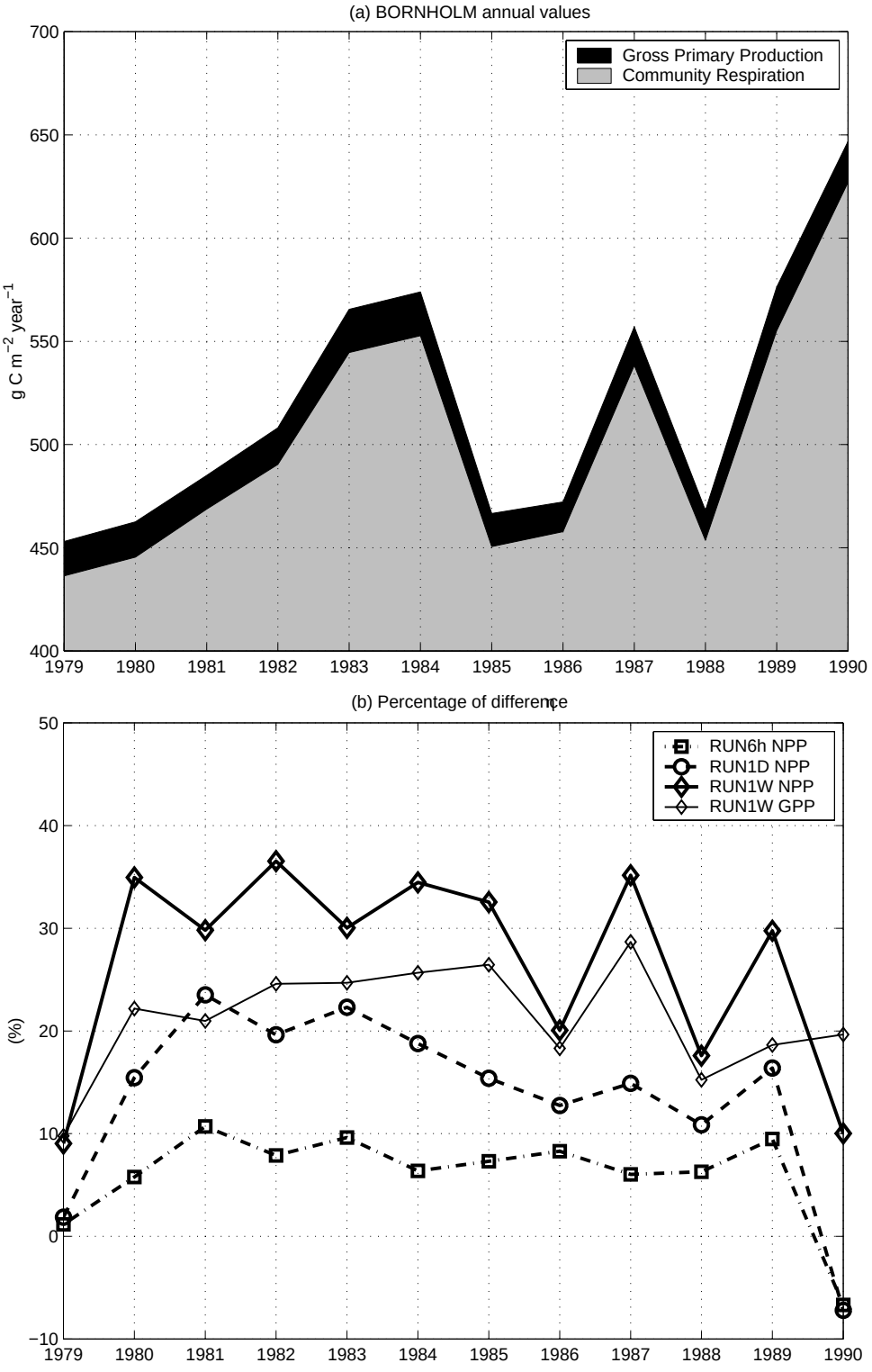

Figure 4.25.: (a) Annual gross carbon primary production (GPP) and ecosystem respiration flux in BORNHOLM. (b) Percentage of difference in the values of NPP and GPP of the standard run with respect to RUN6H, RUN1D and RUN1W.

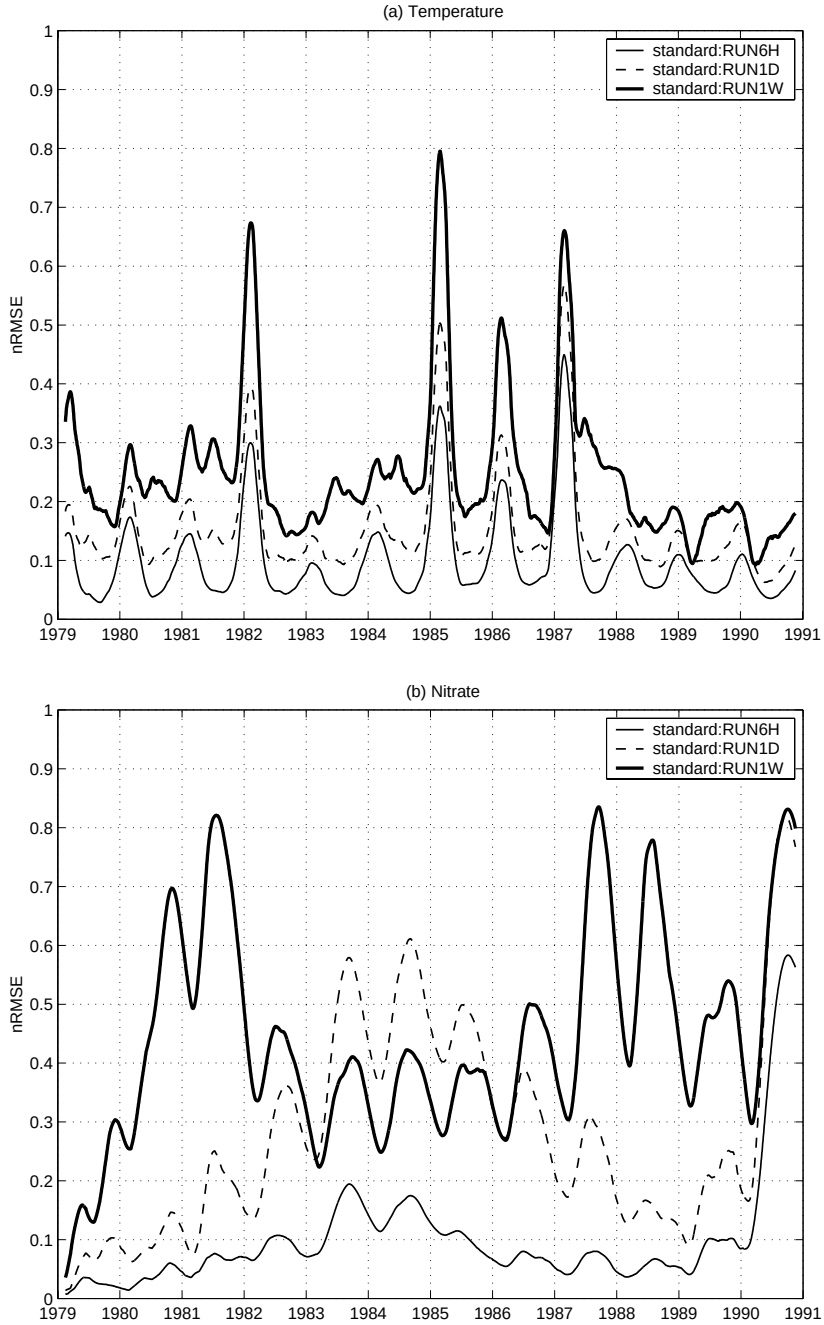

Figure 4.26.: Normalised root mean square differences between model results in BORNHOLM using three-hourly and six-hourly averaged surface fluxes (continuous thin line), three-hourly and daily averaged surface fluxes (dashed thin line) and three-hourly and weekly (thick line).

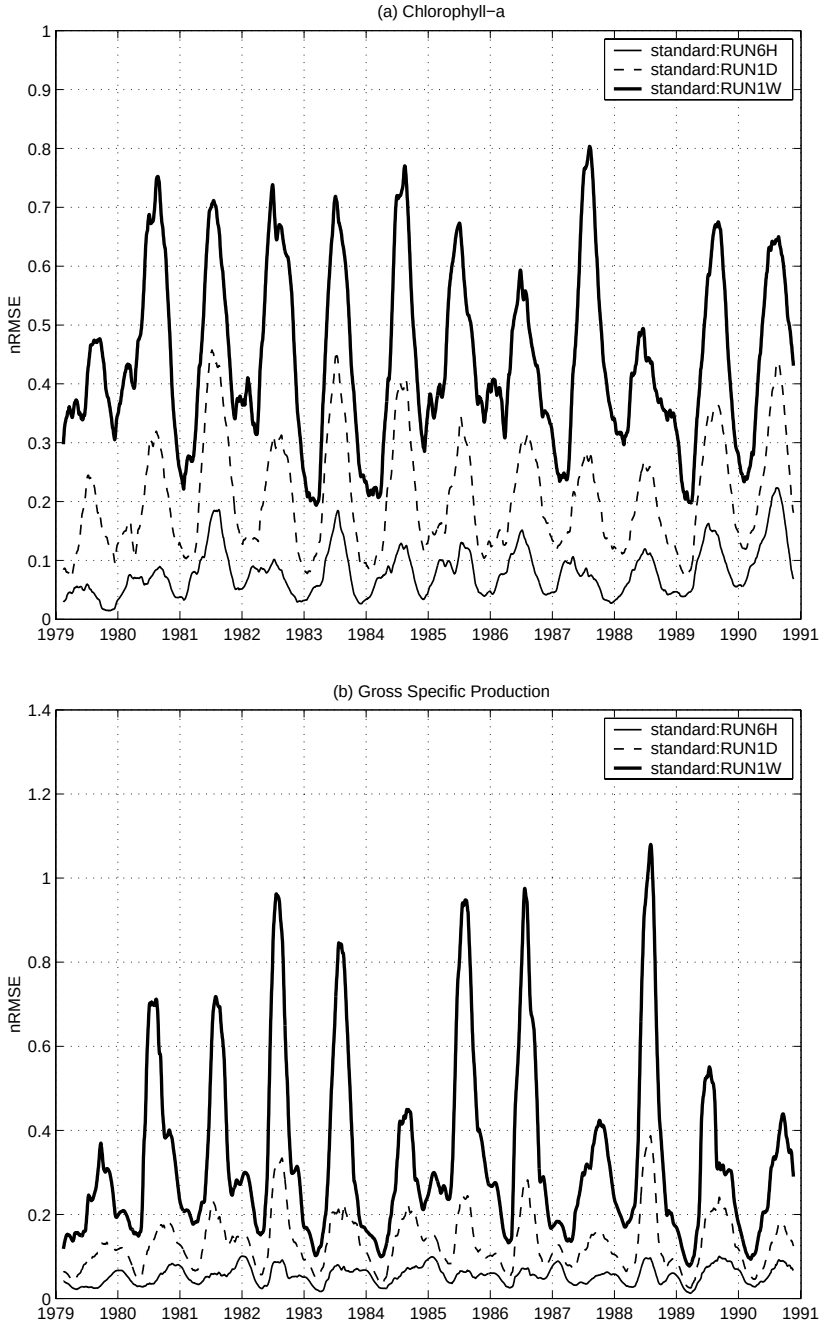

Figure 4.27.: Normalized root mean square differences between model results in BORNHOLM using three-hourly and six-hourly averaged surface fluxes (continuous thin line), three-hourly and daily averaged surface fluxes (dashed thin line) and three-hourly and weekly (thick line).

6. Summary and general conclusions

The study presented in this thesis is principally meant to analyze the genericity of a deterministic, comprehensive marine ecosystem model in combination with various refined representations of hydrodynamical processes, and to evaluate the potential predictability skills of this combined modelling system with specific applications in two rather different coastal basins. This objective has been realized by first developing a modular coupling interface between the Princeton Ocean Model and the European Regional Seas Ecosystem Model, called High Resolution OpenSESAME POM ERSEM (HiROPE). Secondly, this model framework, embedding a composite of "complex" conceptual principles of the functioning of the main biogeochemical processes, has been applied to substantially different marine systems, the Baltic proper and the northern Adriatic Sea.

The basic dissimilarities between the hydrodynamics of this two areas are essential for a detailed assessment of the implemented biogeochemical interactions. Both basins show marked gradients of analogous biological properties which are mainly a consequence of the environmental conditions, which in their turn are the consequence of the interactions between meteorological and hydrodynamical characteristics and external inputs. However, the hydrodynamical features differ substantially in their seasonality. The northern Adriatic Sea shows a seasonal alternation between strongly stratified summer periods and completely mixed autumn/winter conditions, while the Baltic is a brackish sea characterized by a permanent stratification with a welldeveloped mixed layer and limited renewal of deeper waters, especially during the investigated stagnation period (1979-1991).

The generally satisfactory results obtained by the HiROPE implementations are a confirmation of the capability of the generic ecosystem model to respond to local driving abiotic factors and to develop a consistent reasonable representation of the main biogeochemical dynamics. The generic biological first principles of the ERSEM ecosystem model have been throughly controlled for consistency, and a suitable mathematical syntax has been defined in order to accommodate the various biogeochemical cycles of the resolved elements. The description of the differential equations of the biogeochemical model presented in an appendix to this thesis is a revised collection of the original formulations published in ERSEM I/II (BarettaBekker, 1995; BarettaBekker and Baretta, 1997), extended with process formulations that have been found to be necessary during the development of this work and from results of previous applications. In particular the cycling of dissolved organic matter has been improved, with a more refined parameterization of the differential bacterial uptake according to the nutrientcontent of dissolved substrate. Bacterial dynamics have also been improved

with respect to the functional adaptation to anaerobic denitrification processes, a requirement that was strongly felt in the Baltic application, where successions of hypoxic/anoxic events occurred during the investigated period. The inclusion of this last process has been demonstrated to increase the hindcasting capabilities of the model in resolving the nitrogen cycle, suggesting that the addition of more refined parameterizations that create supplemental linkages between the dynamical variables is a valid strategy to be attempted also in the case when parameter definition is only theoretical and not thoroughly corroborated by data.

The application of the same biogeochemical equations to different representations of hydrodynamical processes has lead to interesting considerations on the system properties that can be captured with this type of coupled ecosystem model.

The climatological application in the northern Adriatic Sea (Chapter 3) was aimed at resolving the seasonal cycle of physical and biological components and to investigate the transfer pathways of carbon through the food web in combination with the hydrodynamical regimes. With such a coarse representation of the time-variability of physical processes, the model was mainly able to reproduce the development of the spring and autumn blooms with different dynamics according to the features of the various implementation sites. However, due to the limits of the onedimensional, climatological approach, the main interactions between abiotic factors and biology that can be captured are (1) the Sverdruplike bloom mechanism (controlled by mixed layer shallowing processes and underwater light availability) and (2) the switching between different pathways of carbon recycling (herbivorous, purely-microbial and multivorous food webs, mainly linked to the establishment of stratification and the availability of external nutrient inputs). These are important systemlevel interactions, but they only have a diagnostic role (and limited predictive potentialities), in that they give indications of mean seasonal scale coupled processes. Nevertheless, a comparison of model-simulated rates with available observations have shown an overall agreement in magnitudes and qualitative temporal development. Considering the complexity of both measuring such rates and parameterizing the processes involved, the coarse matching of the order of magnitudes is seen as a highly positive result.

The inclusion of highfrequency scales of variability in the meteorological forcing functions has lead to the appearance of more complex interactions between physical driving factors and biological responses. The one-dimensional applications in the Baltic proper presented in Chapter 4 have in fact shown a satisfactory hindcasting of the decadal system behavior during the recent, long stagnation period. The lack of biologically relevant observations has reduced the analysis to the comparisons of hydrochemical components and especially oxygen, that has been found to be an optimal proxy for analyzing the interactions between production/consumption processes and the turbulent transport processes in the water column interior. The overall persistent anoxic conditions are interpreted, in the light of model results, as a combined effect of the permanently stratified conditions and the preferential recycling of nutrients, which maintains a substantial summer production that continously fuels the bottom layers with reduced organic matter. It is also possible to infer that these processes are enhanced by the availability of external nutrient sources (maybe also via biological nitrification pathways) as

well as by the diapycnal turbulent diffusion of remineralized bottom nutrients. The latter implies that the resolution of intermediate/deep water turbulent mixing processes is of paramount importance in the determination of the biological system behavior.

Another interesting result of these Baltic applications is that the models have given indications that local highfrequency variability in the physical forcing is the driver for much of the observed seasonal and interannual variability (decadal). Time-averaging of the meteorological forcing leads to damping of the vertical exchange fluxes with an overall reduction of the biological activity especially of primary producers. The model responds to the shortscale events in the hydrodynamics with a marked nonlinear behavior that acts in the direction of generating positive feedbacks in the biology, for example sustaining the maintenance of summer phytoplankton under strongly stratified conditions. The observed changes in the simulated interannual variability also indicate that longterm (and perhaps large-scale) variability is the integral of a cascade of variability at the smaller scales. This long-term discrepancy could be larger for integration periods longer than a decade - for instance, in the case of climate change studies - and this underestimation could become important in the predictability of system behavior in terms of carbon and nutrient budgets of the basin.

Finally, the complete threedimensional highresolution implementation in the northern Adriatic Sea (Chapter 5) posed a formidable task, the coupling of highfrequency mesoscale coastal variability with empirical biogeochemical equations that have seldom been tested at such scales. Results are absolutely preliminary and the practical limitations of the implemented experiments make a careful interpretation necessary. The presence of approximate solutions to several practical problems such as the numerical coupling issues, the applications of open boundary conditions and the limitations due to the lack of important processes of coastal areas (e.g.: river discharge of suspended sediments and re suspension/deposition mechanisms), hamper the generalization of the model results. However this work has demonstrated that such a highresolution coupling is feasible with over-the-counter PC-hardware and with Open Source non-proprietary software, and has helped to pinpoint the single components and methodologies that need to be thoroughly analyzed in separate specific experiments to enhance the applicability of the models.

The analysis of the predictability skills conducted by means of the Observational System Simulation Experiment methodology has given indications that the predictability of coastal ecosystem behavior is strongly connected to the knowledge of proper hydrodynamical conditions and other abiotic/biotic external forcing functions. The presence of a diffuse food web as in ERSEM is more of a help to the settingup of initial conditions than a limitation. This concept can be generalized by stating that in a comprehensive ecosystem model, the functional role of a variable and the existence of “weak” linkages with the other components appears to be more relevant (in terms of model behavior) than the initial conditions. This conclusion is demonstrably valid in the context of this specific application which imparts a substantial control from the external forcing functions (the Po River runoff). Further experiments performed in different periods (summer stratified conditions, onset of a spring bloom, etc.) are necessary to thoroughly clarify the impact of incomplete initialization of model variables.

Considering all the results from the different applications, an overall comment is that the main uncertainties on the predictive capabilities of coupled ecosystem models are linked to the definition and parameterization of the processes involved. As stated in the Introduction to this thesis, models are simply necessary tools to be used for the development of ecosystem theory, and their importance has to be considered also in the measure of their contribution to systems understanding. In particular, by means of the analysis of discrepancies with observations, the application of the model allowed to identify processes that need to be refined or further investigated with the aid of coherent datasets and specific experiments. They are summarized as follows:

- the parameterization of light availability in general, intended as the proper estimate of the underwater light climate as driven by the amount of suspended light-attenuating particles, and the photoacclimation property of the different phytoplankton functional groups;
- the relevance of the benthic system in the longterm evolution (read also "predictability") of coastal processes. ERSEM embodies a complete parameterization of benthic biological processes and early-diagenetic dynamics in the sediments, and they have been found to be necessary. Due to time limitation and the need of specific knowledge on such processes, results from the benthic system have not been thoroughly analyzed in this thesis, but deserve a dedicated study because of their contribution to the overall system behavior.
- the paradox of the parameterization of respiration rates. Oxygen (especially saturation) has been found to be a good proxy to system level production/consumption processes. However, values of dissolved oxygen are in satisfactory agreement with observations in the Baltic applications but always underestimated in the 3D Adriatic implementation and overestimated in the climatological runs. This implies a differential response according to the implementation of hydrodynamical processes that needs to be clarified. In general, also from the Baltic experiments, there are indications that the carbon respiration rates are too high and this could explain the low phytoplankton standing stocks observed during summertime in the Baltic (with a consequent reduced export of carbon from the euphotic zone) and in the 3D Adriatic.
- The occurrence of temporal succession and spatial differentiation in the modelled phytoplankton components have partially confirmed the role and the importance of having different functional groups that can adapt to the specific environmental conditions. Results have shown that the various groups respond to specific driving factors according to the features implemented in the parameterizations. In this light, the impact of species with peculiar functionalities such as mixotrophy should be considered in future developments (as already done in a mesocosm experiment by Baretta-Bekker *et al.*, 1998).

Summarizing the previous concepts, it can be said that the predictability of ecosystem behavior is directly connected to *what* we want to predict and *how* we are performing the prediction. This apparently trivial statement is of importance to distinguish the forecasting of ecosystem evolution from

the forecasting of weather or oceanic currents. What has been learned from the present study is that, in these terms, “predictability” suggests too much when applied to ecosystem behavior. Ecosystem behaviour is unpredictable with a mechanistic approach because there are no abstract generally valid approximations of marine ecosystems, from which a hierarchical set of refinements can be extracted, as when going from idealized to real geophysical fluids. It must therefore be recognized that alternative representations of the ecosystem may lead to different qualitative and quantitative conclusions regarding how physical processes affect population and biogeochemical dynamics. It is also important to remark that this analysis of predictability is not properly a study of forecasting capabilities, because the performed applications are mainly hindcasting experiment, in that “known” external forcing functions from the past have been used. This means that the predictive capabilities strongly depend from the specific application that is performed.

In some cases, it is sometimes possible to find “simplifications” or shortcuts to the system behavior, for example derived from the observation that in a certain system nitrogen is the limiting nutrient, and hence to implement a model that resolves only the N cycle. However, there are no practicable ways to find out whether N is really the only key variable, and also for how long it will remain such. Therefore, the degree of predictability is limited, because it is our way to examine the system which is limited. As living marine organisms can simplistically be abstracted to variable mixtures of C, N, P and Si, a minimum requirement for deterministic models is to solve at least the cycling of these elements; the alternative is to find another nonmechanistic approach to system functioning. Thus, the only way for having a more overall view of the predictability skill of coupled ecosystem models is to implement all significant chemical and biological processes, and apply such a model to different realistic scenarios with different spatial and temporal resolution. The external dynamical variability, if appropriately introduced into the model, will do its work, selecting the key variables and the main cycling mechanisms under the prevailing abiotic dynamics. This is actually the approach used in this work, where the same modelling system with a considerable amount of variables and linkages has been applied to distinctly different shallow water ecosystems, and the response of the modelled biological parameters has been analyzed both theoretically and by comparing model results with real *in situ* observations. Unfortunately, it is not known what the reliability of the modelled biological fluxes is, and only the comparison with fluxes also measured *in situ* or at least biological observations at high frequency, can help in establishing whether the variability of ecological components can be properly represented with this type of deterministic models. This problem was clear from the beginning and - in spite of this tacit degree of uncertainty - it was still possible to draw out some interesting information; perhaps more about the behavior of the specific coupled ecosystem model instead of about the behavior of real marine ecosystems, but still useful for the comprehension of systems theory in general.

Usually, ecological modellers concentrate their effort on the representation of the system state at certain moments in time, relegating the dynamical processes that connect the points in the phase state to second order. The main worry is thus finding appropriate analytical/numerical/statistical methods

to bring the model trajectories “back on track”, that is, as close as possible to the incomplete picture that it is supposed to represent the real state of the system at that moment. However, analyzing the results of this thesis, it seems that it is indeed the dynamics or better “the fluxes”, and not the “states”, which determine the ecosystem behavior and its response to the abiotic/biotic variability. It was in fact possible to demonstrate with the OSSE methodology that the uncertainties in the initial state of the pelagic system can be partially recovered thanks to the presence of regulating feedbacks in the functional parameterizations, but that the evolution of the system from one state to the other is basically linked to the weak coupling among the considered dynamical processes. This means that the representation of hydrodynamical variability, the definition and resolution of boundary processes, the introduction of new source terms or (maybe) the implementation of new biological state variables, affect the system behavior (read also “predictability of the system behavior”) more than the utilization of incomplete initial conditions. A proper representation of the plasticity in the biotic interactions (the food web) is thus the major challenge.

Bibliography

[1] A. Adamec. Predictability of quasi-geostrophic ocean flow: sensitivity to varying model vertical resolution. *J. Phys. Oceanogr.*, 19:1753–1764, 1989.

[2] D.L. Aksnes and J.K. Egge. A theoretical model for nutrient uptake in phytoplankton. *Mar. Ecol. Prog. Ser.*, 70:65–72, 1991.

[3] J.I. Allen, J.C. Blackford, and P.J. Radford. A 1-D vertically resolved modelling study of the ecosystem dynamics of the Middle and Southern Adriatic Sea. *J. Mar. Sys.*, 18:265–286, 1998.

[4] J.I. Allen, R.H.M. Howland, N. Bloomer, and R.J. Uncles. Simulating the Spring Phytoplankton Bloom in the Humber Plume (UK). *Mar. Poll. Bull.*, 37(3-7):295–305, 1999.

[5] P.M. Allen. Ecology, thermodynamics, and self-organization: towards a new understanding of complexity. In R.E. Ulanowicz and T. Platt, editors, *Ecosystem theory for biological oceanography*, pages 3–26, Ottawa, Canada, 1985. Department of Fisheries and Oceans, Canadian Bulletin of Fisheries and Aquatic Sciences.

[6] J.S. Almeida, M.A.M. Reis, and M.J.T. Carrondo. A unifying kinetic model of denitrification. *J. Theor. Biol.*, 186(2):241–249, 1997.

[7] V. Anderson, P. Nival, and R.P. Harris. Modelling of a planktonic ecosystem in an enclosed water column. *J.mar. biol. Ass. U.K.*, 67:407–430, 1987.

[8] A. Artegiani, D. Bregant, E. Paschini, N. Pinardi, F. Raicich, and A. Russo. The Adriatic Sea General Circulation. Part I: Air-Sea Interactions and Water Masses Structure. *J. Phys. Oceanogr.*, 27:74–96, 1997a.

[9] A. Artegiani, D. Bregant, E. Paschini, N. Pinardi, F. Raicich, and A. Russo. The Adriatic Sea General Circulation. Part II: Baroclinic Circulation Structure. *J. Phys. Oceanogr.*, 27:97–114, 1997b.

[10] L.B. Axell. On the variability of Baltic Sea deep-water mixing. *J. Geophys. Res*, 103(C10):21667–21682, 1998.

[11] F. Azam. Microbial control of oceanic carbon flux: the plot thickens. *Science*, 280:694–696, 1998.

[12] F. Azam, T. Fenchel, J.G. Field, J.S. Gray, L.A. Meyer-Reil, and F. Thingstad. The ecological role of water-column microbes in the sea. *Mar. Ecol. Prog. Ser.*, 10:257–263, 1983.

[13] F. Azam, S. Fonda Umani, and E. Funari. Significance of bacteria in the mucilage phenomenon in the northern Adriatic Sea. *Ann. Ist. Super. Sanitá*, 35(3):411–419, 1999.

[14] F. Azam, J. Fry, P.LeB. Williams, and G. Herndl. *Investigating marine microbial loops: new tools and perspectives*, volume 11 of *CIESM Workshop Series*. CIESM, 2000.

[15] V. Barale, C.R. McClain, and P. Malanotte-Rizzoli. Space and time variability of the surface color field in the northern Adriatic Sea. *J. geophys. Res.*, 91:12957–12974, 1986.

[16] J.W. Baretta, W. Ebenhoeh, and P. Ruardij. The European Regional Seas Ecosystem Model, a complex marine ecosystem model. *Neth. J. Sea Res.*, 33(3-4):233–246, 1995.

[17] J.W. Baretta and P. Ruardij. *Tidal flat estuaries: simulation and analysis of the Ems estuary*, volume 71 of *Ecol. Studies*. Springer Verlag, Heidelberg, 1988.

[18] J.G. Baretta-Bekker, J.W. Baretta, and W. Ebenhoeh. Microbial dynamics in the marine ecosystem model ERSEM II with decoupled carbon assimilation and nutrient uptake. *J. Sea Res.*, 38(3/4):195–212, 1997.

[19] J.G. Baretta-Bekker, J.W. Baretta, A.S. Hansen, and B. Riemann. An improved model of carbon and nutrient dynamics in the microbial food web in marine enclosures. *Aquat. Microb. Ecol.*, 14:91–108, 1998.

[20] J.G. Baretta-Bekker, J.W. Baretta, and E.K. Rasmussen. The microbial food web in the European Regional Seas Ecosystem Model. *Neth. J. Sea Res.*, 33(3-4):363–379, 1995.

[21] J.G. Baretta-Bekker and J.W. Baretta (eds.). European Regional Seas Ecosystem Model II (1993-1996). *J. Sea Res. (special issue)*, 38(3-4):169–436, 1997.

[22] J.G. Baretta-Bekker, B. Riemann, J.W. Baretta, and E.K. Rasmussen. Testing the microbial loop concept by comparing mesocosm data with results from a dynamical simulation model. *Mar. Ecol. Prog. Ser.*, 106:187–198, 1994.

[23] J.G. Baretta-Bekker (ed.). European Regional Seas Ecosystem Model I (1990-1993). *Neth. J. Sea Res. (special issue)*, 33(3-4):229–483, 1995.

[24] M.B. Beck. Water quality modeling: a review of the analysis of uncertainty. *Water Resour. Res.*, 23:1393–1442, 1987.

[25] M.J. Behrenfeld and P.G. Falkowski. Photosynthetic rates derived from satellite-based chlorophyll concentration. *Limnol. and Oceanogr.*, 42(1):1–20, January 1997.

[26] R.A. Berner. *Early diagenesis: A theoretical approach*. Princeton Univ. Press, Princeton, 1980.

[27] J.C. Blackford. An analysis of benthic biological dynamics in a North Sea ecosystem model. *J. Sea Res.*, 38(3-4):213–230, 1997.

[28] J.C. Blackford and P.J. Radford. A structure and methodology for marine ecosystem modelling. *Neth. J. Sea Res.*, 33(3-4):247–260, 1995.

[29] A.F. Blumberg and G.L. Mellor. A description of a three-dimensional coastal ocean circulation model. In N.S. Heaps, editor, *Three-dimensional coastal ocean model*, pages 1–16. American Geophysical Union, 1987.

[30] D.R. Bouldin. Models for describing the diffusion of oxygen and other mobile constituents across the mud-water interface. *J. Ecol.*, 56:77–87, 1968.

[31] F.P. Bretherton, R.E. Davis, and C.B. Fandry. A technique for objective analysis and design of oceanographic experiments applied to MODE-73. *Deep Sea Res.*, 23:539–582, 1976.

[32] K.H. Brink. Hydrographic observations in the coastal ocean. In K. H. Brink and A. R. Robinson, editors, *The Sea*, volume 10, pages 359–366. John Wiley & Sons, Inc., 1998.

[33] W.S. Broecker and T.H. Peng. Gas exchange between air and sea. *Tellus*, 26:21–35, 1973.

[34] N. Broekhuizen, M.R. Heath, S.J. Hay, and W.S.C. Gurney. Modelling the dynamics of the North Sea's mesozooplankton. *Neth. J. Sea Res.*, 33(3-4):381–406, 1995.

[35] H.S. Carlslaw and J.C. Jaeger. *Conduction of heat in solids*. Oxford University Press, London, 1946.

[36] E.F. Carter and A.R. Robinson. Analysis models for the estimation of oceanic fields. *J. Atmos. Oceanic Technol.*, 4:49–74, 1987.

[37] J. A. Carton. How predictable are the geostrophic currents in the recirculation zone of the North Atlantic. *J. Phys. Oc.*, 17:751–762, June 1997.

[38] S. Castellari, N. Pinardi, and K. Leaman. A model study of air-sea interactions in the Mediterranean Sea. *J. Mar. Sys.*, 18(1-3):89–114, 1998.

[39] B. Cataletto, E. Feoli, S. Fonda Umani, and Sun Cheng-Yong. Eleven years of time-series analysis on the net-zooplankton community in the Gulf of Trieste. *ICES J. Mar. Sc.*, 52:669–687, 1995.

[40] B. Cermelj, A. Bertuzzi, and J. Faganeli. Modelling of pore water nutrient distribution and benthic fluxes in shallow coastal waters (Gulf of Trieste, Northern Adriatic). *Water, Air and Soil Poll.*, 99:435–444, 1997.

[41] I. Cerovecki, Z. Pasaric, M. Kuzmic, J. Brana, and M. Orlic. Ten day variability of the summer circulation in the North Adriatic. *Geofizika*, 8:67–81, 1991.

[42] J. Charney, M. Halem, and R. Jastrow. Use of incomplete historical data to infer the present state of the atmosphere. *J. Atmos. Sci.*, page 1162, 1969.

[43] J.S. Choi, A. Mazmunder, and R.I.C. Hansell. Measuring perturbation in a complicated, thermodynamic world. *Ecol. Modell.*, 117:143–158, 1999.

[44] C. Copin-Montégut. Consumption and production on scales of a few days of inorganic carbon, nitrate and oxygen by the planktonic community: results of continuous measurements at the Dyfamed Station in the northwestern Mediterranean Sea (May 1995). *Deep-Sea Res. I*, 47:447–477, 2000.

[45] S.H. Cousins. The trophic continuum in marine ecosystems: structure and equations for a predictive model. In R.E. Ulanowicz and T. Platt, editors, *Ecosystem theory for biological oceanography*, pages 76–93. Can. Bull. Fish Aquat. Sci. (213), 1985.

[46] S. Cozzi, G. Catalano, and M. Lipizer. Importanza e distribuzione spazio-temporale delle frazioni organiche disciolte dell'azoto e del fosforo nel bacino del nord Adriatico. In *Atti della Associazione Italiana di Oceanologia e Limnologia*, pages 21–32, Genova, 1999. Volume 13 (1). (In Italian).

[47] L.G. Davidavichiene and D.A. Sopauckiene. Inputs of nitrogen and phosphorus compounds from atmosphere. In I.N. Davidan and O.P. Savchuk, editors, *"Baltica" Project. Problems of studies and mathematical modelling of the Baltic SEa ecosystem. Issue 4. Main tenedencies of the ecystem's evolution.*, pages 112–118. Gidrometeoizdat, Leningrad, 1989. (In Russian).

[48] D. Degobbis, S. Fonda Umani, P. Franco, A. Malej, R. Precali, and N. Smodlaka. Changes in the northern Adriatic ecosystem and the hypertrophic appearenc of gelatinous aggregates. *Sc. Total. Env.*, 165:43–58, 1995.

[49] D. Degobbis, A. Malej, and S. Fonda Umani. The mucilage phenomenon in the northern Adriatic Sea. A critical review of the present scientific hypotheses. *Ann. Ist. Super. Sanitá*, 35(3):373–381, 1999.

[50] D. Degobbis, R. Precali, I. Ivancic, N. Smodlaka, D. Fuks, and S. Kveder. Long-term changes in the northern Adriatic ecosystem related to anthropogenic eutrophication. *Int. J. Env. Poll.*, 13(1-6):495–533, 2000.

[51] F.W. Dobson and S.P. Smith. Bulk model of solar radiation at the sea. *Q. J. R. Meteorol. Soc.*, 114:165–182, 1988.

[52] M.R. Droop. Some thoughts on nutrient limitation in algae. *J. Phycol.*, 9:264–272, 1973.

[53] H.W. Ducklow and C.A. Carlson. Oceanic bacterial production. In K.C. Marshall, editor, *Advances in microbial ecology*, chapter 12, pages 113–181. Plenum Press, 1992.

[54] J.A. Dusenberry, R.J. Olson, and S.W. Chisolm. Field observations of oceanic mixed layer dynamics and picophytoplankton photoacclimation. *J. Mar. Sys.*, 24:221–232, 2000.

[55] W. Ebenhöh. Stability in models versus stability in real ecosystems. *Senckenbergiana marit.*, 27(3/6):251–254, 1996.

[56] W. Ebenhöh. Critical analysis of the status quo in marine ecosystem modelling. In J. Fischer, J. Baretta, F. Colijn, and N.N. Flemming, editors, *Bio-ecological observations in operational oceanography*, page 27. EuroGOOS Publication No. 15, Southampton Oceanography Centre, 2000.

[57] W. Ebenhöh, J.G. Baretta, and J.W. Baretta. The primary production module in the marine ecosystem model ERSEM II with emphasis on the light forcing. *J. Sea Res.*, 38:173–193, 1997.

[58] W. Ebenhöh, K. Kohlmeier, and P.J. Radford. The benthic biological submodel in the European Regional Seas Ecosystem Model. *Neth. J. Sea Res.*, 33(3-4):423–452, 1995.

[59] ECMWF. The description of the ECMWF/WCRP Level III-A global atmospheric data archive. Technical report, European Center for Medium-range Weather Forecast, 1994.

[60] K. Eilola and A. Stigebrandt. On the seasonal nitrogen dynamics of the Baltic proper biogeochemical reactor. *J. Mar. Res.*, 57(4):693–713, 1999.

[61] G.T. Evans. The role of models and data sets in the Joint Global Ocean Flux Study. *Deep Sea Res. I*, pages 1369–1389, 1999.

[62] P.G. Falkowski. Light-shade adaptation and vertical mixing of marine phytoplankton: a comparative field study. *J. Mar. Res.*, 41:215–237, 1983.

[63] M.J.R. Fasham, H.W. Ducklow, and S.M. McKelvie. A nitrogen-based model of plankton dynamics in the oceanic mixed layer. *J. Mar. Res.*, 48:591–639, 1990.

[64] K. Fennel, M. Losch, J. Schröter, and M. Wenzel. Testing a marine ecosystem model: sensitivity analysis and parameter optimization. *J. Mar. Sys.*, 28:45–63, 2001.

[65] W. Fennel and T. Neumann. The mesoscale variability of nutrients and plankton as seen in a coupled model. *Germ. J. Hydrog.*, 48(1):49–71, 1996.

[66] R. La Ferla, C. Bacci, G. Chiodo, S. Parrino, and A. Zoppini. Stime di abbondanza e di biovolume batteriplanctonico nell'Adriatico settentrionale: confronto tra AO e DAPI. *Biologia Marina Mediterranea*, 5(1):750–753, 1998. in Italian.

[67] S. Fonda Umani. Pelagic production and biomass in the Adriatic Sea. *Sci. Mar.*, 60:65–77, 1996.

[68] S. Fonda Umani, C.Y. Sun, E. Feoli, B. Cataletto, M. Cabrini, and L. Milani. Is it possible to identify any plankton succession in the Gulf of Trieste (Northern Adriatic Sea)? In A. Eleftheriou, A.D. Ansell, and C.J. Smith, editors, *Biology and Ecology of Shallow Coastal Waters*, pages 59–65. 28th European Marine Biology Symposium, 1995.

[69] S. Fonselius. *On the stagnant conditions in the Baltic*, volume 14 of *Abstracts of Gothenburg dissertations in science*. Almqvist & Wiskell, Stockholm, 1969. 12 pp.

[70] S. Fonselius. Oxygen and hydrogen sulphide conditions in the Baltic Sea. *Marine pollution bulletin*, 12(6):187–194, 1981.

[71] B. Galperin, L.H. Kanta, S. Hassid, and A.Rosati. A quasi-equilibrium turbulent energy model for geophysical flows. *J. Atmos. Sci.*, 45:55–62, 1988.

[72] M. Giani, A. Boldrin, G. Matteucci, F. Frascari, M. Gismondi, and S. Rabitti. Downward fluxes of particulate carbon, nitrogen and phosphorus in the north-western Adriatic Sea. *Sc. Tot. Env.*, 266:125–134, 2001.

[73] M. Giani, M. Gismondi, F. Savelli, A. Boldrin, and S. Rabitti. Carbonio organico, azoto e fosforo particellati nell'Adriatico settentrionale: distribuzione verticale e variabilitá temporale. In *Atti della Associazione Italiana di Oceanologia e Limnologia*, pages 55–65, Genova, 2000. Volume 13 (2). (In Italian).

[74] J.K. Gibson, P.K. Kallberg, S. Uppala, A. Nomura, and E. Serrano. Era description. ECMWF Re-analysis Project Report Series 1, ECMWF, 1997.

[75] P. Giordani, D.E. Hammond, W.M. Berelson, G. Montanari, R. Poletti, A. Milandri, M. Frignani, L. Langone, M. Ravaioli, G. Rovatti, and E. Rabbi. Benthic fluxes and nutrient budgets for sediments in the northern Adriatic Sea: burial and recycling efficiencies. In R.A. Vollenweider, R. Marchetti, and R. Viviani, editors, *Marine coastal eutrophication*, pages 251–276. Elsevier, 1992.

[76] J.C. Goldman, D.A. Caron, and M.R. Dennet. Regulation of gross growth efficiency and ammonium regeneration in bacteria by substrate C:N ratio. *Limnol. Oceanogr.*, 32(6):1239–1252, 1987.

[77] H.H. Gran. On the conditions for the production of plankton in the sea. *Rapp. P-v. Reun. Cons. Int. Exp. Mer.*, 75:37–46, 1931.

[78] E. Graneli, P. Carlsson, J.T. Turner, P.A. Tester, C. Bechemin, R. Dawson, and E. Funari. Effects of N:P:Si ratios and zooplankton grazing on phytoplankton communities in the northern

Adriatic Sea. I. Nutrients, phytoplankton biomass, and polysaccharide production. *Aquat. Microb. Ecol.*, 18:37–54, 1999.

[79] D.B. Haidvogel and A. Beckmann. Numerical models of the coastal ocean. In Kenneth H. Brink and Allan R. Robinson, editors, *The Sea*, volume 10, pages 457–482. John Wiley & Sons, Inc., 1998.

[80] HELCOM. First periodic assessment of the state of the marine environment of the Baltic Sea, 1980-1985. Balt. Sea Environ. Proc. No. 17 B, HELCOM, 1987.

[81] HELCOM. Deposition of airborne pollutants in the baltic sea area: 1983 - 1985 and 1986. Balt. Sea Environ. Proc. No. 35 B, HELCOM, 1989.

[82] HELCOM. Second periodic assessment of the state of the marine environment of the Baltic Sea, 1984-1988; Background document. Balt. Sea Environ. Proc. No. 35 B, HELCOM, 1990.

[83] HELCOM. Third periodic assessment of the state of the marine environment of the Baltic Sea, 1989-1993; Background document. Balt. Sea Environ. Proc. No. 64 B, HELCOM, 1996.

[84] R.A. Herbert. Nitrogen cycling in coastal marine ecosystems. *FEMS Mic. Rev.*, 23:563–590, 1999.

[85] E.E. Hofmann and C.M. Lascara. Overview of Interdisciplinary Modeling for Marine Ecosystems. In K. H. Brink and A. R. Robinson, editors, *The Sea*, volume 10, pages 507–540. John Wiley & Sons, Inc., 1998.

[86] D.C. Hurd. Interaction of biogenic opale, sediment and seawater in the central equatorial Pacific. *Geochim. cosmochim. acta*, 37:2257–2282, 1973.

[87] G.C. Hurtt and R.A. Armstrong. A pelagic ecosystem model calibrated with BATS data. *Deep Sea Res. II*, 43:653–683, 1996.

[88] G.C. Hurtt and R.A. Armstrong. A pelagic ecosystem model calibrated with BATS and OWSI data. *Deep Sea Res. I*, 46:27–61, 1999.

[89] S.E. Jørgensen. Ecological modelling and systems ecology. *Ecol. Model.*, 117:1–2, 1999.

[90] J.T.O. Kirk. *Light and photosynthesis in aquatic ecosystems*. Cambridge University Press, Cambridge, 1983.

[91] O. Klepper, J.C.H. Peters, J.P.G. Van de Kamer, and P. Eilers. The calculation of primary production in an estuary. A model that incorporates the dynamic response of algae, vertical mixing and basin morphology. In A. Marani, editor, *Advances in environmental modelling*, pages 373–394. Elsevier, Amsterdam, 1988.

[92] C. Kohlmeier and W. Ebenhöh. The stabilizing role of cannibalism in a predator-prey system. *Bull. Math. Biol.*, 57(3):401–411, 1995.

[93] G. Korres, N. Pinardi, and A. Lascaratos. The ocean response to low-frequency interannual atmospheric variability in the Mediterranean Sea. Part II: empirical orthogonal functions analysis. *J. Clim.*, 13:732–745, 2000.

[94] V.H. Kourafalou. Process studies on the Po River plume, North Adriatic Sea. *J. Geophys. Res.*, 104(C12):29963–29985, 1999.

[95] J. Kuparinen and A. Heinaenen. Inorganic nutrient and carbon controlled bacterioplankton growth in the Baltic Sea. *Estuar. Coast. Shelf Sci.*, 37:271–285, 1993.

[96] G. Lacroix and P. Nival. Influence of meteorological variability on primary production dynamics in the ligurian sea (NW Mediterranean Sea) with a 1D hydrodynamic/biological model. *J. Mar. Sys.*, 16:23–50, 1998.

[97] A. Lascaratos, R.G. William, and E. Tragou. A mixed-layer study of the formation of Levantine Intermediate Water. *J. Geophys. Res.*, 98(C8):14,739–14,749, 1993.

[98] S. Lee and J.A. Fuhrman. Relationships between biovolume and biomass of naturally derived bacterioplankton. *Appl. Env. Microbiol.*, 53:1298–1303, 1987.

[99] D.R. Legates and C.J. WIllmott. Mean seasonal and spatial variability in gauge-corrected global precipitation. *Int. J. Climatol.*, 10:111–127, 1990.

[100] L. Legendre and F. Rassoulzadegan. Plankton and nutrient dynamics in marine waters. *Ophelia*, 41:153–172, 1995.

[101] A Lehmann and H.-H. Hinrichsen. On the thermohaline variability of the Baltic Sea. *J. Mar. Sys.*, 25(3-4):333–357, 2000.

[102] P.F.J. Lermusiaux. Data assimilation via error subspace statistical estimation. Part II: Middle Atlantic Bight shelfbreak front simulations and ESSE validation. *Monthly Weather Review*, 127:1408–1432, 1999.

[103] P.S. Liss and L. Merlivat. Air-sea gas exchange rates: introduction and synthesis. In P. Buat-Menard, editor, *The role of air-sea exchange in Geochemical cycling*, pages 113–127. 1986.

[104] C.J. Lozano, A.R. Robinson, H.G. Arango, A. Gangopadhyay, Q. Sloan, P.J. Haley, L. Anderson, and W. Leslie. An Interdisciplinary Ocean Prediction System: Assimilation strategies and structured data models. In P. Malanotte-Rizzoli, editor, *Modern Approaches to Data Assimilation in Ocean Modeling*, pages 413–451. Elsevier Science B.V., 1996.

[105] D. R. Lynch and C. E. Naimie. Hydrographic data assimilation on Georges Bank. In M. L. Spaulding and A. F. Blumberg, editors, *Estuarine and Coastal Modeling*, pages 523–539. American Society of Civil Engineers, 1997. 5th international conference, Alexandria, Virginia.

[106] A. Maggiore, M. Zavatarelli, M.G. Angelucci, and N. Pinardi. Surface heat and water fluxes in the Adriatic Sea: Seasonal and interannual variability. *Phys. Chem. Earth*, 23(5-6):561–567, 1998.

[107] P. Malanotte-Rizzoli and A. Bergamasco. The dynamics of the coastal region of the Northern Adriatic Sea. *J. Phys. Oceanogr.*, 13(1105-1130), 1983.

[108] A. Malej and S. Fonda Umani. Evoluzione delle interazioni trofiche nell'ecosistema del Golfo di Trieste. In *Evoluzione dello stato trofico in Adriatico: analisi degli interventi attuati e future linee di intervento*, pages 61–70. Regione Emilia-Romagna, Provincia di Ravenna, Autoritá di bacino del fiume Po, 1995.

[109] A. Malej, P. Mozetic, V. Malacic, S. Terzic, and M. Ahel. Phytoplankton responses to freshwater inputs in a small semi-enclosed gulf (Gulf of Trieste, Adriatic Sea). *Mar. Ecol. Prog. Ser.*, 120:111–121, 1995a.

[110] K.H. Mann. Towards predictive models for coastal marine ecosystems. In L.R. Pomeroy and J.J. Alberts, editors, *Concepts of Ecosystem Ecology*, pages 291–316. Springer-Verlag, 1988.

[111] R. Marchetti, A. Provini, and G. Crosa. Nutrient load by the River Po into the Adriatic Sea, 1968/87. *Mar. Pollut. Bull.*, 20(4):168–172, 1989.

[112] R. Marchetti and N. Verna. Quantification of the phosphorus and nitrogen loads in the minor rivers of the Emilia-Romagna coast (Italy). *Sci. Total Environ.*, Suppl.:315–336, 1992.

[113] R. Margalef. From hydrodynamic processes to structure (information) and from information to process. In R.E. Ulanowicz and T. Platt, editors, *Ecosystem theory for biological oceanography*, pages 200–220. Can. Bull. Fish Aquat. Sci. (213), 1985.

[114] J. Marra. Phytoplankton photosynthetic response to vertical movement in a mixed layer. *Mar. Biol.*, 46:203–208, 1978.

[115] R.J. Matear. Parameter optimization and analysis of ecosystem models using simulated annealing: a case study at Station P. *J. Mar. Res.*, 53:571–607, 1995.

[116] G. L. Mellor. *Users guide for a three-dimensional primitive equation numerical ocean model*. Princeton University, 1998.

[117] G.L. Mellor. Retrospect on oceanic boundary layer modeling and second moment closure. In P. Mueller and D. Henderson, editors, *Acts of the Hawaiian Winter Workshop*, January 1989.

[118] G.L. Mellor. An equation of state for numerical models of ocean and estuaries. *Journal Atmospheric and Oceanic Tech.*, 8:609–611, 1991.

[119] G.L. Mellor and T. Yamada. Development of a Turbulence Closure Model for Geophysical Fluid Problems. *Rev. Geoph. Space Phys.*, 20(4):851–875, 1982.

[120] T. Melvasalo. Regional marine environmental management and the GPA-LBA: perspectives and the need for scientific support. *Oc. Coast. Manag.*, 43:713–724, 2000.

[121] P. Mozetič, S. Fonda Umani, B. Cataletto, and A. Malej. Seasonal and inter-annual plankton variability in the Gulf of Trieste in the northern Adriatic. *ICES J. Mar. Sc.*, 55(4):711–722, 1998.

[122] M. Murakami, Y. Oonishi, and H. Kunishi. Heat and salt balances in the Seto Inland Sea. *J. Oc. Soc. Japan*, 45(3):204–216, 1989.

[123] J.J. Naudin, V. Malacic, and M. Celio. Hydrological characteristics of the Gulf of Trieste (Northern Adriatic) during high fresh-water input in early summer. In *Proceedings of the workshop "Physical and biogeochemical processes in the Adriatic Sea"*, pages 71–81, Portonovo (Ancona), Italy, 1996.

[124] N. Nyholm. Kinetics of nitrogen-limited algal growth. *Prog. Wat. Tech.*, 8:347–358, 1977.

[125] I. Obernosterer, P. Ruardij, and G.J. Herndl. Spatial and diurnal dynamics of dissolved organic matter (DOM) fluorescence and H_2O_2 and the photochemical oxygen demand of surface water DOM across the subtropical Atlantic Ocean. *Lymnol. Oceanogr.*, 46(3):632–643, 2001.

[126] E.P. Odum. *Systems Ecology*. J. Whiley and Sons, Toronto, 1983.

[127] S. Olenin. Some biological consequences of deep water stagnation in the eastern Gotland Basin, Baltic Sea in 1980s. In R.V. Thurston, editor, *Environmental studies in the Nemunas River Basin, Lithuania*, volume EPA/600/R-94/155, pages 147–155. Athens, Georgia, USA, 1994.

[128] Anders Omstedt and Lars B. Axell. Modeling the seasonal, interannual, and long-term variations of salinity and temperature in the Baltic proper. *Tellus*, 50A:637–652, 1998.

[129] M. Orlic, M. Gacic, and P.E. La Violette. The currents and circulation of the Adriatic Sea. *Oceanologica Acta*, 15:109–124, 1992.

[130] C. Osterroht and H. Thomas. New production enhanced by nutrient supply from non-Redfield remineralisation of freshly produced organic material. *J. Mar. Sys.*, 25:33–46, 2000.

[131] E.D. Palma and R.P. Matano. On the implementation of passive open boundary conditions for a general circulation model: The barotropic mode. *J. Geoph. Res*, 103(C1):1319–1341, 1998.

[132] E.D. Palma and R.P. Matano. On the implementation of open boundary conditions for a general circulation model: The three-dimensional case. *J. Geophys. Res*, 105(C4):8605–8628, 2000.

[133] C.A. Paulson and J.J. Simpson. Irradiance measurements in the upper ocean. *J. Phys. Oceanogr.*, 7:952–956, 1977.

[134] M. Pettine, S. Capri, M. Manganelli, L. Patrolecco, A. Puddu, and A. Zoppini. The dynamics of DOM in the northern Adriatic Sea. *Est. Coast. Shelf Sci.*, 52:471–489, 2001.

[135] M. Pettine, L. Patrolecco, M. Camusso, and S. Crescenzio. Transport of carbon and nitrogen to the northern Adriatic Sea by the Po River. *Est. Coast. Shelf Sci.*, 46:127–142, 1998.

[136] M. Pettine, L. Patrolecco, M. Manganelli, S. Capri, and M.G. Farrace. Seasonal variations of dissolved organic matter in the northern Adriatic Sea. *Mar. Chem.*, 64:153–169, 1999.

[137] J.D. Pietrzak. A comparison of advection schemes for ocean modelling. Technical Report 95-8, Danish Meteorological Institute, 1995.

[138] L. Piker, R. Schmaljohann, and J.F. Imhoff. Dissimilatory sulfate reduction and methane production in Gotland Deep sediments Baltic Sea during a transition period from oxic to anoxic bottom water (1993-1996). *Aquat. Microb. Ecol.*, 14:183–193, 1998.

[139] T. Platt. Structure of marine ecosystems: its allometric basis. In R.E. Ulanowicz and T. Platt, editors, *Ecosystem theory for biological oceanography*, pages 55–64. Can. Bull. Fish Aquat. Sci. (213), 1985.

[140] T. Platt, K.H. Mann, and R.E. Ulanowicz. *Mathematical models in biological oceanography*. UNESCO press, Paris, 1981. 156 pp.

[141] L.R. Pomeroy, E.C. Hargrove, and J.J. Alberts. The ecosystem perspective. In L.R. Pomeroy and J.J. Alberts, editors, *Concepts of Ecosystem Ecology*, pages 1–17. Springer-Verlag, 1988.

[142] D. Prandle, C.F. Jago, S.E. Jones, D.A. Purdie, and A. Tappin. The influence of horizontal circulation on the supply and distribution of tracers. *Phil. Trans. R. Soc. Lond.*, 343(1669):405–422, 1993.

[143] Rodolph W. Preisendorfer. *Principal Component Analysis in meteorology and Oceanography*, volume 17 of *Developments in Atmospheric Science*. Elsevier, 1988.

[144] PRISMA1. Rapporto tematica "Cicli biogeochimici ed indagini ecofisiologiche". Technical report, Consiglio Nazionale delle Ricerche, Roma, 1999. M. Giani and A. Puddu (eds.), in italian.

[145] A. Puddu, R. La Ferla, A. Allegra, C. Bacci, M. Lopez, F. Oliva, and C. Pierotti. Seasonal and spatial distribution of bacterial production and biomass along a salinity gradient (Northern Adriatic Sea). *Hydrobiologia*, 363:271–282, 1998.

[146] A. Puddu, A. Zoppini, and M. Pettine. Dissolved organic matter and microbial food web interactions in the marine environment: the case of the Adriatic Sea. *Int. J. Env. Poll.*, 13(1-6):473–494, 2000.

[147] L. Rahm, A. Jönsson, and F. Wulff. Nitrogen fixation in the baltic proper: an empirical study. *J. Mar. Sys.*, 25:239–248, 2000.

[148] F. Raicich. Note on the flow rates of the Adriatic rivers. Technical Report RF 02/94, Consiglio Nazionale delle Ricerche, Istituto Sperimentale Talassografico, 1994.

[149] W.H. Raymond. High-order low-pas implicit tangent filters for use in finite area calculations. *Mon. Wea. Rev.*, 116:2132–2141, 1988.

[150] A.C. Redfield, B. Ketchum, and F. Richards. The influence of organisms on the composition of seawater. In M. Hill, editor, *The Sea*, pages 26–77. Interscience, New York, 1963.

[151] N. Revelante and M. Gilmartin. The relative increase of larger phytoplankton in a subsurface chlorophyll maximum of the northen Adriatic Sea. *J. Plankton Res.*, 17(17):1535–1562, 1995.

[152] H. Ridderinkhof. On the effects of variability in meteorological forcing on the vertical structure of a stratified watercolumn. *Continental Shelf Research*, 12(1):25–36, 1992.

[153] R. Riegman, B.R. Kuipers, A.A.M. Noordeloos, and H.J. Witte. Size-differential control of phytoplankton and the structure of plankton communities. *Neth. J. Sea Res.*, 31(3):255–265, 1993.

[154] R.B. Rivkin and L. Legendre. Biogenic carbon cycling in the upper ocean: effects of microbial respiration. *Science*, 291:2398–2400, 2001.

[155] A.R. Robinson. Physical processes, field estimation and an approach to interdisciplinary ocean modeling. *Earth Science Reviews*, 40:3–54, 1995.

[156] A.R. Robinson, P.F. Lermusiaux, and N.Q. Sloan III. Data assimilation. In K.H. Brink and A.R. Robinson, editors, *The Sea*, volume 10, pages 541–594. John Wiley & Sons, Inc., 1998.

[157] A.R. Robinson and P.F.J. Lermusiaux, editors. *Workshop on the assimilation of biological data in coupled physical/ecosystem models*, CNR Research Area, Bologna, Italy, June 28-30, 1999, 2000. GLOBEC.

[158] A.R. Robinson, J.J. McCarthy, and B.J. Rotschild. Interdisciplinary ocean science is evolving and a systems approach is essential. *J. Mar. Sys.*, 22:231–239, 1999.

[159] U. Rönner and F. Sörensson. Denitrification rates in the low-oxygen waters of the stratified Baltic proper. *Appl. Environ. Microbiol.*, 50:801–806, 1985.

[160] P. Ruardij, J.W. Baretta, and J.G. Baretta-Bekker. SESAME, a Software Environment for Simulation and Analysis of Marine Ecosystems. *Neth. J. Sea Res.*, 33(3-4):261–270, 1995.

[161] P. Ruardij, H. Van Haren, and H. Ridderinkhof. The impact of thermal stratification on phytoplankton and nutrient dynamics in shelf seas: a model study. *J. Sea Res.*, 38(3-4):311–331, 1997.

[162] P. Ruardij and W. Van Raaphorst. Benthic nutrient regeneration in the ERSEM ecosystem model of the North Sea. *Neth. J. Sea Res.*, 33(3-4):453–483, 1995.

[163] R.N. Sambrotto, G. Savidge, C. Robinson, P. Boyd, T. Takahashi, D.M. Karl, C. Langdon, D. Chipman, J. Marra, and L. Codispoti. Elevated consumption of carbon relative to nitrogen in the surface ocean. *Nature*, 363:248–250, 1993.

[164] D.R. Schink, N.L. Guinasso, and K.A. Fanning. Processes affecting the concentration of silica at the sediment-water interface of the atlantic ocean. *Geophys. Res*, 80:3013–3031, 1975.

[165] H. Scholten and A.C. Smaal. The ecophysiological response of mussels (*mytilus edulis*) in mesecosms to a range of inorganic nutrient loads: simulations with the model EMMY. *Aquatic Ecol.*, 33:83–100, 1999.

[166] S. Schulz, W. Kaiser, and G. Breuel. A comparison of biological data from 1976-1990 and 1991 - the influence of a warm winter. Technical Report 1992/L:19, ICES, 1992.

[167] R. Shapiro. Smoothing, filtering and boundary effects. *Rev. Geophys. Space Phys.*, 8(2):359–387, 1970.

[168] R. Shapiro. The use of linear filtering as a parametrization of atmospheric diffusion. *J. Atmos. Sci.*, 28:523–531, 1971.

[169] S.Hellerman and M. Rosenstein. Normal monthly wind stress over the world ocean with error estimates. *J. Phys.Oceanogr.*, 13:1093–1104, 1983.

[170] C.P. Slomp and W. Van Raaphorst. Nutrient early diagenesis in the sandy sediments of the Dogger Bank area, North Sea: pore water results. Technical report, NIOZ, 1990.

[171] C.P. Slomp and W. Van Raaphorst. Forms of phosphorus in North Sea sediments and fluxes across the sediment-water interface. In W. Van Raaphorst and J.P. Boon, editors, *The integrated North Sea programme 1991-1992, preliminary results.*, volume 9 of *NIOZ-report*, pages 20–23. NIOZ, 1993.

[172] P.K. Smolarkiewicz. A simple positive definite advection transport scheme with small implicit diffusion. *Mon. Wea. Rev.*, 111:479–486, 1983.

[173] P.K. Smolarkiewicz. A fully multidimensional positive definite advection transport algorithm with small implicit diffusion. *J. Comput. Phys.*, 54:325–362, 1984.

[174] SMR-ARPA. Progetto SINA: analisi e progettazione delle reti di monitoraggio ambientale su base regionale e sub-regionale. Technical report, Servizio Meteorologico Regionale (ARPA), Regione Emilia Romagna, 1999. In Italian.

[175] A. Sokolov and F. Wulff. Swingstations: a web-based client tool for the baltic environmental database. *Computers and Geosciences*, 25:863–871, 1999.

[176] U. Sommer. *Planktologie*. Springer-Verlag, Berlin, 1994.

[177] Y.H. Spitz, J.R. Moisan, and M.R. Abbott. Configuring an ecosystem model using data from the Bermuda Atlantic Time Series (BATS). *Deep Sea Res. II*, 48:1733–1768, 2001.

[178] Y.H. Spitz, J.R. Moisan, M.R. Abbott, and J.G. Richman. Data assimilation and a pelagic ecosystem model: parameterization using time series observations. *J. Mar. Sys.*, 16:51–68, 1998.

[179] M. Stachowisch. Mass mortality in the Gulf of Trieste: the course of community destruction. *Marine Ecol. P.S.Z.N*, 5:243–264, 1984.

[180] J. H. Steele. Environmental control of photosynthesis in the sea. *Limnol. Oceanogr.*, 7:137–150, 1962.

[181] A. Stigebrandt. A model for the vertical circulation of the Baltic deep water. *J. Phys. Oc.*, 17:1772–1785, 1987.

[182] A. Stigebrandt. Computations of oxygen fluxes through the sea surface and the net production of organic matter with application to the Baltic and adjacent seas. *Limnol. Oceanogr.*, 36(3):444–454, 1991.

[183] A. Stigebrandt and L. Djurfeldt. Control of production of organic matter in the ocean on short and long terms by stratification and remineralization. *Deep Sea Res. II*, 43:23–35, 1996.

[184] P. Stålnacke. *Nutrient loads to the Baltic Sea*. PhD thesis, Linköping University, Sweden, 1996.

[185] P. Stålnacke, A. Grimvall, K. Sundblad, and A. Tonderski. Estimation of riverine loads of nitrogen and phosphorus to the Baltic Sea, 1970-1993. *Environ. Monit. Assess.*, 58:173–200, 1998.

[186] M. Stramska and T.D. Dickey. Phytoplankton blooms and the vertical structure of the ocean. *J. Mar. Res.*, 51:819–842, 1993.

[187] F. Stravisi. Some characteristics of the circulation in the Gulf of Trieste. *Thalassia Jugosl.*, 19(1/4):355–363, 1983a.

[188] F. Stravisi. The vertical structure annual cycle of the mass field parameters in the Gulf of Trieste. *Boll. Oceanol. Teor. Appl.*, 1:239–250, 1983b.

[189] B. Sturm, M. Kuzmic, and M. Orlic. An evaluation and interpretation of CZCS-derived patterns on the Adriatic shelf. *Oceanol. Acta*, 15(1):13–23, 1992.

[190] N. Supić and M. Orlić. Seasonal and interannual variability of the northern Adriatic surface fluxes. *J. Mar. Sys.*, 20:205–229, 1999.

[191] H.V. Sverdrup. On conditions for the vernal blooming of phytoplankton. *J. Cons. Perm. Int. Exp. Mer*, 18:287–295, 1953.

[192] H. Thomas, V. Ittekkot, C. Osterroht, and B. Schneider. Preferential recycling of nutrients - the ocean's way to increase new production and to pass nutrient limitation? *Limnol. Oceanogr.*, 44(8):1999–2004, 1999.

[193] D.W. Townsend, M.D. Keller, M.E. Sieracki, and S.G. Ackleson. Spring phytoplankton blooms in the absence of vertical water column stratification. *Nature*, 360:59–62, 1992.

[194] L. Tuominen, A. Heinanen, J. Kuparinen, and L.P. Nielsen. Spatial and temporal variability of denitrification in the sediments of the northern Baltic proper. *Mar. Ecol. Prog. Ser.*, 172:13–24, 1998.

[195] R.E. Ulanowicz. *Growth and development: ecosystem phenomenology*. Springer-Verlag, New York, 1986.

[196] R.E. Ulanowicz and T. Platt, editors. *Ecosystem theory for biological oceanography*. Can. Bull. Fish Aquat. Sci. 213, 1985.

[197] J.J. Vallino. Improving marine ecosystem models: use of data assimilation and mesocosm experiments. *J. Mar. Res.*, 58:117–164, 2000.

[198] R.A. Varela, A. Cruzado, and J.E. Gabaldon. Modelling primary production in the North Sea using the European Regional Seas Ecosystem Model. *Neth. J. Sea Res.*, 33(3-4):337–361, 1995.

[199] M. Vichi. The influence of high-frequency surface forcing on productivity in the euphotic layer. In J. Fischer, J. Baretta, F. Colijn, and N.N. Flemming, editors, *Bio-ecological observations in operational oceanography*, pages 29–30. EuroGOOS Publication No. 15, Southampton Oceanography Centre, 2000.

[200] M. Vichi, J.W. Baretta, and P. Ruardij. Interannual and long-term variability in Baltic ecosystem dynamics: causes and implications. Technical Report Project 8130, Danish Hydraulic Institute, September 1999.

[201] M. Vichi, N. Pinardi, M. Zavatarelli, G. Matteucci, M. Marcaccio, M.C. Bergamini, and F. Frascari. One-dimensional ecosystem model tests in the Po Prodelta Area (Northern Adriatic Sea). *Env. Mod. Soft.*, 13:471–481, 1998a.

[202] M. Vichi, M. Zavatarelli, and N. Pinardi. Seasonal modulation of microbial-mediated carbon fluxes in the Northern Adriatic Sea. *Fish. Oceanogr.*, 7(3/4):182–190, 1998b.

[203] R.A. Vollenweider, A. Rinaldi, and G. Montanari. Eutrophication, structure and dynamics of a marine coastal system: results of a ten-year monitoring along the Emilia-Romagna coast. In R.A. Vollenweider, R. Marchetti, and R. Viviani, editors, *Marine Coastal Eutrophication*, pages 63–106, Amsterdam, 1992. Regione Emilia-Romagna, Elsevier.

[204] X.H. Wang and N. Pinardi. Modelling the dynamics of sediment transport and resuspension in the northern Adriatic Sea. *J. Geophys. Res.*, 2002. (in press).

[205] A. Weiss. The solubility of nitrogen, oxygen and argon in water and seawater. *Deep Sea Res.*, 17:721–735, 1970.

[206] F. Wulff and L. Rahm. A database and its tools. In F. Wulff, editor, *Large-scale environmental effects and ecological processes in th Baltic Sea. Research program for the period 1990-1995 and background documents.*, number 3856, chapter 13, pages 217–225. SNV Report, Stockholm, Sweden, 1990.

[207] F. Wulff, L. Rahm, A.K. Hallin, and J. Sandberg. A nutrient budget model of the Baltic Sea. In F. Wulff, L. Rahm, and P. Larsson, editors, *A systems analysis of the changing Baltic Sea*, Ecological studies. Springer, 1998.

[208] F. Wulff and A. Stigebrandt. A time-dependent budget model for nutrients in the Baltic Sea. *Glob. Biogeochem. Cycles*, 3(1):63–78, 1989.

[209] M. Xue. High-order monotonic numerical diffusion and smoothing. *Mon. Wea. Rev.*, 128(8):2853–2864, 2000.

[210] R. Zaccone, R. La Ferla, G. Caruso, and M. Azzaro. Attivita' proteasica e respiratoria microbica in due aree dell'Adriatico settentrionale. In *Atti XII Congresso AIOL*, pages 33–44. Associazione Italiana di Limnologia ed Oceanografia, 1999. in Italian.

[211] M. Zavatarelli, J.W. Baretta, J.G. Baretta-Bekker, and N. Pinardi. The dynamics of the Adriatic Sea ecosystem; an idealized model study. *Deep Sea Res.*, 47:937–970, 2000.

[212] M. Zavatarelli, D. Bregant, F. Raicich, A. Russo, and A. Artegiani. Climatological biogeochemical characteristic of the Adriatic Sea. *J. Mar. Sys.*, 18:227–263, 1998.

[213] M. Zavatarelli, N. Pinardi, and A. Gennari. The Adriatic Sea Modeling System: a nested approach. *Ann. Geophys.*, 2002. (accepted for publication).

[214] M. Zavatarelli, N. Pinardi, V.H. Kourafalou, and A. Maggiore. Diagnostic and prognostic model studies of the Adriatic Sea circulation: the seasonal variability. *J. Geophys. Res.*, 107(C1):4/1–4/20, 2002.

[215] U. Zweifel. Consumption of dissolved organic carbon by marine bacteria and demand for inorganic nutrients. *Mar. Ecol. Progr. Ser.*, 101:23–32, 1993.

APPENDICES

List of Equation Boxes

A. Review of the ERSEM III biogeochemical equations. The pelagic model

A.1. The mathematical formulation of the biogeochemical processes

The generic partial differential equation describing the rate of change for the Eulerian model state variable $C(\vec{x},t)$ indicating the concentration in time and space of a generic biogeochemical constituent of ERSEM (Table A.1) is written in the following form:

$$\frac{\partial C}{\partial t} = \left.\frac{\partial C}{\partial t}\right|_{phys} + \left.\frac{\partial C}{\partial t}\right|_{bio} \tag{A.1}$$

where the total time rate of change is given by the algebraic sum of a source term solely due to physical transport processes and by a source term determined by biogeochemical processes. The formulation of the first term on the right hand side of (A.1) is treated in Appendix C. Here and in the following sections we will focus on the last term of (A.1), concerning the parameterization of the biogeochemical processes.

The state variables of ERSEM III (Figure A.2) can be of two types: functional groups and ordinary state variables. The concept of functional group has been presented in Sections 2.1 and 2.2.3, while with ordinary state variables we intend non-living components both organic and inorganic that participate to the biogeochemical cycling of the modeled elements. Ordinary state variables can be scalars or vectors, while a functional group state variable can only be a vector. In the present formulation, each functional group state variable is formally written as a four-dimensional vector varying in time and space $G_i(\vec{x},t)$, $i = 1,2,3,4$. The components of the vector represent the projection of the functional group into the major biological elements considered in the model, *i.e.* carbon (C), nitrogen (N), phosphorus (P) and silica (Si) as shown in Figure A.1. For ease of reading and in order to adhere to the original ERSEM code notation (Blackford and Radford, 1995), the following formal identity is applied:

$$G_i \equiv (G_1, G_2, G_3, G_4) \equiv (G_c, G_n, G_p, G_s).$$

Such conventions are particularly useful for future extensions of the model parameterization; in the deterministic description of particular marine ecosystems it could be necessary to introduce other basic constituents of biological cells such as micronutrients (Fe, K, Na, etc.) that are not considered in the current implementation. In such cases, the number of dimensions of the functional group vector can be increased in order to extend to the required components, also adding the relative dynamical differential equations for those vector components.

The basic idea of the mathematical notation is that the biological rate term in (A.1) can be written using two different formulations, which correspond to two different interpretation levels: 1) flux form; and 2) functional process form. In *flux form*, the biogeochemical rate of change of the model state variable component C is written as:

$$\left.\frac{\partial C}{\partial t}\right|_{bio} = \left.\frac{\partial C}{\partial t}\right|_{V_1}^{e_1} - \left.\frac{\partial C}{\partial t}\right|_{V_2}^{e_2} - \left.\frac{\partial C}{\partial t}\right|_{V_3}^{e_3} \cdots + \left.\frac{\partial C}{\partial t}\right|_{V_n}^{e_n}, \tag{A.2}$$

where the right hand side contains the series of source and sink terms. The superscripts e are the abbreviations indicating the process which determines the variation (the complete list is given in Table A.2). The subscripts V indicate the state variable(s) or functional group vector component(s) involved. If $V = C$, we refer to intra-group fluxes such as cannibalism. In (A.2), the sign of each flux term is algebraically written and the following identity, which is actually an expression of the mass conservation law, is always verified:

$$\left.\frac{\partial C}{\partial t}\right|_{V}^{e} = \left.\frac{\partial V}{\partial t}\right|_{C}^{e}. \tag{A.3}$$

Instead, in an equation written in the *functional process form*, the formulation of the dynamic dependencies on other variables is made explicit, *i.e.*: all the fluxes of (A.2) are given in the complete functional parameterization. Although this is the more complete mathematical form, it is more difficult to read and interpret at a glance, especially when trying to distinguish which processes affect the variable dynamics.

In the following sections we will describe the structure of the pelagic model components first giving the set of differential equations in the flux form in a separate box of equations and then describing the parameterization of the source/sink terms in the text.

Variable	Type	Constituent	Description	Reference
$N^{(1)}$	OSV	P	Phosphate (mmol P m^{-3})	Baretta et al., 1995
$N^{(3)}$	OSV	N	Nitrate (mmol N m^{-3})	"
$N^{(4)}$	OSV	N	Ammonium (mmol N m^{-3})	"
$N^{(5)}$	OSV	Si	Silicate (mmol Si m^{-3})	"
$N^{(6)}$	OSV	R	Reduction equivalents, HS^- (mmol S m^{-3})	*this work*
$O^{(2)}$	OSV	O	Dissolved Oxygen (mmol O_2 m^{-3})	Baretta et al., 1995; Liss and Merlivat, 1986; Weiss, 1972
$O^{(3)}$	OSV	C	Carbon Dioxide (mg C m^{-3}, sink term)	-
$P_i^{(1)}$	FG	C N P Si	Diatoms (mg C m^{-3} and mmol N-P-Si m^{-3})	Varela et al.,1995; Ebenhoeh et al, 1997; Baretta-Bekker et al., 1997
$P_i^{(2)}$	FG	C N P	Flagellates (mg C m^{-3} and mmol N-P m^{-3})	"
$P_i^{(3)}$	FG	C N P	Picophytoplankton (")	"
$P_i^{(4)}$	FG	C N P	Large Phytoplankton - Dinoflagellates (")	"
B_i	FG	C N P	Pelagic Bacteria (")	Baretta-Bekker et al., 1995; Baretta-Bekker et al., 1997
$Z_i^{(3)}$	FG	C N P	Carnivorous Mesozooplankton (")	Broekhuizen et al., 1995
$Z_i^{(4)}$	FG	C N P	Omnivorous Mesozooplankton (")	"
$Z_i^{(5)}$	FG	C N P	Microzooplankton (")	Baretta-Bekker et al., 1995; Baretta-Bekker et al., 1997
$Z_i^{(6)}$	FG	C N P	Heterotrophic Flagellates (")	"
$R_i^{(1)}$	FG	C N P	Dissolved Organic Detritus (")	Baretta et al., 1995
$R_i^{(6)}$	FG	C N P Si	Particulate Organic Detritus (")	"
$L_{P(j)}$	OSV	-	Photoadaptation property (mg C m^{-3} W m^{-2})	Ebenhoeh et al., 1997

Table A.1.: List of functional groups (FG) and ordinary state variables (OSV) for the pelagic model and references to the original parameterization of the implemented processes. For global state variables like nutrients and organic matter the reference to the general descriptive publication (Baretta *et al.*, 1995) is given.

Abbreviation	Comment
gpp	Gross primary production
rsp	Respiration
prd	Predation
out	Excretion/Release
exu	Exudation
upt	Uptake

Table A.2.: List of all the abbreviations used to indicate the biogeochemical processes in (A.2).

A.1.1. The ERSEM food matrix

One of the more concise but appropriate methods for describing trophic interactions in a complex food web is to build a food matrix. Each element of the matrix represents the percentage of availability/preference of that particular trophic level with regard to the others. The values in the food matrix are a peculiarity of each ecosystem and therefore it reflects the specific model implementation. We describe here a sort of standard food matrix, which is mainly derived from the ERSEM II standard values and the experience of the ERSEM applications.

The mathematical form of the rectangular matrix used in the pelagic model is written as:

$$\delta_{Z,X} = \begin{bmatrix} \delta_{Z^{(3)},P^{(1)}} & \cdots & \delta_{Z^{(3)},B} \\ \vdots & \vdots & \vdots \\ \delta_{Z^{(6)},P^{(1)}} & \cdots & \delta_{Z^{(6)},B} \end{bmatrix} \tag{A.4}$$

where X are the preys

$$X \equiv \left\{ P_i^{(1)}, P_i^{(2)}, P_i^{(3)}, P_i^{(4)}, Z_i^{(3)}, Z_i^{(4)}, Z_i^{(5)}, Z_i^{(6)}, B_i \right\}$$

and Z the predators

$$Z \equiv \left\{ Z_i^{(3)}, Z_i^{(4)}, Z_i^{(5)}, Z_i^{(6)} \right\}.$$

The numerical values of the pelagic food matrix are shown in Table A.3. In the description of the model equations we will refer to them in order to derive the proper dynamical equations for the predation terms and food sources in general.

A.2. Phytoplankton

Primary producers in ERSEM are divided in four principal functional types representing on a first approximation the spectrum of functional behavior of phytoplankton in marine systems. The modelled phytoplankton groups are implemented as vectors as described in Section A.1, and give the time and space variation of the phytoplankton standing biomass in terms of carbon, nitrogen, phosphorus and

	Preys								
Predators	$P_i^{(1)}$	$P_i^{(2)}$	$P_i^{(3)}$	$P_i^{(4)}$	$Z_i^{(3)}$	$Z_i^{(4)}$	$Z_i^{(5)}$	$Z_i^{(6)}$	B_i
$Z_i^{(3)}$	0	0	0	0	1.0	1.0	0	0	0
$Z_i^{(4)}$	1.0	0.75	0	0	0	1.0	1.0	0	0
$Z_i^{(5)}$	0.7	1.0	0.1	0.1	0	0	1.0	1.0	0.1
$Z_i^{(6)}$	0	0.2	1.0	0	0	0	0	0.2	1.0

Table A.3.: Pelagic food matrix $\delta_{Z,X}$ for the reference standard model. See Table A.1 for an explanation of symbols.

silica cell content. The operational model definitions of the phytoplankton functional groups are:

- diatoms (state variable vector $P_i^{(1)}$), ESD = 20-200μ, unicellular eukaryotes enclosed by a silica frustule eaten by micro- and mesozooplankton;
- autotrophic nanoflagellates (state variable vector $P_i^{(2)}$), ESD = 2-20μ, motile unicellular eukaryotes comprising smaller dinoflagellates and other autotrophic microplanktonic flagellates eaten by heterotrophic nanoflagellates, micro- and mesozooplankton;
- picophytoplankton (state variable vector $P_i^{(3)}$), ESD = 0.2-2μ, smallest autotrophic unicellular organisms grazed by heterotrophic nanoflagellates, with an almost total preferential use of ammonium nitrogen instead of other nitrogen species;
- inedible or partially unpalatable phytoplankton (state variable vector $P_i^{(4)}$), ESD = 20-200μ, that represents a wide group of phytoplankton species, also comprising larger species belonging to the previous groups (for instance dinoflagellates) but also those that during some period of the year develop a form of (chemo)defense to predator attack. This group generally has low growth rates and small or zero food matrix elements with respect to micro- and mesozooplankton groups.

The model set of equations for the carbon and nutrient components of the standard primary producer vector P_i are given in Equation Box 1, and the equations for every member of this functional group are obtained by substituting $P_i^{(1)}, P_i^{(2)}, P_i^{(3)}, P_i^{(4)}$ for the symbol P_i. All groups are modelled identically except for the silica vector component, which is only considered in the diatom dynamics ($P_i^{(1)}$) while for the other groups is set to 0 as shown in (A.5d). The different set of predators for each phytoplankton group is not considered in the flux form equations, but is reflected in the values of the food matrix elements presented in Section A.1.1.

A.2.1. Environmental regulating factors

Most of the source terms given in Equation Box 1 and described in the next sections, are parameterized by means of regulating factors, which contain the functional response of the organism to environmental conditions such as temperature, light, inorganic nutrients or local food availability. These factors

Equation Box 1 Flux form equations for the phytoplankton functional group.

$$\left.\frac{\partial P_c}{\partial t}\right|_{bio} = \left.\frac{\partial P_c}{\partial t}\right|_{O^{(3)}}^{gpp} - \left.\frac{\partial P_c}{\partial t}\right|_{O^{(3)}}^{rsp} - \left.\frac{\partial P_c}{\partial t}\right|_{R_c^{(1)}}^{exu} - \left.\frac{\partial P_c}{\partial t}\right|_{R_c^{(1)}}^{lys} - \left.\frac{\partial P_c}{\partial t}\right|_{R_c^{(6)}}^{lys} - \sum_j \left.\frac{\partial P_c}{\partial t}\right|_{Z_c^{(j)}}^{prd} \tag{A.5a}$$

$$\left.\frac{\partial P_n}{\partial t}\right|_{bio} = \left.\frac{\partial P_n}{\partial t}\right|_{N^{(3)},N^{(4)}}^{upt} - \left.\frac{\partial P_n}{\partial t}\right|_{R_n^{(1)}}^{lys} - \left.\frac{\partial P_n}{\partial t}\right|_{R_n^{(6)}}^{lys} - \frac{P_n}{P_c}\sum_j \left.\frac{\partial P_c}{\partial t}\right|_{Z_c^{(j)}}^{prd} \tag{A.5b}$$

$$\left.\frac{\partial P_p}{\partial t}\right|_{bio} = \left.\frac{\partial P_p}{\partial t}\right|_{N^{(1)}}^{upt} - \left.\frac{\partial P_p}{\partial t}\right|_{R_p^{(1)}}^{lys} - \left.\frac{\partial P_p}{\partial t}\right|_{R_p^{(6)}}^{lys} - \frac{P_p}{P_c}\sum_j \left.\frac{\partial P_c}{\partial t}\right|_{Z_c^{(j)}}^{prd} \tag{A.5c}$$

$$\left.\frac{\partial P_s}{\partial t}\right|_{bio} = \left.\frac{\partial P_s}{\partial t}\right|_{N^{(5)}}^{upt} - \left.\frac{\partial P_s}{\partial t}\right|_{R_s^{(6)}}^{lys} - \frac{P_s}{P_c}\sum_j \left.\frac{\partial P_c}{\partial t}\right|_{Z_c^{(j)}}^{prd} \tag{A.5d}$$

$$\text{if } P_s = P_s^{(1)}, \text{ otherwise } \left.\frac{\partial P_s}{\partial t}\right|_{bio} = 0$$

have been grouped together in this separate section because they are common to many source/sink terms and they represent the explicit formulation of the organism functionalities. The net growth rate of phytoplankton depends mainly on light, temperature, nutrient availability and, according to Droop (1973) and Nyholm (1977), on the internal nutrient storage. In order to account for the environmental and intracellular conditions in the parameterized functional response of phytoplankton, a set of non-dimensional regulating factors has been defined and discussed in the following. As a general rule, the value of the regulating factors is 1 under optimum conditions (no regulation) and tends towards 0 when phytoplankton is limited by one of the environmental factors.

Temperature regulating factor

The dependence on the environmental water temperature T is common to all the parameterizations of the functional groups and of many other biogeochemical processes. It is written in an exponential form as

$$f^T = Q_{10}^{\frac{T-T_0}{T_0}} \quad T_0 = 10^o C \tag{A.6}$$

where Q_{10} is the characteristic temperature coefficient specific to the involved functional group or chemical reaction. In the case of phytoplankton, Q_{10_P} is set to 2 for all the groups, indicating that the potential growth rate doubles every $10^o C$. This is the only regulating factor that can get a value larger than 1.

Light regulating factor

The parameterization of the light utilization by phytoplankton is a complicated task, nonetheless its proper identification is of paramount importance because it controls the main flow of inorganic car-

bon in marine ecosystems. Ebenhöh *et al.* (1997) focused on the mathematical aspects of the light dependence of primary producers, showing that the depth-integrated effect of irradiance on the primary production in the water column mainly depends on the day length and extinction coefficient (Behrenfeld and Falkowsky, 1997). Therefore, the basic parameterization used in ERSEM I and II was mainly based on the calculation of daily averaged production rates integrated over the light period (Ebenhöh *et al.*, 1997). Such scheme is also maintained in ERSEM III, because of the high degree of uncertainties in the definition of the phytoplankton light response curve with the use of instantaneous light. Clearly, we expect that the short-term variability of vertical and horizontal transport processes imparted by the high-resolution hydrodynamical models plays an important role in the determination of the amount of light-attenuating particles in the water column; neglecting the response of phytoplankton to instantaneous changes in the ambient light might lead to incorrect estimation of primary productivity and hence of the formation of organic particles. Improving the description of the underwater light climate, perhaps also taking the spectral composition into account is expected to improve the forecasting capability of current prognostic models.

We here summarize the main aspects of the light parameterization in phytoplankton, that lead to the formulation of the following light regulating factor, referring to Ebenhöh *et al.* (1997) for a more extensive treatment:

$$f_P^I = \frac{1}{p_{opt} D} \int_{-D}^{0} p\left(p_{opt},\, I_{PAR}/I_P^{opt}\right)\, dz \tag{A.7}$$

We assume that the Photosynthetic Available Radiation (PAR) $I_{PAR}(\vec{x},t)$ is derived from the shortwave irradiance term of the physical model (Section C.4.2) taking into account the extinction due to suspended living particles (the self-shading effect is indeed an important feature in the phytoplankton blooms dynamics). Thus, the irradiance used as forcing functions for the calculation of production rates is written as:

$$I_{PAR} = \varepsilon_{PAR}\, Q_S\, e^{(\lambda_v + \lambda_{bio})z} \tag{A.8}$$

where ε_{PAR} is the coefficient determining the portion of PAR (usually 0.5), λ_v is the background extinction of water and

$$\lambda_{bio} = \sum_j c_{P(j)} P_c^{(j)} + c_{R^{(6)}} R_c^{(6)} + c_{ISM} ISM \tag{A.9}$$

is the extinction due to phytoplankton groups, particulate detritus and suspended inorganic matter, respectively. The *c* constants are the specific contributions to the total extinction coefficient of each suspended substance. It is important to state that the value of Q_S in (A.8) is usually evaluate as plane irradiance, while for the photosynthetic processes the use of the scalar irradiance should be preferable (Kirk, 1983). We assume that the effect of such simplification is negligible in the computation of daily-averaged values, although it could be of importance when resolving the photosynthetic process

with higher temporal resolution.

It is also assumed that, within a layer, the phytoplankton response to the light is uniform as the biomass distribution. The non-dimensional factor (A.7) is computed as the ratio between the productivity function p averaged over the layer of depth D and the maximal productivity p_{opt} at the optimal irradiance I_p^{opt}. The productivity function (the so-called p/I curve) is a complex function of the irradiance in the layer, the optimal irradiance $I_p^{opt}(\vec{x},t)$ and the maximal productivity p_{opt}. Note that the optimal irradiances are ordinary state variables, one for each phytoplankton group (see Section A.2.2 for further details). The productivity function used in the model can be chosen from a set of functions ranging from a simple ramp function (the standard case)

$$p = p_0 \min(1, I_{PAR}/I_{opt})$$

to more complex functions (see Kirk, 1983 and Ebenhöh *et al.*, 1997 for a review) such as:

$$p(y = I_{PAR}/I_{opt}) = p_0 y e^{1-y}$$

that includes the photoinibition process (Steele, 1962) or

$$p(y = I_{PAR}/I_{opt}) = p_0 \frac{(2+a)y}{1+ay+y^2},\ a \geq 0$$

that describes a family of hyperbolic curves (Klepper *et al.*, 1988). Ebenhöh *et al.* (1997) made an extensive sensitivity analysis for ERSEM II, concluding that the model is very sensitive to the formulation of the p/I curve, especially in the case of high-turbidity environment. However, there are reasons to think that the sensitivity depends from the specifications and spatial resolution of the hydrodynamical model that governs the mixing dynamics of the particles. Further experiments are therefore needed to analyze the real impact of this basic process in coupled models.

Nutrient regulating factors

The nutrient uptake processes in phytoplankton are decoupled from the photosynthetic carbon assimilation process. This parameterization has been introduced in ERSEM II (Baretta-Bekker *et al.*, 1997) based on conclusions from the analysis of the ERSEM I model results in the North Sea application (Baretta *et al.*, 1995) and from a mesocosm simulation (Baretta-Bekker *et al.*, 1994; 1995). The discrepancies between simulated and observed microbial food web and primary producer dynamics were interpreted as consequences of the lack of the phytoplankton release of carbohydrates on the one hand, and of the absence of luxury consumption of nutrients by phytoplankton on the other hand. There are many indications in the world ocean of decoupled interactions between the uptake of dissolved inorganic carbon and nutrients (Sambrotto *et al.*, 1993; Copin-Montégut, 2000; Thomas *et al.* 1999; Osterroht and Thomas, 2000), therefore the inclusion of such processes appeared mandatory in deterministic models aiming at achieving any predictability skill. The effect of this parameterization

has been thoroughly discussed in a mesocosm simulation by Baretta-Bekker *et al*. (1998) and the major conclusions were that luxury uptake of nutrients has an effect only when nutrients are close to depletion, and the decoupling of carbon and nutrient uptake has major consequences in nutrient-replete situations. The basic idea of the decoupling is that the Redfield ratio (Redfield *et al*., 1963) is considered as the threshold value between a nutrient-limiting and a non-limiting situation, and that the intra-cellular varying nutrient/carbon quota in phytoplankton always vary within a fixed range around this threshold. The Redfield ratios for the modelled nutrient components are introduced in the model equations with the constant parameters given in Table A.4.

According to the values given by Sommer (1994), the minimum quota for nitrogen and phosphorus correspond to the nutrient content of the structural parts of the cell and are taken to be half the Redfield ratio as follows:

$$n_P^{\min} = \frac{Rr_c^n}{2},\ p_P^{\min} = \frac{Rr_c^p}{2}. \tag{A.10}$$

The maximum values are the maximum storage capacity of phosphorus and nitrogen with respect to carbon, taken to be twice the Redfield ratio:

$$n_P^{\max} = 2\,Rr_c^n,\ p_P^{\max} = 2\,Rr_c^p. \tag{A.11}$$

Due to the high natural variability of these functional biological parameters, the value of 2 has to be considered as indicative, and it is a suggested value based on the experience of the past model applications. The minimum quota (A.10) are used in conjunction with the Redfield ratio for determining the internal nutrient status of cells. The regulating factors for the nutrient limitation depend on the difference between the minimum reference values and the actual (realized) dynamical internal quota as:

$$f_P^n = \min\left(1, \max\left(0, \frac{P_n/P_c - n_P^{\min}}{Rr^n - n_P^{\min}}\right)\right) \tag{A.12}$$

$$f_P^p = \min\left(1, \max\left(0, \frac{P_p/P_c - p_P^{\min}}{Rr^p - p_P^{\min}}\right)\right) \tag{A.13}$$

In order to make the decoupling effective, these non-dimensional parameters are only applied to the carbon loss terms and not to the assimilation of CO_2 through photosynthesis.

The dynamics of silica in diatoms remains coupled to the uptake of inorganic carbon as will be shown in (A.18a). This approach reflects the lack of internal storage capacity for Si in diatoms. A

Michaelis-Menten function controls the regulating factor for silica

$$f^s_{P^{(1)}} = \frac{N^{(5)}}{N^{(5)} + h^s_{P^{(1)}}} \tag{A.14}$$

as a function of the external availability of dissolved silica (state variable $N^{(5)}$) where $h^s_{P^{(1)}}$ is the half-saturation constant of silicate concentration in the water.

The combined effect of the regulating factors for nutrient limitation can be parameterized in several ways. The traditional approach applies the Liebig principle of the most limiting nutrient as in

$$f^{n,p}_P = \min\left(f^p_P,\ f^n_P\right); \quad f^{n,p,s}_{P^{(1)}} = \min\left(f^{n,p}_{P^{(1)}},\ f^s_{P^{(1)}}\right), \tag{A.15}$$

although different combinations such as the geometric mean $f^{p,n}_P = \sqrt{f^p_P\ f^n_P}$ can be specified as well.

A.2.2. Light adaptation

Autotrophic cells keep a record of the light history that affects the productivity during daylight, and moreover, if moved to different depths, cells adapt to the new light environment quickly, in about few days, with a process known as photoacclimation (Marra, 1978; Falkowsky, 1983; Kirk, 1983). Theoretical single-cell models have suggested that the distribution of photoacclimative properties within a population of phytoplankton cells is indeed a physical/biological coupled process, basically related to the mixing dynamics (Dusenberry *et al*., 2000 and references therein). Considering this process into a biomass based coupled model is a major but necessary task, because Ebenhöh *et al*. (1997) have shown that the implementation of photoacclimation in ERSEM II was essential for a correct simulation of the low phytoplankton stocks over the winter periods. Therefore, this feature is (partially) taken into account in ERSEM with the introduction of a set of ordinary state variables (one for each phytoplankton group) called the photoadaptation $L_{P(j)}$. This is a phytoplankton property bound to the biomass, and it is defined as the product of the carbon biomass with the optimal irradiance value as (suppressing the index j):

$$L_P = I^{opt}_P \cdot P_c \tag{A.16}$$

in which I^{opt}_P is in turn defined as the bulk light intensity that gives the maximum potential growth rate in a homogeneous phytoplankton population. As shown in the previous section, I^{opt}_P is used in the determination of the light regulating factor (A.7). The dynamics of the photoadaptation property follows a first order kinetics

$$\left.\frac{\partial L_P}{\partial t}\right|_{bio} = \nu^I_P \left(\tilde{I}^{opt}_P - I^{opt}_P\right) P_c \tag{A.17}$$

where $\tilde{I}_{opt}$ is the reference optimal irradiance to which the phytoplankton is adapting with frequency ν_P^I (in general set to 4 days for a full acclimation). The following forms can be chosen in the model:

$$\tilde{I}_P^{opt} = \min\left(I_P^{\max}, \max\left(I_P^{\min}, I\right)\right)$$

which is a constrained ramp function between the ranges of reactivity of the photosynthetic unit $\left(I_P^{\min}, I_P^{\max}\right)$, and

$$\tilde{I}_P^{opt} = \min\left(I_P^{\max}, \max\left(I_P^{\min}, 2\frac{I_P^{\max}}{I_P^{\max}+I}I\right)\right),$$

which prescribes a slightly faster adaptation at lower intensity and a smooth saturation towards the maximum allowed intensity $I_P^{\max}$. All these parameters can be set to different values for each phytoplankton group.

Equation Box 2 Source/sink terms in functional process form for the phytoplankton carbon dynamics (A.5a).

$$\left.\frac{\partial P_c}{\partial t}\right|_{O^{(3)}}^{gpp} = r_{_P} P_c = f_{_P}^T\, f_{_P}^I \left(f_{_{P^{(1)}}}^s\right) r_{0_P} P_c \tag{A.18a}$$

$$\left.\frac{\partial P_c}{\partial t}\right|_{R_c^{(1)}}^{exu} = \left[\alpha_{_P} + (1-\alpha_{_P})\left(1 - f_{_P}^{n,p}\right)\right] \left.\frac{\partial P_c}{\partial t}\right|_{O^{(3)}}^{gpp} \tag{A.18b}$$

$$\left.\frac{\partial P_c}{\partial t}\right|_{R_c^{(6)}}^{lys} = \varepsilon_{_P}^{n,p} \frac{h_{_P}^{p,n,s}}{f_{_P}^{p,n,s} + h_{_P}^{p,n,s}} d_{0_P} P_c \tag{A.18c}$$

$$\left.\frac{\partial P_c}{\partial t}\right|_{R_c^{(1)}}^{lys} = (1-\varepsilon_{_P}^{n,p}) \frac{h_{_P}^{p,n,s}}{f_{_P}^{p,n,s} + h_{_P}^{p,n,s}} d_{0_P} P_c \tag{A.18d}$$

$$\left.\frac{\partial P_c}{\partial t}\right|_{O^{(3)}}^{rsp} = f_{_P}^T\, b_{_P}\, P_c + \gamma_{_P} \left\{ \left.\frac{\partial P_c}{\partial t}\right|_{O^{(3)}}^{gpp} - \left.\frac{\partial P_c}{\partial t}\right|_{R_c^{(1)}}^{exu} \right\} \tag{A.18e}$$

$$\left.\frac{\partial P_c}{\partial t}\right|_{Z_c^{(j)}}^{prd} = \frac{\delta_{_{Z^{(j)},P}}\, f_{_{Z^{(j)},P}}^{dns}\, P_c}{F_c} \left.\frac{\partial Z_c^{(j)}}{\partial t}\right|_{P_c, Z_c^{(j)}}^{prd} \tag{A.18f}$$

A.2.3. Carbon dynamics

We here describe the carbon phytoplankton equation introduced in Box 1, Equation (A.5a), and given in the complete functional process form in Box 2. The first term on the right side of (A.5a) is the potential carbon assimilation rate (gross primary production) given in (A.18a), where the f parameters (see Section A.2.1) are the regulating factors respectively for temperature, light and, (only in the case

of diatoms), silicate. The constant parameter r_{0_P} represents the maximum potential specific growth rate at the reference temperature (10^oC) under optimal irradiance conditions. Following the considerations given above, the potential uptake of carbon in primary producers is not dependent on external or internal nutrient limitation except for diatoms, where any carbon uptake cannot occur without a proportional growth of the enclosing theca. According to (A.18a), the gross primary production rate (the uptake of inorganic carbon) is not a function of the nutrient availability, but only the loss terms are dependent on the internal nutrient status. In fact, in the case of intra-cellular nutrient shortage, not all the photosynthesized carbon can be converted into body mass and the non-assimilated part is released in the form of dissolved carbohydrates ($R_c^{(1)}$). This exudation rate is parameterized as in (A.18b) taking into account the dependency on the gross growth rate (A.18a), modulated by the constant fraction of activity excretion (α_p) and the nutrient limitation $f_P^{p,n}$.

The term lysis includes all the non-resolved mortality processes that disrupt the cell wall/membrane, such as mechanical causes, viruses, bacteria and yeasts. The lysis of cells generates both dissolved and particulate detritus; the structural parts of the cell are not as easily degradable as cytoplasm, therefore the percentage going to DOC is inversely proportional to the internal nutrient content and limited by the minimum structural content in the following way:

$$\varepsilon_P^{n,p} = \min\left(1, \frac{p_P^{\min}}{P_p/P_c}, \frac{n_P^{\min}}{P_n/P_c}\right). \tag{A.19}$$

This equation provides that the carbon and nutrients in the structural part of the cell, which are assumed to have $p^{\min}$ and $n^{\min}$ nutrient ratios as described in previous section, are always released as particulate components. It is assumed that the lysis rate is partitioned between particulate and dissolved detritus according to (A.19) and increases with nutrient stress $f_P^{p,n,s}$, using the threshold parameter $h_P^{p,n,s}$ that represents the half-saturation constant of a Michaelis-Menten form as in (A.18c) and (A.18d) where the parameter d_{0_P} is the constant specific potential lysis rate. Respiration is the sum of the basal respiration, which is independent from the production rates, and the activity respiration as shown in (A.18e). The basal respiration is only a function of the biomass, temperature (through the regulating factor f_P^T) and the specific constant rate b_p. The activity respiration is a constant fraction (γ_P) of the assimilated carbon, which is in turn derived from the gross primary production (A.18a) minus the exudation losses calculated in (A.18b).

The grazing loss terms due to zooplankton predation in (A.5) are written in functional process form in (A.18f). They involve some functional terms of the dynamics of the zooplankton functional groups that are described in Section A.4 in (A.49). The flux of carbon to each predator is primarily controlled by the value of the food matrix elements $\delta_{Z^{(j)},P}$ given in Table A.3. Therefore, some of the predation fluxes can be set to 0 and the interaction between the related trophic levels can be modified according to the specific applications of the model.

A.2.4. Nutrient dynamics

This section describes the nutrient dynamics given in Box 1. The uptake of nutrients from the dissolved pools of nitrogen and phosphorus (the first terms on the right hand side of (A.5b) and (A.5c) are:

$$\left.\frac{\partial P_n}{\partial t}\right|^{upt}_{N^{(3)},N^{(4)}} = \min\left(u_n^{ext}, u_n^{int}\right) P_c \tag{A.20}$$

$$\left.\frac{\partial P_p}{\partial t}\right|^{upt}_{N_p^{(1)}} = \min\left(u_p^{ext}, u_p^{int}\right) P_c \tag{A.21}$$

We distinguish two different rates of uptake, the first (u^{ext}) dependent on the external nutrient concentration when the cell is "empty" (*i.e.* containing only structural nutrients), and the second (u^{int}) dependent on the internal nutrient storage, according to the kinetics described by Droop (1973).

For the nitrogen species, the external uptake is linearly proportional to the dissolved pools of nitrate $\left(N^{(3)}\right)$ and ammonium $\left(N^{(4)}\right)$,

$$u_n^{ext} = \lambda_3^{ext} N^{(3)} + \lambda_4^{ext} N^{(4)} \tag{A.22}$$

where λ_3^{ext} and λ_4^{ext} indicates the constant permeability coefficients of the membrane for nitrate and ammonium, respectively (Aksnes and Egge, 1991). They are set to different values prescribing a preference for ammonium with respect to nitrate; the present implementation prescribes a total ammonium preference factor for picophytoplankton $\left(P_i^{(3)}\right)$.

For phosphate, the external uptake rate is simply written as:

$$u_p^{ext} = \lambda_1^{ext} N^{(1)} \tag{A.23}$$

where λ_1^{ext} is the specific membrane affinity for orthophosphate (Aksnes and Egge, 1991).

The internal rate accounts for the uptake of nutrients due to (net) growth processes plus the amount necessary to replenish the intracellular storage. In the case of nitrogen it becomes:

$$u_n^{int} = g_P\, n_P^{\max} + \nu_P \left[n_P^{\max} - \frac{P_n}{P_c}\right] \tag{A.24}$$

where ν_P is the maximum specific replenishment rate, and g_P is the net specific carbon growth rate, obtained from (A.5a) and defined as:

$$g_P = \frac{1}{P_c}\left(\left.\frac{\partial P_c}{\partial t}\right|_{O^{(3)}}^{gpp} - \left.\frac{\partial P_c}{\partial t}\right|_{O^{(3)}}^{rsp} - \left.\frac{\partial P_c}{\partial t}\right|_{R_c^{(1)}}^{exu} - \left.\frac{\partial P_c}{\partial t}\right|_{R_c^{(1)}}^{lys} - \left.\frac{\partial P_c}{\partial t}\right|_{R_c^{(6)}}^{lys}\right) \tag{A.25}$$

with units of d^{-1}.

In the case of phosphorus, equation (A.24) is written as:

$$u_p^{int} = g_P\, p_P^{\max} + \nu_P \left[p_P^{\max} - \frac{P_p}{P_c}\right]. \tag{A.26}$$

The high-resolution coupled models have shown to be quite insensitive with respect to variations of this parameter, and a time scale of 1 day is a reasonable value for most applications. It is important to note that the reference ratios used in (A.24) and (A.26) are the maximal nutrient/carbon ratios described in Section A.2.1, in order to allow phytoplankton to assimilate nutrients at rates higher than the carbon growth rates (the so-called "luxury consumption").

In the case of nitrogen, we distinguish between the involved nitrogen species. If the total flow in (A.20) is greater than 0, then the flow is partitioned over the nitrate and ammonium uptake:

$$\left.\frac{\partial P_n}{\partial t}\right|_{N^{(3)},N^{(4)}}^{upt} > 0 \Rightarrow \begin{cases} \left.\frac{\partial P_n}{\partial t}\right|_{N^{(3)}}^{upt} = \frac{\lambda_3^{ext} N_n^{(3)}}{u_n^{ext}} \left.\frac{\partial P_n}{\partial t}\right|_{N^{(3)},N^{(4)}}^{upt} \\ \left.\frac{\partial P_n}{\partial t}\right|_{N^{(4)}}^{upt} = \frac{\lambda_4^{ext} N_n^{(4)}}{u_n^{ext}} \left.\frac{\partial P_n}{\partial t}\right|_{N^{(3)},N^{(4)}}^{upt} \end{cases} \tag{A.27}$$

If the total flow is lower than 0 (as in case of "dark respiration"), then the virtual excretion is redirected only to the ammonium pool:

$$\left.\frac{\partial P_n}{\partial t}\right|_{N^{(3)},N^{(4)}}^{upt} < 0 \Rightarrow \begin{cases} \left.\frac{\partial P_n}{\partial t}\right|_{N^{(3)}}^{upt} = 0 \\ \left.\frac{\partial P_n}{\partial t}\right|_{N^{(4)}}^{upt} = \left.\frac{\partial P_n}{\partial t}\right|_{N^{(3)},N^{(4)}}^{upt} \end{cases} \tag{A.28}$$

The lysis process affects phytoplankton nutrient content exactly as the carbon content in (A.18c). In the following we only give the equation for phosphorus:

$$\left.\frac{\partial P_p}{\partial t}\right|_{R_p^{(6)}}^{lys} = p_P^{\min}\left.\frac{\partial P_c}{\partial t}\right|_{R_c^{(6)}}^{lys} \tag{A.29}$$

$$\left.\frac{\partial P_p}{\partial t}\right|_{R_p^{(1)}}^{lys} = \frac{h_p^{p,n,s}}{f_P^{p,n,s}+h_P^{p,n,s}} d_{0_P} P_p - \left.\frac{\partial P_p}{\partial t}\right|_{R_p^{(6)}}^{lys} \tag{A.30}$$

For the silicate dynamics (A.5d) there is no internal storage (but only structural), therefore the uptake is directly dependent on the net specific organic carbon uptake as follows:

$$\left.\frac{\partial P_s^{(1)}}{\partial t}\right|_{N^{(5)}}^{upt} = g_{_{P^{(1)}}}\, s_{P^{(1)}}^{\max} P_c^{(1)} \tag{A.31}$$

where $g_{_{P^{(1)}}}$ is (A.25) for diatoms.

Silicate is released only in particulate form, because it is incorporated in the diatom theca. The loss term of particulate silicate due to lysis processes is:

$$\left.\frac{\partial P_s^{(1)}}{\partial t}\right|_{R_s^{(6)}}^{lys} = \frac{h_p^{p,n,s}}{f_P^{p,n,s}+h_P^{p,n,s}} d_{0_P} P_s^{(1)}. \tag{A.32}$$

Since microzooplankton and mesozooplankton do not have a Si component, the predation involving a silica flux (last terms in (A.5d)) are not included in zooplankton dynamics. Silicate is not ingested but directly transferred to the silicate component of POM $\left(R_s^{(6)}\right)$ as shown in (A.67d).

A.2.5. Chlorophyll-*a* computation

Chlorophyll-*a* in the model is a diagnostic variable and not an ordinary state variable. It is assumed that chlorophyll content has a fixed ratio with respect to carbon content, which is different among the functional groups. This is a strong approximation of the real world because the C/Chl ratio is extremely variable and the normal range of variability found in the ocean is between 25 and 75 (Ducklow and Carlson, 1992). The standard ERSEM conversion factors (c_P^{chl}) are 50 for flagellates $P_i^{(2)}$, picophytoplankton $P_i^{(3)}$ and dinoflagellates $P_i^{(4)}$, and 25 for diatoms $P_i^{(1)}$, because it is assumed that part of the carbon in non-siliceous phytoplankton is structural and thus cannot contain chloroplasts. The diagnostic computation of Chlorophyll-*a* concentration is done according to the following equation:

$$Chla = \sum_{j=1}^{4} \frac{P_c^{(j)}}{c_P^{chl}} \tag{A.33}$$

A.2.6. Phytoplankton sinking velocity

The sinking of phytoplankton has been included in the model since from the first version of ERSEM (Varela *et al.*, 1995) because it is widely accepted that nutrient limitation results in elevated sinking velocity of certain phytoplankton species. This term does not properly belongs to the biological processes because it is actually a physical process affected by biological factors. In fact, the phytoplankton sinking velocity is a component of the vertical velocity used in the transport model equations (Appendix C). It is parameterized as a background sinking velocity ω^{sink} modulated by a threshold function of the nutrient stress as follows:

$$w_P^{sink} = \omega^{sink} \max\left(0, l^{sink} - f_P^{p,n,s}\right) \tag{A.34}$$

where l^{sink} is the nutrient regulating factor value under which the process occurs. In the current implementation the sinking process is in general used only for diatoms, but it can be applied to the other groups as well.

Equation Box 3 Flux form equations for the bacteria functional group.

$$\left.\frac{\partial B_c}{\partial t}\right|_{bio} = \left.\frac{\partial B_c}{\partial t}\right|_{R_c^{(1)}}^{bcd} + \left.\frac{\partial B_c}{\partial t}\right|_{R_n^{(6)}}^{bcd} - \left.\frac{\partial B_c}{\partial t}\right|_{O^{(3)}}^{rsp} - \left.\frac{\partial B_c}{\partial t}\right|_{R_c^{(1)}}^{out} - \sum_j \left.\frac{\partial B_c}{\partial t}\right|_{Z_c^{(j)}}^{prd} \tag{A.35a}$$

$$\left.\frac{\partial B_n}{\partial t}\right|_{bio} = \frac{R_n^{(1)}}{R_c^{(1)}} \left.\frac{\partial B_c}{\partial t}\right|_{R_c^{(1)}}^{bcd} + \frac{R_n^{(6)}}{R_c^{(6)}} \left.\frac{\partial B_c}{\partial t}\right|_{R_n^{(6)}}^{bcd} + f_B^n \left.\frac{\partial B_n}{\partial t}\right|_{N^{(4)}}^{upt,rel} + - \frac{B_n}{B_c} \left.\frac{\partial B_c}{\partial t}\right|_{R_c^{(1)}}^{out} - \frac{B_n}{B_c} \sum_j \left.\frac{\partial B_c}{\partial t}\right|_{Z_c^{(j)}}^{prd} \tag{A.35b}$$

$$\left.\frac{\partial B_p}{\partial t}\right|_{bio} = \frac{R_p^{(1)}}{R_c^{(1)}} \left.\frac{\partial B_c}{\partial t}\right|_{R_p^{(1)}}^{bcd} + \frac{R_p^{(6)}}{R_c^{(6)}} \left.\frac{\partial B_c}{\partial t}\right|_{R_p^{(6)}}^{bcd} + f_B^p \left.\frac{\partial B_p}{\partial t}\right|_{N^{(1)}}^{upt,rel} + - \frac{B_p}{B_c} \left.\frac{\partial B_c}{\partial t}\right|_{R_c^{(1)}}^{out} - \frac{B_p}{B_c} \sum_j \left.\frac{\partial B_c}{\partial t}\right|_{Z_c^{(j)}}^{prd} \tag{A.35c}$$

$$\left.\frac{\partial B_s}{\partial t}\right|_{bio} = 0 \tag{A.35d}$$

A.3. Pelagic bacteria

Bacteria equation formulations have evolved after the original ERSEM I concept given in Baretta-Bekker *et al.* (1995) as the understanding of their functionalities has increased. In ERSEM II, the parameterization was extended in order to include the bacteria uptake of dissolved nutrients (Baretta-Bekker *et al.* 1997) because bacteria have been found to compete with phytoplankton under certain

conditions. Some ERSEM-II model applications illustrating the implication of such process can be found in Baretta-Bekker *et al*. (1998) for a mesocosm setup and Vichi *et al*. (1998b) for a one-dimensional implementation. In addition, the dynamics of the dissolved organic matter (DOM), which is one of the burning issues in the current microbial ecology topics, was not made explicit in the original ERSEM implementation (Baretta-Bekker *et al*., 1995), while the standard ERSEM III formulation defines DOM as an ordinary vector state variable with a dynamics basically dependent on its nutrient content.

Pelagic bacteria (B_i) in the model are a large group comprising free-living heterotrophic bacteria that utilize non-living organic substrate, both in dissolved ($R_i^{(1)}$) and particulate (detritus $R_i^{(6)}$) form . Bacteria functionalities have been set up to consider both aerobic and anaerobic processes, allowing bacteria to also degrade substrate under hypoxic or anoxic conditions, switching to a nitrate-based metabolism. The equations in flux form for all the vector components are given in Equation Box 3.

Equation Box 4 Source/sink terms in functional process form of the bacteria carbon and nutrient dynamics (A.35).

$$\left.\frac{\partial B_c}{\partial t}\right|_{R_c^{(1)},R_c^{(6)}}^{bcd} = \min\left(G^{env}, G^{sub}\right) \tag{A.36a}$$

$$G^{env} = f_B^{n,p}\, f^T\, r_{0_B} B_c \tag{A.36b}$$

$$G^{sub} = \nu_{R^{(6)}}\, f_{R^{(6)}}^{n,p} R_c^{(6)} + \nu_{R^{(1)}}\, f_{R^{(1)}}^{n,p} R_c^{(1)} \tag{A.36c}$$

$$\left.\frac{\partial B_c}{\partial t}\right|_{O^{(3)}}^{rsp} = b_B\, f_B^T\, B_c + \left[1 - \eta_B - \eta_B^o\left(1 - f_B^o\right)\right] \left.\frac{\partial B_c}{\partial t}\right|_{R_c^{(1)},R_c^{(6)}}^{bcd} \tag{A.36d}$$

$$\left.\frac{\partial B_c}{\partial t}\right|_{R_c^{(1)}}^{out} = f_B^T\, d_{0_B}\, B_c \tag{A.36e}$$

$$\left.\frac{\partial B_p}{\partial t}\right|_{N^{(1)}}^{upt,rel} = \nu_B^p \left(\frac{B_p}{B_c} - p_B^{\max}\right) B_c \tag{A.37a}$$

$$\left.\frac{\partial B_n}{\partial t}\right|_{N^{(4)}}^{upt,rel} = \nu_B^n \left(\frac{B_n}{B_c} - n_B^{\max}\right) B_c \tag{A.37b}$$

A.3.1. Carbon dynamics

The formulation of the carbon uptake (usually referred to as the bacterial carbon demand, BCD) in (A.35a) is given in functional process form in (A.36a). It is regulated either by the environmental factors or by the availability the substrate itself if limiting. The environmental control (A.36b) defines the carbon demand in case of non-limiting substrate, and it is a function of the bacterioplankton physiological state and the environmental temperature. The non-dimensional factor $f_B^{n,p}$ controls the

health status of bacterioplankton as a function of the intracellular ratios with respect to the internal nutrient content:

$$f_B^{n,p} = \min\left(q^n, q^p\right) \tag{A.38}$$

$$q^p = \min\left(1, \frac{B_p/B_c}{p^{opt}}\right) \qquad q^n = \min\left(1, \frac{B_n/B_c}{n^{opt}}\right) \tag{A.39}$$

where p^{opt} and n^{opt} are the Goldman *et al.* (1987) P:C and N:C intracellular reference ratios in model units (mmol nutrient/mg C).

The other term (A.36c) is the carbon demand dependent on the dissolved and particulate substrate "quality" and some "characteristic", size-defined time scales for the uptake process ($\nu_{R^{(1)}}, \nu_{R^{(6)}}$) . The quality of the substrate is defined on the basis of the N:C and P:C ratios in $R_i^{(1)}$ and $R_i^{(6)}$ through a non-dimensional factor computed according to a Liebig formulation:

$$f_{R^{(j)}}^{n,p} = \min\left(1, \frac{R_p^{(j)}/R_c^{(j)}}{p^{opt}}, \frac{R_p^{(j)}/R_c^{(j)}}{n^{opt}}\right), \quad R^{(j)} = R1, R6. \tag{A.40}$$

This factor tends toward 0 when the available substrate is nutrient-depleted, and to 1 in case of optimal N and P content with respect to the reference intracellular ratios p^{opt} and n^{opt}.

From (A.36a), we can derive the partitioned bacterial uptake from the two detrital sources that is further used in the formulation of the bacteria dynamics (A.35b, A.35c):

$$\left.\frac{\partial B_c}{\partial t}\right|_{R_c^{(j)}}^{bcd} = \frac{\min\left(G^{env}, G^{sub}\right)}{G^{sub}} \nu_{R^{(j)}} f_{R^{(j)}}^{n,p} R_c^{(j)} \quad , \quad R^{(j)} = R^{(1)}, R^{(6)} \tag{A.41}$$

The respiration sink term in (A.35a) is divided in basal and activity respiration as shown in (A.36d). The basal respiration is parameterized as for phytoplankton with a constant specific respiration rate b_B and the regulating factor for temperature given in (A.6). The parameter η_B in the activity respiration term represents the bacterial growth efficiency (BGE) under oxic situations, and η_B^o is the efficiency decrease under low oxygen conditions. This parameterization has been chosen in order to consider the differences in the energetics of the metabolic pathways in relation to the oxygen availability, since anaerobic bacteria have a lower actual BGE because they need to burn (respire) more carbon in order to produce the same amount of energy. The oxygen regulating factor is parameterized with a cubic form of the Michaelis-Menten formulation as:

$$f_B^o = \frac{\left(O^{(2)}\right)^3}{\left(O^{(2)}\right)^3 + \left(h_B^o\right)^3} \tag{A.42}$$

where the dissolved oxygen concentration $O^{(2)}$ is considered, and h_B^o is the concentration at which metabolic functionalities are halved. This steep sigmoid has been chosen to efficiently separate the bacteria functionalities under aerobic conditions from the anaerobic metabolism as further explained in Section A.5.2.

Concerning the remaining loss terms, It has been assumed that bacteria in the model have no carbon losses except for respiration (A.36d) and a first-order background mortality (A.36e) meant to mimic viral lysis. Possibly the continuous renewal and the consequent excretion of capsular material should be taken into account in future developments. The specific mortality rate d_{0_B} is constant and modulated by the temperature factor. Note that all bacterial lysis products go to the DOM pool.

The heterotrophic flagellates are major predators on bacteria, but the predation term (the last one in equation (A.35a)) can be extended to other groups. Bacteria can also be preyed by microzooplankton, because of the possible presence of filamentous bacteria within the bacterial functional group. The predation flux by microzooplankton can be easily derived from (A.49) substituting the corresponding component of vector B_i to the symbol X and considering the food matrix element $\delta_{Z,B}$ in Table A.3.

A.3.2. Nutrient dynamics

Nutrient dynamics are mostly connected to carbon dynamics, except for the direct nutrient uptake and remineralization processes as shown in the dynamical equations for nitrogen (A.35b) and phosphorus (A.35c) components. The growth rate of the P-component in bacteria is related to the phosphorus content in particulate and dissolved organic matter via the bacterial carbon demand rates computed in (A.41). The uptake/remineralization term from or to the dissolved nutrient pool is given in (A.37a), where ν_B^p is the constant specific maximum uptake rate (in d^{-1}). Depending on the internal nutrient-to-carbon ratios, bacteria can behave as remineralizers or as competitors with the phytoplankton, taking up inorganic nutrients directly from the water. In the model this is achieved using the non-dimensional parameter f_B^p that gets different values according to the following equations::

$$f_B^p = \begin{cases} -1 & \text{if } \dfrac{B_p}{B_c} - p_B^{\max} > 0 \\ \dfrac{N^{(1)}}{N^{(1)} + h_B^p} & \text{if } \dfrac{B_p}{B_c} - p_B^{\max} < 0 \end{cases} \tag{A.43}$$

In case the nutrient ratio is higher than the maximum one allowed in the cell, there is a nutrient excretion and f_B^p in (A.35c) becomes equal to -1. In the opposite case, when bacteria have lower

internal ratios, they take inorganic phosphate directly from the water as a function of the nutrient concentration in a Michaelis-Menten form (h_B^p is the half-saturation concentration value) competing for resources with the phytoplankton.

The nitrogen dynamics in (A.35b) involves only ammonium, and the uptake/release term shown in (A.37b) is similar to the phosphorus uptake (A.37a) where v_B^n is the constant specific maximum uptake rate and the form of $f_B^n$is derived as in (A.43) substituting the ammonium concentration $\left(N^{(4)}\right)$ to phosphate and the relative half-saturation concentration value for dissolved ammonium.

Equation Box 5 Flux form equations for the zooplankton functional groups (the terms in brackets are only valid for mesozooplankton).

$$\left.\frac{\partial Z_c}{\partial t}\right|_{bio} = \left.\frac{\partial Z_c}{\partial t}\right|_{P_c,Z_c}^{prd} - \left.\frac{\partial Z_c}{\partial t}\right|_{R_c^{(1)},R_c^{(6)}}^{out} - \left.\frac{\partial Z_c}{\partial t}\right|_{O^{(3)}}^{rsp} - \sum_x \left.\frac{\partial Z_c}{\partial t}\right|_{Z_c^{(x)}}^{prd} - \left(\left.\frac{\partial Z_c}{\partial t}\right|_{R_c^{(6)}}^{lim}\right) \tag{A.44a}$$

$$\left.\frac{\partial Z_n}{\partial t}\right|_{bio} = \left.\frac{\partial Z_n}{\partial t}\right|_{P_n,Z_n}^{prd} - \left.\frac{\partial Z_n}{\partial t}\right|_{R_n^{(1)},R_n^{(6)}}^{out} - \left.\frac{\partial Z_n}{\partial t}\right|_{N^{(4)}}^{out} - \frac{Z_n}{Z_c}\sum_x \left.\frac{\partial Z_c}{\partial t}\right|_{Z_c^{(x)}}^{prd} - \left(\left.\frac{\partial Z_n}{\partial t}\right|_{N^{(4)}}^{lim}\right) \tag{A.44b}$$

$$\left.\frac{\partial Z_p}{\partial t}\right|_{bio} = \left.\frac{\partial Z_p}{\partial t}\right|_{P_n,Z_n}^{prd} - \left.\frac{\partial Z_p}{\partial t}\right|_{R_p^{(1)},R_p^{(6)}}^{out} - \left.\frac{\partial Z_n}{\partial t}\right|_{N^{(1)}}^{out} - \frac{Z_p}{Z_c}\sum_x \left.\frac{\partial Z_c}{\partial t}\right|_{Z_c^{(x)}}^{prd} - \left(\left.\frac{\partial Z_p}{\partial t}\right|_{N^{(1)}}^{lim}\right) \tag{A.44c}$$

$$\left.\frac{\partial Z_s}{\partial t}\right|_{bio} = 0 \tag{A.44d}$$

A.4. Zooplankton

There are four different zooplanktonic groups in the model, with different positions in the food web and parameter values, but with similar parameterization schemes:

- microzooplankton *s.s.*, state variable $Z_j^{(5)}$, representing the biomass concentration of heterotrophic microzooplankton with a ESD within the range 20- 200 μm, excluding flagellates and naupliar/larval stages of multicellular zooplankton or meroplanktonic larvae of benthic organisms;
- heterotrophic nanoflagellates, state variable $Z_j^{(6)}$, protozoa with dimensions between 2 and 20 μm, mainly grazing upon picophytoplankton and bacteria.
- carnivorous mesozooplankton $Z_j^{(3)}$, including copepods such as *Pareuchaeta*, annelids such as *Tomopteris*, chaetognaths and cnidarians;
- omnivorous mesozooplankton $Z_j^{(4)}$, mainly composed of calanoid copepods.

Mesozooplankton is defined in the model as any permanent member of the zooplankton community which is between 200 μm and 3 to 4 cm long as an adult, also embracing many species that are

traditionally considered part of the microzooplankton when in juveniles stages (Broekhuizen *et al*., 1995). Both micro- and mesozooplankton groups also indulge in "cannibalism", preying on other members of their own functional group. This flux usually acts as a stabilizer of the group dynamics, as demonstrated by Kohlmeyer and Ebenhöh (1995).

Mesozooplankton is included in ERSEM III using the parameterization of ERSEM I (Broekhuizen *et al*., 1995), to which reference is made for a complete explanation of the underlying biological processes. We propose here a review of the equations described in Broekhuizen *et al*. (1995) in order to write them according to the new common mathematical formulation. Because of the problems connected with the description of this complex individual-based population by a bulk biomass model, the mesozooplankton functional groups in this framework should be only considered as a sort of background top-down control on the dynamics of primary producers and (more indirectly) on the microbial food web. The coupling with finer spatial resolution hydrodynamical model has now made the lack of parameterization of the vertical migration more important. While in ERSEM I (Broekhuizen *et al*., 1995) migration was assumed to occur at a finer spatial and time scale than that at which the model was designed to operate, when dealing with a high-resolution spatial representation of phytoplankton vertical distribution, the migration strategy of mesozooplankton becomes dominant. Therefore, the model skill with respect to the reproduction of observed mesozooplankton behavior strongly relies on a proper tuning of parameters such as feeding rates and volume search in order to account for the lack of more appropriate parameterizations of such ecological aspects.

Similar to the previous functional group descriptions, hereinafter we will refer only to the generic zooplankton state variable vector Z_i and the specific dynamical equations in flux form can be obtained from Box 5 substituting the corresponding variable name. The main difference between mesozooplankton and microzooplankton is that the former has constant nutrient-to-carbon internal ratios (Broekhuizen *et al*., 1995; Anderson *et al*., 1987). Therefore, all the carbon loss fluxes have also a correspondent loss term in the nutrient equations, and an additional flux for balancing the excess of the other components with respect to the limiting element is added in the equations (cf. terms in brackets on the right hand sides of (A.44)).

A.4.1. Microzooplankton

The microzooplankton source and sink terms to be used in (A.44) are shown in their functional process forms in Box 6. The first term on the right hand side of (A.44a) is the carbon flux from predation (grazing) given in (A.45a). The subscripts on the flux form derivative indicate that zooplankton preys upon both phytoplankton and some zooplankton guilds as well (the list of the preyed functional groups is shown in Table A.3, although it generally depends on the specific implementation). The gross secondary production is parameterized as a function of the maximum specific daily ingestion rate g_Z regulated by the temperature and by a type II response with respect to the food availability, with h_Z being the half-saturation constant for the total food. If we indicate with X each food source (e.g.: diatoms $P_i^{(1)}$, bacteria B_i, etc.), the total availability of food is a vector whose components are:

Equation Box 6 Source/sink terms in functional process form for the microzooplankton dynamics (A.44).

$$\left.\frac{\partial Z_c}{\partial t}\right|_{P_c,Z_c}^{prd} = f_z^T\, r_{0_Z}\frac{F_c}{F_c+h_z^F}Z_c \tag{A.45a}$$

$$\left.\frac{\partial Z_c}{\partial t}\right|_{R_c^{(1)},R_c^{(6)}}^{out} = \alpha_z(1-\eta_z)\left.\frac{\partial Z_c}{\partial t}\right|_{P_c,Z_c}^{prd} + \left[d_{0_Z}+\left(1-f_z^o\right)\, d_z^o\right]Z_c \tag{A.45b}$$

$$\left.\frac{\partial Z_c}{\partial t}\right|_{O^{(3)}}^{rsp} = b_z\, f_z^T\, Z_c + (1-\alpha_z)(1-\eta_z)\left.\frac{\partial Z_c}{\partial t}\right|_{P_c,Z_c}^{prd} \tag{A.45c}$$

$$\left.\frac{\partial Z_l}{\partial t}\right|_{P_l,Z_l}^{prd} = \frac{F_l}{F_c}\left.\frac{\partial Z_c}{\partial t}\right|_{P_c,Z_c}^{prd} \qquad l=n,p \tag{A.46a}$$

$$\left.\frac{\partial Z_l}{\partial t}\right|_{R_l^{(1)},R_l^{(6)}}^{out} = \zeta^l_{R^{(1)}}\frac{Z_l}{Z_c}\left.\frac{\partial Z_c}{\partial t}\right|_{R_l^{(1)}}^{out} + \frac{Z_l}{Z_c}\left.\frac{\partial Z_c}{\partial t}\right|_{R_l^{(6)}}^{out}, \quad l=n,p \tag{A.46b}$$

$$\left.\frac{\partial Z_p}{\partial t}\right|_{N^{(1)}}^{out} = \nu_z^p \max\left(0,\frac{Z_p}{Z_c}-p_z^{\max}\right)Z_p \tag{A.46c}$$

$$\left.\frac{\partial Z_n}{\partial t}\right|_{N^{(4)}}^{out} = \nu_z^n \max\left(0,\frac{Z_n}{Z_c}-n_z^{\max}\right)Z_n \tag{A.46d}$$

$$F_i = \sum_X \delta_{Z,X}\; f_{Z,X}^{dns}\; X_i \tag{A.47}$$

where $\delta_{Z,X}$ is the food matrix element for predator Z upon prey X given in Table A.3, and the density regulating factor is written in a sigmoid form:

$$f_{Z,X}^{dns} = \frac{X_c}{X_c+\mu_z}. \tag{A.48}$$

The constant parameter μ_z is the biomass threshold [mg C m^{-3}] where the density regulating factor of each prey is 0.5 (the consumers eat more from the more abundant sources). The gross secondary production (A.45a) corresponds to the sum of all the predation loss terms in the general carbon equations for the other functional groups being preyed by microzooplankton. Applying the exchange rule defined in (A.3), the reference equation for all the predation fluxes is:

$$\left.\frac{\partial Z_c}{\partial t}\right|_{X_c}^{prd} = \left.\frac{\partial X_c}{\partial t}\right|_{Z_c}^{prd} = \frac{\delta_{Z,X}\, f_{Z,X}^{dns}\, X_c}{F_c}\left.\frac{\partial Z_c}{\partial t}\right|_{P_c,Z_c}^{prd} \tag{A.49}$$

This term also represents the predation of other groups upon microzooplankton or the carbon flux due to cannibalism (last term in equation (A.44)). For instance, according to Table A.3, microzooplankton $Z_i^{(5)}$ is preyed by omnivorous mesozooplankton $Z_i^{(4)}$. Such flux is, for example, written in functional form as:

$$\left.\frac{\partial Z_c^{(5)}}{\partial t}\right|_{Z_c^{(4)}}^{prd} = \frac{\delta_{Z^{(4)},Z^{(5)}}\, f^{dns}_{Z^{(4)},Z^{(5)}}\, Z_c^{(5)}}{F_c}\, \left.\frac{\partial Z_c^{(4)}}{\partial t}\right|_{P_c,Z_c}^{prd} \tag{A.50}$$

The next carbon loss term in (A.44a) is presented in (A.45b), and it represents the sum of the excretion and mortality rates. Microzooplankton functional dynamics are essentially parameterized with a partitioning approach. It is assumed that a constant fraction η_z of the ingested organic matter is assimilated, and the reminder is partitioned into excretion and respiration losses with another constant fraction α_z. The excreted fraction α_z is further divided into the particulate and dissolved organic forms using a constant percentage ε_z:

$$\begin{cases} \left.\dfrac{\partial Z_c}{\partial t}\right|_{R_c^{(6)}}^{out} = (1-\varepsilon_z)\, \left.\dfrac{\partial Z_c}{\partial t}\right|_{R_c^{(1)},R_c^{(6)}}^{out} \\ \left.\dfrac{\partial Z_c}{\partial t}\right|_{R_c^{(1)}}^{out} = \varepsilon_z\, \left.\dfrac{\partial Z_c}{\partial t}\right|_{R_c^{(1)},R_c^{(6)}}^{out} \end{cases} \tag{A.51}$$

The natural mortality rate, the last one in (A.45b), is composed of a constant specific daily rate d_z^0, and an oxygen-dependent rate d_z^o, scaled by the environmental regulating factor for oxygen written in the common Michaelis-Menten form

$$f_z^o = \frac{O_{sat}}{O_{sat} + h_z^o} \tag{A.52}$$

where O_{sat} is the oxygen saturation and h_z^o is the percentage of saturation where metabolic respiration is half the one under oxygen saturated conditions.

Continuing in the description of the carbon terms in the general equation (A.44a), the functional process form of the respiration term is divided in basal and activity respiration (linked to the gross secondary production) as shown in (A.45c). The activity respiration is simply derived by difference with (A.45b), while the constant basal respiration rate at 10^oC (b_z) is increased or decreased by the temperature regulating factor defined in (A.6).

The nutrient dynamics for microzooplankton, shown in (A.46) of Equation Box 6, are mainly derived from carbon dynamics. The nutrient fluxes from the functional groups that are being eaten by the microzooplankton, are calculated considering the nutrient content of the total food availability as in

(A.46a). The excretion flux is partitioned into particulate and dissolved detritus following the carbon dynamics in (A.51) and according to (A.46b), where $\zeta^{j}_{R^{(1)}}$ is a non-dimensional factor equal or lower than 1 parameterizing the tendency of organisms to retain more nutrients within the cellular walls with respect to carbon. The other output terms in (A.44b) and (A.44c) are given in (A.46c,A.46d), and they represent the direct excretion of inorganic nutrients in the water. The excretion is in the form of phosphate and urea, but the latter in the model is assumed to be as labile as the ammonium, therefore the flux is directly to the $N^{(4)}$ pool. Such excretions can exist only when the internal nutrient quota are higher than the maximum allowance, and are controlled by the parameters ν^{n}_{Z} and ν^{p}_{Z}, which are the maximum constant specific rates of the release process (d^{-1}), and $n_Z^{\max}$, $p_Z^{\max}$ that are the maximum internal quota for nitrogen and phosphorus, respectively.

Equation Box 7 Source/sink terms in functional process form for the mesozooplankton flux equations given in Box 5.

$$\left.\frac{\partial Z_c}{\partial t}\right|^{prd}_{P_c,Z_c} = f_z^T\, r_{0_Z}\, \frac{F_z}{F_z + \frac{r_{0_Z}}{v_z}} Z_c \tag{A.53a}$$

$$\left.\frac{\partial Z_c}{\partial t}\right|^{out}_{R_c^{(6)}} = \alpha_z \left.\frac{\partial Z_c}{\partial t}\right|^{prd}_{P_c,Z_c} + d_{0_Z}\, f_z^T\, Z_c + d_z^{dns}\, Z_c^{\beta_Z} \tag{A.53b}$$

$$\left.\frac{\partial Z_c}{\partial t}\right|^{rsp}_{O^{(3)}} = b_z\, f_z^T\, Z_c + \gamma_z \left.\frac{\partial Z_c}{\partial t}\right|^{prd}_{P_c,Z_c} \tag{A.53c}$$

$$\left.\frac{\partial Z_l}{\partial t}\right|^{prd}_{P_l,Z_l} = \frac{F_l}{F_c} \left.\frac{\partial Z_c}{\partial t}\right|^{prd}_{P_c,Z_c} \qquad l = n, p \tag{A.54a}$$

$$\left.\frac{\partial Z_n}{\partial t}\right|^{out}_{N^{(4)}} = b_z\, f_z^T\, Z_n \tag{A.54b}$$

$$\left.\frac{\partial Z_n}{\partial t}\right|^{out}_{N^{(1)}} = b_z\, f_z^T\, Z_p \tag{A.54c}$$

$$\left.\frac{\partial Z_l}{\partial t}\right|^{out}_{R_l^{(6)}} = l_z^{\max} \left.\frac{\partial Z_c}{\partial t}\right|^{out}_{R_c^{(6)}} \qquad l = n, p \tag{A.54d}$$

A.4.2. Mesozooplankton

For mesozooplankton, the functional process forms of the terms in the general zooplankton equation (A.44) are similar to the ones for microzooplankton, with the addition of some additional fluxes in order to account for the different population behavior of metazoans (Box 7). The gross secondary production flux in (A.53a) is written as a type II functional response, where f_z^T is the regulating factor for environmental temperature given in (A.6), v_z is the constant search volume, r_{0_Z} is the maximum potential specific growth rate (the inverse of the more commonly used handling time) and the total

availability of food is a vector F_i computed similarly to (A.47) but not including any prey density factor:

$$F_i = \sum_X \delta_{Z,X} X_i \tag{A.55}$$

where $\delta_{Z,X}$ is the food matrix element (cfr. (A.4) for mesozooplankton Z upon prey X, and the set of food sources can be derived from Table A.3. The predation loss term due to the mesozooplankton predation entering in (A.5a) and (A.44a) is again similar to the microzooplankton term (A.49) but without the density regulating factor. This means that mesozooplankton is assumed to consume each prey taxon in proportion to its instantaneous abundance in the local environment. In virtue of the high diversity in this functional group, this choice was thought to be less unrealistic than prescribing a switching behavior (Broekhuizen *et al*., 1995). However, one consequence of this assumption is that consumers can exert a strong predation pressure on a prey group because of the high abundance of another one.

As in the case of microzooplankton, the functional dynamics are based on the partitioning of the active ingestion flux. The main difference with respect to microzooplankton is that all the partitioning coefficients are constrained by the following relationship

$$\eta_z + \alpha_z + \gamma_z = 1 \tag{A.56}$$

where η_z is the assimilation fraction, α_z the portion excreted in the form of faecal pellets and γ_z the fraction released as carbon dioxide during the respiration. Among the excretion terms toward the detrital fraction of the organic matter, we also consider the losses due to mortality as shown in (A.53b), because mesozooplankton is a large group and it is assumed that has no exchange with the dissolved organic fraction. In (A.53b), the defecation rate is a constant fraction α_z of the secondary gross production (A.53a), which is the active carbon inflow, while the mortality rates are instead proportional to the population biomass only. Here mortality is divided in natural and density-dependent mortality, where d_{0_Z} is the specific daily rate of the natural mortality, and d_z^{dns} is the constant specific density-dependent mortality rate regulated by the non-dimensional exponent β_z, which should be in principle scaled to the average dimension of the parameterized species. Since mesozooplankton is the top predator in ERSEM III, these terms aquire importance because they represent the closure terms at the top of the food chain.

The respiration term in (A.53c) is normally divided in rest and activity respiration. According to the assumptions given above, the activity respiration is a fixed fraction of the total carbon uptake derived from (A.56), while, as already done in the other functional groups, the basal respiration is a constant rate (b_z) modulated by the environmental temperature.

Due to the assumption of the invariability of the internal nutrient quotas, the nitrogen and phosphorus dynamics in (A.44b) and (A.44c) are directly linked to the carbon dynamics considering the

nutrient content of the food sources, as shown in process form in (A.54a). Also in the case of the respiration flux there must be a release of nutrients associated to the carbon loss toward the carbon dioxide pool. This is only valid for the rest respiration as shown in (A.54b) and (A.54c), because the losses of nutrient for the activity respiration are accounted for in the assimilation balance described in the next section. The fluxes to the POP and PON pools shown in (A.54d) are likewise derived from the carbon excretion to the POC component.

A.4.3. The assimilation balance

In order to maintain constant the internal nutrient quota in the organisms, the non-limiting components that have been assimilated in excess have to be released in the water. These fluxes have been already introduced in the general dynamics for mesozooplankton in (A.44). Carbon is released as particulate detritus $R_c^{(6)}$, phosphorus as phosphate $N^{(1)}$ and nitrogen as ammonium $N^{(4)}$.

In order to determine the limiting component, the nutrient to carbon ratios of the assimilation fluxes is computed as follows:

$$\Gamma_z^l = \frac{(1-\alpha_z)\left.\dfrac{\partial Z_l}{\partial t}\right|_{P_l,Z_l}^{prd}}{\eta_z \left.\dfrac{\partial Z_c}{\partial t}\right|_{P_c,Z_c}^{prd}}, \quad l = n, p \tag{A.57}$$

Then, the assimilation ratios are cross-compared with the fixed nutrient-to-carbon ratios $n_z^{\max}$ and $p_z^{\max}$. If both Γ_z^n and Γ_z^p are greater than the fixed internal ratios, then carbon is limiting and the balance fluxes in Box 5 are:

$$\left.\frac{\partial Z_c}{\partial t}\right|_{R_c^{(6)}}^{lim} = 0 \tag{A.58a}$$

$$\left.\frac{\partial Z_n}{\partial t}\right|_{N^{(4)}}^{lim} = (1-\alpha_z)\left.\frac{\partial Z_n}{\partial t}\right|_{P_n,Z_n}^{prd} - n_z^{\max}\eta_z \left.\frac{\partial Z_c}{\partial t}\right|_{P_c,Z_c}^{prd} \tag{A.58b}$$

$$\left.\frac{\partial Z_p}{\partial t}\right|_{N^{(1)}}^{lim} = (1-\alpha_z)\left.\frac{\partial Z_p}{\partial t}\right|_{P_p,Z_p}^{prd} - p_z^{\max}\eta_z \left.\frac{\partial Z_c}{\partial t}\right|_{P_c,Z_c}^{prd} \tag{A.58c}$$

If nitrogen is limiting $\left(\Gamma_z^n < n_z^{\max}\right)$, then the fluxes are only towards particulate detritus and dissolved phosphate:

$$\left.\frac{\partial Z_c}{\partial t}\right|^{lim}_{R_c^{(6)}} = \eta_z \left.\frac{\partial Z_c}{\partial t}\right|^{prd}_{P_c,Z_c} - \frac{(1-\alpha_z)}{n_z^{\max}} \left.\frac{\partial Z_n}{\partial t}\right|^{prd}_{P_n,Z_n} \tag{A.59a}$$

$$\left.\frac{\partial Z_n}{\partial t}\right|^{lim}_{N^{(4)}} = 0 \tag{A.59b}$$

$$\left.\frac{\partial Z_p}{\partial t}\right|^{lim}_{N^{(1)}} = (1-\alpha_z) \left.\frac{\partial Z_p}{\partial t}\right|^{prd}_{P_p,Z_p} - p_z^{\max} \frac{(1-\alpha_z)}{n_z^{\max}} \left.\frac{\partial Z_n}{\partial t}\right|^{prd}_{P_n,Z_n} \tag{A.59c}$$

And last, if phosphorus is limiting $\left(\Gamma_z^p < p_z^{\max}\right)$, we have:

$$\left.\frac{\partial Z_c}{\partial t}\right|^{lim}_{R_c^{(6)}} = \eta_z \left.\frac{\partial Z_c}{\partial t}\right|^{prd}_{P_c,Z_c} - \frac{(1-\alpha_z)}{p_z^{\max}} \left.\frac{\partial Z_p}{\partial t}\right|^{prd}_{P_p,Z_p} \tag{A.60a}$$

$$\left.\frac{\partial Z_n}{\partial t}\right|^{lim}_{N^{(4)}} = (1-\alpha_z) \left.\frac{\partial Z_n}{\partial t}\right|^{prd}_{P_n,Z_n} - n_z^{\max} \frac{(1-\alpha_z)}{p_z^{\max}} \left.\frac{\partial Z_p}{\partial t}\right|^{prd}_{P_p,Z_p} \tag{A.60b}$$

$$\left.\frac{\partial Z_p}{\partial t}\right|^{lim}_{N^{(1)}} = 0 \tag{A.60c}$$

A.5. Dissolved inorganic components

In this section we describe the dynamics of the inorganic hydrochemical species that are resolved in the current version of the model, namely inorganic nutrients (phosphate, nitrate, ammonium and silicate), dissolved oxygen and reduction equivalents. The variable reduction equivalent was originally defined only in the benthic model, and it has been introduced in the pelagic model (state variable $N^{(6)}$) in order to account for the propagation of anoxic conditions from the water-sediment interface to the upper layers. It is assumed that reduction equivalents have the properties of sulphide, and they are measured in mmol S m^{-3}.

A.5.1. Nutrients

The pelagic cycles of dissolved inorganic nutrients are linked to the functional group dynamics. Therefore, the nutrient flux form equations given in Equation Box 8 are essentially a collection of all the flux terms already explained in the description of the functional groups shown in the previous sections. All the terms in Box 8 are expressed with the explicit signs, unless indicated by the presence of a regulating factor, as, for instance, in the case of the bacteria nutrient uptake/release in (A.61a) and (A.61c). Therefore, the equations can be rewritten by applying the exchange rule defined in (A.3).

Here follows a brief summary of the processes acting on the nutrient pools in the pelagic model.

The biochemical cycle of phosphate $N^{(1)}$ in (A.61a) is affected by the phytoplankton uptake (A.27), the bacterial uptake/release (A.37a) and the excretion from the zooplankton groups, (A.46c)

Equation Box 8 Flux form equations for the dissolved inorganic nutrients, phosphate, nitrate, ammonium and silicate.

$$\left.\frac{\partial N^{(1)}}{\partial t}\right|_{bio} = -\sum_{j=1}^{4}\left.\frac{\partial P_p^{(j)}}{\partial t}\right|_{N^{(1)}}^{upt} + f_B^p \left.\frac{\partial B_p}{\partial t}\right|_{N^{(1)}}^{upt,rel} + \sum_{j=3}^{6}\left.\frac{\partial Z_p^{(j)}}{\partial t}\right|_{N^{(1)}}^{out} \tag{A.61a}$$

$$\left.\frac{\partial N^{(3)}}{\partial t}\right|_{bio} = -\sum_{j=1}^{4}\left.\frac{\partial P_n^{(j)}}{\partial t}\right|_{N^{(3)}}^{upt} + \left.\frac{\partial N^{(3)}}{\partial t}\right|_{N^{(4)}}^{nit} - \left.\frac{\partial N^{(3)}}{\partial t}\right|_{sink_n}^{denit} \tag{A.61b}$$

$$\left.\frac{\partial N^{(4)}}{\partial t}\right|_{bio} = -\sum_{j=1}^{4}\left.\frac{\partial P_n^{(j)}}{\partial t}\right|_{N^{(4)}}^{upt} + f_B^p \left.\frac{\partial B_n}{\partial t}\right|_{N^{(4)}}^{upt,rel} + \sum_{j=3}^{6}\left.\frac{\partial Z_n^{(j)}}{\partial t}\right|_{N^{(4)}}^{out} - \left.\frac{\partial N^{(4)}}{\partial t}\right|_{N3}^{nit}$$

$$\left.\frac{\partial N^{(5)}}{\partial t}\right|_{bio} = -\left.\frac{\partial P_s^{(1)}}{\partial t}\right|_{N^{(5)}}^{upt} + \left.\frac{\partial R_s^{(6)}}{\partial t}\right|_{N^{(5)}}^{rmn} \tag{A.61c}$$

and (A.54c).

For nitrate $N^{(3)}$ (A.61b), the pelagic fluxes involve the phytoplankton uptake described in (A.5b) and the nitrification and denitrification process parameterizations that, being dependent on the redox conditions of the water column, will be described in the next section together with the dynamics of oxygen and reduction equivalents.

Ammonium (A.61c) is consumed by phytoplankton as described in (A.27) and remineralized (or utilized) by bacteria according to the quality of the substrate and their internal content of nitrogen (see (A.37b) and (A.40)). Zooplankton participates in the ammonium dynamics through the excretion of urea, which is assumed to be directly available in the form of ammonium, as shown in (A.46d) for microzooplankton and (A.54b) for mesozooplankton.

The pelagic cycle of silicate is quite simple in the model because of the many uncertainties linked to the complex dynamics of such element in the water. Silicate concentration was originally only affected by diatom uptake (A.31) and we have introduced a simple first-order reaction in ERSEM III, concerning the dissolution of biogenic silicate in the form of frustules as

$$\left.\frac{\partial R_s^{(6)}}{\partial t}\right|_{N^{(5)}}^{rmn} = \Lambda^s_{R^{(6)}}\, f^T_{R^{(6)}}\, R_s^{(6)} \tag{A.62}$$

where $\Lambda^s_{R^{(6)}}$ is the constant specific dissolution rate and $f^T_{R^{(6)}}$ is the regulating factor for temperature parameterized with the characteristic coefficient as usual.

A.5.2. Aerobic and anaerobic processes

Since many coastal ocean areas with a strong seasonal or permanent stratification manifest the occasional appearance of hypoxic or even anoxic conditions, it is necessary to introduce some pro-

Equation Box 9 Flux form equations for dissolved oxygen and reduction equivalents.

$$\left.\frac{\partial O^{(2)}}{\partial t}\right|_{bio} = \Omega_c^o \sum_{x=1}^{4} \left(\left.\frac{\partial P_c^{(x)}}{\partial t}\right|_{O^{(3)}}^{gpp} - \left.\frac{\partial P_c^{(x)}}{\partial t}\right|_{O^{(3)}}^{rsp} \right) - \Omega_c^o \, f_B^o \left.\frac{\partial B_c}{\partial t}\right|_{O^{(3)}}^{rsp} + \\ -\Omega_c^o \sum_{x=3}^{6} \left.\frac{\partial Z_c^{(x)}}{\partial t}\right|_{O^{(3)}}^{rsp} - \Omega_n^o \left.\frac{\partial N^{(4)}}{\partial t}\right|_{N^{(3)}}^{nit} - \frac{1}{\Omega_o^r} \left.\frac{\partial N^{(6)}}{\partial t}\right|_{sink_r}^{reox} \tag{A.63a}$$

$$\left.\frac{\partial N^{(6)}}{\partial t}\right|_{bio} = \Omega_o^r \Omega_c^o \left(1 - f_{B1}^o\right) \left.\frac{\partial B_c}{\partial t}\right|_{O^{(3)}}^{rsp} - \Omega_o^r \widetilde{\Omega}_n^o \left.\frac{\partial N^{(3)}}{\partial t}\right|_{sink_n}^{denit} - \left.\frac{\partial N^{(6)}}{\partial t}\right|_{sink_r}^{reox} \tag{A.63b}$$

cess parameterization that can describe chemical reactions under varying redox conditions. The major biochemical processes affected by redox conditions implemented in the model are nitrification/denitrification, sulphate reduction and reoxidation of reduction equivalents. One of the main problems related to the modelling of temporal successions of aerobic and anaerobic conditions is that some components are removed from the water and different species and metabolic pathways are favored by the new conditions. The numerical simulation of such behavior is quite complicated because some components reach concentrations that are close to zero with the risk of producing negative values as a result of the numerical integration. In the model, the problem has been approached in a functional way by allowing the simultaneous coexistence of oxygen and reduction equivalents and the actual oxygen concentration is determined considering the sum of the two components according to the concept of negative oxygen proposed by Fonselius (1969). The concentration of reduction equivalents - that in the model is equivalent to the presence of HS^- ions - is converted to oxygen by means of the stoichiometric coefficient $\Omega_o^r = 0.5$ (mmol S) (mmol O_2)$^{-1}$ and eventually is added to the dissolved O_2 concentration. Therefore, all the aerobic processes involve the consumption/production of dissolved oxygen and all the anaerobic ones the production/consumption of reduction equivalents and the global redox state is determined by the sum of the two.

The dynamics of these components are shown in Box 9. The planktonic net production of oxygen in (A.63a) is derived from the algebraic sum of gross primary production and community respiration, also subtracting the losses due to nitrification and reoxidation of reduction equivalents. All the source/sink terms are converted into oxygen units by means of the stoichiometric coefficients given in Table A.4. Equation (A.63b) shows the complementary dynamics of reduction equivalents that involves anaerobic processes. Since bacteria are active both under aerobic and anaerobic conditions the bacterial oxygen demand (A.36d) is partitioned into oxygen consumption and reduction equivalent production by using the oxygen regulating factor f_{B1}^o described in (A.42). The formation of reduction equivalents is parameterized converting the biological oxygen demand of bacteria (under low oxygen conditions) into sulphide ions by using the stoichiometric coefficient Ω_o^r as in the first term on the right side of (A.63b). The utilization of nitrate as an electron acceptor in microbial metabolic reactions is parameterized in an indirect way. Firstly, when the oxygen level falls below the threshold level and

$f^o_{B1} < 1$, the metabolic formation of reduction equivalents begins according to the bacterial oxygen demand (A.36d). However, the denitrification reaction is favored with respect to the pure anaerobic sulpho-reduction, therefore a portion of this oxygen demand should be redirected towards the denitrification process. In order to achieve this net effect, the changes in the redox conditions also enhance the denitrification flux in the following way:

$$\left.\frac{\partial N^{(3)}}{\partial t}\right|^{denit}_{sink_n} = \Lambda^{denit}_{N^{(3)}}\, f^T_{N^{(3)}} \left[\frac{1}{M^*_o}\,\Omega^o_c\left(1-f^o_B\right)\left.\frac{\partial B_c}{\partial t}\right|^{rsp}_{O^{(3)}}\right] N^{(3)} \tag{A.64}$$

where $\Lambda^{denit}_{N^{(3)}}$ is the specific denitrification rate at the reference anoxic mineralization M^*_o at 10^o C. The term at the numerator is the actual anoxic mineralization (bacterial oxygen demand), derived from the bacterial respiration. This consumption flux is not redirected (as production rate) to the amount of N_2 in the water, because this variable is not explicitely formulated in the model but considered as an infinite pelagic sink term ($sink_n$). Therefore, if nitrate is still present in the water, the rate of production of reduction equivalent $N^{(6)}$ is converted in nitrate consumption, mimicking the bacteria-mediated denitrification reactions.

Furthermore, until there is some oxygen left, reduction equivalents are also fast reoxidized with the following rate:

$$\left.\frac{\partial N^{(6)}}{\partial t}\right|^{reox}_{sink_r} = \Lambda^{reox}_{N^{(6)}}\, f^T_{N^{(6)}}\, \frac{O^{(2)}}{O^{(2)}+h^o_{N^{(6)}}} N^{(6)} \tag{A.65}$$

where $\Lambda^{reox}_{N^{(6)}}$ is the (constant) specific daily reoxidation rate, $f^T_{N^{(6)}}$ is the temperature regulating factor and $h^o_{N^{(6)}}$ is a half-saturation concentration set to a very small oxygen concentration (10 mmol O_2 m^{-3}). When oxygen and nitrate are completely depleted the two last terms in (A.63b) become zero and the process turns to a strict anaerobic formation of sulphide ions coupled to the availability of the organic substrate.

The last parameterized process dealing with the redox conditions is nitrification, which is a source/sink term of the nitrate (A.61b) equation, ammonium (A.61c), and oxygen (A.63a). Nitrification in the model is written as a first-order term:

$$\left.\frac{\partial N^{(4)}}{\partial t}\right|^{nit}_{N^{(3)}} = \Lambda^{nit}_{N^{(4)}}\, f^T_{N^{(4)}}\, \frac{O^{(2)}}{O^{(2)}+h^o_{N^{(4)}}}\, O_{sat}\, N^{(4)} \tag{A.66}$$

where Λ^{nit}_{N4} is the constant specific nitrification rate, O_{sat} the fraction of oxygen saturation, and the regulating factors are similar to the ones shown in (A.65).

Equation Box 10 Flux form equations for dissolved and particulate organic detritus.

$$\left.\frac{\partial R_c^{(1)}}{\partial t}\right|_{bio} = \sum_{j=1}^{4} \left.\frac{\partial P_c^{(j)}}{\partial t}\right|_{R_c^{(1)}}^{out} + \left.\frac{\partial B_c}{\partial t}\right|_{R_c^{(1)}}^{out} - \left.\frac{\partial B_c}{\partial t}\right|_{R_c^{(1)}}^{bcd} + \sum_{j=5}^{6} \left.\frac{\partial Z_c^{(j)}}{\partial t}\right|_{R_c^{(1)}}^{out} \tag{A.67a}$$

$$\left.\frac{\partial R_l^{(1)}}{\partial t}\right|_{bio} = \sum_{j=1}^{4} \left.\frac{\partial P_l^{(j)}}{\partial t}\right|_{R_l^{(1)}}^{out} + \left.\frac{\partial B_l}{\partial t}\right|_{R_l^{(1)}}^{out} - \left.\frac{\partial B_l}{\partial t}\right|_{R_l^{(1)}}^{upt} + \sum_{j=5}^{6} \left.\frac{Z_l^{(j)}}{Z_c^{(x)}} \frac{\partial Z_c^{(j)}}{\partial t}\right|_{R_c^{(1)}}^{out} \qquad l = n, p \tag{A.67b}$$

$$\left.\frac{\partial R_c^{(6)}}{\partial t}\right|_{bio} = \sum_{j=1}^{4} \left.\frac{\partial P_c^{(j)}}{\partial t}\right|_{R_c^{(6)}}^{out} - \left.\frac{\partial B_c}{\partial t}\right|_{R_c^{(6)}}^{bcd} + \sum_{j=5}^{6} \left.\frac{\partial Z_c^{(j)}}{\partial t}\right|_{R_c^{(6)}}^{out} + \sum_{j=3}^{4} \left.\frac{\partial Z_c^{(j)}}{\partial t}\right|_{R_c^{(6)}}^{out} \tag{A.67c}$$

$$\left.\frac{\partial R_l^{(6)}}{\partial t}\right|_{bio} = \sum_{j=1}^{4} \left.\frac{\partial P_l^{(j)}}{\partial t}\right|_{R_l^{(6)}}^{out} - \left.\frac{\partial B_l}{\partial t}\right|_{R_l^{(6)}}^{upt} + \sum_{j=3}^{6} \left.\frac{Z_l^{(j)}}{Z_c^{(j)}} \frac{\partial Z_c^{(j)}}{\partial t}\right|_{R_c^{(6)}}^{out} \qquad l = n, p$$

$$\left.\frac{\partial R_s^{(6)}}{\partial t}\right|_{bio} = \left.\frac{\partial P_s^{(1)}}{\partial t}\right|_{R_s^{(6)}}^{out} + \frac{P_s^{(1)}}{P_c^{(1)}} \sum_{j=4}^{5} \left.\frac{\partial P_c^{(1)}}{\partial t}\right|_{Z_c^{(j)}}^{prd} - \left.\frac{\partial R_s^{(6)}}{\partial t}\right|_{N^{(5)}}^{rmn} \tag{A.67d}$$

A.6. Dissolved and particulate organic matter

The source/sink terms in functional process form for dissolved and particulate organic matter (ordinary state variables $R_i^{(1)}$ and $R_i^{(6)}$) shown in Box 10 are the consequence of the production/consumption rates described in the functional group parameterizations in the previous sections. Dissolved organic matter (DOM) is produced by phytoplankton, bacteria and microzooplankton and used as organic substrate by bacteria as shown in (A.67a) and (A.67b). The carbon, nitrogen and phosphorus component of particulate detritus (shown in (A.67c) and (A.67d) respectively) are excreted by all the members of the planktonic community except bacteria, which are the only utilizers of this component according to (A.36c). The pelagic cycle of biogenic silica is instead restricted to the release of diatom frustule through mortality and other lysis processes as in (A.32) and via micro- mesozooplankton predation and sloppy feeding with the addition of the chemical dissolution shown in (A.62).

Symbol	Value	Description
Mw^c	12	Molar weight of Carbon (mg C)
Rr_c^n	$\frac{16}{106 \cdot Mw^c}$	N:C Redfield ratio (mmol N mg C^{-1})
Rr_c^p	$\frac{1}{106 \cdot Mw^c}$	P:C Redfield ratio (mmol P mg C^{-1})
Rr_c^s	$\frac{15}{106 \cdot Mw^c}$	Si:C Redfield ratio (mmol Si mg C^{-1})
Ω_c^o	$\frac{1}{Mw^c}$	Stoichiometric coefficient in respiration and photosynthesis (mmol O_2 mg C^{-1})
Ω_n^o	2	Stoichiometric coefficient in nitrification reaction (mmol O_2 mmol N^{-1})
$\widetilde{\Omega}_n^o$	5/4	Stoichiometric coefficient in denitrification reaction (mmol O_2 mmol N^{-1})
Ω_o^r	1/2	Stoichiometric coefficient in sulphate reduction (mmol HS^- mmol $O_2{}^{-1}$)

Table A.4.: Functional constants and stoichiometric coefficients of biochemical reactions.

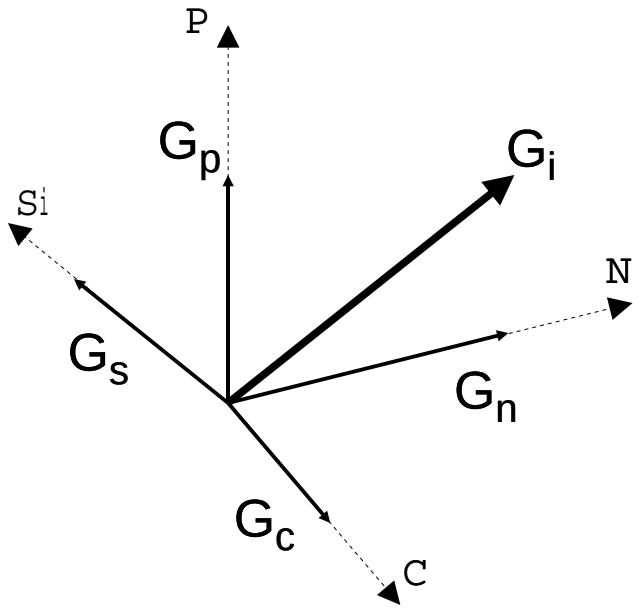

Figure A.1.: Visual schematization of the 4-dimensional functional group vector.

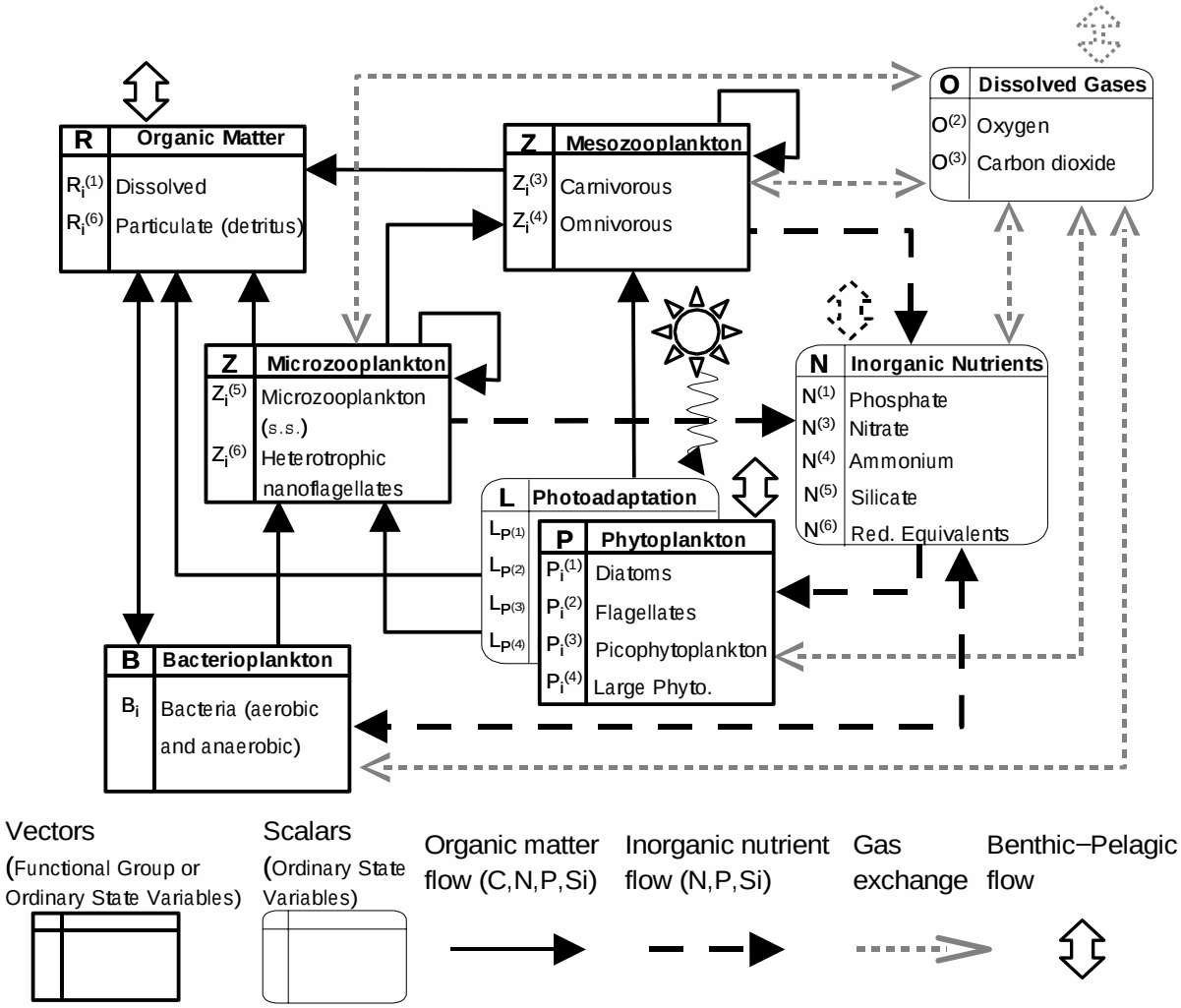

Figure A.2.: Scheme of the pelagic model.

B. Review of the ERSEM III biogeochemical equations. The benthic model

B.1. Introduction

This Appendix describes the equations for the benthic model applying the mathematical formulation defined for the pelagic model (Section A.1). The pelagic and the benthic systems are connected each other through the water-sediment interface, which is located at depth $\tilde{z} = -H$ in the pelagic system of coordinates, where H is the bottom depth. The system of coordinates for the benthic model is reverted (Figure B.2), starting from $z = 0$ at the interface and going downward to the total depth of the modelled sediment layers ($D_{tot} = 0.3$ m). Therefore, fluxes are considered positive downwards, and the fluxes from the benthic to the pelagic system are negative.

The main processes considered in the benthic model are:

- deposition and incorporation of particulate organic matters from the pelagic system;
- cycling of carbon and macronutrients through the benthic food web;
- early-diagenesis (oxic and anoxic mineralization) with a semi-analytical description of the dissolved nutrient dynamics in the pore-waters and subsequent molecular exchanges with the nutrient pools in the water column.

Physical resuspension processes are not included in the present formulation, although they are considered to be an important mechanism for nutrient mobility especially in shallow coastal waters. Parameterization schemes describing this process need to be introduced in future developments, particularly in the case of three-dimensional transport models that can solve the horizontal current structure and the bottom boundary layer. Therefore, the generic equations for the benthic variables do not have any physical transport term as in (A.1), but only biological source or sink terms.

The list of the ERSEM III benthic state variables (functional groups and ordinary state variables) is summarized in Table B.1 and the schematic interactions are illustrated in Figure B.1. It is important to remind that the present description of the model equations is intended to be a formal (re)writing of the biogeochemical concepts already presented in the previous ERSEM I (Baretta, 1995) and ERSEM II (Baretta-Bekker and Baretta, 1997) publications, plus some new additional processes and refinements.

Hence, we refer to the specific papers also listed in Table B.1 for a detailed explanation of the underlying theoretical and experimental reasons at the basis of the parameterization. In the case of the definition of new processes, further specific details and justifications will be given in the text.

The ERSEM III benthic model is essentially a layer model in which the concentrations of the benthic functional groups and of the other ordinary state variables (representing the organic/inorganic compounds and dissolved gases) are treated as bulk values in the sediments. Therefore, the units are given per meter squared, and the depth of the bottom layer of the water column is taken into account in the unit conversions concerning the exchange fluxes at the interface with the pelagic system. The sediments are divided in three main dynamical layers where different processes take place. The benthic organisms are supposed to act from the sediment surface to a depth of a few centimeters, mainly depending on the oxic conditions and the availability of resources. The benthic anaerobic decomposers can instead extend to the bottom of the modeled layers, but always limited by the penetration depth of the organic matter. In the oxic layer (Figure B.2), whose thickness is defined by the ordinary state variable $D^{(1)}$, the aerobic mineralization processes occur and the nitrification of ammonium is also considered. Most of the life cycles of the benthic functional groups take place in this layer. In the denitrification and anoxic layers, separated by the sulphide horizon depth (ordinary state variable $D^{(2)}$), the anaerobic mineralization is the main process that controls the distribution of the dissolved nutrients. This is the layer where nitrate and sulphate are considered to be the main electron-acceptors used in the bacterial functional dynamics for the decomposition of the organic matter. Below the sulphide horizon depth, only strict anaerobic processes such as sulphate reduction occurs.

B.2. Pelagic-benthic coupling

The main input to the benthic system is the sedimentation of particles from the water column that enters into the organic matter pools in the sediments ($Q_i^{(6)}$ and $Q_i^{(1)}$). Sedimentation is a physical process partly mediated by biological dynamics, as in the case of diatom sinking (cfr. Section A.2.6). Since the last layer of the pelagic model coincides with the first layer of the benthic, the sedimentation flux is a boundary condition for both the equation sets. Actually, the incorporation of pelagic components into the benthic system depends on the net sedimentation rates at the bottom that result from the interaction between resuspension and deposition processes. Since none of these processes is considered in the current formulation, in the physical model we assume that the vertical velocity at the bottom is zero, and that all the sinking matter is deposited and remains in the benthic system. The flux to the benthic system is considered with a simplified approach, in which we assume that the incorporation velocity (or surface burial rate w_{bur}) is a constant value that multiplied by the concentrations of the sinking variables gives the output rates from the water column to the sediments. In the

Variable	Type	Constituent	Description	Reference
$K^{(1)}$	OSV	P	Phosphate in oxic layer (mmol P m^{-2})	Ruardij and Van Raaphorst, 1995
$K1^{(1)}$	OSV	P	Phosphate in denitrification layer (mmol P m^{-2})	"
$K2^{(1)}$	OSV	P	Phosphate in anoxic layer (mmol P m^{-2})	"
$K^{(3)}$	OSV	N	Nitrate in the sediments (mmol N m^{-2})	"
$K^{(4)}$	OSV	N	Ammonium in oxic layer (mmol N m^{-2})	"
$K1^{(4)}$	OSV	N	Ammonium in denitrification layer (mmol N m^{-2})	"
$K2^{(4)}$	OSV	N	Ammonium in anoxic layer (mmol N m^{-2})	"
$K^{(5)}$	OSV	Si	Silicate in the sediments (mmol Si m^{-2})	"
$K^{(6)}$	OSV	R	Reduction equivalents, Fe(II), Mn(II), HS^- (mmol S m^{-2})	"
$G^{(2)}$	OSV	O	Dissolved Oxygen (O_2) in oxic layer (mmol O_2 m^{-2})	Ebenhoeh et al, 1995; Ruardij and Van Raaphorst, 1995
$G^{(3)}$	OSV	C	Dissolved CO_2 in the sediments (mg C m^{-3})	"
$Y_i^{(1)}$	FG	C N P	Epibenthic Predators (*megabenthos*) (mg C m^{-2} or mmol nut. m^{-2})	Ebenhoeh et al, 1995; Blackford, 1997
$Y_i^{(2)}$	FG	C N P	Deposit Feeders (")	"
$Y_i^{(3)}$	FG	C N P	Filter Feeders (")	"
$Y_i^{(4)}$	FG	C N P	Meiobenthos	"
$Y_i^{(5)}$	FG	C N P	Infaunal Predators (")	"
$H_i^{(1)}$	FG	C N P	Aerobic Benthic Bacteria (")	"
$H_i^{(2)}$	FG	C N P	Anaerobic Benthic Bacteria (")	"
$D^{(1)}$	OSV	-	Oxic layer depth (m)	Ruardij and Van Raaphorst, 1995
$D^{(2)}$	OSV	-	Sulfide Horizon depth (m)	"
$D^{(6)}$	OSV	-	Average penetration depth for the C-component in detritus (m)	Ebenhoeh et al, 1995
$D^{(7)}$	OSV	-	As above but for the N-component	"
$D^{(8)}$	OSV	-	As above but for the P-component	"
$D^{(9)}$	OSV	-	As above but for the Si-component	"
$Q_i^{(1)}$	OSV	C N P	Dissolved Organic Matter in the oxic layer (mg C m^{-2} or mmol nut. m^{-2})	-
$Q1_i^{(1)}$	OSV	C N P	Dissolved Organic Matter in the anoxic layer (")	-
$Q_i^{(6)}$	OSV	C N P Si	Particulate Organic Detritus in the sediments (")	Ebenhoeh et al, 1995; Ruardij and Van Raaphorst, 1995

Table B.1.: List of state variables for the benthic model and references to the original parameterization of the implemented processes.

case of phytoplankton and organic detritus, these are written as

$$\left.\frac{\partial Q_i^{(6)}}{\partial t}\right|_{R_i^{(6)},P_i^{(1)}}^{sed} = w_{bur}\left[\left(R_i^{(6)}\right)_{z=-H} + \xi_i \sum_j \left(1-\psi_{P^{(j)}}\right)\left(P_i^{(j)}\right)_{z=-H}\right] \quad i=c,n,p,s \qquad \text{(B.1)}$$

$$\left.\frac{\partial Q_i^{(1)}}{\partial t}\right|_{P_i}^{sed} = w_{bur}\,\xi_i \sum_j \psi_{P^{(j)}}\left(P_i^{(j)}\right)_{z=-H} \quad i=c,n,p \qquad \text{(B.2)}$$

where it is also considered that phytoplankton is fractionated into particulate and dissolved components, mainly for mechanical reasons. The pelagic state variables $R_i^{(6)}$ and $P_i^{(j)}$ are the particulate detritus and the phytoplankton functional groups (only those ones that sink) described in Appendix A. The parameter $\psi_{P^{(j)}}$ is different for each phytoplankton group. It indicates the fraction of the biomass that is considered to be labile and it is readily available in dissolved phase. Nutrients are considered to be more available than carbon in such phase, therefore the non-dimensional constant ξ_i has been introduced, which is 1 for carbon and usually larger than one for the other nutrients.

B.3. The benthic food matrix

The formulation of the standard food matrix for the benthic food web is the same described in the pelagic model (Section A.1.1). The benthic food matrix is indicated as $\phi_{Y,X}$:

$$\phi_{Y,X} = \begin{bmatrix} \phi_{Y^{(1)},P^{(1)}} & \cdots & \phi_{Y^{(1)},H^{(2)}} \\ \vdots & \vdots & \vdots \\ \phi_{Y^{(5)},P^{(1)}} & \cdots & \phi_{Y^{(5)},H^{(2)}} \end{bmatrix} \qquad \text{(B.3)}$$

where X are the food sources

$$X \equiv \left\{P_i^{(1)}, P_i^{(2)}, P_i^{(3)}, P_i^{(4)}, Y_i^{(1)}, Y_i^{(2)}, Y_i^{(3)}, Y_i^{(4)}, Y_i^{(5)}, H_i^{(1)}, H_i^{(2)}, Q_i^{(6)}, R_i^{(6)}\right\}$$

and Z the consumers

$$Y \equiv \left\{Y_i^{(1)}, Y_i^{(2)}, Y_i^{(3)}, Y_i^{(4)}, Y_i^{(5)}\right\}.$$

The reference values of the benthic food matrix, mostly derived from the ERSEM II standard values, are shown in Table B.2. This matrix has a slightly different meaning with respect to the pelagic one because it also includes non-living resources such as detritus in the sediments and in the water column.

	Food Sources											
Consumers	$Y_i^{(1)}$	$Y_i^{(2)}$	$Y_i^{(3)}$	$Y_i^{(4)}$	$Y_i^{(5)}$	$P_i^{(1)}$	$P_i^{(2)}$	$P_i^{(3)}$	$H_i^{(1)}$	$H_i^{(2)}$	$Q_i^{(6)}$	$R_i^{(6)}$
$Y_i^{(1)}$	1.0	0.7	1.0	0	0.5	0	0	0	0	0	0	0
$Y_i^{(2)}$	0	0	0	1.0	0	0	0	0	0	0	0.1	0
$Y_i^{(3)}$	0	0	0	0	0	1.0	1.0	1.0	1.0	0	0.1	1.0
$Y_i^{(4)}$	0	0	0	1.0	0	0	0	0	1.0	1.0	0.3	0
$Y_i^{(5)}$	0	1.0	0	0.5	1.0	0	0	0	0	0	0	0

Table B.2.: Benthic food matrix $\phi_{Y,X}$ for the reference standard model. See Tab. B.1 for an explanation of symbols.

Equation Box 11 Flux form equations for the functional groups of the benthos.

$$\left.\frac{\partial Y_c}{\partial t}\right|_{bio} = \sum_X \left.\frac{\partial Y_c}{\partial t}\right|_{X_c}^{upt} - \left.\frac{\partial Y_c}{\partial t}\right|_{G^{(3)}}^{rsp} - \left.\frac{\partial Y_c}{\partial t}\right|_{Q_c^{(6)}}^{out} - \sum_j \left.\frac{\partial Y_c}{\partial t}\right|_{Y_c^{(j)}}^{prd} - \left.\frac{\partial Y_c}{\partial t}\right|_{Q_c^{(6)}}^{lim} \tag{B.4a}$$

$$\left.\frac{\partial Y_n}{\partial t}\right|_{bio} = \sum_X \left.\frac{\partial Y_c}{\partial t}\right|_{X_c}^{upt} - \left.\frac{\partial Y_n}{\partial t}\right|_{Q_n^{(6)}}^{out} - \frac{Y_n}{Y_c}\sum_j \left.\frac{\partial Y_c}{\partial t}\right|_{Y_c^{(j)}}^{prd} - \left.\frac{\partial Y_n}{\partial t}\right|_{K^{(4)}}^{lim} \tag{B.4b}$$

$$\left.\frac{\partial Y_p}{\partial t}\right|_{bio} = \sum_X \frac{X_p}{X_c}\left.\frac{\partial Y_c}{\partial t}\right|_{X_c}^{upt} - \left.\frac{\partial Y_p}{\partial t}\right|_{Q_p^{(6)}}^{out} - \frac{Y_p}{Y_c}\sum_j \left.\frac{\partial Y_c}{\partial t}\right|_{Y_c^{(j)}}^{prd} - \left.\frac{\partial Y_p}{\partial t}\right|_{K^{(1)}}^{lim} \tag{B.4c}$$

B.4. Benthic organisms

The definition of the functional groups belonging to the benthos has not changed with respect to the previous versions, and we give here a brief summary of the group specifications presented in Ebenhöh et al. (1995) and Blackford (1997). The structure of the food web is conceived as divided in a "surface" chain composed of epibenthic predators and filter feeders, and a "subsurface" chain with meiobenthic organisms, deposit feeders, infaunal predators and microbial decomposers that will be specifically discussed in the next section. All these organisms, except meiobenthos and microbes, have dimensions larger than 1 mm, even reaching sizes of several centimeters as in the case of epibenthic predators. Benthic primary producers are not considered in the standard model, although they could be responsible of a substantial part of the autotrophic production in coastal areas where the euphotic zone reaches the bottom layers.

From a mathematical point of view, the benthic functional groups are treated as multidimensional vectors, but the 4th dimension, which represents the silicate component, is not considered in any of the groups. Therefore, the functional groups are essentially 3-dimensional vectors with only the C, N and P components, and the dynamics of Si will be omitted in their description.

The 5 functional groups are:

- Epifaunal predators (state variable vector $Y_i^{(1)}$), large mobile organisms usually classified as megabenthos. Since there are no other epifaunal groups, this component can also include other

smaller size predators and the immobile epifaunal organisms (excluding filter feeders);

- Deposit feeders (state variable vector $Y_i^{(2)}$), a wide group comprising all the organisms whose diet consists of benthic detritus and smaller organisms belonging to the meiobenthic community;

- Filter feeders (state variable vector $Y_i^{(3)}$), is a large functional group composed of immobile (or slowly moving) organisms that feeds directly from the pelagic system by filtering the suspended particles in the surrounding waters. The prototype of this group are molluscs;

- Meiobenthos (state variable vector $Y_i^{(4)}$), complex ensemble of heterotrophs characterized by a size of about 1 mm. This group comprises both protozoa and animals with different kind of functional specializations but with a small impact on the sediment distribution through bioturbation and bioirrigation mechanisms. They are the main ecological consumers of benthic bacteria;

- Infaunal predators (state variable vector $Y_i^{(5)}$), specialized heterotrophs that prefer preys of a size comparable to themselves. Their predation pressure usually extends within the oxygen horizon, with a substantial bioturbation of the organic matter distribution.

All the groups also indulge in cannibalism, because, as demonstrated by Kohlmeyer and Ebenhöh (1995), these fluxes stabilize the oscillations of the functional group dynamics. Besides, this flux is especially important for meiobenthos, because it can be demonstrated that the introduction of an artificial cannibalism flux also makes the trophic position of a group independent from the degree of aggregation (Ulanowicz, 1986; Ebenhöh et al., 1995).

The set of flux form equations for the benthic organisms is presented in Equation Box 11. As done for the pelagic model, we will refer to the generic group Y, and the dynamics of each functional group can be derived by substituting the corresponding symbol. An exception is necessary for the group of filter feeders, for which we reserve the specific Section B.4.2 in order to account for their different ecological role.

Benthic organism physiology is supposed to be affected by the water temperature (we assume sediments are in a thermal equilibrium with the water) with the usual form of the regulating factor also presented in the pelagic model:

$$f^T = Q_{10}^{\frac{T-T_0}{T_0}} \quad T_0 = 10^o C \tag{B.5}$$

where Q_{10} is the characteristic temperature coefficient that can have different values for each group. Oxygen dependence is parameterized as a function of the oxic layer thickness $D^{(1)}$ with the following

ramp function:

$$f_Y^o = \begin{cases} 1 & \text{if } D^{(1)} > D^* \\ \dfrac{D^{(1)}}{D^*} & \text{if } 0 \le D^{(1)} \le D^* \end{cases}$$

where D^* is a threshold critical depth of the oxic layer set to about 5 mm. This is a very simple parameterization, because the response of benthic organisms to hypoxic or even anoxic conditions is quite complex and different from species to species. For filter feeders and epibenthic organisms that live on the surface, there is an alternative function (Blackford, 1997) that depends on the oxygen concentration in the water column and it is the same used for pelagic bacteria:

$$f_Y^o = \frac{\left(O^{(2)}\right)^3}{\left(O^{(2)}\right)^3 + h_Y^o} \tag{B.6}$$

where h_Y^o is the half-saturation threshold.

Other important parameters are the ideal depths where the activity of the benthic organisms is located. These depths, which are different for each sub-group, are indicated by the symbol m_Y. They will be used in the determination of the changes in the vertical distribution of the sediment detritus (Section B.6). Epifaunal predators and filter feeders are supposed to spend their lifetime on the sediment surface, therefore we put $m_{Y^{(1)}}, m_{Y^{(3)}} = 0$. Meiobenthos is allowed to move within a fixed range of maximum and minimum depths $m_{Y^{(4)}}^{\min}$ and $m_{Y^{(4)}}^{\max}$. Their virtual activity depth is put in the middle of this range disregarding the oxygen distribution in the sediments, because this group is assumed to survive a permanence in anoxic environments for relatively brief periods. The deposit feeders are located at half the mean intrusion depth of the organic detritus, $m_{Y^{(2)}} = D^{(6)}/2$, and the infaunal predators can extend their activity only within the oxic layer and are located at $m_{Y^{(5)}} = D^{(1)}/2$.

Equation Box 12 Source/sink terms in functional process forms for the functional groups of the benthos.

$$\left.\frac{\partial Y_c}{\partial t}\right|_{X_c}^{upt} = r_{0_Y} f_Y^T f_Y^o \frac{f_{Y,X}^{dns} \phi_{Y,X} X_c}{F_Y + h_Y^F} Y_c \tag{B.7a}$$

$$\left.\frac{\partial Y_c}{\partial t}\right|_{G^{(3)}}^{rsp} = b_Y f_Y^T Y_c + \gamma_Y \sum_X \left(1 - \alpha_{Y,X}\right) \left.\frac{\partial Y_c}{\partial t}\right|_X^{upt} \tag{B.7b}$$

$$\left.\frac{\partial Y_c}{\partial t}\right|_{Q_c^{(6)}}^{out} = \sum_X \alpha_{Y,X} \left.\frac{\partial Y_c}{\partial t}\right|_{X_c}^{upt} + d_{0_Y} f_Y^T Y_c \tag{B.7c}$$

$$\left.\frac{\partial Y_l}{\partial t}\right|_{X_l}^{upt} = \frac{X_l}{X_c} \left.\frac{\partial Y_c}{\partial t}\right|_{X_c}^{upt} \quad l = n, p \tag{B.7d}$$

$$\left.\frac{\partial Y_l}{\partial t}\right|_{Q_l^{(6)}}^{out} = \xi_Y \frac{Y_l}{Y_c} \left.\frac{\partial Y_c}{\partial t}\right|_{Q_c^{(6)}}^{out} \quad l = n, p \tag{B.7e}$$

B.4.1. Carbon and nutrient dynamics

The functional process form of the terms in (B.4) are shown in Equation Box 12. The processes affecting the consumers are uptake of food sources, respiration, release (faeces production and mortality) and predation. An additional term (indicated by the subscript lim) is introduced in order to allow the excretion of those components that are in excess. This process is derived from the assumption of constant internal nutrient to carbon ratios and will be described in Section B.4.3. The calculation of any single uptake rate (B.7a) involves a potential growth rate that is modulated by the environmental factors and the estimation of the apparent availability of the food sources implemented with a Type II feeding response (the parameter h_Y^F controls the shape of the Type II function). The availability of each source is derived from the benthic food matrix element (B.3) and Table B.2 for the organism Y upon the source X. The total food availability is the sum of all the available food sources as follows:

$$F_Y = \sum_X f_{Y,X}^{dns} \phi_{Y,X} X_c \tag{B.8}$$

in which a density regulating factor written in a Michaelis-Menten form is considered:

$$f_{Y,X}^{dns} = \frac{\phi_{Y,X} X_c}{\phi_{Y,X} X_c + \mu_Y}. \tag{B.9}$$

This factor introduces a selective approach to the consumer uptake dynamics, directing the feeding towards the more abundant resources and avoiding the total consumption of the less abundant ones. The parameter μ_Y determines the choice threshold, which is typical of each consumer.

When an organism can feed upon benthic detritus (see Table B.2), which has an implicit vertical distribution (Section B.6), such distribution has to be considered in the determination of the food availability. Availability is computed by defining a portion of the sediment where the organism can be found, delimited by a minimum and a maximum depth $\left[m_Y^{\min}, m_Y^{\max}\right]$ in meters. If we consider the vertical density distribution of detritus shown below in (B.23), the availability is written as

$$\widetilde{Q}_c^{(6)} = Q_c^{(6)} \int_{m_Y^{\min}}^{m_Y^{\max}} \frac{\rho_{Q^{(6)}}(z, D^{(6)})}{\rho 0_{Q^{(6)}}} dz \tag{B.10}$$

The new variable $\widetilde{Q}_c^{(6)}$ is used in (B.8) to calculate the total food sources. The availability for the nutrient-components in the detritus are derived accordingly considering the respective depth distributions for nitrogen ($D^{(7)}$) and for phosphate ($D^{(8)}$).

The loss terms in (B.7b) and (B.7c) are computed from the partitioning of the uptake rates into one portion that is assimilated and one that is excreted. Usually the fraction of the excreted part ($\alpha_{Y,X}$) is the same for all the food sources except for detritus $\widetilde{Q}_i^{(6)}$, which is usually higher because the assimilation efficiency of detritus is lower compared to the living sources. A portion γ_r of the assimilated carbon is respired to the carbon dioxide pool $G^{(3)}$ as energy cost for the uptake dynamics as shown in (B.7b).

The basal respiration is added to that as a function of the environmental temperature and of the specific daily basal respiration rate (b_Y). The mortality term is instead added to the release flux (B.7c). This process is parameterized as a simple first-order process depending on the daily specific mortality rate. It is important to note that this is the closure term for the carbon food web dynamics in the benthic system, because there are no higher trophic level predators in ERSEM III. In fact, predation exists only among the benthic functional groups, and it is straightforward to derive the predation loss terms from (B.7a), substituting the proper trophic interaction factors listed in Table B.2.

The processes affecting the nutrient dynamics in (B.4b) and (B.4c) are essentially derived from the carbon terms. In particular, the uptake (B.7d) depends on the nutrient content of each food source, and the excretion (B.7e) from the nutrient ratios in the functional groups itself. The nutrients in excess are released in inorganic form as shown below in (B.12b) and (B.12c).

B.4.2. Filter feeders

Some modifications of the standard parameterizations are necessary in order to take into account the filtration process and the uptake from the pelagic variables which are expressed as volume concentrations. The set of food sources for filter feeders can be derived from Table B.2. The benthic detritus utilization is considered to be coming from resuspension processes, which are not yet explicitly parameterized in the model. A theoretical resuspension will be considered though.

As defined in Ebenhöeh et al. (1995), we introduce a parameter (d_w) that describes the unequal distribution of suspended matter in the water layer above the sediments. This is written as a concentration factor multiplied by the depth of the layer which is accessed by filter feeders. If $d_w = 3$ m, it can mean both a concentration factor of 10 and the water layer can be filtered up to the height of 30 cm, or a concentration factor of 100 and only 3 cm of filtration layer. This parameter is applied to the food concentrations in the water column in (B.7a) and (B.8) in order to give the correct units for the benthic state variables. The availability of the benthic detritus is still given by (B.10) , but it has a different meaning. $\widetilde{Q}_c^{(6)}$ now represents the actual amount of detritus that has been resuspended from the surface $m_{Y3}^{\min} = 0$ to the depth $m_{Y3}^{\max}$, and it is available in the same filtration layer as the other pelagic sources.

B.4.3. Assimilation balance

Since the internal C:N:P ratio is supposed to remain constant, there is an assimilation balance to release the components in excess according to the limiting one. This is expressed in the last terms of (B.4). Let G_Y^c and G_Y^l, $l = n, p$ be the net secondary production for the carbon and nutrient components defined as follows:

$$G_Y^c = \sum_X \left.\frac{\partial Y_c}{\partial t}\right|_{X_c}^{upt} - \left.\frac{\partial Y_c}{\partial t}\right|_{G^{(3)}}^{rsp} - \left.\frac{\partial Y_c}{\partial t}\right|_{Q_c^{(6)}}^{out} \tag{B.11a}$$

$$G_Y^l = \sum_X \frac{X_l}{X_c} \left.\frac{\partial Y_c}{\partial t}\right|_{X_c}^{upt} - \left.\frac{\partial Y_l}{\partial t}\right|_{Q_l^{(6)}}^{out} \tag{B.11b}$$

Evaluating the difference $G_Y^l - l_Y^{\max} G_Y^c$ where we make use of the maximum nutrient:carbon ratios $l_Y^{\max} = (n_Y^{\max}, p_Y^{\max})$, we can derive the inorganic nutrients or carbon release (detritus) as:

$$\left.\frac{\partial Y_c}{\partial t}\right|_{Q_c^{(6)}}^{lim} = \max\left(0, -\frac{G_Y^p - p_Y^{\max} G_Y^c}{p_Y^{\max}}\right) + \max\left(0, -\frac{G_Y^n - n_Y^{\max} G_Y^c}{n_Y^{\max}}\right) \tag{B.12a}$$

$$\left.\frac{\partial Y_n}{\partial t}\right|_{K^{(4)}}^{lim} = G_Y^n - n_Y^{\max}\left(G_Y^c - \left.\frac{\partial Y_c}{\partial t}\right|_{Q_c^{(6)}}^{lim}\right) \tag{B.12b}$$

$$\left.\frac{\partial Y_p}{\partial t}\right|_{K^{(1)}}^{lim} = G_Y^p - p_Y^{\max}\left(G_Y^c - \left.\frac{\partial Y_c}{\partial t}\right|_{Q_c^{(6)}}^{out}\right) \tag{B.12c}$$

Equation Box 13 Flux form equations for benthic decomposers.

$$\left.\frac{\partial H_c}{\partial t}\right|_{bio} = \left.\frac{\partial H_c}{\partial t}\right|_{Q_c^{(1)},Q_c^{(6)}}^{upt} - \left.\frac{\partial H_c}{\partial t}\right|_{G^{(3)}}^{rsp} - \left.\frac{\partial H_c}{\partial t}\right|_{Q_c^{(1)}}^{out} - \sum_j \left.\frac{\partial H_c}{\partial t}\right|_{Y_c^{(j)}}^{prd} - \left.\frac{\partial H_c}{\partial t}\right|_{Q_c^{(1)}}^{lim} \tag{B.13a}$$

$$\left.\frac{\partial H_n}{\partial t}\right|_{bio} = \left.\frac{\partial H_n}{\partial t}\right|_{Q_n^{(1)},Q_n^{(6)}}^{upt} + \left.\frac{\partial H_n}{\partial t}\right|_{K^{(4)}}^{upt} - \left.\frac{\partial H_n}{\partial t}\right|_{Q_n^{(1)}}^{out} - \frac{H_n}{H_c}\sum_j \left.\frac{\partial H_c}{\partial t}\right|_{Y_c^{(j)}}^{prd} - \left.\frac{\partial H_n}{\partial t}\right|_{K^{(4)}}^{lim} \tag{B.13b}$$

$$\left.\frac{\partial H_p}{\partial t}\right|_{bio} = \left.\frac{\partial H_p}{\partial t}\right|_{Q_p^{(1)},Q_p^{(6)}}^{upt} + \left.\frac{\partial H_p}{\partial t}\right|_{K^{(1)}}^{upt} - \left.\frac{\partial H_p}{\partial t}\right|_{Q_p^{(1)}}^{out} - \frac{H_p}{H_c}\sum_j \left.\frac{\partial H_c}{\partial t}\right|_{Y_c^{(j)}}^{prd} - \left.\frac{\partial H_p}{\partial t}\right|_{K^{(1)}}^{lim} \tag{B.13c}$$

B.5. Benthic decomposers

Two different groups of microbial decomposers are considered, whose definitions are basically unchanged with respect to ERSEM I and II:

- aerobic bacteria (functional group $H_l^{(1)}$), a wide group of decomposers that needs oxygen for their functional dynamics;
- anaerobic bacteria (functional group $H_l^{(2)}$), which combines the functionality of both the nitrate and sulphate reducers.

The main assumptions concerning the parameterization of this ERSEM group can be found in Ebenhöh et al. (1995) and Blackford (1997). Here we give a detailed description of only the mathematical equations, leaving the biochemical considerations to the cited literature. The ERSEM III formulation of bacteria dynamics for carbon and nutrients is shown in Equation Box 13 for the generic group H_l. Since the functional dynamics of the two groups are spatially separated by the oxic horizon, aerobes and anaerobes interact with different pools in the sediments. The dynamics shown in (B.13) and in

the other equations below are written as referred to the aerobic bacteria. In the derivation of the specific dynamics for the anaerobic decomposers the variables belonging to the aerobic layer have to be substituted by the corresponding ones in the anaerobic layers. For example, the dissolved carbon pool in the oxic layer ($Q_c^{(1)}$) applies in the case of aerobes $H_i^{(1)}$, while $Q1_c^{(1)}$ in the case of anaerobes $H_i^{(2)}$; the same is valid for nutrients with phosphate $K^{(1)}$ and $K1^{(1)}$ (see Table B.1 or Figure B.1 for the list and descriptions of the variables).

As also done for the benthos, we define some variables that describe the location of the bacterial activity in the sediments. The parameters are $\left[m_H^{\min}, m_H^{\max}, m_H\right]$ and represents respectively the minimum and maximum depth where the group can be found, and the mean depth where the bacterial decomposition activity takes place. The definitions of the location variables for the two groups are the following:

$$\begin{aligned} m^{\min}_{H^{(1)}} &= 0 \quad ; \quad & m^{\min}_{H^{(2)}} &= D^{(1)} \\ m^{\max}_{H^{(1)}} &= D^{(1)} \quad ; \quad & m^{\max}_{H^{(2)}} &= d_{tot} \\ m_{H^{(1)}} &= \min\left(D^{(1)}, \frac{D^{(6)}}{2}\right) \quad ; \quad & m_{H^{(2)}} &= \max\left(D^{(1)}, \frac{D^{(6)}}{2}\right) \end{aligned} \tag{B.14}$$

Note that the average location of bacteria is controlled either by the oxic horizon or by the detritus penetration depth. A combination of these parameters defines the non-dimensional regulating factor for oxygen of the aerobic bacteria:

$$f^o_{H^{(1)}} = \frac{m_{H^{(1)}} - m^{\min}_{H^{(1)}}}{\left(m_{H^{(1)}} - m^{\min}_{H^{(1)}}\right) + h^m_{H^{(1)}}} \tag{B.15}$$

where h_H^m is the layer thickness that defines the half-saturation value. For the anaerobes, this factor is set to 1.

B.5.1. Carbon dynamics

Equation Box 14 shows the functional process form of the source/sink terms in the dynamics of bacteria. The parameterized functional processes are the uptake from particulate and dissolved organic matter, respiration, excretion and predation. The predation term is not described here because it can be easily derived from (B.7a) considering that bacteria are mainly predated by the meiobenthic community.

Benthic bacteria in ERSEM III are modelled differently with respect to the previous versions, because the growth term given in (B.16a) is mainly controlled by the quality and the availability of the substrate (more similarly to the pelagic bacteria shown in Section A.3). Thus, two different uptake rates are considered and compared, one depending on the environmental limiting factors (B.16b) and the other depending on the substrate availability (B.16c). The regulating factors involves temperature (B.5) and oxygen conditions (B.15), and they are meant to limit the growth in the case of excess of

Equation Box 14 Source/sink terms in functional process forms for benthic decomposers.

$$\left.\frac{\partial H_c}{\partial t}\right|^{upt}_{Q_c^{(1)},Q_c^{(6)}} = \min\left(G_H^{env}, G_H^{sub}\right) \tag{B.16a}$$

$$G_H^{env} = f_H^T\, f_H^o\, r_{0_H}\, H_c \tag{B.16b}$$

$$G_H^{sub} = \left(f_H^q\, \nu_H^{fast} + \nu_H^{slow}\right) \widetilde{Q}_c^{(6)} + \nu_H^{diss}\, Q_c^{(1)} \tag{B.16c}$$

$$\left.\frac{\partial H_c}{\partial t}\right|^{rsp}_{G^{(3)}} = b_H\, f_H^T\, H_c + \gamma_H \left.\frac{\partial H_c}{\partial t}\right|^{upt}_{Q_c^{(1)},Q_c^{(6)}} \tag{B.16d}$$

$$\left.\frac{\partial H_c}{\partial t}\right|^{out}_{Q_c^{(1)}} = \varepsilon_H \left.\frac{\partial H_c}{\partial t}\right|^{upt}_{Q_c^{(6)}} + d_{0_H}\left(1 - f_H^o\right) H_c \tag{B.16e}$$

$$\left.\frac{\partial H_l}{\partial t}\right|^{upt}_{Q_l^{(1)},Q_l^{(6)}} = \xi_H \left(\frac{Q_l^{(1)}}{Q_c^{(1)}} \left.\frac{\partial H_c}{\partial t}\right|^{upt}_{Q_c^{(1)}} + \frac{Q_l^{(6)}}{Q_c^{(6)}} \left.\frac{\partial H_c}{\partial t}\right|^{upt}_{Q_c^{(6)}}\right) \quad l = n, p \tag{B.17a}$$

$$\left.\frac{\partial H_n}{\partial t}\right|^{upt}_{K^{(4)}} = n_H^{opt} \frac{K^{(4)}}{K^{(4)} + h_H^n} \left.\frac{\partial H_c}{\partial t}\right|^{upt}_{Q_c^{(1)},Q_c^{(6)}} \tag{B.17b}$$

substrate with a balanced nutrient-content.

The control of the substrate is expressed by the second rate (B.16c). Firstly, the total availability of particulate detritus is computed as in (B.10), according to the bacteria and substrate penetration depths. Secondly, in order to mimic the different degrees of reactivity of the organic matter, we introduce two different specific uptake velocities. One is faster (ν_H^{fast}), but is modulated by the nutrient content of the detritus via the non-dimensional quality factor

$$f_H^q = \min\left(1, \frac{\widetilde{Q}_n^{(6)}/\widetilde{Q}_c^{(6)}}{n_H^{opt}}, \frac{\widetilde{Q}_p^{(6)}/\widetilde{Q}_c^{(6)}}{p_H^{opt}}\right). \tag{B.18}$$

This regulating factor compares the detritus nutrient-content with the optimal nutrient:carbon ratios of bacteria (n_H^{opt}, p_H^{opt}) by applying a Liebig formulation for the choice of the limiting one. The other uptake rate is much slower (ν_H^{slow}) and is independent from the amount of nutrients in the substrate. The uptake of dissolved organic matter is similar, a first-order process with a constant rate ν_H^{diss} involving $Q_i^{(1)}$ when considering aerobic bacteria, and $Q1_i^{(1)}$ in the anaerobic case. Finally, the actual consumption rates for each detrital component are derived from the total uptake rate as follows:

$$\left.\frac{\partial H_c}{\partial t}\right|_{Q_c^{(1)}}^{upt} = \frac{\nu_H^{diss} Q_c^{(1)}}{G_H^{sub}} \left.\frac{\partial H_c}{\partial t}\right|_{Q_c^{(1)},Q_c^{(6)}}^{upt} \tag{B.19}$$

$$\left.\frac{\partial H_c}{\partial t}\right|_{Q_c^{(6)}}^{upt} = \frac{\left(f_H^q \nu_H^{fast} + \nu_H^{slow}\right) \widetilde{Q}_c^{(6)}}{G_H^{sub}} \left.\frac{\partial H_c}{\partial t}\right|_{Q_c^{(1)},Q_c^{(6)}}^{upt} \tag{B.20}$$

The respiration term (B.16d) is partitioned in basal and activity respiration as for pelagic bacteria, where γ_H is the respired fraction of the uptake and b_H the constant basal respiration rate. The same formulation is applied to both aerobic and anaerobic bacteria, but in the case of anoxic processes the related oxygen consumption flux is directed to the pool of reduction equivalents instead of the benthic oxygen as shown below in (B.32) and (B.63). The parameter $\gamma_{H^{(2)}}$ is about twice the one for aerobic bacteria, considering the differences in the energetics of the metabolic reactions under hypoxic/anoxic conditions.

The carbon loss terms in (B.16e) are the excretion and the oxygen-dependent mortality. Excretion means the POM to DOM decomposition by extracellular enzymes, and is modelled as a constant fraction (ε_Y) of the substrate uptake. The parameter d_{0_H} is the specific daily mortality rate and this mortality term is zero for anaerobic bacteria because $f^o_{H^{(2)}} = 1$.

B.5.2. Nutrient dynamics and assimilation balance

In describing the functional process terms of nutrient dynamics (B.13b) and (B.13c), we have to distinguish between the two functional groups, because the pools of inorganic nutrients and dissolved substrate that can be accessed are different. The uptake of organic matter is directly derived from the carbon term as shown in (B.17a), where, in the case of anaerobic bacteria, the dissolved pool below the oxic layer ($Q1_i^{(1)}$) is consumed. Since bacteria are efficient in the degradation of the nutrient components of organic matter, it has been defined a parameter $\xi_H \geq 1$ that introduces a preference factor for organic nutrients with respect to carbon.

Bacteria in the model are also allowed to directly take up inorganic nutrients from the sediments. This input is proportional to the nutrient concentration (through a Michaelis-Menten formulation) and to the bacteria nutrient requirements according to the optimal nutrient:carbon quota. In (B.17b) we give the nutrient uptake functional form in the case of ammonium. The other fluxes can be derived taking into account that aerobic bacteria $(H_i^{(1)})$ establish nutrient fluxes between the ammonium and phosphate pools above the oxygen horizon, respectively $K^{(4)}$ and $K^{(1)}$. Anaerobic bacteria exchange nutrients with the ammonium and phosphate pools in the denitrification layer, respectively $K^{(14)}$ and $K^{(11)}$. The resources in the anoxic layer are assumed as not available to the anaerobic decomposers, because usually the denitrification layer extends down to the maximum modeled sediment depth.

The nutrient uptake, together with the carbon uptake, are actually gross input fluxes. In fact, since benthic bacteria are supposed to have almost constant ratios among the intracellular constituents, the inputs are eventually compensated by excretion fluxes if the nutrient (or carbon) uptake is higher than

the optimal one (fluxes indicated by the superscript *lim* in Box 13). The correction for the component in excess is evaluated as previously done for benthic organisms in (B.12).

Equation Box 15 Flux form equations for the particulate organic matter in the sediments and for the mean penetration depths.

$$\left.\frac{\partial Q_c^{(6)}}{\partial t}\right|_{bio} = \sum_j \left(\left.\frac{\partial Y_c^{(j)}}{\partial t}\right|_{Q_c^{(6)}}^{out} + \left.\frac{\partial Y_c^{(j)}}{\partial t}\right|_{Q_c^{(6)}}^{lim} - \left.\frac{\partial Y_c^{(j)}}{\partial t}\right|_{Q_c^{(6)}}^{upt} \right) - \sum_j \left.\frac{\partial H_c^{(j)}}{\partial t}\right|_{Q_c^{(6)}}^{upt} + \left.\frac{\partial Q_c^{(6)}}{\partial t}\right|^{sed} \quad \text{(B.21a)}$$

$$\left.\frac{\partial Q_l^{(6)}}{\partial t}\right|_{bio} = \sum_j \left(\left.\frac{\partial Y_l^{(j)}}{\partial t}\right|_{Q_l^{(6)}}^{out} - \left.\frac{\partial Y_l^{(j)}}{\partial t}\right|_{Q_l^{(6)}}^{upt} \right) - \sum_j \left.\frac{\partial H_l^{(j)}}{\partial t}\right|_{Q_l^{(6)}}^{upt} + \left.\frac{\partial Q_l^{(6)}}{\partial t}\right|^{sed} \qquad l = n, p \quad \text{(B.21b)}$$

$$\left.\frac{\partial Q_s^{(6)}}{\partial t}\right|_{bio} = \left.\frac{\partial Q_s^{(6)}}{\partial t}\right|^{sed} - \left.\frac{\partial Q_s^{(6)}}{\partial t}\right|_{K^{(5)}}^{diss} - \left.\frac{\partial Q_s^{(6)}}{\partial t}\right|_{sink_s}^{diss} \quad \text{(B.21c)}$$

$$\left.\frac{\partial D^{(i)}}{\partial t}\right|_{bio} = \sum_j \frac{m_{Y^{(j)}} - D^{(i)}}{Q_c^{(6)}} \left.\frac{\partial Q_c^{(6)}}{\partial t}\right|_{Y^{(j)}} + \sum_j \frac{m_{H^{(j)}} - D^{(i)}}{Q_c^{(6)}} \left.\frac{\partial Q_c^{(6)}}{\partial t}\right|_{H_c^{(j)}} + + \frac{D^{(i)}}{Q^{(6)}} \left.\frac{\partial Q^{(6)}}{\partial t}\right|^{sed} + \left.\frac{\partial Q^{(6)}}{\partial t}\right|_{Y}^{tur} \qquad i = 6, 7, 8 \quad \text{(B.22a)}$$

$$\left.\frac{\partial D^{(9)}}{\partial t}\right|_{bio} = \frac{D^{(9)}}{Q_s^{(6)}} \left.\frac{\partial Q_s^{(6)}}{\partial t}\right|^{sed} + \left.\frac{\partial Q_s^{(6)}}{\partial t}\right|_{Y}^{tur} \quad \text{(B.22b)}$$

B.6. The organic matter in the sediments

As already introduced in the description of the benthic organisms, the organic matter in the benthic model is divided in two fractions, the particulate and the dissolved. The dissolved fraction is treated as a dissolved component in the pore-waters and it is described by two ordinary state variables: $Q_1^{(1)}$ indicating the total amount in the oxic layer, and $Q1_l^{(1)}$ that is the vector for the total DOM in the anaerobic layers. They will be described, together with the other dissolved components, in Section B.7 because the chosen parameterization requires a specific resolution method.

Particulate detritus in the sediment is indicated by the vector state variable $Q_q^{(6)}$ and, although representing the bulk of organic matter in all the layers, it has an implicit vertical distributions. In fact, the density vertical profiles are not explicitly described, but parameterized using a mean intrusion depth D, which is also an ordinary state variable. The average intrusion depths are different for each detritus component, and we have $D^{(6)}$ for the C-component $Q_c^{(6)}$, $D^{(7)}$ for $Q_n^{(6)}$, $D^{(8)}$ for $Q_p^{(6)}$ and $D^{(9)}$ for $Q_s^{(6)}$. Since the dynamics are the same for all the components, in the following description the superscripts in D and the subscripts in $Q^{(6)}$ will be omitted.

According to Ebenhöh et al. (1995), the detritus vertical distribution is defined as a normalized function of z and D written as:

$$q(z) = Q^{(6)} \frac{\rho_{Q^{(6)}}(z, D)}{\rho 0_{Q^{(6)}}} \tag{B.23}$$

where the non-dimensional density function $\rho_{Q^{(6)}}$ is an exponential decrease cut off at the total depth of the sediments D_{tot}:

$$\rho_{Q^{(6)}}(z, D) = e^{-\alpha z}; \quad \rho 0_{Q^{(6)}} = \frac{1}{\alpha}\left(1 - e^{-\alpha D_{tot}}\right) \tag{B.24}$$

with $\alpha = 1/D$. It is easy to demonstrate that

$$\int_0^{D_{tot}} q(z)dz = Q^{(6)}$$

and it comes that the ordinary state variable D is defined as the center of mass of the vertical distribution as follows:

$$\int_0^{D_{tot}} z\, q(z)\, dz = D\, Q^{(6)}.$$

The total amount of organic matter in the sediments changes because of the biological activity and the sedimentation processes. Therefore, we can collect all the terms involving particulate detritus from the general equations for the benthos described in the previous sections, and obtain the equations for $Q_i^{(6)}$ shown in Equation Box 15. The processes affecting the concentration are specifically the uptake and release by benthic organisms and bacteria, the sedimentation and the dissolution of biogenic silica in (B.22b), which will be described in Section B.7.5. The sedimentation terms are defined as the inflows of particulate organic matter and sinking phytoplankton coming from the water column, and can be derived from (B.1).

All these terms also enter in the dynamical equations for the average intrusion depths $D^{(j)}$ in (B.22). The functional groups changes the vertical distribution according to their own location in the sediments, which is implemented as the parameters m_Y and m_H defined in the previous sections. All the terms involving detritus consumption/production fluxes from (B.21) are converted into relative fluxes and then multiplied by a nudging term function of the location where the consumption takes place. The contribution of sedimentation is modelled similarly to the biological terms, but the interaction depth is in this case the water-sediment interface, thus $m = 0$. Therefore, the deposition of new material at surface always leads to a decrease in the average penetration depth because the bulk of the material is located closer to the surface.

The effects of bioturbation in (B.22) are included in a very simple way. The presence of benthic organisms leads to a redistribution of the detritus vertical profile, moving or shifting layers from the surface to a certain depth with a consequent change in the penetration depth. The chosen mechanism

simulates the exchange of a surface layer with one at a fixed depth δ^{tur} giving:

$$\left.\frac{\partial D^{(j)}}{\partial t}\right|_{Y}^{tur} = \frac{\tau_0^{tur} f_Y^{tur}}{D^{(j)}} \left(1 - e^{-\delta^{tur}/Di_m}\right) \qquad j = 6,\ldots,9 \tag{B.25}$$

where τ_0^{tur} is a physical diffusion constant [m^{2}d^{-1}], modulated by an intensification factor depending on the biological activity as follows:

$$f_Y^{tur} = 1 + f_Y^T \, f_0^{tur} \frac{\sum_j \psi_{Y(j)}^{tur} Y_c^{(j)}}{\sum_j \psi_{Y(j)}^{tur} Y_c^{(j)} + h_Y^{tur}}. \tag{B.26}$$

The intensification factor (B.26) is a function of temperature as in (B.5) and of the density of benthic organisms Y, multiplied by a weight coefficient ψ_Y^{tur} that determines the contribution of each functional group to the bioturbation. The semi-saturation value h_Y^{tur} should roughly correspond to the mean density of benthic organisms in the area, and f_0^{tur} is the maximum enhancement factor.

B.7. Benthic nutrients and other dissolved components

A detailed description and the basic assumptions of the benthic nutrient model used in ERSEM can be found in Ruardij and Van Raaphorst (1995). Here we will summarize the main dynamical equations and especially the links with the other components of the benthic and pelagic system. The form of the generic equation for the dissolved nutrients $C(\vec{x},t)$ comes from Berner (1980):

$$(p+1)\frac{\partial C}{\partial t} = D\frac{\partial^2 C}{\partial z^2} - kC + M \tag{B.27}$$

where we distinguish a vertical diffusion process (horizontal diffusions are neglected), a first order loss-rate with constant specific rate k and a zero order mineralization $M(z,t)$. The parameter p is the non-dimensional adsorption coefficient which - especially in the case of phosphate - is dependent on the porosity of the sediments found in the area (Slomp and Van Raaphorst, 1993). Sorption of dissolved constituents is considered to be a fast process, and consequently the pore water concentration and the sorbent phase are in equilibrium.

Considering the layers defined in the benthic system (Figure B.2), the source/sink terms in (B.27) are assumed to be vertically uniform in the oxic layer while have an exponential decrease according to the detritus distribution (B.23) in the anoxic layers. The number of differential equations used to describe the dynamics vary from nutrient to nutrient according to the specific kind of processes and the number of prescribed boundary conditions.

The semi-analytical method used in the determination of the time evolution of benthic nutrients is the following (Ruardij and Van Raaphorst, 1995):

1. A steady-state analytical solution $C_{eq}(z)$ is calculated for each differential equation valid in the layer, given the proper boundary conditions and source/sink terms (biochemical remineralization or other chemical reactions, such as nitrification, etc.);

2. The vertically integrated concentration at the equilibrium (K_{eq}) is evaluated, and eventually the average transient value is derived according to the following nudging equation:

$$K_{tr} = K_{eq} + \frac{\Delta t}{\tau_a}(K - K_{eq})\left(1 - e^{-\frac{\Delta t}{\tau_a}}\right), \tag{B.28}$$

The other known variables are the initial value from previous time step (K) and the ratio between the actual time step and the adaptation time $(\Delta t/\tau_a)$. The transient profile is actually the average value over the current time step taking into account the equilibrium value after a longer time step. The adaptation time is derived from the general analytical solution of (B.27),

$$\tau_\alpha = \frac{p+1}{k + \pi^2 DH^{-2}} \tag{B.29}$$

and represents the time necessary to reach the steady-state profile or concentration (Carslaw and Jaeger, 1946; with H the depth of the layer);

3. The effective transient profiles in each layer $C_{tr}(z)$ are derived assuming the same form of the steady-state solutions, and the integration constants are recalculated with an inverse modelling technique by imposing the transient total concentration K_{tr} as the new constraint (note that this is usually done only in the first more reactive layer). This is equivalent to the introduction of a new apparent mineralization term in the first layer dynamics, that gives the total transient concentration K_{tr} as solution after the current time step;

4. The transient solution is substituted on the right hand side of (B.27), and then vertically integrated within the layer boundaries z_0 and z_1 to obtain the expression for the rate of change of the total amount of nutrient in the layer:

$$\frac{\partial K}{\partial t} = \phi D\left[\frac{\partial C_{tr}}{\partial z}(z_1) - \frac{\partial C_{tr}}{\partial z}(z_0)\right] - \phi k \int_{z_0}^{z_1} C_{tr}(z)\, dz + \phi M(z_1 - z_0) \tag{B.30}$$

The concentration gradients at the boundaries are calculated from the analytical form of $C_{tr}(z)$, deriving the fluxes between the sediment layers and the water-sediment interface (in the form of the Fick's law). Equation (B.30) is then solved with the numerical integration in order to quantify the forward-in-time bulk state in each specified layer $(K(z, t+\Delta t))$. In order to assure conservation of mass at the bottom layer $(z = D_{tot})$, it is also necessary to define an infinite source/sink (one for each nutrient component N and P) that acts as nutrient buffer from the deeper sediments. This flux will be indicated by the subscript $source_i$ or $sink_i$ with $i = n, p$.

In the following, the description of the benthic nutrient, oxygen and dissolved organic matter dynamics

is given, where the above method is applied to all the sets of differential equations. The variable names used in the analytical equations are different from the state variables carried by the model because of the need to introduce continuous functions according to the semi-analytical solving method. The relations between the analytical profiles and the corresponding state variables will always be indicated.

A detailed description of the methodology will be given for the ammonium case in the next section, while for the other components only the dynamical equations and boundary conditions are shown.

B.7.1. Inputs to the benthic nutrient model

The main fluxes into the benthic nutrient model are the oxic and anoxic mineralizations, which come from the degradation of the organic matter in the sediments. The mineralization fluxes are measured in units of oxygen consumed during the respiration processes, both under oxic and anoxic conditions. In the case of anoxic processes, the biological oxygen demand is converted into units of reduction equivalents using the stoichiometric conversion factor between oxygen and sulphide (Ω^{γ}_{o}, Table A.4), and this flux is subtracted from the pool of reduction equivalents instead of oxygen.

The aerobic mineralization is derived from the carbon dynamics of the benthic organisms and aerobic bacteria as follows:

$$M_o^{BT} = \frac{1}{\phi D^{(1)}} \left(\Omega_c^o \sum_j \left. \frac{\partial Y_c^{(j)}}{\partial t} \right|_{G^{(3)}}^{rsp} + \Omega_c^o \left. \frac{\partial H_c^{(1)}}{\partial t} \right|_{G^{(3)}}^{rsp} \right) \tag{B.31}$$

where the conversion parameter Ω^o_c is explained in Table A.4. Note that units are converted to pore-water fluxes by means of the sediment porosity (ϕ) and the oxic layer thickness because this process is assumed to be homogeneously distributed in the first layer.

The total anoxic mineralization considers the respiration of anaerobic bacteria (B.16d) and the vertical distribution of the organic carbon in the sediments (Section B.6) as:

$$M_o^{AT} = \frac{\Omega_c^o}{\phi \int_{D^{(1)}}^{D_{tot}} e^{-\alpha_c (z - D^{(1)})}\, dz} \left. \frac{\partial H_c^{(2)}}{\partial t} \right|_{G^{(3)}}^{rsp}. \tag{B.32}$$

The exponential decrease is written according to (B.24) with the depth-scale coefficient defined as $\alpha_c = 1/D^{(6)}$.

The nutrient mineralization fluxes that are used in the pore-water nutrient dynamics involve the biological regeneration of phosphate and ammonium in the sediments. They are derived from the corresponding nutrient dynamics of the standard benthic organisms and decomposers (B.4b), (B.4c),

(B.13b), (B.13c) in the following way:

$$M_n^{BT} = \frac{1}{\phi D^{(1)}} \left(\sum_j \frac{\partial Y_n^{(j)}}{\partial t}\bigg|_{K^{(4)}}^{lim} + \frac{\partial H_n^{(1)}}{\partial t}\bigg|_{K^{(4)}}^{lim} - \frac{\partial H_n^{(1)}}{\partial t}\bigg|_{K^{(4)}}^{upt} \right) \tag{B.33a}$$

$$M_p^{BT} = \frac{1}{\phi D^{(1)}} \left(\sum_j \frac{\partial Y_p^{(j)}}{\partial t}\bigg|_{K^{(1)}}^{lim} + \frac{\partial H_p^{(1)}}{\partial t}\bigg|_{K^{(1)}}^{lim} - \frac{\partial H_p^{(1)}}{\partial t}\bigg|_{K^{(1)}}^{upt} \right) \tag{B.33b}$$

As shown in (B.32), the nutrient anoxic mineralization is assumed to have an exponential decrease with depth following the distribution of the N-, P-components in the organic matter, in which $\alpha_n = 1/D^{(7)}$ and $\alpha_p = 1/D^{(8)}$ are the e-folding coefficients. The nutrient fluxes are completely controlled by the anaerobic bacteria dynamics as follows:

$$M_n^{AT} = \frac{1}{\phi \int_{D^{(1)}}^{D_{tot}} e^{-\alpha_n (z - D^{(1)})}\, dz} \left(\frac{\partial H_n^{(2)}}{\partial t}\bigg|_{K1^{(4)}}^{lim} - \frac{\partial H_n^{(2)}}{\partial t}\bigg|_{K1^{(4)}}^{upt} \right) \tag{B.34a}$$

$$M_p^{AT} = \frac{1}{\phi \int_{D^{(1)}}^{D_{tot}} e^{-\alpha_p (z - D^{(1)})}\, dz} \left(\frac{\partial H_p^{(2)}}{\partial t}\bigg|_{K1^{(1)}}^{lim} - \frac{\partial H_p^{(2)}}{\partial t}\bigg|_{K1^{(1)}}^{upt} \right) \tag{B.34b}$$

Another variable whose parameterization is common to all the dissolved components is the diffusion coefficient D in (B.27). These coefficients are assumed to be composed of a constant part representing the physical molecular diffusion (D_0, different for each dissolved substance), multiplied by the porosity, the temperature regulating factor (B.5) and a biological enhancement factor (f_Y^{irr}) as follows:

$$D = \phi\, f^T\, f_Y^{irr}\, D_0.$$

The biological enhancement factor is an input to the benthic nutrient model and simulates the bioirrigation process, which contributes to the mobility of dissolved nutrients in the pore-waters. It is expressed in a way similar to the bioturbation factor in (B.26)

$$f_Y^{irr} = 1 + f_Y^T\, f_0^{irr} \frac{\sum_j \psi_Y^{irr} Y_c^{(j)}}{\sum_j \psi_Y^{irr} Y_c^{(j)} + h_Y^{irr}} \tag{B.35}$$

considering that the weight coefficients (ψ_Y^{irr}) are different from the one used in the bioturbation because the contributing organisms may be different. The bioirrigation factor is always larger than or equal to 1 and has a sigmoidal shape controlled by the environmental temperature as well.

B.7.2. Ammonium

The processes affecting the dynamics of ammonium in the pore-waters largely depend on the redox conditions. In order to solve the strong vertical variability of this component, the ammonium dynamics in the sediments are estimated in all the three layers as shown in Equation Box 16. In the

Equation Box 16 Flux form equations of ammonium in the sediments.

$$\frac{\partial K^{(4)}}{\partial t} = \frac{\partial K^{(4)}}{\partial t}\bigg|_{N^{(4)}}^{diff} + \frac{\partial K^{(4)}}{\partial t}\bigg|_{K1^{(4)}}^{diff} + \frac{\partial K_n^{(4)}}{\partial t}\bigg|_{D^{(1)}}^{shift} + \frac{\partial K^{(4)}}{\partial t}\bigg|_{K^{(3)}}^{nit} + \sum_j \frac{\partial Y_n^{(j)}}{\partial t}\bigg|_{K^{(4)}}^{lim} + \\ + \frac{\partial H_n^{(1)}}{\partial t}\bigg|_{K^{(4)}}^{lim} - \frac{\partial H_n^{(1)}}{\partial t}\bigg|_{K^{(4)}}^{upt} \tag{B.36a}$$

$$\frac{\partial K1^{(4)}}{\partial t} = \frac{\partial K1^{(4)}}{\partial t}\bigg|_{K2^{(4)}}^{diff} - \frac{\partial K^{(4)}}{\partial t}\bigg|_{K1^{(4)}}^{diff} + \frac{\partial K^{(4)}}{\partial t}\bigg|_{D^{(1)}}^{shift} + \frac{\partial K1^{(4)}}{\partial t}\bigg|_{D^{(2)}}^{shift} + \\ + \pi_A \left(\frac{\partial H_n^{(2)}}{\partial t}\bigg|_{K1^{(4)}}^{lim} - \frac{\partial H_n^{(2)}}{\partial t}\bigg|_{K1^{(4)}}^{upt} \right) \tag{B.36b}$$

$$\frac{\partial K2^{(4)}}{\partial t} = \frac{\partial K2^{(4)}}{\partial t}\bigg|_{source_n}^{diff} - \frac{\partial K1^{(4)}}{\partial t}\bigg|_{K2^{(4)}}^{diff} + \frac{\partial K1_n^{(4)}}{\partial t}\bigg|_{D^{(2)}}^{shift} + \\ + (1-\pi_A) \left(\frac{\partial H_n^{(2)}}{\partial t}\bigg|_{K1^{(4)}}^{lim} - \frac{\partial H_n^{(2)}}{\partial t}\bigg|_{K1^{(4)}}^{upt} \right) \tag{B.36c}$$

oxic layer we have the diffusion terms from the denitrification layer and to the water column, the nitrification terms and the remineralization (ammonification) terms from (B.33a). In the anoxic layers only remineralization from (B.34a) and vertical diffusion are considered. The bulk of ammonium in each layer is also determined by the shifting of the layers due to changes in the oxygen penetration (fluxes indicated by the superscript *shift*). These fluxes will be described in Section B.7.9 because they are common to all the dissolved components. The partitioning coefficient π_A has been introduced because there is no explicit sub-division in the anaerobic layers for biological processes. This stems from the simplified assumption that there is biology only until the denitrification layer. Hence, the uptake/remineralization fluxes have to be artificially divided according to the exponential distribution of the N-component in detritus (cfr. (B.23)) as follows:

$$\pi_A = \frac{\int_{D^{(1)}}^{D^{(2)}} e^{-\alpha_n (z - D^{(1)})}\, dz}{\int_{D^{(1)}}^{D_{tot}} e^{-\alpha_n (z - D^{(1)})}\, dz}. \tag{B.37}$$

Equations (B.36) are derived from the application of the semi-analytical methodology described above. We first present the set of differential equations for the pore water concentration - according to the generic form (B.27) - that describes the dynamics of dissolved ammonium in the model:

$$(p_A+1)\frac{\partial A_1}{\partial t} = D_A\frac{\partial^2 A_1}{\partial z^2} - k_A A_1 + M_n^{BT} \quad 0 \le z \le D^{(1)} \tag{B.38a}$$

$$(p_A+1)\frac{\partial A_2}{\partial t} = D_A\frac{\partial^2 A_2}{\partial z^2} + M_n^{AT} e^{-\alpha_n(z-D^{(1)})} \quad D^{(1)} < z \le D^{(2)} \tag{B.38b}$$

$$(p_A+1)\frac{\partial A_3}{\partial t} = D_A\frac{\partial^2 A_3}{\partial z^2} + M_n^{AT} e^{-\alpha_n(z-D^{(1)})} \quad D^{(2)} < z \le D_{tot} \tag{B.38c}$$

where $A_j(z,t)$, $j = 1,2,3$ are the profiles in the oxic, denitrification and anoxic layers, respectively. The oxic and anoxic mineralization terms are derived from (B.33a) and (B.34a), while nitrification is parameterized with a first-order nitrification term as follows:

$$k_{_A} = f_{_A}^T \, f_{_A}^o \, k_{0_A}. \tag{B.39}$$

The constant specific daily rate k_{0_A} is scaled by the regulating factors depending on temperature and oxygen, respectively expressed with the formulation shown in (B.5) and the following Michaelis-Menten form:

$$f_{_A}^o = \frac{\frac{G^{(2)}}{\phi D^{(1)}}}{\frac{G^{(2)}}{\phi D^{(1)}} + h_{_A}^o} \tag{B.40}$$

which involves the pore-water average concentration of oxygen $G^{(2)}$ and a half-saturation value $h_{_A}^o$.

Equations (B.38) are linked to the model state variables in (B.36) by means of the following relationships, in which we also give the definition of the average total concentrations in the pore-waters for each layer that are used as diagnostic variables in the model:

$$K^{(4)} = \phi\,(p_A+1)\int_0^{D^{(1)}} A_1(z)\,dz; \quad M^{(4)} = \frac{K^{(4)}}{\phi D^{(1)}\,(p_A+1)} \tag{B.41a}$$

$$K1^{(4)} = \phi\,(p_A+1)\int_{D^{(1)}}^{D^{(2)}} A_2(z)\,dz; \quad M1^{(4)} = \frac{K1^{(4)}}{\phi\left(D^{(2)}-D^{(1)}\right)(p_A+1)} \tag{B.41b}$$

$$K2^{(4)} = \phi\,(p_A+1)\int_{D^{(2)}}^{D_{tot}} A_3(z)\,dz; \quad M2^{(4)} = \frac{K2^{(4)}}{\phi\left(D_{tot}-D^{(2)}\right)(p_A+1)} \tag{B.41c}$$

.

The functional process form of the equations in Box 16 are given in Box 17, and they are written according to (B.30), making use of the transient solutions of the pore water equations given in (B.38). The transient profiles are computed according to the method described above from the steady-state solutions ($A_j^{eq}(z)$) , which, in turn, are obtained always from (B.38) by applying the following boundary

conditions and continuity constraints:

$$\begin{cases} \left(A_1^{eq}\right)_{z=0} & = & \left(N^{(4)}\right)_{z=-H} \\ \left(A_1^{eq}\right)_{z=D^{(1)}} & = & \left(A_2^{eq}\right)_{z=D^{(1)}}; \quad \left(\dfrac{\partial A_1^{eq}}{\partial t}\right)_{z=D^{(1)}} = \left(\dfrac{\partial A_2^{eq}}{\partial t}\right)_{z=D^{(1)}} \\ \left(A_2^{eq}\right)_{z=D^{(2)}} & = & \left(A_3^{eq}\right)_{z=D^{(2)}}; \quad \left(\dfrac{\partial A_1^{eq}}{\partial t}\right)_{z=D^{(2)}} = \left(\dfrac{\partial A_3^{eq}}{\partial t}\right)_{z=D^{(2)}} \\ \left(\dfrac{\partial A_3^{eq}}{\partial t}\right)_{z\to+\infty} & = & 0 \end{cases} \tag{B.42}$$

where $N^{(4)}$ is the concentration of dissolved ammonium in the water. At the end of the whole procedure we obtain the (B.36), which are numerically integrated forward in time together with the other pelagic and benthic model state variables.

Equation Box 17 Functional forms of the ammonium source/sink terms in Box 16.

$$\left.\frac{\partial K^{(4)}}{\partial t}\right|_{N^{(4)}}^{diff} = \phi D_A \left(\frac{\partial A_1^{tr}}{\partial z}\right)_{z=0} \tag{B.43a}$$

$$\left.\frac{\partial K^{(4)}}{\partial t}\right|_{K1^{(4)}}^{diff} = \phi D_A \left(\frac{\partial A_1^{tr}}{\partial z}\right)_{z=D^{(1)}} \tag{B.43b}$$

$$\left.\frac{\partial K^{(4)}}{\partial t}\right|_{K^{(3)}}^{nit} = \phi k_A \int_0^{D^{(1)}} A_1^{tr}(z)\, dz \tag{B.43c}$$

$$\left.\frac{\partial K1^{(4)}}{\partial t}\right|_{K2^{(4)}}^{diff} = \phi D_A \left(\frac{\partial A_2^{tr}}{\partial z}\right)_{z=D^{(2)}} \tag{B.43d}$$

$$\left.\frac{\partial K2^{(4)}}{\partial t}\right|_{source_n}^{diff} = \phi D_A \left(\frac{\partial A_3^{tr}}{\partial z}\right)_{z=D_{tot}} \tag{B.43e}$$

B.7.3. Nitrate

Nitrate dynamics have a reduced number of interactions with the other benthic components, because they are not regenerated in the sediments but only affected by denitrification and nitrification processes. Therefore, nitrate in the sediment layers is modeled by means of a single flux form equation shown in Box 18 together with the explicit functional process formulation of its terms. We refer to the ammonium dynamics above for a more detailed explanation of the procedure that leads to the formulation of (B.44). Here we limit to the presentation of the main dynamical processes and of their mathematical forms.

Equation Box 18 Flux and functional process form equations for nitrate in the sediments.

$$\frac{\partial K^{(3)}}{\partial t} = \left.\frac{\partial K^{(3)}}{\partial t}\right|_{N^{(3)}}^{diff} + \left.\frac{\partial K^{(3)}}{\partial t}\right|_{source_n}^{diff} + \left.\frac{\partial K^{(3)}}{\partial t}\right|_{K^{(4)}}^{nit} - \left.\frac{\partial K^{(3)}}{\partial t}\right|_{sink_n}^{denit} \tag{B.44}$$

$$\left.\frac{\partial K^{(3)}}{\partial t}\right|_{N^{(3)}}^{diff} = -\phi D_N \left(\frac{\partial N_1^{tr}}{\partial z}\right)_{z=0} \tag{B.45a}$$

$$\left.\frac{\partial K^{(3)}}{\partial t}\right|_{source_n}^{diff} = -\phi D_N \left(\frac{\partial N_2^{tr}}{\partial z}\right)_{z=D^{(2)}} \tag{B.45b}$$

$$\left.\frac{\partial K^{(3)}}{\partial t}\right|_{K^{(4)}}^{nit} = \phi k_A \int_0^{D^{(1)}} A_1^{tr}(z)\, dz \tag{B.45c}$$

$$\left.\frac{\partial K^{(3)}}{\partial t}\right|_{sink_n}^{denit} = \phi d_N \int_{D^{(1)}}^{D^{(2)}} N_1^{tr}(z)\, dz \tag{B.45d}$$

According to the processes affecting this component, the pore-water dynamics have been divided in two layers

$$\frac{\partial N_1}{\partial t} = D_N \frac{\partial^2 N_1}{\partial z^2} + k_A A_1 \quad 0 \le z \le D^{(1)} \tag{B.46a}$$

$$\frac{\partial N_2}{\partial t} = D_N \frac{\partial^2 N_2}{\partial z^2} - d_N N_2 \quad D^{(1)} < z \le D_{tot} \tag{B.46b}$$

with a first-order nitrification term linked to the ammonium concentration (B.38a) in the oxic layer, and a first-order denitrification in the anoxic part. The adsorption coefficient in (B.27) is taken to be 0. The parameterization of the denitrification rate has been improved with respect to the previous ERSEM I/II versions described in Ruardij and Van Raaphorst (1995). As similarly done in the pelagic model (Section A.5.2), the denitrification rate is not constant but linked to the anoxic mineralization in the sediments (B.32) as:

$$d_N = d_{0_N} f^T \frac{M_o^{AT}}{M_o^*} \tag{B.47}$$

where M_o^* is a reference anoxic mineralization at 10º C. This establishes a sort of indirect feedback with the bacterial metabolic activity without an explicit definition of a denitrifier functional group. Clearly, this is still a very simple parameterization with respect to more sophisticated formulations (for example, Almeida *et al.*, 1997), but it allows to incorporate more realistic interactions of the nitrogen cycle in the sediments while maintaining low computational costs and making feasible the coupling with the other physical and ecological processes.

As boundary conditions for the equilibrium solution we consider the nitrate concentration at the water-sediment interface ($N^{(3)}$) and a complete consumption in the deeper sediment layers as

$$\begin{cases} \left(N_1^{eq}\right)_{z=0} & = & \left(N^{(3)}\right)_{\tilde{z}=-H} \\ \left(N_2^{eq}\right)_{z\to+\infty} & = & 0 \end{cases} \tag{B.48}$$

together with the continuity of mass at $z = D^{(1)}$ as in (B.42) for ammonium. The steady-state solution of (B.46a) is connected to the ammonium oxic dynamics shown in (B.38a), and thus the integration coefficients in the equilibrium solution can only slowly adapt to fast-changing profiles. For this reason in the numerical implementation the ratios between coefficients have been prescribed instead of the coefficients themselves, in order to increase the number of degrees of freedom.

As done for the ammonium in (B.41), the model state variable for nitrate in the sediments and the diagnostic average concentration in the pore water can be derived from the following relations:

$$K^{(3)} = \phi \int_0^{D^{(1)}} N_1(z)\, dz + \phi \int_{D^{(1)}}^{D_{tot}} N_2(z)\, dz; \quad M^{(3)} = \frac{K^{(3)}}{\phi D_{tot}(p_N + 1)} \tag{B.49}$$

Equation Box 19 Flux form equations for phosphate in the sediments.

$$\begin{aligned} \frac{\partial K^{(1)}}{\partial t} &= \left.\frac{\partial K^{(1)}}{\partial t}\right|_{K1^{(1)}}^{diff} - \left.\frac{\partial K^{(1)}}{\partial t}\right|_{N1}^{ben} + \left.\frac{\partial K^{(1)}}{\partial t}\right|_{D^{(1)}}^{shift} + \sum_{Yi} \left.\frac{\partial Y_p}{\partial t}\right|_{K1}^{lim} + \\ &\quad + \left.\frac{\partial H_p^{(1)}}{\partial t}\right|_{K1}^{lim} - \left.\frac{\partial H_p^{(1)}}{\partial t}\right|_{K1}^{upt} \end{aligned} \tag{B.50a}$$

$$\begin{aligned} \frac{\partial K1^{(1)}}{\partial t} &= \left.\frac{\partial K1^{(1)}}{\partial t}\right|_{K2^{(1)}}^{diff} - \left.\frac{\partial K^{(1)}}{\partial t}\right|_{K1^{(1)}}^{diff} - \left.\frac{\partial K^{(1)}}{\partial t}\right|_{D^{(1)}}^{shift} + \left.\frac{\partial K1^{(1)}}{\partial t}\right|_{D^{(2)}}^{shift} + \\ &\quad + \pi_P \left(\left.\frac{\partial H_p^{(2)}}{\partial t}\right|_{K1^{(1)}}^{lim} - \left.\frac{\partial H_p^{(2)}}{\partial t}\right|_{K1^{(1)}}^{upt} \right) \end{aligned} \tag{B.50b}$$

$$\begin{aligned} \frac{\partial K2^{(1)}}{\partial t} &= \left.\frac{\partial K2^{(1)}}{\partial t}\right|_{Source_p}^{diff} - \left.\frac{\partial K1^{(1)}}{\partial t}\right|_{K2^{(1)}}^{diff} - \left.\frac{\partial K1^{(1)}}{\partial t}\right|_{D^{(2)}}^{shift} + \\ &\quad + (1 - \pi_P) \left(\left.\frac{\partial H_p^{(2)}}{\partial t}\right|_{K1^{(1)}}^{lim} - \left.\frac{\partial H_p^{(2)}}{\partial t}\right|_{K1^{(1)}}^{upt} \right) \end{aligned} \tag{B.50c}$$

B.7.4. Phosphate

The dynamics of phosphorus are described using 3 layers as shown in Equation Box 19, in order to provide a better description of the vertical variability mainly due to the changes in the adsorption coefficient. Adsorption is dependent on the oxygenation state of the sediment and the particle size; in oxygenated layers, phosphate is bound to Fe(III) and the adsorption coefficient p_P^{ae} is consequently high (250-400:1). The reduction of Fe(III) to Fe(II) in anoxic sediments leads to the mobilization of the adsorbed phosphate, and hence the proportion p_P^{an} between the dissolved and the sorbent phase is lower (approx. 2:1). In the denitrification layer the presence of nitrate should limit the iron oxidation, and we assume the same adsorption coefficient as in the oxic layer. The main processes affecting the phosphorus concentration in the sediments are the vertical diffusion between the layers, and the phosphorus remineralizations given in (B.33b) and (B.34b), which are included as zero-order reactions with an exponential distribution below the oxygen horizon $D^{(1)}$. The partitioning parameter π_P is similar as the one for ammonium in (B.37), with the substitution of the penetration depth scale ($\alpha_P = 1/D^{(8)}$) of the P-component in the organic matter.

In the application of the method described in the beginning of Section B.7, 4 layers are used instead of 3, dividing in two the layer below the sulphide horizon, but the main features can be described by the following set of differential equations:

$$(p_P^{ae}+1)\frac{\partial P_1}{\partial t} = D_P\frac{\partial^2 P_1}{\partial z^2} + M_p^{BT} \quad 0 \le z \le D^{(1)} \tag{B.51a}$$

$$(p_P^{ae}+1)\frac{\partial P_2}{\partial t} = D_P\frac{\partial^2 P_2}{\partial z^2} + M_p^{AT} e^{-\alpha_p(z-D^{(1)})} \quad D^{(1)} < z \le D^{(2)} \tag{B.51b}$$

$$(p_P^{an}+1)\frac{\partial P_3}{\partial t} = D_P\frac{\partial^2 P_3}{\partial z^2} + M_p^{AT} e^{-\alpha_p(z-D^{(1)})} \quad D^{(2)} < z \le D_{tot} \tag{B.51c}$$

.

The source/sink terms of (B.50) are computed according to the semi-analytical resolution method, and the explicit form that utilizes the transient profiles can be obtained by substituting the proper profiles $P_j^{tr}(z),\ j = 1,2,3$ in the Equation Box 17 for ammonium. The boundary conditions applied in the calculation of the steady-state and transient profiles are:

$$\begin{cases} \left(P_1^{eq}\right)_{z=0} = \left(N^{(1)}\right)_{\tilde{z}=0} \\ \left(\dfrac{\partial P_3^{eq}}{\partial t}\right)_{z\to+\infty} = 0 \end{cases} \tag{B.52}$$

where $N^{(1)}$ is the concentration of dissolved phosphate in the seawater at the bottom, plus the continuity of mass and fluxes through the interfaces in the interior.

The relations between the analytical variables used to describe the dynamics of the transient pro-

file, and the ordinary state variables are the following:

$$K^{(1)} = \phi\,(p_P^{ae}+1)\int_0^{D^{(1)}} P_1(z)\,dz; \quad M^{(1)} = \frac{K^{(1)}}{\phi D^{(1)}\,(p_P^{ae}+1)} \tag{B.53a}$$

$$K1^{(1)} = \phi\,(p_P^{ae}+1)\int_{D^{(1)}}^{D^{(2)}} P_2(z)\,dz; \quad M1^{(1)} = \frac{K1^{(1)}}{\phi\left(D^{(2)}-D^{(1)}\right)(p_P^{ae}+1)} \tag{B.53b}$$

$$K2^{(1)} = \phi\,(p_P^{an}+1)\int_{D^{(2)}}^{D_{tot}} P_3(z)\,dz; \quad M2^{(1)} = \frac{K2^{(1)}}{\phi\left(D_{tot}-D^{(2)}\right)(p_P^{an}+1)}. \tag{B.53c}$$

There are still several unresolved problems connected to the modelling of phosphorus dynamics in the sediments. As already introduced above, problems are especially related to the fact that phosphates are primarily bound to iron oxides, and the adsorption coefficients change as a function of the redox conditions. In order to thoroughly reproduce this process, an explicit modelling of the dissolved and sorbent phase is needed, however the introduction of this process would result in slower computations, and cannot be coped with the ERSEM philosophy of a comprehensive ecosystem model. Therefore, some numerical workarounds have been used to prevent the instantaneous change of phase due to the shifting of the sulphide horizon, and they have been grouped together in Section B.7.9, where a detailed explanation is given.

Equation Box 20 Flux form equations for silicate in the sediments.

$$\frac{\partial K^{(5)}}{\partial t} = -\left.\frac{\partial K^{(5)}}{\partial t}\right|_{N^{(5)}}^{diff} + \left.\frac{\partial K^{(5)}}{\partial t}\right|_{source_s}^{diff} + \left.\frac{\partial K^{(5)}}{\partial t}\right|_{D^{(2)}}^{shift} + \left.\frac{\partial Q_s^{(6)}}{\partial t}\right|_{K^{(5)}}^{diss} + \left.\frac{\partial Q_s^{(6)}}{\partial t}\right|_{sink_s}^{diss} \tag{B.54}$$

$$\left.\frac{\partial K^{(5)}}{\partial t}\right|_{N^{(5)}}^{diff} = -\phi D_S \frac{\partial C_{tr}(0)}{\partial z} \tag{B.55a}$$

$$\left.\frac{\partial K^{(5)}}{\partial t}\right|_{source_s}^{diff} = -\phi D_S \left(\frac{\partial C_2^{tr}}{\partial z}\right)_{z=D^{(2)}} \tag{B.55b}$$

$$\left.\frac{\partial Q_s^{(6)}}{\partial t}\right|_{K^{(5)}}^{diss} = \phi s_S \int_0^{D^{(1)}} C_1^{eq}(z)\,dz + \phi s_S \int_{D^{(1)}}^{D^{(2)}} C_2^{eq}(z)\,dz \tag{B.55c}$$

$$\left.\frac{\partial Q_s^{(6)}}{\partial t}\right|_{sink_s}^{diss} = \phi s_S \int_{D^{(2)}}^{D_{tot}} C_2^{eq}(z)\,dz \tag{B.55d}$$

B.7.5. Silicate

The dissolution of biogenic silica is described as a first-order process between biogenic silica and the dissolved fraction. Biogenic silica in the model comes from diatoms' siliceous frustules that sink along the water column as living cells $(P_s^{(1)})$ or particulate detritus $(R_s^{(6)})$ and enter the benthic system as $Q_s^{(6)}$ (Section B.2). Silicate dynamics in the model are described by the equation (B.54) in Equation Box 20, where we also give the functional process forms of the involved fluxes. The dynamics have been defined over the entire modelled sediment depth, although silicate profiles are assumed to have dynamical variations only until the depth of the sulphide horizon $(D^{(2)})$. For this reason, all the dissolution fluxes of the biogenic silicate below that depth will be redirected to the infinite virtual silicate sink in the sediments, without affecting the dissolved phase variable $K^{(5)}$ (see term (B.55d)).

Equation (B.54) originates from the general form of the dissolution process in the pore waters (Hurd, 1973; Schink et al., 1975), which is written as:

$$\frac{\partial C}{\partial t} = D_S \frac{\partial^2 C}{\partial z^2} - s_S \frac{B}{S_\infty} C \tag{B.56}$$

where $C(z,t) = S_\infty - S(z,t)$ is the difference between the actual concentration of dissolved silica and the one at saturation with opaline silica, $B(z,t)$ is the concentration of biogenic opaline silica and s_S is the specific dissolution rate. The concentration at saturated conditions is calculated according to the linear equation

$$S_\infty = S_\infty^* + a_S \left(f_S^T - 1 \right) \tag{B.57}$$

where S_∞^* is the saturated concentration at 10º C (600 mmol Si m^{-3}) and a_S is an empirical coefficient taken to be 400 mmol Si m^{-3}. In the model, the vertical distribution of biogenic silica has been approximated to an exponential function, and the processes in the oxic layer - where a low pore-water concentration is usually found - have been reduced to a simple zero-order source term depending on the average concentration. These assumptions lead to the following set of equations in a two-layered system of pore waters:

$$\frac{\partial C_1}{\partial t} = D_S \frac{\partial^2 C_1}{\partial z^2} + f^T s_S \overline{B_1} \quad 0 \le z \le D^{(1)} \tag{B.58a}$$

$$\frac{\partial C_2}{\partial t} = D_S \frac{\partial^2 C}{\partial z^2} + f^T s_S \frac{B_0 e^{-\alpha_S (z - D^{(1)})}}{S_\infty} C \quad D^{(1)} < z \le D_{tot} \tag{B.58b}$$

The constant dissolution rate (s_S) is only modulated by the environmental temperature, and the mean concentration of biogenic silica in the first oxic layer (B_1) is derived from the vertical distribution of

biogenic detritus as follows:

$$B_0 = \frac{Q_s^{(6)}}{\phi \int_0^{D_{tot}} e^{-\alpha_S z}\, dz} \tag{B.59}$$

$$\overline{B_1} = \frac{B_0}{D^{(1)}} \int_0^{D^{(1)}} e^{-\alpha_S z}\, dz \tag{B.60}$$

where $\alpha_S = 1/D^{(9)}$.

The boundary conditions for (B.58) are:

$$\begin{cases} \left(C_1^{eq}\right)_{z=0} & = & S_\infty - \left(N^{(5)}\right)_{\tilde{z}=-H} \\ \left(\dfrac{\partial C_2^{eq}}{\partial t}\right)_{z\to+\infty} & = & 0 \end{cases} \tag{B.61}$$

where the variable $N^{(5)}$ is the concentration of dissolved silicate in the seawater at the bottom, and the dynamical equations are also linked by prescribing continuity in the concentration and in the flux at the interface with the oxic layer as done for ammonium (B.42).

All the terms in (B.55) are evaluated by means of the transient profiles computed through the semi-analytical resolution method. However, there are some exceptions in the case of the dissolution fluxes (B.55c) and (B.55d), the terms that respectively represent the dissolution in the oxic/denitrification layers and in the anoxic one. Since the silicate dynamics is assumed to vary with very long time scales, the dissolution rates are derived by substituting the steady-state equilibrium profiles instead of the transient profiles. Moreover - as mentioned in the beginning - the fluxes are calculated until the depth $D^{(2)}$, and the reminder (B.55d) is directly added to the sink term for silicate.

Finally, we give the relationships between the model state variables and the analytical profiles with also the derivation of the pore water average concentration $M^{(5)}$:

$$K^{(5)} = \phi \int_0^{D^{(1)}} S_\infty - C_1(z)\, dz + \phi \int_{D^{(1)}}^{D^{(2)}} S_\infty - C_2(z)\, dz; \quad M^{(5)} = \frac{K^{(5)}}{\phi D^{(2)}} \tag{B.62}$$

where, as remarked above, only the profiles down to the sulphide horizon are taken into account.

B.7.6. Reduction equivalents

The model state variable “reduction equivalents” represents all the reduced ions generated in the sulphide layer during the degradation of the organic matter. It is assumed that reduction equivalents have the properties of sulphide (for example, the same diffusion coefficient), and are thus measured in mmol S m^{-2}. The main processes affecting the dynamics are shown in Equation Box 21. They are the production in the anoxic layers through bacterial metabolic reactions and the diffusion towards the oxic layer, where they are eventually reoxidized.

The reoxidation is approximated to a first-order process controlled by a constant specific rate,

Equation Box 21 Flux form equations for reduction equivalents in the sediments.

$$\frac{\partial K^{(6)}}{\partial t} = -\left.\frac{\partial K^{(6)}}{\partial t}\right|_{N6}^{ben} + \left.\frac{\partial K^{(6)}}{\partial t}\right|_{source_r}^{diff} - \left.\frac{\partial K^{(6)}}{\partial t}\right|_{G^{(2)}}^{reox} + \Omega_o^r\,\Omega_c^o\,\left.\frac{\partial H_c^{(2)}}{\partial t}\right|_{G^{(3)}}^{rsp} - \left.\frac{\partial K^{(6)}}{\partial t}\right|_{sink_r}^{denit} \tag{B.63}$$

$$\left.\frac{\partial K^{(6)}}{\partial t}\right|_{N^{(6)}}^{ben} = \phi D_R \left(\frac{\partial R_1^{tr}}{\partial z}\right)_{z=0} \tag{B.64a}$$

$$\left.\frac{\partial K^{(6)}}{\partial t}\right|_{source_r}^{diff} = \phi D_R \left(\frac{\partial R_1^{tr}}{\partial z}\right)_{z=D_{tot}} \tag{B.64b}$$

$$\left.\frac{\partial K^{(6)}}{\partial t}\right|_{G^{(2)}}^{reox} = \phi \sigma_R \int_0^{D^{(1)}} R_{tr}(z)\,dz \tag{B.64c}$$

$$\left.\frac{\partial K^{(6)}}{\partial t}\right|_{sink_r}^{denit} = \phi \Omega_n^r d_N \int_{D^{(1)}}^{D^{(2)}} N_2^{tr}(z)\,dz \tag{B.64d}$$

while the production/consumption rates below the oxygen horizon are functions of the anoxic mineralization and of the denitrification rates. We can express this in the following set of equations:

$$\frac{\partial R_1}{\partial t} = D_R \frac{\partial^2 R_1}{\partial z^2} - \sigma_R R_1 \qquad 0 \le z \le D^{(1)} \tag{B.65a}$$

$$\frac{\partial R_2}{\partial t} = D_R \frac{\partial^2 R_2}{\partial z^2} + \Omega_o^r M_o^{AT} e^{-\alpha_c (z - D^{(1)})} - \Omega_n^r d_N N_2 \quad D^{(1)} < z \le D_{tot} \tag{B.65b}$$

where σ_R is the specific daily reoxidation rate, M_o^{AT} is the average anoxic mineralization according to (B.32) and considering the exponential distribution of the organic matter with $\alpha_c = 1/D^{(6)}$, $N_2(z)$ is the nitrate concentration and d_N is the denitrification rate calculated from (B.47). The parameters Ω_o^r and Ω_n^r represent the stoichiometric coefficients between sulphide and oxygen in the reoxidation process, and between sulphide and nitrogen in the denitrification reaction (Table A.4).

The metabolic denitrification pathway is considered in an indirect way, because the anoxic mineralization (B.32) are converted from oxygen units to reduction equivalents, which in turn are reoxidized by nitrate in the denitrification layer. When nitrate is totally depleted (B.63b) turns into a strict sulphur-reducing process.

The boundary conditions for the calculation of the steady-state profiles are:

$$\begin{cases} \left(R_1^{eq}\right)_{z=0} = \left(N^{(6)}\right)_{\tilde{z}=-H} \\ \left(\dfrac{\partial R_2^{eq}}{\partial t}\right)_{z\to+\infty} = 0 \end{cases} \tag{B.66}$$

where $N^{(6)}$ is the concentration of reduction equivalents in the water column. Additional boundary conditions are the continuity constraints at $z = D^{(1)}$. In order to derive the state variables actually carried by the model, the following expressions are adopted:

$$K^{(6)} = \phi \int_0^{D^{(1)}} R_1(z)\, dz + \phi \int_{D^{(1)}}^{D_{tot}} R_2(z)\, dz; \quad M^{(6)} = \frac{K^{(6)}}{\phi D_{tot}}. \tag{B.67}$$

Equation Box 22 Flux form equations for the dissolved organic matter (C, N, P components) in oxic ($Q_i^{(1)}$) and anoxic ($Q1_i^{(1)}$) sediments.

$$\frac{\partial Q_c^{(1)}}{\partial t} = \frac{\partial Q_c^{(1)}}{\partial t}\bigg|_{Q1_c^{(1)}}^{diff} + \frac{\partial Q_c^{(1)}}{\partial t}\bigg|_{D^{(1)}}^{shift} - \frac{\partial H_c^{(1)}}{\partial t}\bigg|_{Q_c^{(1)}}^{upt} + \frac{\partial H_c^{(1)}}{\partial t}\bigg|_{Q_c^{(1)}}^{out} + \frac{\partial H_c^{(1)}}{\partial t}\bigg|_{Q_c^{(1)}}^{lim} + \frac{\partial Q_c^{(1)}}{\partial t}\bigg|_{P_c}^{sed} \tag{B.68a}$$

$$\frac{\partial Q_l^{(1)}}{\partial t} = \frac{Q_l^{(1)}}{Q_c^{(1)}}\left(\frac{\partial Q_c^{(1)}}{\partial t}\bigg|_{Q1_c^{(1)}}^{diff} + \frac{\partial Q_c^{(1)}}{\partial t}\bigg|_{D^{(1)}}^{shift}\right) - \frac{Q_l^{(1)}}{Q_c^{(1)}}\frac{\partial H_c^{(1)}}{\partial t}\bigg|_{Q_c^{(1)}}^{upt} + \frac{\partial H_l^{(1)}}{\partial t}\bigg|_{Q_l^{(1)}}^{out} + \frac{\partial Q_l^{(1)}}{\partial t}\bigg|_{P_l}^{sed} \quad l = n, p \tag{B.68b}$$

$$\frac{\partial Q1_c^{(1)}}{\partial t} = -\frac{\partial Q1_c^{(1)}}{\partial t}\bigg|_{Q_c^{(1)}}^{diff} - \frac{\partial Q_c^{(1)}}{\partial t}\bigg|_{D^{(1)}}^{shift} - \frac{\partial H_c^{(2)}}{\partial t}\bigg|_{Q1_c^{(1)}}^{upt} + \frac{\partial H_c^{(2)}}{\partial t}\bigg|_{Q1_c^{(1)}}^{out} + \frac{\partial H_c^{(2)}}{\partial t}\bigg|_{Q1_c^{(1)}}^{lim} \tag{B.68c}$$

B.7.7. Dissolved organic matter

The dynamics of DOM in the sediments is mainly controlled by production/consumption terms and by vertical diffusion. We have to distinguish the processes occurring above the oxygen horizon from the ones in the anoxic layers, where the distribution of DOM is only affected by anaerobic bacterial activity. Therefore, the model utilizes 2 ordinary state vectors as already introduced in Section B.6, whose general equations are shown in Equation Box 22 for the C, N and P components. They are derived according to the standard methodology from the following set of differential equations describing the pore water concentration profiles:

$$\frac{\partial Q_1}{\partial t} = D_Q \frac{\partial^2 Q(z)}{\partial z^2} - M_c^{BT} \quad 0 \le z \le D^{(1)} \tag{B.69a}$$

$$\frac{\partial Q_2}{\partial t} = D_Q \frac{\partial^2 Q(z)}{\partial z^2} - \psi_Q Q \quad D^{(1)} < z \le D_{tot} \tag{B.69b}$$

Specifically, in the oxic layer we have a zero-order term describing the total production/consumption and deposition processes derived from (B.13a):

$$M_c^{BT} = \frac{1}{\phi D^{(1)}}\left\{\frac{\partial H_c^{(1)}}{\partial t}\bigg|_{Q^{(1)}}^{upt} - \frac{\partial H_c^{(1)}}{\partial t}\bigg|_{Q^{(1)}}^{out} - \frac{\partial H_c^{(1)}}{\partial t}\bigg|_{Q^{(1)}}^{lim}\right\}. \tag{B.70}$$

In the anoxic layers the uptake process is modelled with a first order term and the specific consumption rate is evaluated using the following equation, derived from the carbon fluxes of anaerobic bacteria in (B.13a) and Box 14:

$$\psi_Q = \frac{\left.\frac{\partial H_c^{(2)}}{\partial t}\right|_{Q1^{(1)}}^{upt} - \left.\frac{\partial H_c^{(2)}}{\partial t}\right|_{Q1^{(1)}}^{out} - \left.\frac{\partial H_c^{(2)}}{\partial t}\right|_{Q1^{(1)}}^{lim}}{Q1_c^{(1)}} \tag{B.71}$$

Boundary conditions for the steady-state solution of (B.68) are:

$$\begin{cases} \left(\frac{\partial Q_1^{eq}}{\partial t}\right)_{z=0} &= 0 \\ \left(\frac{\partial Q_1^{eq}}{\partial t}\right)_{z\to+\infty} &= 0 \end{cases} \tag{B.72}$$

where it is important to note that at the sediment-water interface there is a no-flux condition and the sedimentation flux from the water column (from (B.2)) has been included as source term of the general equations (B.68a) and (B.68b).

The equations are thus solved using the same procedure as for the other dissolved nutrients, and the model state variables can be derived using the following expressions:

$$Q_c^{(1)} = \phi \int_0^{D^{(1)}} Q_1(z)\, dz; \quad Q1_c^{(1)} = \phi \int_{D^{(1)}}^{D_{tot}} Q_2(z)\, dz. \tag{B.73}$$

In the current implementation there are actually no variables describing the average concentrations in the pore-waters.

Equation Box 23 Flux form equations for oxygen and penetration depths of the oxic and denitrification layers.

$$\left.\frac{\partial G^{(2)}}{\partial t}\right|_{bio} = \left.\frac{\partial G^{(2)}}{\partial t}\right|_{O^{(2)}}^{diff} - \Omega_c^o \left(\sum_j \left.\frac{\partial Y_c^{(j)}}{\partial t}\right|_{G^{(3)}}^{rsp} + \left.\frac{\partial H_c^{(1)}}{\partial t}\right|_{G^{(3)}}^{rsp} \right) + -\Omega_n^o \left.\frac{\partial K^{(4)}}{\partial t}\right|_{K^{(3)}}^{nit} - \frac{1}{\Omega_o^r} \left.\frac{\partial K^{(6)}}{\partial t}\right|_{G^{(2)}}^{reox} \tag{B.74}$$

$$\frac{\partial D^{(j)}}{\partial t} = \nu \frac{h_{D^{(j)}}}{h_{D^{(j)}} + D^{(j)}} \left(\frac{D_{eq}^{(j)}}{D^{(j)}}\right)^{\sigma} \left(D_{eq}^{(j)} - D^{(j)}\right) \quad j = 1,2 \tag{B.75}$$

B.7.8. Oxygen distribution and the dynamics of the sulphide horizon

The oxygen dynamics model used in ERSEM has been originally proposed by Bouldin (1968), and partially modified by Ruardij and Van Raaphorst (1995). The main processes affecting the oxygen concentration are the biological oxidation of the organic matter, the nitrification reaction of ammonium and the reoxidation of the reduction equivalents. Most of these terms have already been explained in the previous sections (see equations (B.31), (B.36) and (B.63)), and have been collected in Equation Box 23 to give the general model equation for the ordinary state variable $G^{(2)}$. From the dynamics of oxygen, we also derive the model equations for the ordinary state variable $D^{(1)}$, which is the thickness of the oxic layer used in the other computations. A similar dynamics is also used to derive the dynamical equation for the starting depth of the anaerobic layer, the sulphide horizon $D^{(2)}$.

It is assumed that oxygen in the sediments is in instantaneous equilibrium with the consumption processes at the resolved time scales, therefore the dynamics is not solved by means of the semi-analytical method used for the other dissolved components. Thus, we compute the steady state solution from the equation of the dissolved oxygen in the pore waters, which is written as:

$$\frac{\partial O}{\partial t} = D_O \frac{\partial^2 O}{\partial z^2} - M_o^{BT} - M_o^{nit} - M_o^{rox} \quad 0 \leq z \leq D^{(1)} \tag{B.76}$$

The consumption terms in (B.76) are evaluated as mean values of the corresponding fluxes in (B.36) and (B.63) as follows

$$M_o^{nit} = \frac{\Omega_n^o}{\phi D^{(1)}} \frac{\partial K^{(4)}}{\partial t}\bigg|_{K^{(3)}}^{nit} \tag{B.77}$$

$$M_o^{rox} = \frac{1}{\phi D^{(1)} \Omega_o^r} \frac{\partial K^{(6)}}{\partial t}\bigg|_{G^{(2)}}^{reox} \tag{B.78}$$

and the biological oxygen demand is computed from (B.31). The molecular diffusion coefficient of oxygen (in $m^2\ d^{-1}$) is taken from an empirical relation (Broecker and Peng, 1973) that also includes a temperature correction as follows:

$$D_O = \theta \cdot 8.64 \cdot 10^{-5} \cdot 10^{3.672 - \frac{984.26}{273+T}} \tag{B.79}$$

where θ is a sensitivity factor chosen to be 1.5. The steady-state solution of (B.76) is obtained by applying the following boundary conditions

$$\begin{cases} (O_{eq})_{z=0} = \left(O^{(2)}\right)_{\tilde{z}=-H} \\ \left(\dfrac{\partial O_{eq}}{\partial z}\right)_{z=D^{(1)}} = 0 \\ (O_{eq})_{z \geq D^{(1)}} = 0 \end{cases} \tag{B.80}$$

from which it is possible to derive the maximum oxygen penetration depth at the equilibrium with the consumption fluxes as:

$$D_{eq}^{(1)} = \sqrt{\frac{2D_O\, O^{(2)}}{M_o^{BT} + M_o^{nit} + M_o^{rox}}} \tag{B.81}$$

The actual rate of change of the oxic layer thickness $D^{(1)}$ is evaluated from (B.81) utilizing the dynamics defined in Box 23, equation (B.75). This is a relaxation to the equilibrium thickness in which the relaxing frequency ν_D is modulated by some regulating factors introduced to dampen the shorter scale frequency. The parameter $h_{D^{(1)}}$ is the depth at which the change is limited to half of its actual value and σ is the exponent for the damping function, usually taken to be 2.

Equation (B.75) is then numerically solved forward in time to get an approximation of the new oxic thickness $(D_{t+\Delta t}^{(1)})$. Afterwards, the steady-state solution of (B.76) is again used to derive the concentration of $G^{(2)}$ at the next time step by means of the following:

$$G_{t+\Delta t}^{(2)} \quad = \quad \int_0^{D_{t+\Delta t}^{(1)}} O_{eq}(z)\, dz \tag{B.82}$$

Now we only need to derive the molecular diffusion flux to the water column, which is obtained by difference from (B.74) as follows:

$$\left.\frac{\partial G^{(2)}}{\partial t}\right|_{O^{(2)}}^{diff} = -\frac{\left(G_{t+\Delta t}^{(2)} - G^{(2)}\right)}{\Delta t} - \Omega_c^o \left(\sum_j \left.\frac{\partial Y_c^{(j)}}{\partial t}\right|_{G^{(3)}}^{rsp} + \left.\frac{\partial H_c^{(1)}}{\partial t}\right|_{G^{(3)}}^{rsp} \right) - \Omega_n^o \left.\frac{\partial K^{(4)}}{\partial t}\right|_{K^{(3)}}^{nit} - \frac{1}{\Omega_o^r} \left.\frac{\partial K^{(6)}}{\partial t}\right|_{G^{(2)}}^{reox} \tag{B.83}$$

This flux is a boundary condition for the pelagic equation of dissolved oxygen shown in (MISSING).

The sulphide horizon is defined after Van Raaphorst et al. (1990) as the depth at which nitrate has decreased to 10% of the value at the oxygen horizon depth. From the analytical steady-state solution of (B.46b), the nitrate profile below the oxic penetration depth has an exponential decrease of the form:

$$N_2^{eq}(z) = n_{21} e^{-\sqrt{\frac{d_N}{D_N}} z} \tag{B.84}$$

where n_{21} is an integration constant, D_N is the diffusivity and d_N have been described in (B.39). This exponential function is utilized to derive the new sulphide horizon depth at the equilibrium as follows:

$$\left(N_2^{eq}\right)_{z=D_{eq}^{(2)}} = 0.1 \left(N_2^{eq}\right)_{z=D^{(1)}} \Longrightarrow D_{eq}^{(2)} = \frac{\log 0.1}{\sqrt{\frac{d_N}{D_N}}} + D^{(1)}. \tag{B.85}$$

Similarly to the oxygen horizon depth, the shifting rate is evaluated according to (B.75) where $h_{D^{(2)}}$ is the depth at which the changes are limited to half of their values.

B.7.9. Shifting of the layers

This section describes the calculation of nutrient and organic matter fluxes related to the dynamical shifting of the layer interfaces. These terms have been introduced in the dynamical equations to account for the changes in the mass vertical distribution. Such fluxes are particularly important for the phosphate distribution because of the strong vertical gradients of the adsorption coefficients.

The general form of the shifting terms is the following:

$$\left.\frac{\partial K}{\partial t}\right|_{D^{(j)}}^{shift} = \frac{\phi\,(p+1)}{\Delta t}\int_{D^{(j)}}^{D^{(j)}+\frac{\partial D^{(j)}}{\partial t}\Delta t} X_{tr}(z)\,dz \quad j=1,2 \tag{B.86}$$

where K is the generic total amount of substance in the layer, X_{tr} is the related transient profile and $\partial D^{(j)}/\partial t$ is the time rate of change of the layer depth from (B.75). The sign of the flux depends on the direction of the shifting, being positive for downwards movements.

In the case of phosphates the fluxes are limited by using a dampening factor that has a Michaelis-Menten form:

$$f_{K^{(1)}}^{flux} = \frac{h_{K^{(1)}}}{h_{K^{(1)}} + \frac{1}{K^{(1)}}\left.\frac{\partial K^{(1)}}{\partial t}\right|_{D^{(1)}}^{shift}} \tag{B.87}$$

where $h_{K^{(1)}}$ represents a relative control rate (d^{-1}). The factors for the fluxes between the denitrification and the anoxic layers can be obtained by substituting the appropriate variable names ($K1^{(1)}$ and $K2^{(1)}$). This factor is multiplied by the actual shifting-related flux (B.86) and the result is applied in the dynamical equations described above. This simple parameterization is a compromise between the necessity to have slow response in the behavior of this dissolved nutrient and the possibility to have fast changes in the sediment redox conditions. Refinements of this process need to be addressed in the future, in order to have a more suitable representation of the time-scale interactions.

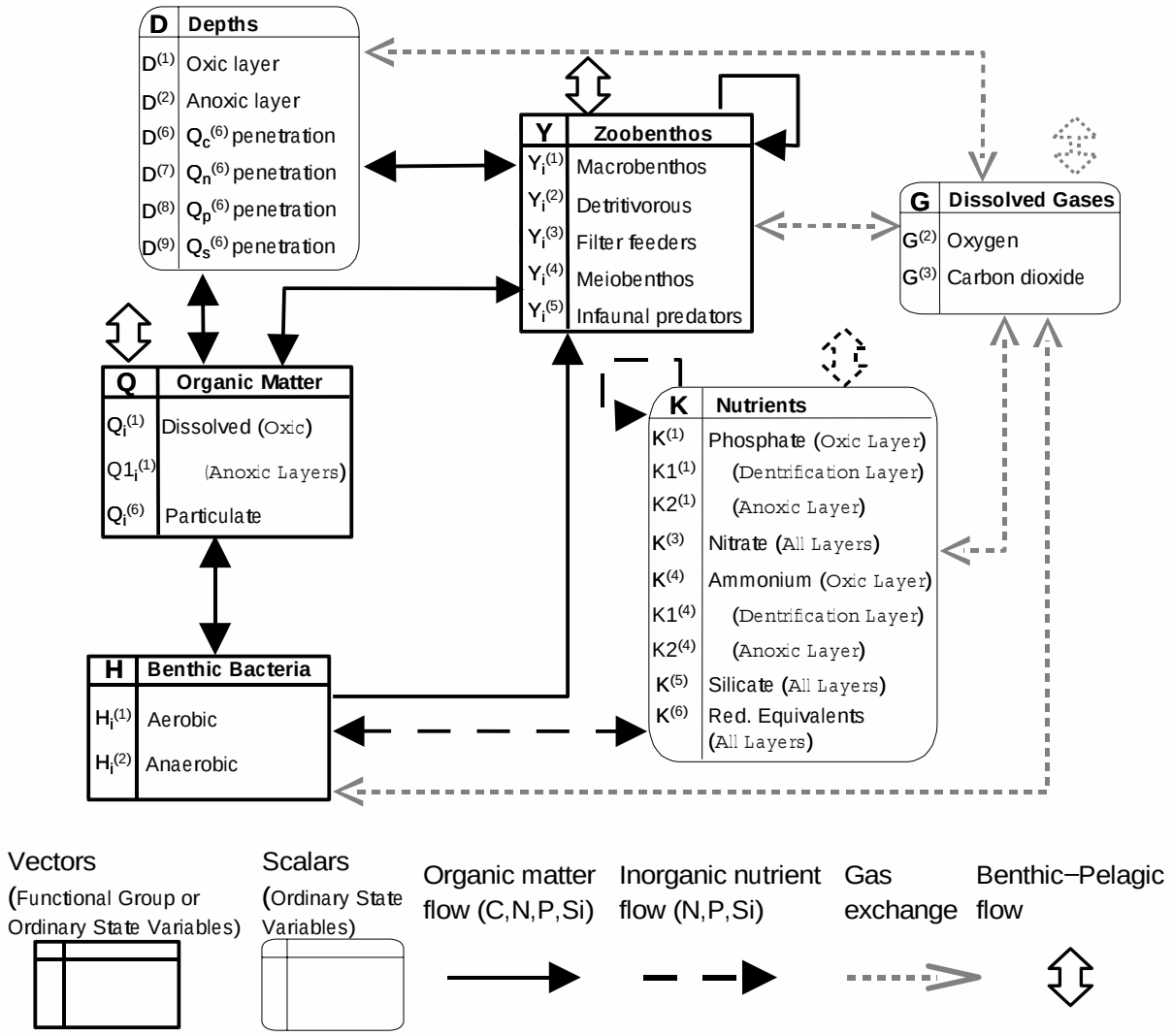

Figure B.1.: Scheme of the benthic model.

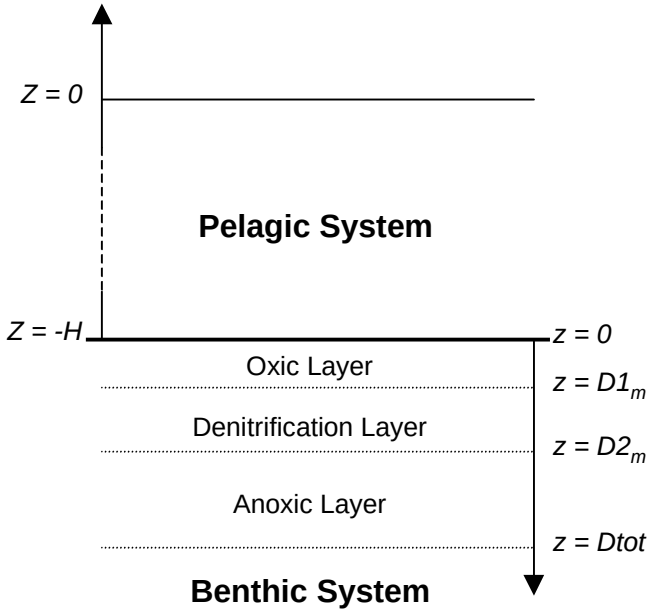

Figure B.2.: The system of coordinates and the modelled sediment layers in the benthic model.

C. The primitive equation transport model (POM)

C.1. Introduction

This Appendix gives the description of the physical transport term in the general dynamical equations (A.1) for the ecosystem state variables, and the fundamental equations for the physical transport models, both for the three-dimensional and the one-dimensional implementations.

The usual general decomposition of the main oceanographic fields in mean flow (slow varying) and turbulent flow (fast varying) is used here :

$$\begin{cases} \mathbf{u} = \mathbf{U} + \mathbf{u}' \\ \mathtt{T} = T + T' \\ \mathtt{S} = S + S' \\ \mathtt{C} = C + C' \end{cases} \tag{C.1}$$

where $\mathbf{u} \equiv (u, v, w)$ is the velocity vector in m/s, $\mathtt{T}$ is the temperature field in *degrees Celsius*, $\mathtt{S}$ is salinity in *psu* (practical salinity units) and $\mathtt{C}$ is the concentration of the pelagic transported biogeochemical component. $\mathbf{U}, \mathbf{u}'$ are, respectively, the long/medium time scale component and the small turbulent component of the velocity field. Likewise, T, S, C indicate the temperature, salinity and substance concentration mean fields and T', S', C' the turbulence-induced fluctuations of the related mean variables.

Substituting these definitions both in the primitive equations of motion[1] and in the generic equation for tracers, and after the application of the *ensemble mean* $\langle\cdot\rangle$ we get the following equations:

$$\frac{D\mathbf{U}_h}{Dt} + \mathbf{f} \times \mathbf{U}_h + \frac{\nabla \mathbf{P}}{\rho_0} - \mathbf{g}\frac{\rho}{\rho_0} - \mathbf{F} = -\frac{1}{\rho_0}\nabla \cdot \langle \tau_{ij} \rangle \tag{C.2}$$

$$\nabla \cdot \mathbf{U} = 0 \tag{C.3}$$

$$\frac{DT}{Dt} + m_T - Q_I = -\nabla \cdot \langle \mathbf{u}' T' \rangle = -\left[\frac{\partial}{\partial x} \langle u' T' \rangle + \frac{\partial}{\partial y} \langle v' T' \rangle + \frac{\partial}{\partial z} \langle w' T' \rangle \right] \tag{C.4}$$

[1] Primitive equations are the Navier-Stokes equations for an incompressible fluid under the hypothesis of hydrostatic equilibrium and the Boussinesq approximation.

$$\frac{DS}{Dt} + m_S = -\nabla \cdot \left\langle \mathbf{u}' S' \right\rangle = -\left[\frac{\partial}{\partial x} \left\langle u' S' \right\rangle + \frac{\partial}{\partial y} \left\langle v' S' \right\rangle + \frac{\partial}{\partial z} \left\langle w' S' \right\rangle \right] \tag{C.5}$$

$$\left. \frac{DC}{Dt} \right|_t + m_C = -\nabla \cdot \left\langle \mathbf{u}' C' \right\rangle = -\left[\frac{\partial}{\partial x} \left\langle u' C' \right\rangle + \frac{\partial}{\partial y} \left\langle v' C' \right\rangle + \frac{\partial}{\partial z} \left\langle w' C' \right\rangle \right] \tag{C.6}$$

$$\rho = \rho\,(T, S) \tag{C.7}$$

where $\mathbf{U}_h \equiv (U, V)$ and

$$\frac{D}{Dt} \equiv \frac{\partial}{\partial t} + U\frac{\partial}{\partial x} + V\frac{\partial}{\partial y} + W\frac{\partial}{\partial z}$$

is the total derivative, $\mathbf{f} \equiv (f,\ f,\ 0)$ is the Coriolis parameter ($f = 2\Omega \sin\theta$), $\mathbf{g} \equiv (0, 0, g)$ is the gravity term and $\left\langle \tau_{ij} \right\rangle$ is the Reynold's stress tensor, which is written as:

$$\left\langle \tau_{ij} \right\rangle = \rho \begin{vmatrix} \langle u'u' \rangle & \langle u'v' \rangle & \langle u'w' \rangle \\ \langle v'u' \rangle & \langle v'v' \rangle & \langle v'w' \rangle \\ \langle w'u' \rangle & \langle w'v' \rangle & \langle w'w' \rangle \end{vmatrix} \tag{C.8}$$

The density of water ρ is expressed as a function of T and S using an approximation of the UNESCO density equation proposed by Mellor (1991); this equation has been shown to give results comparable to the UNESCO general equation (UNESCO, 1981, 1982) in the range of density found in the Baltic Sea and in the Adriatic Sea. The remaining terms in (C.2 - C.6), $\mathbf{F}$, m_T, m_S and m_C indicate the smallest scale processes related to molecular diffusivity, while Q in (C.4) represents the heat due to the vertical divergence of the solar heating.

The Reynold's stresses are rewritten according to:

$$-\left\langle u'w' \right\rangle = K_M \frac{\partial U}{\partial z}; \qquad -\left\langle v'w' \right\rangle = K_M \frac{\partial V}{\partial z}, \tag{C.9a}$$

$$-\left\langle T'w' \right\rangle = K_H \frac{\partial T}{\partial z}; \qquad -\left\langle S'w' \right\rangle = K_H \frac{\partial S}{\partial z}; \qquad -\left\langle C'w' \right\rangle = K_H \frac{\partial C}{\partial z} \tag{C.9b}$$

where K_M e K_H are the turbulent diffusion coefficients. The following equations define the horizontal diffusion coefficients A_M and A_H

$$-\left\langle u'u' \right\rangle = 2A_M \frac{\partial U}{\partial x}; \qquad -\left\langle u'v' \right\rangle = -\left\langle v'u' \right\rangle = A_M \left(\frac{\partial U}{\partial y} + \frac{\partial V}{\partial x} \right); \qquad -\left\langle v'v' \right\rangle = 2A_M \frac{\partial V}{\partial y} \tag{C.10a}$$

$$-\left\langle T'u' \right\rangle = A_H \frac{\partial T}{\partial x}; \qquad -\left\langle S'u' \right\rangle = A_H \frac{\partial S}{\partial x}; \qquad -\left\langle C'u' \right\rangle = A_H \frac{\partial C}{\partial x} \tag{C.10b}$$

$$-\left\langle T'v'\right\rangle = A_H\frac{\partial T}{\partial y};\qquad -\left\langle S'v'\right\rangle = A_H\frac{\partial S}{\partial y};\qquad -\left\langle C'v'\right\rangle = A_H\frac{\partial C}{\partial y}. \tag{C.10c}$$

The turbulence closure scheme for the vertical diffusivities used in this model is the Mellor and Yamada 2.5 (Mellor and Yamada, 1982, hereinafter M-Y) with successive modifications by Galperin *et al*. (1988). The M-Y scheme locally evaluates these two coefficients knowing the amount of turbulent energy in the water column, the local master length scale as a measure of the dimension of eddies, and considering some stability functions as follows:

$$K_M = q\,l\,S_M \tag{C.11}$$

$$K_H = q\,l\,S_H \tag{C.12}$$

Here $q^2 = (\langle u'u'\rangle + \langle v'v'\rangle)$ is twice the turbulent kinetic energy term, l is the master length scale , whereas S_M and S_H are functions of a Richardson number and other empirical constants (Mellor and Yamada, 1982; Mellor, 1989). Hence, the following partial differential equations are added to the set of basic equations, in order to determine the dynamics of q^2 and the master length scale:

$$\frac{Dq^2}{Dt} = \frac{\partial}{\partial z}\left(K_q\frac{\partial q^2}{\partial z}\right) + \frac{\partial}{\partial x}\left(A_H\frac{\partial q^2}{\partial x}\right) + \frac{\partial}{\partial y}\left(A_H\frac{\partial q^2}{\partial y}\right) + P_s + P_b - \varepsilon \tag{C.13}$$

$$\frac{D\left(q^2l\right)}{Dt} = \frac{\partial}{\partial z}\left(K_q\frac{\partial(q^2l)}{\partial z}\right) + \frac{\partial}{\partial x}\left(A_H\frac{\partial(q^2l)}{\partial x}\right) + \frac{\partial}{\partial x}\left(A_H\frac{\partial(q^2l)}{\partial x}\right) + E_1\,l(\frac{P_s}{2} + E_3\frac{P_b}{2})\widetilde{W} - \frac{l\varepsilon}{2} \tag{C.14}$$

where K_q is the vertical eddy diffusivity coefficient for energy, $\widetilde{W}$ is the so-called wall proximity function,

$$P_s = 2K_M\left[\left(\frac{\partial U}{\partial z}\right)^2 + \left(\frac{\partial V}{\partial z}\right)^2\right] \tag{C.15}$$

is the shear production of eddy kinetic energy,

$$P_b = \frac{2g}{\rho_0}K_H\frac{\partial \rho}{\partial z} \tag{C.16}$$

is the buoyancy production due to the vertical structure of the water column and finally

$$\varepsilon = \frac{2q^3}{B_1 l} \tag{C.17}$$

is the Kolmogorov's energy dissipation term (B_1, E_1 and E_3 are empirically determined constants).

For the horizontal diffusion term A_M, the Smagorinsky parameterization of the momentum diffu-

sivity is used:

$$A_M = C_H \Delta x \Delta y \sqrt{\left(\frac{\partial U}{\partial x}\right)^2 + \frac{1}{2}\left(\frac{\partial U}{\partial y} + \frac{\partial V}{\partial x}\right)^2 + \left(\frac{\partial V}{\partial y}\right)^2} \tag{C.18}$$

where Δx and Δy are the grid spacings and C_H is the non-dimensional control parameter. The choice of the Prandtl number N_P also prescribes the value of the horizontal diffusion for the transported variables

$$N_P = \frac{A_M}{A_H}. \tag{C.19}$$

Equation Box 24 Sigma-coordinate equations for the three-dimensional transport model.

$$\frac{\partial DU}{\partial t} + \frac{\partial DU^2}{\partial x} + \frac{\partial DUV}{\partial y} + \frac{\partial DU\omega}{\partial \sigma} - fVD + gD\frac{\partial \eta}{\partial x} + \frac{gD^2}{\rho_0}\int_0^\sigma \left(\frac{\partial \rho}{\partial x} - \frac{\sigma\prime}{D}\frac{\partial D}{\partial x}\frac{\partial \rho}{\partial \sigma\prime}\right) d\sigma\prime \tag{C.20}$$
$$= \frac{\partial}{\partial \sigma}\left(\frac{K_M}{D}\frac{\partial U}{\partial \sigma}\right) + 2\frac{\partial}{\partial x}\left(A_M H\frac{\partial U}{\partial x}\right) + \frac{\partial}{\partial y}A_M H\left(\frac{\partial U}{\partial y} + \frac{\partial V}{\partial x}\right)$$

$$\frac{\partial DV}{\partial t} + \frac{\partial DUV}{\partial x} + \frac{\partial DV^2}{\partial y} + \frac{\partial DV\omega}{\partial \sigma} + fUD + gD\frac{\partial \eta}{\partial y} + \frac{gD^2}{\rho_0}\int_0^\sigma \left(\frac{\partial \rho}{\partial y} - \frac{\sigma\prime}{D}\frac{\partial D}{\partial y}\frac{\partial \rho}{\partial \sigma\prime}\right) d\sigma\prime \tag{C.21}$$
$$= \frac{\partial}{\partial \sigma}\left(\frac{K_M}{D}\frac{\partial V}{\partial \sigma}\right) + 2\frac{\partial}{\partial y}\left(A_M H\frac{\partial V}{\partial y}\right) + \frac{\partial}{\partial x}A_M H\left(\frac{\partial U}{\partial y} + \frac{\partial V}{\partial x}\right)$$

$$\frac{\partial DU}{\partial x} + \frac{\partial DV}{\partial y} + \frac{\partial \omega}{\partial \sigma} + \frac{\partial \eta}{\partial t} = 0 \tag{C.22}$$

$$\frac{\partial DT}{\partial t} + \frac{\partial DUT}{\partial x} + \frac{\partial DVT}{\partial y} + \frac{\partial D\omega T}{\partial \sigma} = \frac{\partial}{\partial \sigma}\left(\frac{K_H}{D}\frac{\partial T}{\partial \sigma}\right) + \frac{\partial}{\partial x}\left(A_H H\frac{\partial T}{\partial x}\right) + \frac{\partial}{\partial y}\left(A_H H\frac{\partial T}{\partial y}\right) + Q_I \tag{C.23}$$

$$\frac{\partial DS}{\partial t} + \frac{\partial DUS}{\partial x} + \frac{\partial DVS}{\partial y} + \frac{\partial D\omega S}{\partial \sigma} = \frac{\partial}{\partial \sigma}\left(\frac{K_H}{D}\frac{\partial S}{\partial \sigma}\right) + \frac{\partial}{\partial x}\left(A_H H\frac{\partial S}{\partial x}\right) + \frac{\partial}{\partial y}\left(A_H H\frac{\partial S}{\partial y}\right) - Q_R \tag{C.24}$$

$$\left.\frac{\partial DC}{\partial t}\right|_{phys} + \frac{\partial DUT}{\partial x} + \frac{\partial DVC}{\partial y} + \frac{\partial D\left(\omega + w_C^{sink}\right)C}{\partial \sigma} = \frac{\partial}{\partial \sigma}\left(\frac{K_H}{D}\frac{\partial C}{\partial \sigma}\right) + \frac{\partial}{\partial x}\left(A_H H\frac{\partial C}{\partial x}\right) + \frac{\partial}{\partial y}\left(A_H H\frac{\partial C}{\partial y}\right) \tag{C.25}$$

C.2. The sigma-coordinate three-dimensional basic equations

A complete and exhaustive description of the Princeton Ocean Model with the definitions of all the variables and equations can be found in Blumberg and Mellor (1997) or in the POM User Guide (Mellor 1998). In Equation Box 24 I summarize the bottom-following equations for the main state variables that are derived from (C.2-C.6) by applying the following sigma transformation,

$$\sigma = \frac{z-\eta}{H+\eta} = \frac{z-\eta}{D} \tag{C.26}$$

where $\eta(x,y,t)$ is the sea surface elevation and $H(x,y)$ is the bottom topography:

The vertical velocity ω is the velocity component normal to the sigma surfaces. In (C.25), the specific sinking velocity of the pelagic state variable C is also added. The shallow water approximation has been assumed in the applications of the model, thus here T is the *in situ* temperature and the pressure dependency of the density has been neglected. The equations for the external mode in POM can be derived by integrating the velocity transport equations (C.22) and (C.20, C.21) from $\sigma = -1$ to $\sigma = 0$ and using the boundary conditions shown below in (C.37), (C.36b) and (C.36a). In all the horizontal diffusion terms, H has been used instead of D as explained in Mellor (1998).

The last term in (C.24) has been added in order to parameterize the dilution effect due to the presence of the strong Po river runoff in the model domain, and is described in Section C.4.3.

Equation Box 25 The one-dimensional transport model equations.

$$\frac{\partial U}{\partial t} - fV = \frac{\partial}{\partial z}\left[(K_M+\chi)\frac{\partial U}{\partial z}\right] \tag{C.27}$$

$$\frac{\partial V}{\partial t} + fU = \frac{\partial}{\partial z}\left[(K_M+\chi)\frac{\partial V}{\partial z}\right] \tag{C.28}$$

$$\frac{\partial P}{\partial z} = -\rho g \tag{C.29}$$

$$\frac{\partial W}{\partial z} = 0 \tag{C.30}$$

$$\frac{\partial T}{\partial t} = \frac{\partial}{\partial z}\left[(K_H+\chi)\frac{\partial T}{\partial z}\right] + Q_I \tag{C.31}$$

$$\frac{\partial S}{\partial t} = \frac{\partial}{\partial z}\left[(K_H+\chi)\frac{\partial S}{\partial z}\right] \tag{C.32}$$

$$\left.\frac{\partial C}{\partial t}\right|_{phys} = \frac{\partial}{\partial z}\left[(K_H+\chi)\frac{\partial C}{\partial z}\right] - w_C^{sink}\frac{\partial C}{\partial z} \tag{C.33}$$

C.3. The one-dimensional model equations

In order to derive the basic equations for the one-dimensional model, all the horizontal terms in (C.2-C.6) are neglected; the equations are expressed in the z coordinate because in the one-dimensional case there are no differences with the sigma coordinate, and the water column depth is set to $D = H$. We also make some assumptions about the terms representing the smaller scale processes in the equations (these assumptions apply also to the vertical diffusion terms of the three-dimensional model). These terms should actually consist only of the molecular diffusion, but in the model they are representative of other unresolved processes as for example internal wave turbulence. In the case of the Baltic proper implementation, the parameterization of these terms has been refined as described in Section 4.3.3. In the standard model, they are parameterized like equations (C.9a) and (C.9b) introducing a background constant diffusivity χ:

$$F_x = \frac{\partial}{\partial z}\left(\chi\frac{\partial U}{\partial z}\right); \qquad F_y = \frac{\partial}{\partial z}\left(\chi\frac{\partial V}{\partial z}\right); \tag{C.34}$$

$$m_T = \frac{\partial}{\partial z}\left(\chi\frac{\partial T}{\partial z}\right); \quad m_S = \frac{\partial}{\partial z}\left(\chi\frac{\partial S}{\partial z}\right); \quad m_C = \frac{\partial}{\partial z}\left(\chi\frac{\partial C}{\partial z}\right) \tag{C.35}$$

The basic equations for the transport model can now be written as shown in Equation Box 25. The main difference between the transport of momentum/tracers and pelagic variable is the presence of the vertical sedimentation term in (C.33). A sinking velocity w_C^{sink} in the model is prescribed for diatoms and particulate organic detritus.

C.4. Boundary conditions

The boundary conditions for the three dimensional model are presented here. The one-dimensional form can be derived considering that $D\,d\sigma = H\,d\sigma = dz$ and that $(\sigma = 0) \equiv (z = 0)$ and $(\sigma = -1) \equiv (z = -H)$. Moreover, the x, y and time coordinates are not indicated in the equations, although the state variable have to be intended as spatial vectors.

C.4.1. Momentum

The boundary conditions for the momentum equations (C.20, C.21) or (C.27, C.28) in the one-dimensional case are:

$$\begin{cases} \dfrac{(K_M+\chi)}{D}\left(\dfrac{\partial \mathbf{U}_H}{\partial\sigma}\right)_{\sigma=0} = -\dfrac{\tau_W}{\rho} \\ \tau_W = \rho_A c_D \left|\mathbf{U}_A\right| \mathbf{U}_A \end{cases} \tag{C.36a}$$

$$\begin{cases} \dfrac{(K_M+\chi)}{D}\left(\dfrac{\partial \mathbf{U}_H}{\partial\sigma}\right)_{\sigma=-1} = \dfrac{\tau_b}{\rho} \\ \tau_b = \rho u_*^2 = \rho k^2 \left(\log\frac{z_{bot}}{z_0}\right)^{-2} |\mathbf{U}_H|\,\mathbf{U}_H \end{cases} \tag{C.36b}$$

where ρ_A is the density of the air, U_A is the wind velocity at 10 m height, c_D is the momentum exchange coefficient at surface calculated according to Hellerman and Rosenstein (1985) and the bottom stress is computed using a logarithmic drag law coefficient where u_* is the shear velocity in the bottom layer ($z_0 = 0.01$m roughness length, $k = 0.4$ Von Karman constant).

For the continuity equations in the three-dimensional case (C.22) we prescribe

$$\omega_{\sigma=0} = \omega_{\sigma=-1} = 0 \tag{C.37}$$

while for eq. (C.30) we choose the constant vertical velocity as $W = 0$.

The boundary conditions on equations (C.13) and (C.14) for the eddy kinetic energy are

$$q^2_{\sigma=0} = B_1^{\frac{2}{3}} \frac{|\tau_W|}{\rho} \tag{C.38a}$$

$$q^2_{\sigma=-1} = B_1^{\frac{2}{3}} u_*^2 \tag{C.38b}$$

$$l_{\sigma=0,-1} = 0 \tag{C.38c}$$

C.4.2. Temperature

Boundary conditions for temperature, (C.23) and (C.31), are:

$$\frac{(K_H+\chi)}{D}\left(\frac{\partial T}{\partial\sigma}\right)_{\sigma=0} = \frac{-Q_b - Q_h - Q_e}{\rho\, c_p} \tag{C.39a}$$

$$\frac{(K_H+\chi)}{D}\left(\frac{\partial T}{\partial\sigma}\right)_{\sigma=-1} = 0 \tag{C.39b}$$

where c_p is the specific heat of water at constant pressure, Q_h is the sensible heat flux, Q_b the long-wave heat flux, Q_e the heat lost due to evaporation (latent heat flux). These values are calculated according to the bulk formulae collected by Castellari *et al.* (1998) and reported in Maggiore *et al.* (1998).

The heat flux gained from the short wave radiation is the term Q_I in equations (C.23, C.31), and it is written as

$$Q_I = \frac{1}{\rho c_p}\frac{\partial I}{\partial z} \tag{C.40}$$

Following Paulson and Simpson (1977), the model parameterizes a partitioning of the incoming short-wave irradiance I in a portion extinguished in the first upper layers (simulating the infrared compo-

nents of the spectrum) and a portion that can penetrate the water column (visible light) as follows:

$$I = Q_S \left[\varepsilon_i e^{\lambda_i z} + (1 - \varepsilon_i) e^{\lambda_v z} \right] \tag{C.41}$$

where Q_S is the astronomical solar radiation flux corrected by cloud cover (Dobson and Smith, 1988). In the model the partitioning coefficient between visible and infrared light (ε_i) is generally set to 0.5, and the value for the infrared extinction coefficient (λ_i) to about 10 m^{-1}. The background extinction coefficient for the visible light (λ_v) is a function of water types, and hence of the amount of light-attenuating dissolved matter present in the water column.

C.4.3. Salinity

Boundary conditions for salinity equation (C.24) or (C.32) differ according to the model setup and applications and the choices are discussed in the specific chapter of the one-dimensional (Chapter 3 and 4) and three-dimensional (Chapter 5) applications. Salinity is used as a proxy for constraining the long term buoyancy of the water column structure and usually in the 1D case a nudging boundary condition is used, which is written in term of salinity data at surface $S^*(t)$:

$$(K_H + \chi) \left(\frac{\partial S}{\partial z} \right)_{z=0} = \alpha_S \left(S - S^*(t) \right)_{z=0} \tag{C.42}$$

where α_S is the relaxation velocity.

In the 3-D case, the general form of the surface condition is:

$$\frac{(K_H + \chi)}{D} \left(\frac{\partial S}{\partial \sigma} \right)_{\sigma=0} = -(E - P) S_{\sigma=0} \tag{C.43}$$

where E is the evaporation rate and P the precipitation rate. The physics of the river runoff dilution effect is parameterized separately in (C.24) in the form of

$$Q_R = \frac{R \Phi_R \left(S - S_R \right)_{\sigma=0}}{DA} \tag{C.44}$$

where $\Phi_R(\vec{x})$ is a normalized scaling coefficient (exponential decaying function of the distance from the river mouth) and S_R is the reference salinity of the inflowing waters at the model boundaries with the river mouths. This parameterization, proposed by Murakami *et al.* (1989) has been preferred to the imposition of a "classical" surface boundary condition because the latter scarcely accelerates the flow and does not provide a proper spreading of the river plume.

At the bottom, the salinity boundary condition is a no-flux condition:

$$\frac{(K_H + \chi)}{D} \left(\frac{\partial S}{\partial \sigma} \right)_{\sigma=-1} = 0 \tag{C.45}$$

C.4.4. Ecological variables

Boundary conditions for (C.33) differ according to the pelagic variable and the model implementation. For functional groups such as phytoplankton or zooplankton both bottom and surface boundary conditions are Von Neumann no-flux specifications. For inorganic nutrients and organic matter, for which external sources are considered, the boundary condition (here given for the generic nutrient N) is written as,

$$(K_H + \chi)\left(\frac{\partial N}{\partial \sigma}\right)_{\sigma=0} = -\left\langle N'w'\right\rangle_{\sigma=0} \tag{C.46}$$

The right hand side in the 1D case can be specified as a nudging term

$$\left\langle N'w'\right\rangle_{z=0} = \alpha_{nut}\left(N - N^*(t)\right)_{z=0} \tag{C.47}$$

where we use climatological time series of surface concentrations N^* and α_{nut} is the relaxation velocity. Alternatively, when data on river or atmospheric loads are available as in the case of the Baltic models presented in Chapter 4, the corresponding nutrient flux is written as:

$$\left\langle N'w'\right\rangle_{z=0} = \frac{L_N}{\Delta z_{z=0}} \tag{C.48}$$

where $L_N(t)$ is the nutrient load time series and the depth of the first layer is used to obtain the proper units for the boundary flux. For the 3D model, the same parameterization used above for salinity is applied. The river is assumed to have a given time-varying nutrient (or dissolved/particulate organic matter) concentration $N_R(t)$ that is transformed into a source term for the general equation (C.25) as in (C.24). The additional source term is computed as in (C.44):

$$Q_N = \frac{R\Phi_R\left(N - N_R\right)_{\sigma=0}}{DA} \tag{C.49}$$

As nutrient bottom boundary conditions we impose the molecular diffusion fluxes of the nutrient benthic remineralization processes computed as described in Section B.7:

$$(K_H + \chi)\left(\frac{\partial N}{\partial \sigma}\right)_{\sigma=-1} = \left.\frac{\partial K}{\partial t}\right|_N^{diff} \Delta z_{\sigma=-1} \tag{C.50}$$

where K is the corresponding nutrient state variable in the sediment and Δz is the depth of the last layer of the vertical grid.

Surface boundary conditions for dissolved oxygen ($O^{(2)}$) are derived from the air-sea gas exchange velocity (α_{ox}) parameterized according to Liss and Merlivat (1986) as a function of the wind velocity, and the dissolved oxygen concentration at saturation, O_{sat} - calculated according to Weiss, 1970 - in

the following way:

$$(K_H + \chi)\left(\frac{\partial O^{(2)}}{\partial \sigma}\right)_{\sigma=0} = \alpha_{ox}\left(O_{sat} - O^{(2)}\right)_{\sigma=0}. \tag{C.51}$$

At the bottom, the boundary condition is equivalent to (C.50) where the water-sediment flux is function of the benthic oxygen demand computed as in Section B.7.8.

Curriculum Vitae

Name: **Marcello Vichi**
Place and date of birth: **Ravenna (Italy), April 6th 1970**
Nationality: **Italian**

Titles

1989: Scientific "Diploma" from Liceo Scientifico "A. Oriani", Ravenna, Italy.
1997: "Laurea" in Marine Environmental Sciences, University of Bologna at Ravenna, Italy.

Language skills

Italian: mother tongue.
English: written and spoken.

Professional experiences

1997: assistant at Laboratorio di Simulazioni Numeriche del Clima e degli Ecosistemi Marini (SINCEM), University of Bologna at Ravenna, Italy.

1997-98: Scientific collaborator at the Marine Geology Institute (IGM-CNR), Bologna, Italy.

1998-2000: Research fellowship (EU Marie-Curie grant) at the Ecological Modelling Centre (DHI Water and Environment, Hoersholm, Denmark).

1999-2000: Visiting scientist at the Royal Netherlands Institute for Sea Research (NIOZ), Texel, The Netherlands.

2000-2002: Ph.D. student at the Faculty of Biology, Geology and Environmental Sciences (FB 7), University of Oldenburg, Germany.

2000-present: Researcher at the National Institute of Geophysics and Volcanology (INGV), Climate Dynamics Group, Bologna, Italy.

Peer-reviewed articles

Vichi M., May W., Navarra A. (2002) Response of a shallow shelf sea ecosystem to a regional climate change scenario. *J. Geoph. Res.*, submitted.

Vichi M., Oddo P., Zavatarelli M.**,** Coluccelli A., Coppini G. Celio M., Fonda Umani S., Pinardi N. (2002). Calibration and validation of a one-dimensional complex marine biogeochemical flux model in different areas of the northern Adriatic Sea. *Annales Geophysicae*, in press.

Vichi M., Zavatarelli M., Pinardi N. (1998) Seasonal modulation of microbial mediated carbon fluxes in the northern Adriatic Sea. A model study. *Fisheries Oceanogr.*, 7(3/4), 182-190.

Vichi M., Pinardi N., Zavatarelli M., Frascari F., Bergamini M.C., Matteucci G., Marcaccio M. (1998) One dimensional ecosystem model tests in the Po prodelta area (northern Adriatic Sea). *Environ. Modelling and Software* 13(5/6), 471-481.

Conference Proceedings

Vichi M. (2000) The influence of high frequency surface forcing functions on productivity in the euphotic layer. In *bio-ecological Observations in Operational Oceanography.* Fischer J., Baretta J., Colijn F. and Flemming N.C. (eds.). EuroGOOS Publication No. 15, Southampton Oceanography Centre, Southampton. ISBN 0-904175-43-X.

Vichi M., Baretta J.W., Ruardij P. (2000) Non linear response in complex ecosystem models: possible implications for the biological data assimilation. In *Workshop on the assimilation of Biological data in Coupled Physical/Ecosystem Models.*, Robinson, A.R. And P.F.J. Lermusiaux (eds.). GLOBEC Special Contribution 3, 152 pp.

Pinardi N., Zavatarelli M., **Vichi M**., Coluccelli A. (2000) Interdisciplinary Modeling: A complex ecosystem approach. In *Workshop on the assimilation of Biological data in Coupled Physical/Ecosystem Models.*, Robinson, A.R. And P.F.J. Lermusiaux (eds.). GLOBEC Special Contribution 3, 152 pp.

Vichi M., Baretta J.W., Ruardij P. (1999) Interannual and long term variability in Baltic ecosystem dynamics. Proc. 3rd BASYS annual science conference, Warnemuende, September 1999, 27 (153).

Zavatarelli M., Pinardi N., **Vichi M**., Allen J.I (1999). The Adriatic Sea ecosystem dynamics: the role of physical and biological processes. *Proc. 2nd EUROGOOS Conf.*, Rome, March 1999, 97.

Baretta J.W., **Vichi M**., Babovic V., Keijzer M. (1999) New tools in marine ecosystem modelling. *Proc. 3nd International Marine Environmental Modelling Seminar*, Lillehammer, April 1999.

Zavatarelli M., Allen J.I, Baretta J.W., Baretta-Bekker J.G, Pinardi N., **Vichi M**. (1998) Developments in the Adriatic Sea ecosystem dynamics modelling. *Proc. 3rd MTP Workshop*, Rhodos, October 1998, 229.

Zavatarelli M., Allen J.I, Pinardi N., **Vichi M**. (1998) Modelling the Adriatic Sea ecosystem dynamics: from 1D to high resolution 3D models. *Proc. Int. Workshop: The Oceanography of the Adriatic Sea*, Trieste, September 1998, 60.

Vichi M., Pinardi N., Zavatarelli M., Frascari F., Bergamini M.C., Matteucci G., Marcaccio M. (1998 A one-dimensional model study of the biogeochemical seasonal cycles in the Po prodelta area (northern Adriatic Sea). *Annales Geophysicae*, 16(Suppl. II), C597.

Vichi M., Zavatarelli M., Pinardi N. (1998) Seasonal modulation of microbial mediated carbon fluxes in the northern Adriatic Sea. A model study. *Proc. 1st GLOBEC Open Science meeting, Paris*, March 1998, N. 67.

Vichi M., Zavatarelli M., Pinardi N. (1998) Calibration and validation of a one-dimensional ecosystem model in the Po prodelta area (northern Adriatic Sea). *Proc. 2nd International Marine Environmental Modelling Seminar,* Lillehammer, March 1998.

Technical reports

Babovic V., Baretta J.W., **Vichi M**., Keijzer M. (1999) New methods in ecological modelling in the context of BASYS. *DHI Tech. Report, Project 8103/8130, October 1999*, 10 pp.

Vichi M., Baretta J.W., Ruardij P. (1999) Interannual and long-term variability in Baltic ecosystem dynamics: causes and implications. *DHI Tech. Report, Project 8130, September 1999*, 151 pp.

Vichi M., Pinardi N., Zavatarelli M., Frascari F. (1998) Interazione tra forzante idrodinamico e cicli biogeochimici nel Mare Adriatico Settentrionale: esperimenti numerici. *IMGA-CNR Tech. Rep., 3/98*, 170 pp.

Vichi M., Pinardi N., Zavatarelli M. (1998) Sviluppo e calibrazione di un modello unidimensionale di ecosistema nella stazione S1. *Progetto PRISMA I, relazione finale*, 47 pp.

Theses

Vichi M. (1997) Interazione tra forzante idrodinamico e cicli biogeochimici nel Mare Adriatico Settentrionale: esperimenti numerici. *Tesi di Laurea in Scienze Ambientali (indirizzo marino), Univ. Bologna, Sede Ravenna, Fac. Sci. MM FF NN*, 218 pp.

Vichi M. (2002) Predictability studies of coastal marine ecosystem behavior. Ph.D thesis, Oldenburg University, Germany.

Erklärung:

Hiermit versichere ich, dass ich diese Arbeit selbständig verfasst und keine anderen als die angegebenen Quellen und Hilfsmittel benutzt habe

Unterschrift

Ort, Datum